PhD Thesis ‖ Dissertation

Two-Photon Initiators and Macromers for Biomedical Applications

ausgeführt zum Zwecke der Erlangung

des akademischen Grades eines Doktors der technischen Wissenschaften

unter der Leitung von

Univ.Prof. Dipl.-Ing. Dr.techn. Robert Liska

Univ.Ass. Dipl.-Ing. Dr.techn. Stefan Baudis

E163 – Institut für Angewandte Synthesechemie

eingereicht an der TU Wien, Fakultät für Technische Chemie

von
Elise Zerobin ‖ 0826417
Witthauergasse 19/12, 1180 Wien
Wien, 1. Februar 2021

Die approbierte gedruckte Originalversion dieser Dissertation ist an der TU Wien Bibliothek verfügbar.
The approved original version of this doctoral thesis is available in print at TU Wien Bibliothek.

Die approbierte gedruckte Originalversion dieser Dissertation ist an der TU Wien Bibliothek verfügbar.
The approved original version of this doctoral thesis is available in print at TU Wien Bibliothek.

Die approbierte gedruckte Originalversion dieser Dissertation ist an der TU Wien Bibliothek verfügbar.
The approved original version of this doctoral thesis is available in print at TU Wien Bibliothek.

Look up at the stars and not down at your feet

Stephen Hawking

1942-2018

Die approbierte gedruckte Originalversion dieser Dissertation ist an der TU Wien Bibliothek verfügbar.
The approved original version of this doctoral thesis is available in print at TU Wien Bibliothek.

Danke

Robert: für die Möglichkeit, diese Dissertation in deiner Arbeitsgruppe zu verfassen. Danke für dieses einzigartige Projekt, in dem ich mich fachlich sowie persönlich weiterentwickeln konnte. Danke für die unzähligen *team building* Seminare und dein Bestreben eine angenehme Arbeitsatmosphäre zu schaffen.

Stefan: für deine fachliche Betreuung und dein unbändiges Bestreben zur Perfektion.

Aleks: für deinen stets direkten Input und für die Möglichkeit, meinen Horizont in die Welt der Physik, Biologie und Medizin zu erweitern.

Simone: für deine ehrliche Unterstützung und Förderung.

Triumph4Rat® - Hofi und Schnöll: für eure unbändige Ehrlichkeit und diese großartige Freundschaft.

Team des FBMC: Thank you all for making those 3 years some incredible ones. Danke insbesondere an **Yazgan**, mit dir habe ich persönliche sowie berufliche Höhen und Tiefen immer teilen und mich stets auf deine ehrliche Meinung verlassen können. Danke auch an meine ambitionierten WahlpraktikantInnen und Bachelorstudenten (Stephan und Jakob).

Super Scientific Play-Room Marica, Franziska, Wolfi, Agi, Jasper, Stefan B., Tommaso and of course 2PPeter: for your productive support & expert knowledge regarding physics, (cell) biology, and materials science. Additionally, I'd like to say a huge thank you to the entire team in Belgium! I am so grateful that I was able to get to know you all.

Forschungsgruppe Werkstoffe und Additive Fertigung: für den erfrischenden Maschinenbau-Wind. Einen speziellen Dank auch an **Jürgen Stampfl** für die grandiosen Ski-Seminare und die interdisziplinäre Zusammenarbeit.

Ein großer Dank gebührt meiner **Familie**, die mich aufgezogen, geformt, geprägt und zu dem gemacht hat, was ich heute bin. Ich bin euch unendlich dankbar, dass ihr das Leben so lebenswert macht und dass ich euch immer vertrauen kann.

Mein **Florian**: deine Effizienz und Aufopferung inspirieren mich immer wieder. Ich bin unglaublich dankbar dich an meiner Seite zu haben.

Die approbierte gedruckte Originalversion dieser Dissertation ist an der TU Wien Bibliothek verfügbar.
The approved original version of this doctoral thesis is available in print at TU Wien Bibliothek.
TU Bibliothek Your knowledge hub WIEN

Die approbierte gedruckte Originalversion dieser Dissertation ist an der TU Wien Bibliothek verfügbar.
The approved original version of this doctoral thesis is available in print at TU Wien Bibliothek.

Abstract

Three-dimensional printing and photopolymerization are powerful technologies for the reconstruction of tissue-like functional materials with great relevance for biomedicine. However, conventional high-energy lithographic techniques (UV-polymerization) exhibit considerable limitations, since the provided energy may induce collateral tissue damage along the irradiation pathway. The development of two-photon polymerization enabled the fabrication of hydrogel scaffolds with exceptional resolution, providing enough energy within the focal volume of a focused infrared laser to efficiently induce two-photon polymerization. The water-solubility of the matrix materials (monomers and photoinitiators) are of major importance for the reconstruction of tissue-like hydrogel scaffolds. Furthermore, the solubility in aqueous media and the biocompatibility of the compounds is essential for efficient two-photon polymerization in the presence of cells. Not only the compounds itself, but also the generation of reactive oxygen species, as a consequence of photoexcitation, are limiting factors regarding biocompatibility.

The reduction of those limitations is targeted via a straightforward design of novel two-photon initiators and the association of cleavable moieties into π-conjugated chromophores. The photolabile moieties could possibly reduce the formation of reactive oxygen species, due to their efficient dissociation mechanisms, while preserving biocompatibility. Furthermore, hyaluronic acid is investigated as endogenous substance for the development of hydrogel materials for tissue engineering. Two basic approaches were followed to synthesize cleavable two-photon initiators. On the one hand, photolabile oxime ester moieties were introduced into a well-established cycloketone core structure. On the other hand, photolabile azosulfonate moieties were incorporated into a commercially available azo dye. The photochemical behavior of the synthesized compounds was examined during comprehensive photoreactor studies, while focus was placed on the stilbene-based reference materials, which exhibited severe tendency towards photoisomerization. The efficiency of the novel two-photon initiators was confirmed via two-photon structuring tests in gelatin-based hydrogel formulations and the performance was compared to state-of the art initiators. Especially, the polymerization threshold of the azosulfonate-based two-photon initiators was studied in detail, since exceptionally stable hydrogel materials were obtained at various technically relevant femtosecond-laser wavelengths. Biocompatibility assays on various cell-lines proved their promising cytocompatibility. Finally, hyaluronic acid-based hydrogel formulations were successfully applied as material platform for three-dimensional cell encapsulation using two-photon polymerization. Summarizing, the association of photolabile groups (oxime esters, azosulfonates) to π-conjugated chromophores was successful. Furthermore, hyaluronic acid was confirmed as promising candidate for the fabrication of tissue-like hydrogel materials as long as the molecular weight is kept moderate to ensure solubility in aqueous media.

Die approbierte gedruckte Originalversion dieser Dissertation ist an der TU Wien Bibliothek verfügbar.
The approved original version of this doctoral thesis is available in print at TU Wien Bibliothek.
TU Bibliothek Your knowledge hub WIEN

Die approbierte gedruckte Originalversion dieser Dissertation ist an der TU Wien Bibliothek verfügbar.
The approved original version of this doctoral thesis is available in print at TU Wien Bibliothek.

Kurzfassung

Der 3D Druck und besonders der Einsatz von Photopolymeren für die Geweberekonstruktion sind heutzutage von außerordentlicher Bedeutung für die Biomedizin. Bei der klassischen UV-Polymerisation wird hochenergetisches, kurzwelliges Licht angewandt, wobei es durch Absorption von biologischem Gewebe zur Schädigung von Zellen sowie Verbrennungen der Matrix kommen kann. Zwei-Photonen Polymerisation basiert auf der Technologie von gepulsten, fokussierten Infrarotlasern und ermöglicht aufgrund der Transparenz von biologischem Gewebe gegenüber dem eingesetzten Infrarotlicht, die Herstellung hoch aufgelöster, komplexer drei dimensionaler Strukturen mit einer minimalinvasiven Technik. Hierfür sind wasserlösliche Matrixkomponenten unabdingbar (Monomere sowie Photoinitiatoren), um natürliches Gewebe bestmöglich nachzubilden. Nicht nur die Wasserlöslichkeit, sondern auch ein hohes Maß an Biokompatibilität aller Matrixkomponenten sind für eine effiziente Zwei-Photonen Polymerisation in Gegenwart von Zellen unerlässlich. Außerdem kann es aufgrund von angeregten Zuständen der Photoinitiatoren und der Bildung von reaktiven Sauerstoffspezies zu erheblichem Schaden des umgebenden Gewebes kommen.

Um diese Limitierungen zu reduzieren, befasst sich diese Arbeit mit der gezielten Entwicklung spaltbarer Photoinitiatoren. Getrieben durch die Freisetzung von Kohlenstoffdioxid bzw. Stickstoff können spaltbare funktionelle Gruppen die Bildung von reaktiven Sauerstoffspezies reduzieren und somit zu einer vielversprechenden Biokompatibilität beitragen. Nebst Photoinitiatoren werden in dieser Arbeit auch Makromere weiterentwickelt, die auf einem natürlich vorkommenden Polysaccharid basieren (Hyaluronsäure), um natürliches Gewebe in Form von Hydrogelen optimal nachzubilden. Im Gegensatz zu den bisherig entwickelten Photoinitiatoren, konnten zwei Klassen an spaltbaren Photoinitiatoren synthetisiert werden. Die erste Klasse an Photoinitiatoren wurde über die gezielte Einbindung spaltbarer Oximester Gruppen in bereits etablierte Zykloketon-Kernstrukturen erhalten und die zweite Klasse über die Einführung spaltbarer Azosulfonat Gruppen in einen kommerziell erhältlichen Azofarbstoff. Die Spaltbarkeit der Photoinitiatoren wurde mithilfe von Photoreaktor-studien überprüft, wobei vor allem auf die Fotoprodukte der Stilben-basierten Azosulfonate eingegangen wurde, die als Konkurrenz-reaktion eine außerordentliche Tendenz zur Photoisomerisierung aufweisen. Die Wirksamkeit beider Photoinitiator-klassen wurde mittels Zwei-Photonen Lithographie in Gelatine-basierten Makromeren bestätigt. Hierbei wurde vor allem der Schwellenwert der Polymerisation von Azosulfonaten bei verschiedenen Wellenlängen ermittelt. Zusätzlich konnte durch Stammzellenstudien eine hohe Biokompatibilität der Azosulfonate bewiesen werden. Die Makromere basierend auf Hyaluronsäure konnten sogar dafür verwendet werden, um in Gegenwart von Zellen komplexe 3D Hydrogele zu drucken. Demnach wurde die Entwicklung und Anwendung neuer Zwei-Photonen Initiatoren über die Inkorporation spaltbarer Funktionalitäten (Oximester, Azosulfonate) erfolgreich durchgeführt. Außerdem wurde Hyaluronsäure als hervorragende Basiskomponente für die Entwicklung von Hydrogelstrukturen bestätigt, sofern das Molekulargewicht der Wiederholungseinheit niedrig gehalten wird, um die Löslichkeit der Makromere zu bewahren.

Die approbierte gedruckte Originalversion dieser Dissertation ist an der TU Wien Bibliothek verfügbar.
The approved original version of this doctoral thesis is available in print at TU Wien Bibliothek.
TU Bibliothek Your knowledge hub WIEN

Die approbierte gedruckte Originalversion dieser Dissertation ist an der TU Wien Bibliothek verfügbar.
The approved original version of this doctoral thesis is available in print at TU Wien Bibliothek.

Table of Contents

Introduction	1
Objective	17
General Part	19
Experimental Part	123
Summary	157
Materials and Methods	164
Abbreviations	168
References	170

	Gen.	Exp.
1 Two-Photon Initiators based on Oxime Esters	19	
1.1 State-of-the-Art Oxime Esters	19	
1.2 Synthesis of Oxime Ester-based Two-Photon Initiators	22	123
1.2.1 Preliminary Investigation on a Bimolecular System	22	123
1.2.1.1 Synthesis	23	123
1.2.1.2 Testing	23	124
1.3 Steady-State Photolysis of Oxime Ester-2PIs	46	140
1.4 Two-Photon Polymerization of Oxime Ester-2PIs	50	140
1.5 Conclusion	55	
2 Two-Photon Initiators based on Azosulfonates	59	
2.1 State-of-the-Art Azosulfonates	59	
2.2 Synthesis of Azosulfonate-based Two-Photon Initiators	61	141
2.3 Characterization of Azosulfonate-2PIs	67	144
2.3.1 Photoreactor Studies	67	144
2.3.2 NMR Study of Photoproducts	75	145
2.3.3 HPLC Study of Photoproducts	79	147
2.3.4 Z-Scan Measurements	83	149
2.4 Two-Photon Polymerization of Azosulfonate-2PIs	84	150
2.5 Biocompatibility Studies	93	151
2.5.1 2.5.1 Metabolic Activity	93	151
2.5.2 Cell Permeability	98	152
2.6 Conclusion	103	

Die approbierte gedruckte Originalversion dieser Dissertation ist an der TU Wien Bibliothek verfügbar.
The approved original version of this doctoral thesis is available in print at TU Wien Bibliothek.

3 Hydrogel Materials for Two-Photon Polymerization	107	
3.1 State-of-the-Art Hydrogel Materials	107	
3.2 Synthesis of Hyaluronic Acid-based Macromers	110	152
3.3 Characterization of HAVE Hydrogels	112	153
3.3.1 NMR Analysis	112	153
3.3.2 GPC Analysis	113	153
3.3.3 Photorheology	113	153
3.3.4 Hydrogel Swellability	114	154
3.4 Cell Encapsulation	116	155
3.4.1 UV-Cell Encapsulation	117	155
3.4.2 Cell Encapsulation using Two-Photon Polymerization	120	156
3.5 Conclusion	122	

Die approbierte gedruckte Originalversion dieser Dissertation ist an der TU Wien Bibliothek verfügbar.
The approved original version of this doctoral thesis is available in print at TU Wien Bibliothek.

Introduction

Tissue Engineering

Tissue engineering (TE) is an interdisciplinary field that applies the principles of biology and engineering with the ultimate goal to recreate the complexity of living tissues.[1,2] There is an immense variety of polymers available on the market and researchers constantly strive to improve materials and methods to broaden the horizon towards more economical and ecological solutions. Especially in the field of medicine and the related divisions, such as TE and regenerative medicine, there is a great demand for biocompatible materials.[3] In particular, a better understanding on the dynamic interactions between cells and materials guide the design for more appropriate *in vivo* and *in vitro* models. Since then, it has been long recognized that the microenvironment directly influences cell fate.[4] TE is an highly interdisciplinary field with the motivation to restore, replace or regenerate native tissue. Multiple factors such as the combination of scaffolds, cells and signaling molecules determine the success of TE (Figure 1).

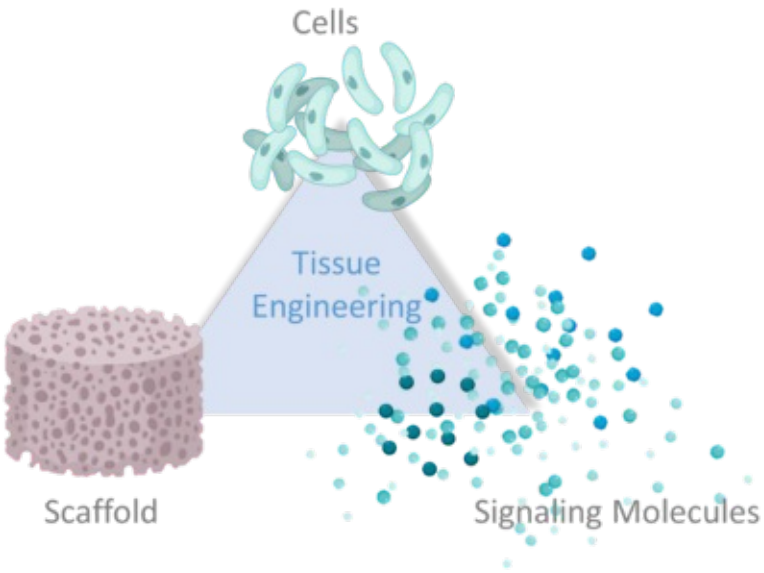

Figure 1: The basic principles of tissue engineering. Cell survival is strongly determined by the surrounding microenvironment (scaffold) and local and systemic active signaling molecules (growth- & transcription factors).

Hydrogels are an important class of biomaterials, widely used in TE with the aim to mimic native tissue.[5,6] Hydrogels are crosslinked polymeric networks, which do not dissolve in aqueous media, hence providing an optimal scaffold matrix element.[7] Their ability to absorb high amount of water and their permeability for nutrients make them especially promising materials for their application in soft tissue regeneration. For their application, following requirements should be fulfilled: biodegradability, structural similarity to the desired type of tissue and mechanical support for tissue growth.[4] Scaffolds provide the defined structural element for cells to properly attach and proliferate within a matrix (cell adhesion, -proliferation, -migration and -differentiation).[8]

Die approbierte gedruckte Originalversion dieser Dissertation ist an der TU Wien Bibliothek verfügbar.
The approved original version of this doctoral thesis is available in print at TU Wien Bibliothek.
TU Bibliothek Your knowledge hub WIEN

Additionally, the development and differentiation of some organs requires dynamic and reciprocal signaling between cells and their microenvironment.[4] TE aims to design such materials with cell-regulative behavior using polymers capable of meeting all these requirements. The versatility of hydrogels supported the further development of these materials from simple water-swollen networks to multi-variant smart materials with tunable bioactive properties.[9] In order to create crosslinked polymeric networks, various building blocks can be used. The large variety of polymers available explains the even greater manifoldness of available macromers.

Polymeric Biomaterials for Tissue Engineering

The development of polymeric biomaterials has played a fundamental role in the improvement of healthcare.[10] Many achievements have been made by the judicious combination of various available materials. The major goal of polymeric biomaterials is the mimicking of native ECM and the morphological appearance of native tissue. According to the replaced tissue (bones, joints, ligaments, vascular grafts, cartilage), different mechanical properties are required.[11] In general, biomaterials can be classified as synthetic, naturally-derived and hybrid materials, depending on the source of the constituting polymer.[12] Since the exploitation of petroleum, a broad range of synthetic materials was developed with wide-spread applications, also in the field of biomedicine (Figure 2).[13,14]

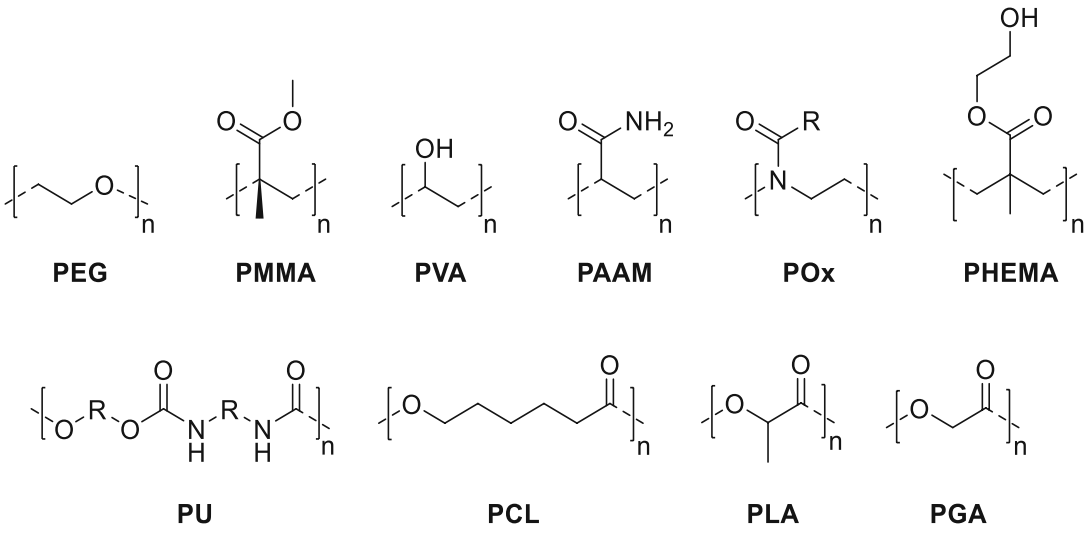

Figure 2: Various synthetic biomaterials are available for the fabrication of biomaterials: poly(ethylene glycol) (PEG), poly(methyl methacrylate) (PMMA), poly(vinyl alcohol) (PVA), poly(acrylamide) (PAAM), poly(2-oxazoline) (POx), poly(hydroxymethyl methacrylate) (PHEMA), poly(urethane) (PU), poly(caprolactone) (PCL), poly(lactic acid) (PLA) and poly(glycolic acid) (PGA).

Many synthetic biomaterials are available, amongst others polyethylene glycol (PEG),[15,16] poly(methyl methacrylate) (PMMA),[17] poly(vinyl alcohol) (PVA),[18] poly(acrylamide) (PAAM),[19,20] poly(2-oxazolines) (POx)[21-24] and poly(hydroxyethyl methacrylate) (PHEMA).[25] However, these hydrophilic macromers often suffer from low- to no biodegradability. By the development of resorbable biomaterials such as poly(lactic acid) (PLA),[26,27] poly(glycolic acid) (PGA),[28,29]

Die approbierte gedruckte Originalversion dieser Dissertation ist an der TU Wien Bibliothek verfügbar.
The approved original version of this doctoral thesis is available in print at TU Wien Bibliothek.
TU Bibliothek Your knowledge hub WIEN

poly(ε-caprolactone) (PCL)[30,31] polymer-breakdown was enabled, which blurred the lines between artificial biomaterial implants and host tissue. For polyesters, different bulk- and surface degradation-rates can be observed, depending on the hydrolysis-rate of ester moieties related to the amount of hydrophilic and -phobic side chains.[32,33] Poly(urethanes) (PUs) are an exceptionally variable class of biopolymers used for cardiovascular prostheses, because the variation of soft- and hard segments enables the guidance of biomaterial-morphology.[34,35]

The portfolio of biomaterials was further expanded by the introduction of naturally-derived biomaterials. Since synthetic hydrogels are considered as bioinert, their clinical success is limited.[36,37] Living tissue is responding to changing physiological, biochemical stimuli but bioinert materials are not without further modification.[38] Naturally-derived biomaterials are especially suitable to reconstruct soft tissues, offering active sites for cells to attach. Many polymers created by nature are biodegradable *per se*, which can be used to engineer biomaterials with variable degradation properties.[39] Polysaccharides and proteins were already explored for various TE applications, such as alginate,[40] agarose,[41] chitosan,[42] hyaluronic acid,[43] fibrin,[44,45] collagen,[46-48] keratin,[49] and gelatin[50-54] (Figure 3).

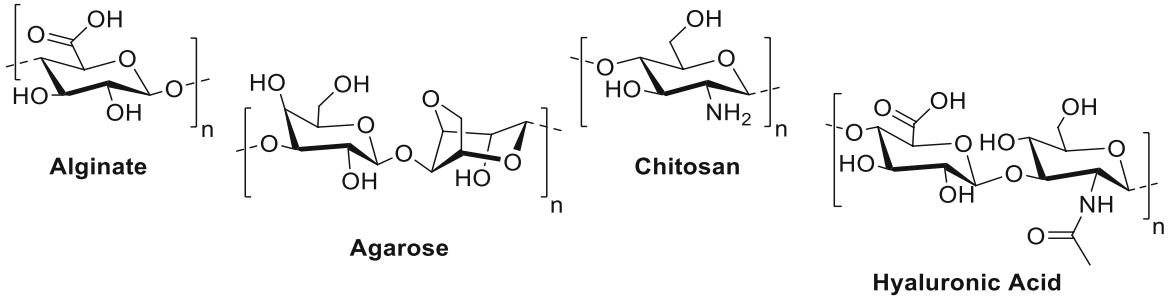

Figure 3: Naturally-derived polysaccharides as biomaterials for tissue engineering.

Alginate and agarose are polysaccharides widely available from plants (brown seaweeds and red algae). Chitosan is derived from chitin and the main component of the exoskeleton of insects and crustacean. Hyaluronic acid (HA) is a major component of the ECM (cartilage, dermis and the vitreous humor, Figure 4) with high clinical relevance.[55]

Figure 4: Hyaluronic acid is a naturally-occurring biopolymer, widely present in native tissue, such as joints (a),[56] the dermis (b)[57] and the vitreous humor of the eye c).[58]

Die approbierte gedruckte Originalversion dieser Dissertation ist an der TU Wien Bibliothek verfügbar.
The approved original version of this doctoral thesis is available in print at TU Wien Bibliothek.
TU Bibliothek Your knowledge hub WIEN

HA is an attractive hydrogel material for a wide range of biomedical applications including regenerative medicine, drug delivery and scaffolds for cell culture.[59] HA's extremely high water binding capacity enables the fabrication of tissue scaffolds similar to the native ECM.[59-61] Although natural polymers, such as HA, provide a close reproduction to the ECM, the lack of mechanical properties still limits these materials being applied as 3D scaffolds at load bearing regions.[62] Consequently, chemical modification allows the development of biomaterials with independently tunable mechanical properties (Figure 5).[63,64]

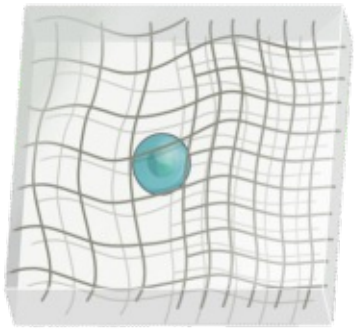

Figure 5: The crosslinking density of macromers controls the mechanical properties of hydrogels.[62]

For HA, the chemical modification of functional moieties (hydroxyl-, carboxyl-) is a powerful tool to control mechanics and degradability after crosslinking.[59] A broad variety of functional groups were already introduced (furan, maleimide, thiol, methacrylate, acrylate and vinyl ester, Figure 6).

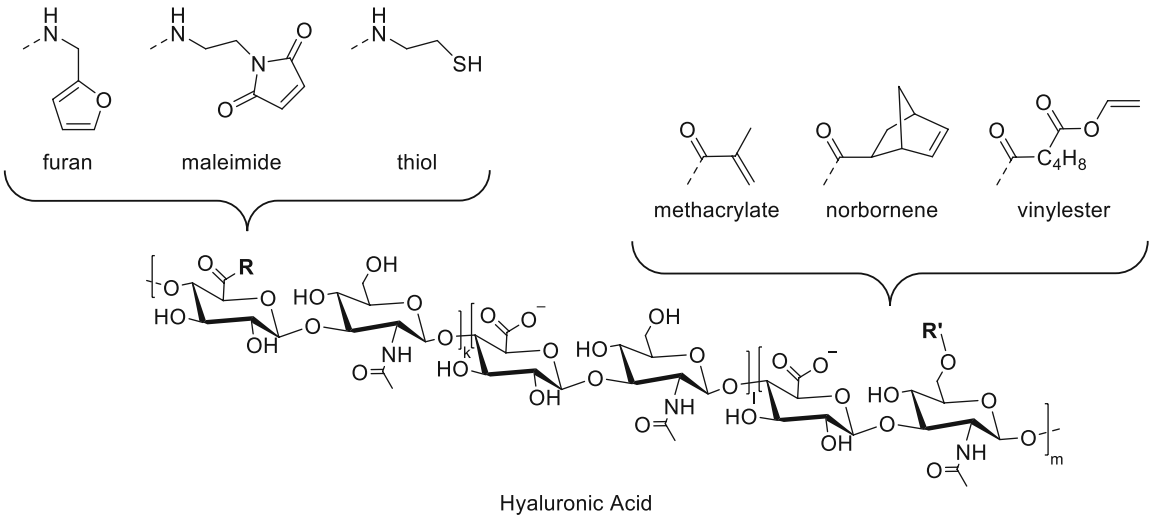

Figure 6: Hyaluronic acid is available for modification on the active site of the carboxylic acid (left) and the primary alcohol (right).

Chemical modifications enable the crosslinking of macromers via various external stimuli such as temperature, electricity, pH, magnetic field, pressure, sound and light.[65] By this, biomaterials became increasingly important, mainly because of their stimuli-responsive behavior. The response of the polymer can differ according to the concept applied, such as a change in shape, color or solubility.[66] Certainly, a highly important group of polymers are those undergoing major changes in solubility either by a change of temperature (e.g. 37°C for gelatin) or by light-induced processes.

Die approbierte gedruckte Originalversion dieser Dissertation ist an der TU Wien Bibliothek verfügbar.
The approved original version of this doctoral thesis is available in print at TU Wien Bibliothek.
TU Bibliothek Your knowledge hub WIEN

Many natural phenomena and vital processes on earth (photosynthesis) are initiated by the electromagnetic radiation of the sun (UV, Vis, IR light).[67] In a similar way, external triggers such as UV light can be used to trigger photochemical reactions in hydrogel precursor formulations, inducing the crosslinking of reactive macromers.

Radical Photopolymerization

Radical photopolymerization is a type of polymerization initiated by the optical absorption of a photoinitiator (PI) molecule. Subsequently, reactive radicals are created inducing polymerization in the presence of reactive monomers (Scheme 1). The mechanism proceeds (propagation) via the radical addition on reactive double bonds at the lower substituted site.[68] The polymerization is progressing until termination occurs (recombination, disproportionation and O_2 inhibition).

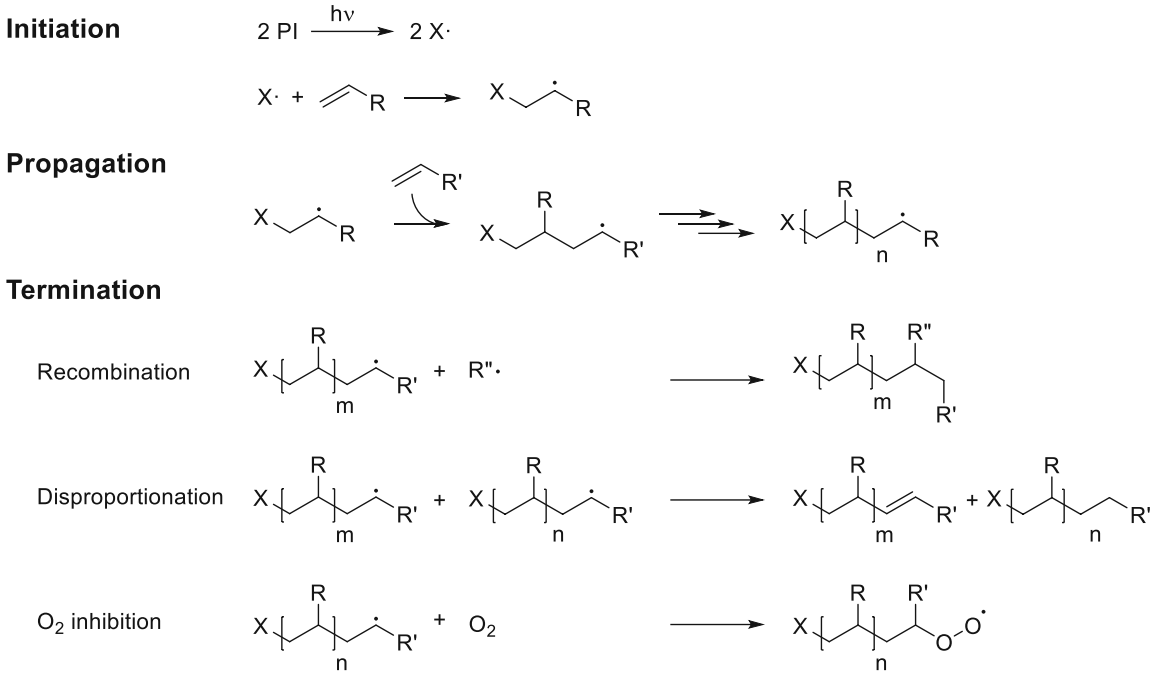

Scheme 1: The mechanism of radical photopolymerization.

Generally, there are different types of PIs, depending on the molecular mechanism of how radicals are generated.[69] For Norrish type I PIs, unimolecular α-cleavage occurs preferentially from the n-π* electronic states of ketones (Scheme 2).[70] Norrish type II reactions proceed via a bi-molecular mechanism of a PI (sensitizer) and a co-initiator. Several studies suggested the improved efficiency of type I compared to type II PIs.[71] This is caused by the intrinsic limitations for bimolecular systems, such as limited electron transfer between sensitizer and co-initiator. Furthermore, photoinduced back electron transfer can significantly decrease initiation efficiency, since the ground state of the parent system can be regenerated.[70,72] Classical bi-molecular type II systems, like ketone/amines are applied in dental medicine, where camphorquinone serves as PI and tertiary amines as co-initiators.[71] Lithium phenyl-2,4,6-trimethylbenzoylphosphinate (Li-TPO) is

Die approbierte gedruckte Originalversion dieser Dissertation ist an der TU Wien Bibliothek verfügbar.
The approved original version of this doctoral thesis is available in print at TU Wien Bibliothek.
TU Bibliothek Your knowledge hub WIEN

one representative of a water-soluble type I PI, which was already intensively studied for hydrogel fabrication (Scheme 2).[73]

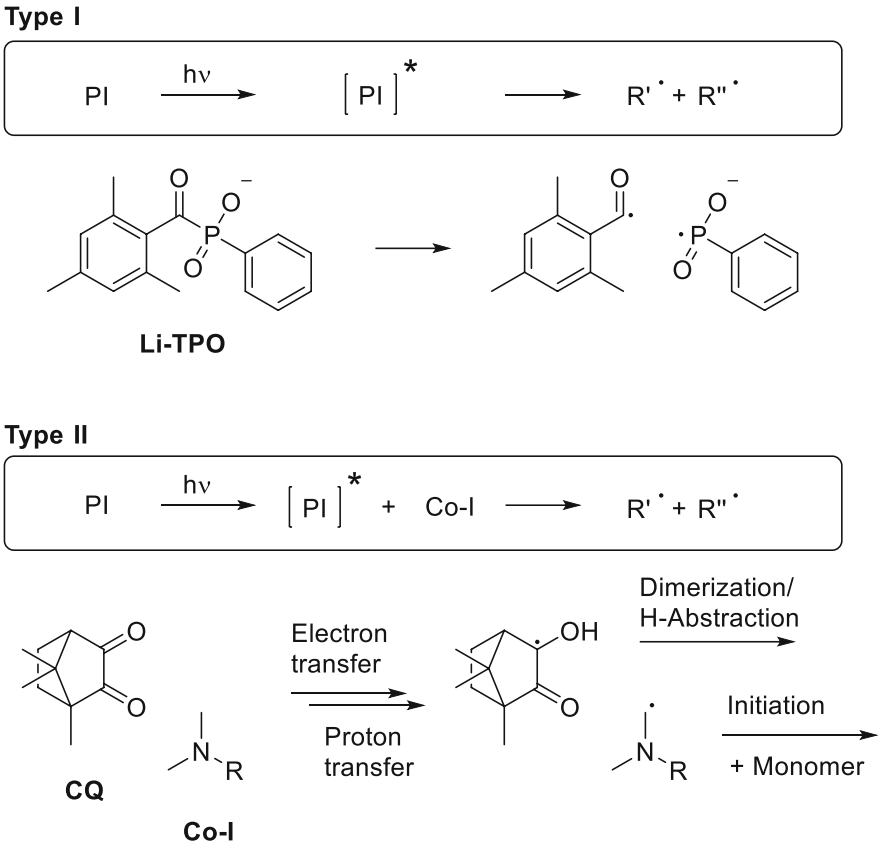

Scheme 2: Unimolecular (type I) fragmentation and bi-molecular (type II) reaction of a photoinitiator (PI) upon excitation with light (hν). The type II mechanism proceeds via the reaction of an excited-state molecule ([PI]) with a co-initiator (Co-I) under the formation of free reactive radicals (R'·, R''·). Examples are depicted on the right: Li-TPO as a representative of Norrish type I PIs and camphorquinone (CQ) in combination with tertiary amines (Co-I) as representatives of Norrish type II PIs.*

Most radicals are transient species and will react with vinylic macromers. Hence, radical photopolymerization can be used for the crosslinking of macromers to generate hydrogels. Therefore, precursor molecules (e.g. polysaccharides) must be chemically modified to introduce reactive double bounds. Although, acrylates are readily applied, due to their high curing rates and good storage stability,[74] they are more and more associated with problems of irritancy and cytotoxicity due to potential harmful acrylic acid degradation products.[75] Vinyl ester (VE) macromers instead, showed improved cytocompatibility over state-of-the-art acrylate macromers.[76] Typically, free-radical polymerization of acrylates suffers from stress development[77] and oxygen inhibition,[78] highly undesired for aqueous systems. Moreover, heterogeneous polymer network structures with broad glass transition temperatures and high shrinkage stress are generated.[79] Thiol-ene chemistry is a concept often applied when homogeneous polymer networks with lower shrinkage are desired.[80] Additionally, the limited photoreactivity of VEs compared to acrylates, in particular when abstractable hydrogens are present, can be boosted by the introduction of reactive thiols.[81] Moreover, the rapid reaction rate and lower sensitivity

Die approbierte gedruckte Originalversion dieser Dissertation ist an der TU Wien Bibliothek verfügbar.
The approved original version of this doctoral thesis is available in print at TU Wien Bibliothek.
TU Bibliothek Your knowledge hub WIEN

towards O_2 make thiol-ene reactions especially promising for the preparation of hydrogels. Furthermore, thiol-ene reactions occur under very mild conditions (aqueous media, room temperature, physiological pH values), highly attractive when applied in the field of TE. The difference between thiol-ene chemistry of VE macromers and the homopolymerization mechanism of state-of-the-art acrylate macromers is described hereafter (Scheme 3).[81]

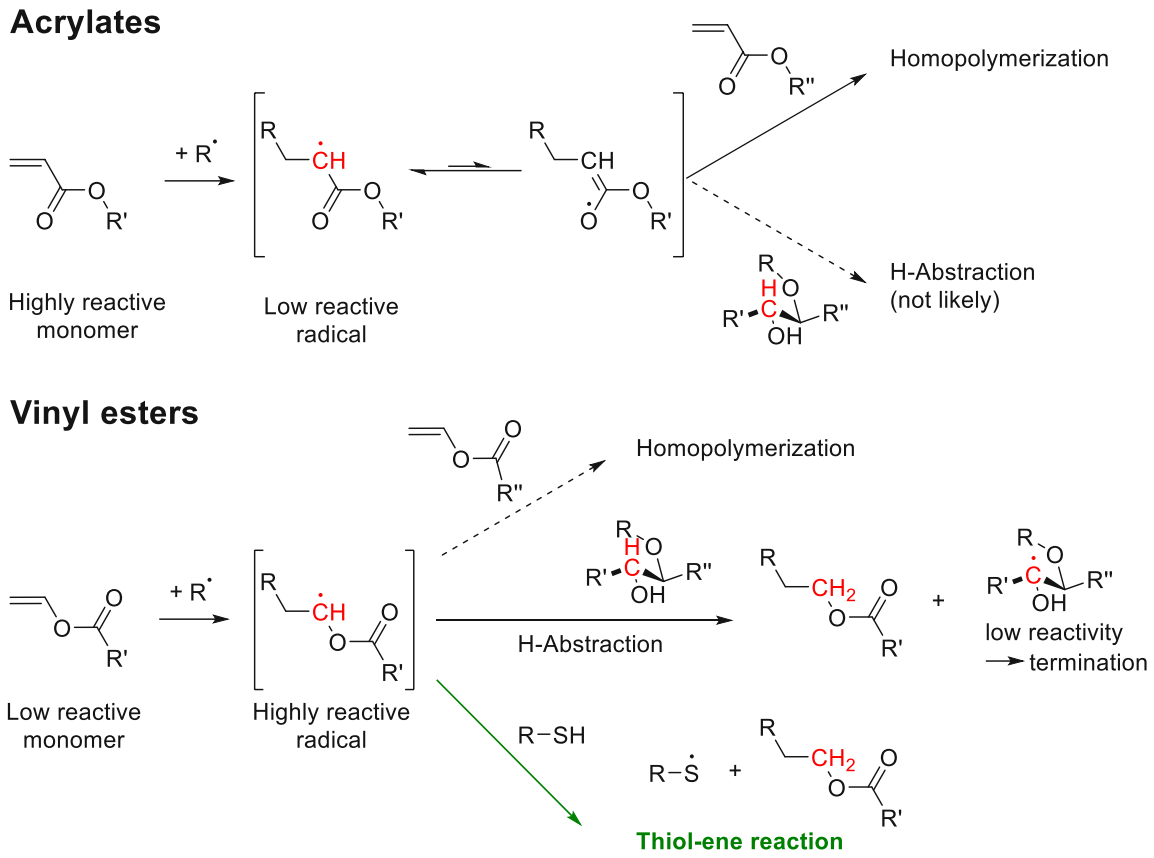

Scheme 3: Reaction mechanisms for the homopolymerization of acrylates (top) and the thiol-ene reaction of vinyl esters (bottom).

There are two major classes of radical photopolymerization: reactions following a chain-growth or step-growth mechanism. In contrast to the free-radical chain-propagation mechanism of acrylate systems, thiol-ene reactions proceed by a step-growth or a mixed mechanism, facilitated by a free-radical chain-transfer.[82] Compared to VE, acrylates proceed via homopolymerization, due to the high reactivity of the acrylate monomer driven by the resonance-stabilization of the radicals. Side reactions, which lower the reactivity of acrylates (H-abstraction), are not very likely. In case of the VEs, the resulting radical is not resonance stabilized, making it very reactive. Therefore, side reactions like H-abstraction are very likely and lead to termination of the polymerization process. By introducing thiols into the system, the H-abstraction can be directed to a substrate, which generates radicals that do not terminate the polymerization, but yield in highly reactive thiyl radicals. The thiyl radicals react with further VE macromers resulting in a homogeneous network formation. Since the polymerization proceeds rapidly and the gel-point is retarded until relatively high functional group conversions, thiol-ene reactions are leading to

Die approbierte gedruckte Originalversion dieser Dissertation ist an der TU Wien Bibliothek verfügbar.
The approved original version of this doctoral thesis is available in print at TU Wien Bibliothek.
TU Bibliothek Your knowledge hub WIEN

polymers with low shrinkage stress.[83,84] Thiol-ene chemistry can be employed to an enormous range of both thiols and macromers (enes), enabling the adjustment of physical and mechanical properties of polymer networks. More and more, acrylates get substituted with more biocompatible macromers, like VEs since the toxicity of hydrogel macromers are of crucial importance to understand cell microenvironment and cell viability.[85] Hence, photopolymerization offers the possibility to generate a great variety of dynamic and complex biomaterials. Besides the crosslinking mechanism, the type of material processing determines final network properties. A broad variety of techniques are available to locally expose photosensitive monomer mixtures to light, creating three-dimensional (3D) polymer structures.

Additive Manufacturing Technologies

Additive Manufacturing Technologies (AMT) is a rapidly evolving field with the ability to replicate complex native tissue generating 3D matrices for TE.[86] AMT is a computer-controlled process, where objects are fabricated via solidification of monomer mixtures or powders.[87] There is a great number of techniques, including extrusion-based and powder bed fusion techniques, but in this thesis, special focus is laid on lithography-based techniques for regenerative medicine. Literature provides an extensive overview on AMT-manufactured cell culture matrices.[88-97] Three main groups of lithography-based AMTs (L-AMTs) are discussed hereafter, laser-based stereolithography (SLA), digital light processing (DLP)-based SLA and two-photon polymerization (2PP, Figure 7). L-AMTs are extremely versatile technologies with the ability to use different light sources and pattern generators (lasers, lamps, LEDs, galvanometer scanners for SLA and digital micromirror device for DLP). Given the common approach of irradiating photosensitive monomer mixtures with light, SLA is using a moveable UV laser spot to initiate photopolymerization. The fabrication of constructs can either be realized through a bottom-up or top-down approach. During the printing process, a movable platform within a vat then immerses the cured part with another layer of monomer mixture and the laser scanning process is repeated. In contrast, DLP supports the strategy of projecting a whole cross-section of the desired structure onto the bottom of a transparent vat using an optical system. By the simultaneous projection of multiple points, processing times can be reduced.[98] In a DLP process, every layer consists of pixels, building up a layer of quadratic elements (Figure 7).

Die approbierte gedruckte Originalversion dieser Dissertation ist an der TU Wien Bibliothek verfügbar.
The approved original version of this doctoral thesis is available in print at TU Wien Bibliothek.
TU Bibliothek Your knowledge hub WIEN

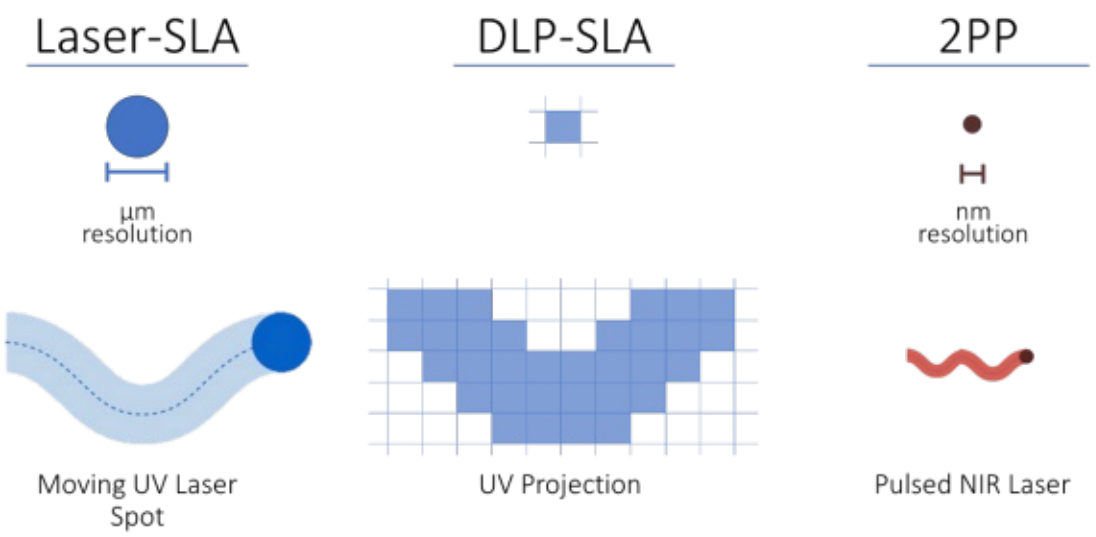

Figure 7: Lithography-based additive manufacturing technologies (AMTs) for soft tissue fabrication. Laser-based stereolithography (SLA) and digital light processing (DLP) both are using UV light to initiate polymerization. For two photon polymerization (2PP) a NIR laser is used enabling 3D printing with extremely high resolution (~ 50 nm)[99].

However, for SLA and DLP there are issues with accuracy and surface finish of the printed parts.[100] They typically require post-processing techniques such as removal of unreacted monomer mixture inside cavities or voids. In some cases, post-curing is required in order to reach maximum strength and stability.[101] The feature size for DLP (few tens of microns) is determined by the x-y resolution of the pixel and for SLA by the area of the laser beam combined with the speed at which the laser is moving.[102,103] However, another flourishing technology enables 3D printing with outstanding resolution and feature size in the sub-micrometer range.[99] 2PP is using a focused NIR laser beam, which is scanned in a 3D pattern through a photoresist. Instead of pixels, 2PP enables the 3D printing of volumetric pixels (voxels).[104] This technology is especially advantageous for biological applications, since cellular absorbers of native tissue (water, melanin, hemoglobin) are relatively transparent to the applied NIR light in comparison with tissue absorption in the visible spectrum.[105]

Two-Photon Polymerization

Two-Photon Polymerization (2PP) is a multiphoton lithography process with widespread applications such as optical data storage,[106] photonic crystals,[107] waveguides,[108] micro needles,[109] microfluidics,[110-112] and 3D cell matrices.[113-119] Due to high tissue penetration of the applied NIR light, 2PP is especially suitable for biological applications.[105] 2PP enables the microfabrication of complex tissue scaffolds with amongst the highest resolution of all AMTs, including feature sizes of down to 50 nm.[99] The major difference to above mentioned approaches (Laser-SLA, DLP-SLA), which are based on single-photon absorption, is the principle of multiphoton absorption (Figure 8, a). In particular, the excitation of PIs cannot only occur via absorption of one photon but also

Die approbierte gedruckte Originalversion dieser Dissertation ist an der TU Wien Bibliothek verfügbar.
The approved original version of this doctoral thesis is available in print at TU Wien Bibliothek.
TU Bibliothek Your knowledge hub WIEN

via the simultaneous absorption of two photons. This was already described by Maria Göppert-Mayer in 1931.[120]

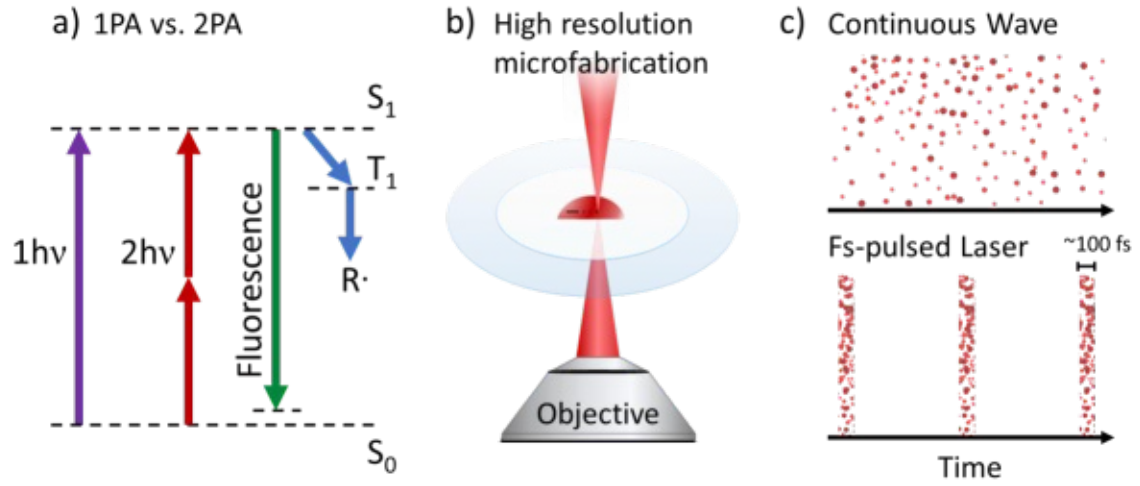

Figure 8: The excitation of a photoinitiator molecule from the ground- (S_0) to the excited singlet state (S_1) can occur via the absorption of one- (1PA) and two photons (2PA, a). The required high photon density is achieved by the spatial compression of photons within the focal area of a NIR-laser (b) and by the temporal compression of photons using a fs-pulsed laser beam (c).

Up until her death, she was not able to proof her theoretical calculations in the laboratory. However, with the development of solid-state femtosecond (fs) lasers (titanium:sapphire crystal) the proposed mechanism could be demonstrated.[121] In contrast to continuous wave lasers, providing a continuous photon-flux over time, pulsed lasers generate ultrashort pulses supplying an extremely high density of photons in extraordinary small timeframes ($100 \cdot 10^{-15}$ s, Figure 8, c). This advantage can be used to increase the photon density at the focal area, therefore increasing the chance for two-photon absorption (2PA) to occur. The fundamental principle of 2PP is based on the non-linear absorption of light. Particularly, the transition probability for the absorption of two photons is proportional to the square of the intensity of the laser pulse,[122] in contrast to one-photon absorption, which follows Lambert-Beer law.[123] Since the absorption only occurs in the focal volume of the laser beam, where the intensity is high enough, the remaining medium is transparent to the applied NIR light. Upon excitation of a PI to the excited singlet state (S_1, Figure 8, a) several relaxation pathways are possible. Radicals, required for radical photopolymerization are commonly proposed to be generated upon intersystem-crossing to an excited triplet state (T_1).[70,124] In contrast to fluorescent dyes, where high fluorescence yields are desired, here the generation of radicals is crucial for polymerization. It is proposed that two photons with half the energy (or twice the wavelength, IR light) can excite electrons in the same way as one photon with double the energy (or half the wavelength, UV light).[125] The immense photon density required in order to induce 2PP is achieved by the spatial compression of photons within the focal volume (voxel) of the pulsed laser beam (Figure 8, b). A practical 2PP-setup was developed, enabling extremely high structuring velocities of up to 1000 $mm \cdot s^{-1}$ and shorter processing times compared to state-of-the-art systems.[126,127] The fs-pulsed laser beam is generated within a chamber

Die approbierte gedruckte Originalversion dieser Dissertation ist an der TU Wien Bibliothek verfügbar.
The approved original version of this doctoral thesis is available in print at TU Wien Bibliothek.
TU Bibliothek Your knowledge hub WIEN

containing a mode-locked Ti:sapphire cavity. The beam is then guided towards waveplate (WP), beam splitter (BS) and acousto-optic modulator (AOM), responsible for laser power adjustment and diffraction (Figure 9). The pinhole is blocking the zeroth order of the beam and the first order beam is guided through a beam expander (BE) to the galvanometer scanner (GS), where the scanning in x- and y- direction is realized. A lens-system is focusing the beam onto the back-focal plane of the objective, where it is focused in the photoreactive monomer mixture. The vertical movement (z-axis) of the focal area is controlled by a motorized stage.

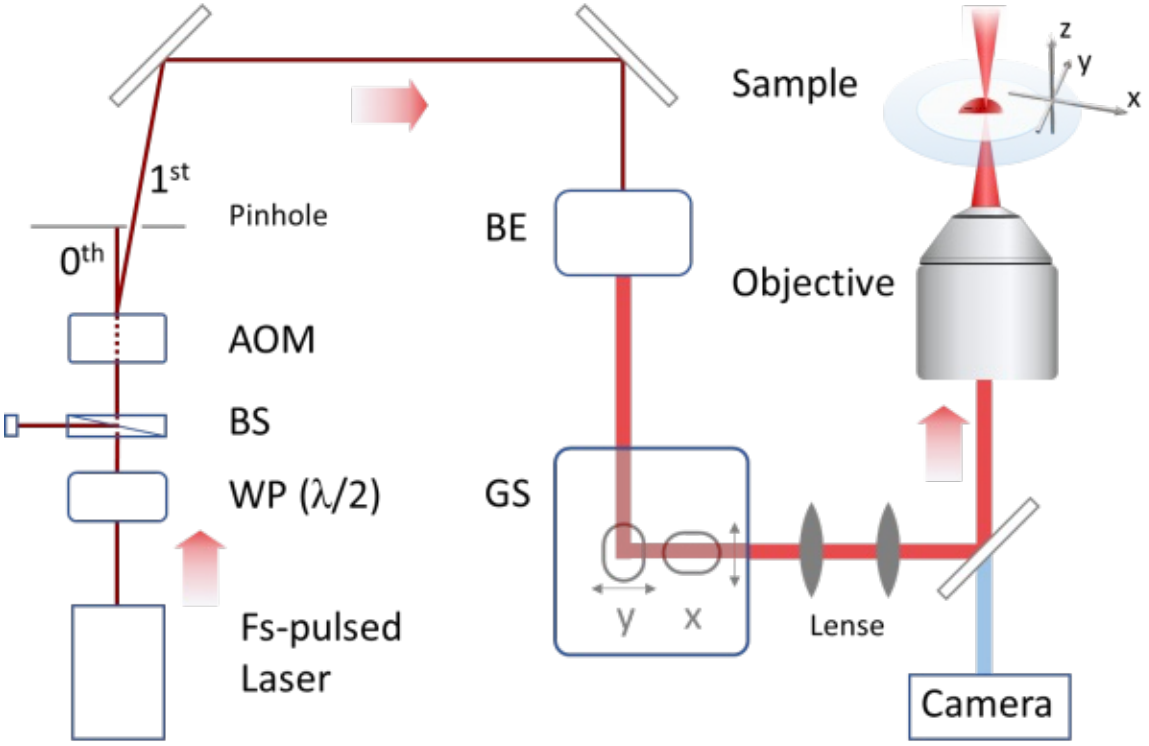

Figure 9: For Two-Photon Polymerization, a tunable femtosecond-(fs) pulsed laser beam is generated in a titanium-doped sapphire crystal. The maximum power of the laser beam is adjusted via a waveplate (WP), responsible for polarization and a beam splitter (BS), separating s- from p-polarized light. The acousto-optic modulator (AOM) is shifting the frequency of the wave and generates diffraction patterns of several orders. The 1st order laser beam is extracted by a pinhole, while a shutter is controlling the exposure time. The beam is guided to the beam expander (BE) and the galvanometer scanner (GS), where it is directed along the x- and y-axis. Mirrors and lenses are projecting the beam onto the back focal plane of a microscope objective, creating the desired object inside the sample. A motorized x-y stage and a z-movable stage are supporting the printing process.[126,127]

The extraordinary high light intensities within the focal area, combined with the small voxel size in the nanometer range enable high-resolution 3D fabrication of photoreactive monomer mixtures. Besides the pulsed character of the laser, providing the required photon density, fs-lasers offer high degree of tunability in the range of 690 nm – 1040 nm. Depending on the absorbent, the precursor formulation can be selectively irradiated with the desired wavelength. Not only, the invention of pulsed lasers was a breakthrough for this technology, but also the development of highly efficient two-photon initiators.

Die approbierte gedruckte Originalversion dieser Dissertation ist an der TU Wien Bibliothek verfügbar.
The approved original version of this doctoral thesis is available in print at TU Wien Bibliothek.
TU Bibliothek Your knowledge hub WIEN

Two-Photon Initiators

Two-photon initiators (2PIs) are photoactive molecules capable of entering excited states by absorption of two photons with lower energy (longer wavelength) compared to single photons with higher energy (shorter wavelength).[125] The most significant characteristic of 2PIs is their excellent photophysical and -chemical activity being excited by low-energy NIR irradiation, especially suitable for biological applications, where low tissue damage is favored. 2PIs must exhibit strong absorbance at the applied wavelength as well as high quantum efficiency in generating reactive radicals, necessary for radical photo polymerization. The capability of absorbing two photons simultaneously at a given wavelength is quantified using the 2PA cross-section (σ_{2PA}), given in the unit Göppert-Mayer (1 GM = 10^{-50} cm^4 s $photon^{-1}$ $molecule^{-1}$). 2PA heavily depends on how the energy of the ground- and excited state is defined, which is characterized by the structural moieties of the 2PI. The nonlinear optical properties of two-photon active fluorophores was already investigated for optical polarization storage technology[128,129] as well as for bioimaging.[130,131] Major findings were made in the molecular design of 2PIs with increased σ_{2PA}.[132] Key elements proposed are an extended π-conjugation, sufficient co-planarity, intramolecular charge transfer and mesomeric dipole moments.[103] Dipolar-, quadrupolar-, octupolar- and more generally multipolar push-pull-systems with various electron-donating or electron-withdrawing groups are promoting factors for high σ_{2PA}.[125,133] However, this characteristic value alone does not guarantee the generation of reactive radicals, since the energy can dissipate via various other competing pathways (fluorescence, thermal relaxation, isomerization, back electron transfer).[134,135] Principally, there are numerous available photoactive molecules, but here the class of 2PIs is divided into categories with particularly different mechanistic pathways: [136,137] on the one hand 2PIs, known as sensitizers and on the other hand, 2PIs following photodissociation mechanisms (e.g. cleavage, Figure 10).

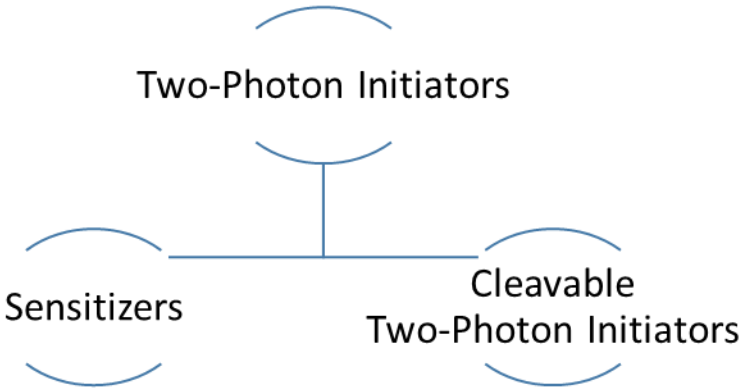

Figure 10: Here, two-photon initiators (2PIs) are divided into two major classes: sensitizers and cleavable 2PIs.

Commonly, sensitizers are following a bimolecular mechanism promoted by a photoinduced electron- or energy transfer from the two-photon excited sensitizer to another molecule.[136] Cleavable 2PIs are promoted homolytic bond cleavage upon photoexcitation, a mechanism very

Die approbierte gedruckte Originalversion dieser Dissertation ist an der TU Wien Bibliothek verfügbar.
The approved original version of this doctoral thesis is available in print at TU Wien Bibliothek.
TU Bibliothek Your knowledge hub WIEN

well-known from UV photopolymerization. Generally, molecules following a bimolecular mechanism (sensitizers) tend to lengthen the overall timescale of photoinitiation, resulting in potential delayed structuring efficiency.[136] By the introduction of photolabile groups, short-lived triplet states are generated favorable for the generation of reactive radicals (see also Figure 8). Usually, homolytic bond dissociation requires electronic localization at the cleavable bond, engaging the photodissociation character of the bond.[136] A broad range of photolabile moieties have been introduced in literature, most prominent examples being o-nitrobenzyl esters[138,139] and oxime esters.[140,141] Still, these tunable materials additionally need to show increased 2PA. UV-PIs usually suffer from low σ_{2PA}, owing to the relatively small conjugated π-systems, additionally leading to low structuring performance during 2PP.[142] Extremely high laser power and low writing speed (prolonged exposure time) are required in order to compensate the inefficiency of these molecules. Additionally, harsh exposure conditions could possibly lead to severe tissue damage.[143] One common approach to synthesize 2PIs includes the association of a π-conjugated chromophore (increased σ_{2PA}) with state-of-the-art PIs used for UV photopolymerization. Over the last two decades, a very large spectrum of 2PIs was developed, including α-β-unsaturated ketones,[144] coumarins,[145] thioxanthones,[146] 1,3-diketones,[147] triazines,[148] acyl-phosphine oxides,[149] carbazole,[150] anthraquinone-[151] and anthracene derivatives.[152] A selection of commonly used 2PIs is given hereafter (Figure 11).

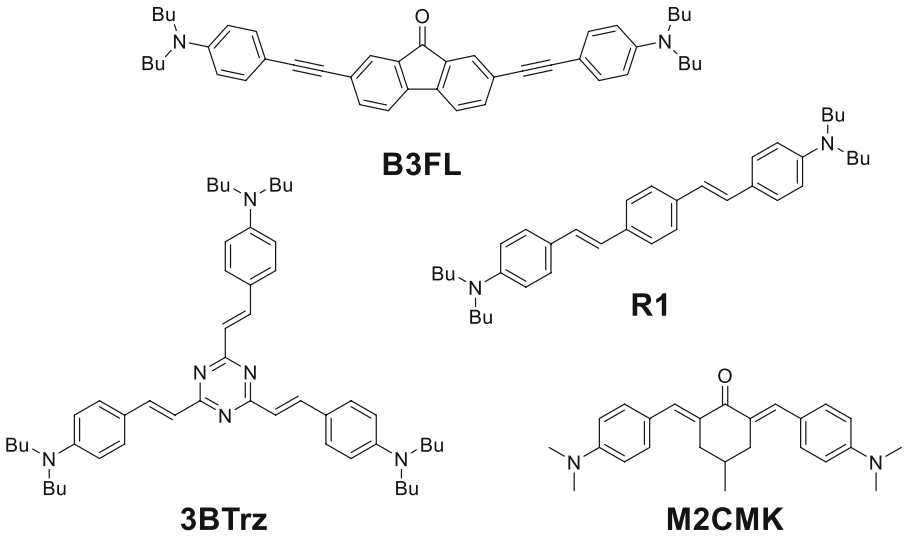

Figure 11: Examples of organo-soluble two-photon initiators, including their characteristic absorption maxima (1PA). B3FL[114] λ_{max}^{1PA} = 396 nm, R1 λ_{max}^{1PA} = 428 nm, 3BTrz[148] λ_{max}^{1PA} = 434 nm and M2CMK[144,153] λ_{max}^{1PA} = 432 nm.

For the microfabrication of hydrogels, water-solubility is of crucial importance. At first, commercially available hydrophilic fluorescent dyes were used to ensure solubility in aqueous systems. Chromophores, which are usually used in biological microscopy (Eosin Y, Rose Bengal, Rhodamine B) were tested as 2PI sensitizers.[154] However, due to their possible cellular uptake and potential generation of radical induced oxygen species (ROS) within the cell, cytotoxicity becomes an issue.[155] The generation of ROS upon photoexcited species is very well known, however this photoinduced oxidation process is only desired, where targeted apoptosis or necrosis is

Die approbierte gedruckte Originalversion dieser Dissertation ist an der TU Wien Bibliothek verfügbar.
The approved original version of this doctoral thesis is available in print at TU Wien Bibliothek.
TU Bibliothek Your knowledge hub WIEN

desired.[156-158] Unless, specifically engineered to target cancer cells (photodynamic therapy, PDT), cytotoxicity of 2PIs needs to be strictly avoided, especially when applied for the fabrication of hydrogel scaffolds in the presence of cells. Photodamage is usually restricted to the near vicinity of the sensitizer due to the limited diffusional range of $^1O_2$.[157] Still, phototoxic effects in surrounding media can occur via the generation of secondary ROS initially generated from $^1O_2$.[159] The control of light exposure might be the most effective strategy to limit phototoxicity although there are many factors determining phototoxicity (excitation wavelength, -intensity, -duration, 2PI concentration and -localization, cell type and -medium).[160] Due to the applied IR light, reduced photodamage is proposed to be a principal benefit of 2PP. Although, the overall exposure is reduced compared to one-photon excitation, severe photodamage can occur in the focal volume.[161,162] Therefore, a new generation of water-soluble 2PIs were introduced, showing improved cell-compatibility and high processability in the same time (DAS, P2CK, Figure 12).

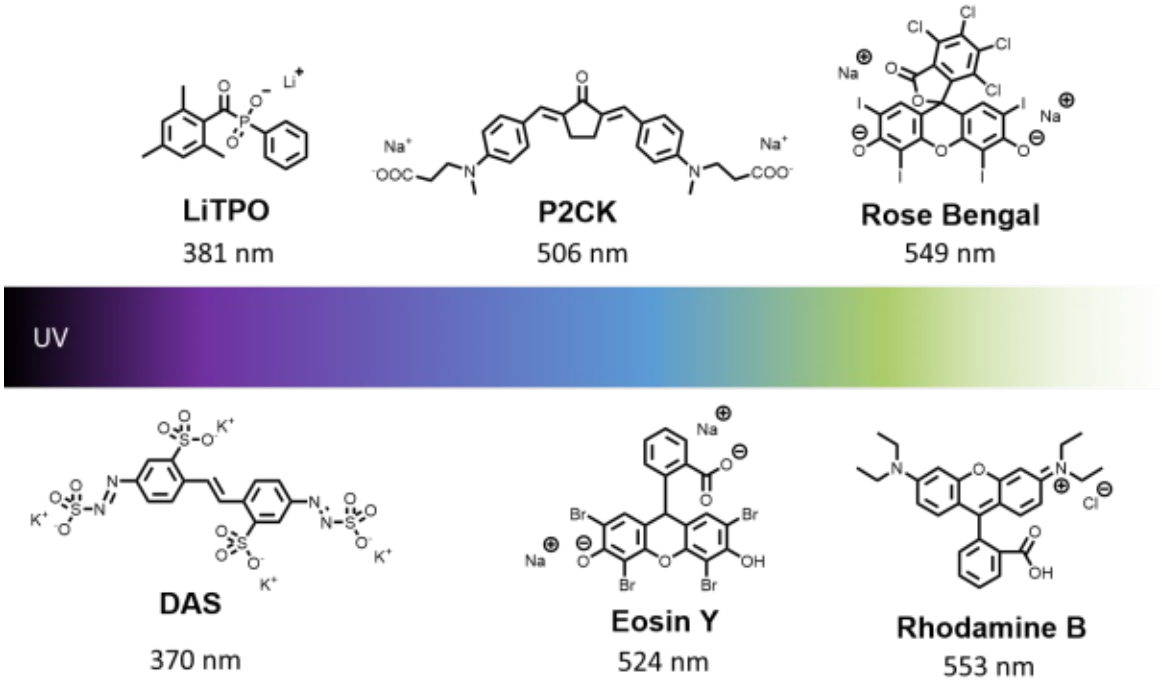

Figure 12: Examples of water-soluble chromophores used for photopolymerization and their characteristic λ_{max}^{1PA}. LiTPO is mentioned as a reference on the one side of the electromagnetic spectrum, since it is the most commonly used photoinitiator for UV-cell encapsulation.[163] On the other end of the spectrum, classical water-soluble 2PIs are given (DAS,[164] P2CK,[165] Eosin Y,[166] Rhodamine B[167]).

Cytotoxicity is not only determined by photoinduced processes, driven by the laser power and -exposure time and photothermal damage, but also by the dark toxicity of the 2PI. Reducing the concentration of 2PIs is an easy and straightforward approach to reduce dark-toxicity. Hence, high σ_{2PA} is required even at extremely low concentrations, still ensuring efficient two-photon-induced polymerization.

The success of TE is regulated by a combination of choosing suitable compounds for the construction of biocompatible hydrogel materials, as well as the sensitive adaption of factors determining cell-survival. With a growing understanding on the existing biomaterials, research is

Die approbierte gedruckte Originalversion dieser Dissertation ist an der TU Wien Bibliothek verfügbar.
The approved original version of this doctoral thesis is available in print at TU Wien Bibliothek.
TU Bibliothek Your knowledge hub WIEN

continuing to engineer tailor-made polymers for biomedical applications. In contrast to the bioinert synthetic polymers introduced in the early 20th century, now a new generation of smart materials are available, leading to the coherent integration of biomaterials into the human body. Ongoing collaborative research between chemists, biologists, physicists, and physicians is continuing to lead to more and more economical and ecological solutions.

Die approbierte gedruckte Originalversion dieser Dissertation ist an der TU Wien Bibliothek verfügbar.
The approved original version of this doctoral thesis is available in print at TU Wien Bibliothek.
TU Bibliothek Your knowledge hub WIEN

Die approbierte gedruckte Originalversion dieser Dissertation ist an der TU Wien Bibliothek verfügbar.
The approved original version of this doctoral thesis is available in print at TU Wien Bibliothek.

Objective

Tissue engineering (TE) is an established field within the medical sector, aiming to create, regenerate and replace native tissue for the human body.[62] 3D cell culture matrices are of great importance for TE, since they excellently mimic entities of endogenous tissue. Hydrogel scaffolds with extraordinarily high resolution can be fabricated via a rapidly growing technology referred to as two-photon polymerization (2PP). At the same time, the applied low-energy NIR light, is capable of initiating polymerization inside a matrix with reduced photodamage of tissue and cells. Amongst the multiple factors, determining the successful application of materials in TE (scaffolds, cells, signaling molecules, processing parameters, biocompatibility, biodegradability and bioactivity of the final polymeric network) there are two major classes of compounds, which will be especially considered in this work. On the one hand, macromers required to build polymeric networks and on the other hand, two-photon initiators (2PIs) required for the absorption of the applied irradiation energy and for initiating polymerization.

Although outstanding progress has been made, currently available 2PIs are exhibiting limitations to a certain extent. Most 2PIs are prone to sensitize molecules within the matrix, creating reactive oxygen species, eventually harming surrounding tissue. Furthermore, relatively long-lived triplet state occupation of excited electrons potentially leads to loss of energy (through non-radiative decay, fluorescence, or phosphorescence) and consequently leading to reduced radical-generation-rate. Although sensitizers can induce tissue damage, they still exhibit extraordinarily high two-photon absorption cross-section (σ_{2PA}), favorable for efficient structuring processes. Two different approaches are proposed to increase 2PI structuring efficiency. Additionally, despite of the tedious molecular engineering of the current state-of-the-art 2PIs, their low water-solubility leads to an intrinsic barrier for further biological applications. Therefore, strategies are proposed, to enhance their solubility in aqueous systems.

A major aim of this thesis is the association of π-conjugated chromophores (driving σ_{2PA} properties) with covalently coupled photolabile groups. For this, two different approaches should be followed, combining the concept of photosensitization with photolability.

First, oxime ester (OE) moieties should be introduced into a two-photon active chromophore, since OEs tend to decompose upon irradiation.[168] The proposed dissipation of the excitation-energy, promoted by N-O bond cleavage combined with the kinetic driving force of decarboxylation, is hypothesized to increase radical-generation-rate. The OE-moiety should be covalently coupled to a well-established benzylidene cycloketone chromophore, known for its high σ_{2PA}. Multiple OE-derivatives should be synthesized, by the introduction of different coupling agents, hence adjusting the electronic structure of the final 2PIs. Furthermore, ionizable substituents should be introduced to increase hydrophilicity and water-solubility of resulting OE-2PIs.

Die approbierte gedruckte Originalversion dieser Dissertation ist an der TU Wien Bibliothek verfügbar.
The approved original version of this doctoral thesis is available in print at TU Wien Bibliothek.
TU Bibliothek Your knowledge hub WIEN

Second, photolabile azo-sulfonate (AS) moieties should be incorporated, since terminal AS groups tend to decompose upon photoexcitation. Similar to the concept above, the kinetic driving force of the generation of gaseous nitrogen is hypothesized to create photolabile AS-2PIs. For this, a commercially available azo dye should be chosen to serve as two-photon active chromophore. A suitable hydrophilic compound with the respective functional groups is proposed to extend the portfolio of water-soluble 2PIs, exhibiting strong absorbance above 400 nm.

Both synthesized 2PIs (OE, AS) should be tested in well-established hydrogel materials (gelatin methacrylate) using 2PP. In a final step, biocompatible macromers based on naturally occurring polysaccharides should be synthesized. Hyaluronic acid (HA) should be used as model compound and reactive vinyl ester (VE) groups should be introduced to the polymer backbone (HAVE). Macromer length and crosslinking density are adjusted accordingly and are hypothesized to determine characteristic hydrogel network parameters (swelling ratio, mass loss profiles). Moreover, HAVE should be investigated as biocompatible hydrogel macromer for direct 3D cell-encapsulation via 2PP.

Die approbierte gedruckte Originalversion dieser Dissertation ist an der TU Wien Bibliothek verfügbar.
The approved original version of this doctoral thesis is available in print at TU Wien Bibliothek.
TU Bibliothek Your knowledge hub WIEN

General Part

1 Two-Photon Initiators based on Oxime Esters

1.1 State-of-the-Art Oxime Esters

Oxime esters (OEs), also referred to as O-substituted oximes have been widely explored in the last decades.[169] On the one hand, OEs were used as starting materials for the synthesis of amines, amides, nitriles and heterocycles such as pyrrole-, pyridine- and quinoline derivatives. On the other hand, OE-functionalities were coupled to various bioactive molecules enabling studies on their specific pharmacological importance (anti-bacterial,[170] -fungal,[171,172] -inflammatory, -oxidant,[173] and insecticidal activity, Figure 13).[171,174-178170]

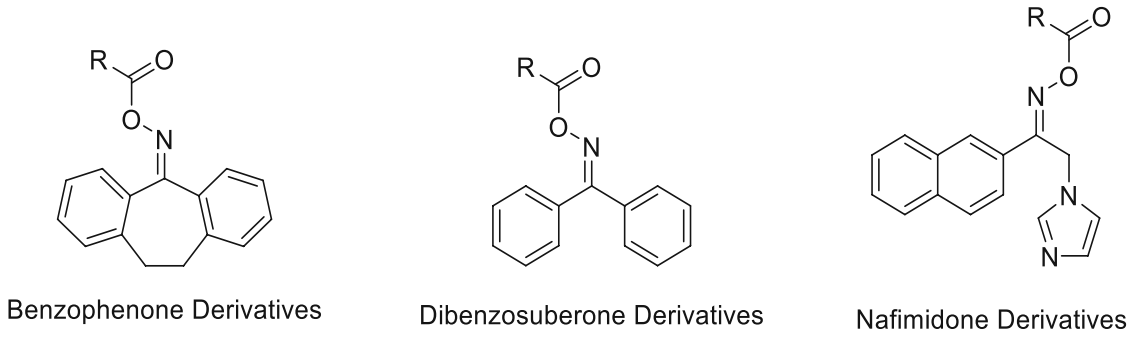

Figure 13: Benzophenone- and dibenzosuberone derivatives were developed in order to selectively interact with neurotransmitter[174] and nafimidone derivatives were studied for their applications as antiepileptic drugs.[175]

Besides the importance of OE-in medicine, their photoactive behavior was soon reported.[179] Compounds that damage DNA upon irradiation, known as photo nucleases have been increasingly interesting for photodynamic therapy (PDT). This field was further opened via the investigation of quinoline derivatives on their nucleolytic activity without mentioning OE-cleaving mechanism in detail.[180] Photocleavable hydrogels in general are an innovative class of recently developed functional materials.[181] After all, Barton esters were already introduced in the 80ies with the aim to promote radical chemistry.[182] The cleaving mechanism was well established, which is occurring via two main pathways. Cleavage is either introduced via a radical starter, directed by the driving force of stable Sn-S bond formation, or via direct photolytic- or thermal trigger. All mechanisms result in a N-O cleavage process, followed by a fast entropy-driven decarboxylation mechanism (Scheme 4).[183-186]

Die approbierte gedruckte Originalversion dieser Dissertation ist an der TU Wien Bibliothek verfügbar.
The approved original version of this doctoral thesis is available in print at TU Wien Bibliothek.

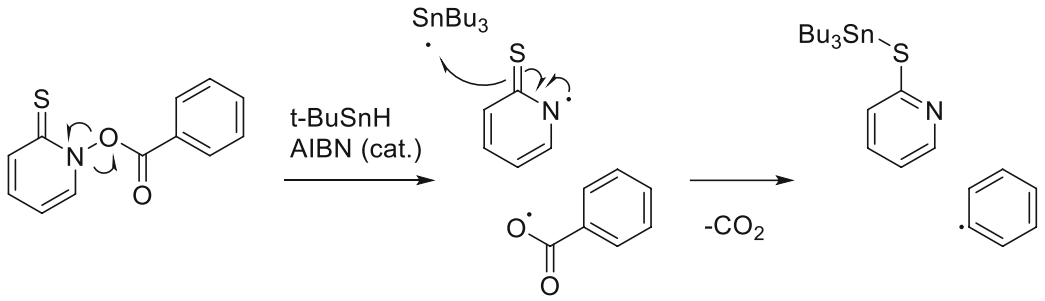

Scheme 4: Mechanism of Barton decarboxylation. Cleavage of a Barton ester can be promoted by a radical starter (AIBN) resulting in a stable Sn-S bond formation. Cleavage can be initiated by temperature or light.[187]

Promoted by the structural similarity to Barton esters, the cleaving mechanism of OEs is comparable.[188,189] In general, iminyl radicals are an important class of nitrogen-centered radicals readily available from various oxime derivatives. Upon external stimuli (UV irradiation, thermolysis, transition-metal catalysis, oxidants) the labile N-O bond cleaves. Subsequently, the driving force of decarboxylation leads to the generation of reactive radicals (Scheme 5).

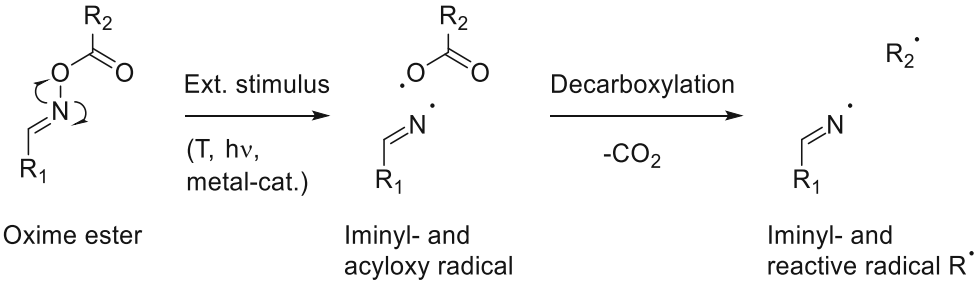

Scheme 5: Cleavage mechanism of OE derivatives into iminyl- and acyloxy radicals. Subsequent decarboxylation leads to the formation of reactive radicals available for radical polymerization.

Besides the importance of OEs in the medicinal field, we were interested in applying OE derivatives in 2PP. Various studies have been performed on the photochemical and -physical behavior of OEs. The photoinduced decomposition of some O-acyl oximino ketones was already studied at the end of the last century.[190] Furthermore, O-acyl oximes have been investigated as photobase generators, claiming insensitivity to oxygen inhibition compared to photoradical-generators.[191] Various spectroscopic methods (fluorescence quantum yield, steady-state photolysis, electron spin resonance-spin trapping) were used in order to proof photophysical and -chemical properties of coumarin-OE derivatives.[192] Photolysis of aldoxime esters was presented in the presence of the sensitizer methoxyacetophenone in the early 2000s.[193] Furthermore, OE derivatives and their reactivities were investigated in the presence of benzophenone sensitizers and compared to monomolecular Type I PIs (Darocur 1173).[194] Subsequent studies were performed, comparing OEs of typical bimolecular systems with sensitizers covalently coupled to OE functionalities.[168] Laser flash photolysis and photochemically induced dynamic nuclear polarization (CIDNP) experiments resulted in a deeper understanding on OEs initiation mechanisms. In particular, it was shown that radical initiation mechanisms proceed via a triplet energy transfer from the sensitizer, followed by a cleavage of the labile oxime N-O bond.[140] The formed carboxylate radicals are transforming

Die approbierte gedruckte Originalversion dieser Dissertation ist an der TU Wien Bibliothek verfügbar.
The approved original version of this doctoral thesis is available in print at TU Wien Bibliothek.
TU Bibliothek Your knowledge hub WIEN

into carbon-centered radicals upon decarboxylation, inducing polymerization. However, it was shown that the formed iminyl radicals do not contribute to the initiation process at the observed time scale. Still, cis–trans isomerization at the C=N double bond was observed in CIDNP experiments. A deeper understanding on photoinduced reaction pathways of oxime esters was reported lately.[195] Here, the wavelength-dependent initiation behavior was studied in the presence of a monomer by applying density functional theory calculations together with pulsed laser polymerization and size exclusion chromatography – electrospray ionization mass spectrometry. Contrary to the expectations, highest monomer-conversion was found at a wavelength, far off the 1PA absorption maximum of the PIs. Potential explanations were mentioned, such as a limited penetration depth of the incident light as a consequence of the high molar extinction coefficient at the absorption maximum, causing radical formation only at the outermost layer of the formulation. Although this hypothesis could not be proven, another radical formation pathway was suggested involving conical intersections between electronic states of the PIs.[196] Recently, OEs and their application in 2PP was first reported.[197] Also, carbazole-based 2PA modules associated with photocleavable OEs were introduced for multiphoton stereolithography (Figure 14).[136]

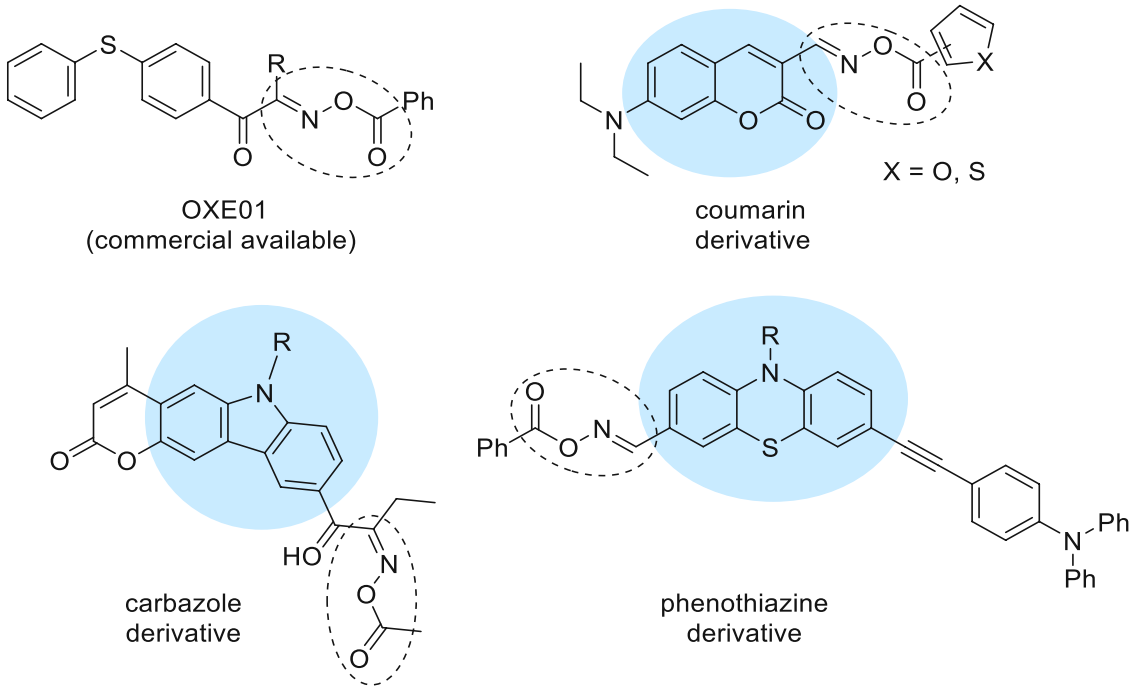

Figure 14 Overview on state-of-the-art OEs applied in photopolymerization. A deeper understanding on the cleaving mechanism of commercially available OXE01 was presented in literature [195] and various OE derivatives based on phenothiazine[198], carbazole[136] and coumarin[192] were introduced.

Furthermore, phenothiazine-substituted OEs were studied in literature and tested as free radical photoinitiators under visible light conditions.[198] In a previous study, they reported the incorporation of carbazole, phenothiazine and triphenyl-amine groups serving as electron donors for photosensitizer moieties. Ground state absorption and fluorescence spectra revealed knowledge on the π-π* transitions character of O-acyloximes.[199] Moreover, various patents on OE

Die approbierte gedruckte Originalversion dieser Dissertation ist an der TU Wien Bibliothek verfügbar.
The approved original version of this doctoral thesis is available in print at TU Wien Bibliothek.

PIs were published.[200-206] The application of OEs in microelectronics via photolithography and the photopolymerization kinetics of OE PIs was reported in the beginning of the previous decade.[207,208] Especially, the dissociation of OEs under visible light irradiation was reported.[209]

The studies reviewed here support the hypothesis that OEs serve as adequate compounds for the development of novel 2PIs. Besides being an important intermediate in organic chemistry, OEs can promote various photodriven reactions. The fast homolytic cleavage of these moieties should be examined for the application in 2PP.

1.2 Synthesis of Oxime Ester-based Two-Photon Initiators

1.2.1 Preliminary Investigation on a Bimolecular System

The type of sensitizer is crucial for the development of novel 2PIs. The absorption profile of 2PIs determines structuring efficiency during 2PP. Besides the previously introduced chromophores based on coumarin, carbazole, quinoline and phenothiazines, linear and cyclic benzylidene ketone-based 2PIs were introduced in the last years.[144] In general, 2PIs with long conjugation length and strong donor- and acceptor groups are of great interest when high initiation efficiency and quantum yields are required. Previous studies established classical aldol condensations as powerful tool to couple commercially available cycloketones with N-substituted benzaldehydes.[153] Via this method, several linear and cyclic benzylidene ketone-based 2PIs with dialkylamino groups were synthesized, instead of going along the expensive metal-catalyzed synthesis routes, such as Wittig, Horner-Wadsworth-Emmons, Heck and Sonogashira Coupling.[210-213] Due to the promising performance of cycloketones (high 2PA-cross section, broad processing window, high quantum yield for reactive radicals) these compounds were chosen to serve as central sensitizers for 2PIs developed within this thesis. The significant improved solubility of 4-methylcyclohexanone electron acceptors compared to cyclohexanone-based compounds, guided the synthesis strategy towards the derivatization of well-established 2,6-bis(4-(dimethylamino)benzylidene)-4-methylcyclohexanone (M2CMK, Figure 15).

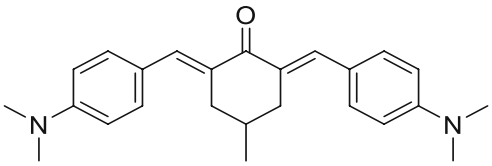

M2CMK

Figure 15: State-of-the-art organo-soluble 2PI (M2CMK).[153]

In this thesis, a thorough study was performed to examine the performance-relationship between oxime ester (OE) moieties and literature-known sensitizer (M2CMK). The performance during 2PP should be examined for formulations containing various molar ratios of sensitizer (M2CMK) and OE as co-initiator.

Die approbierte gedruckte Originalversion dieser Dissertation ist an der TU Wien Bibliothek verfügbar.
The approved original version of this doctoral thesis is available in print at TU Wien Bibliothek.
TU Bibliothek Your knowledge hub WIEN

1.2.1.1 Synthesis

First, reference sensitizer (M2CMK) was synthesized according to literature.[153] Finely powdered sodium hydroxide was dissolved in minimal amount of EtOH and added dropwise to a solution of 4-methylcyclohexanone (MCK) in EtOH. Subsequently, dimethylamino benzaldehyde (DMBA) was dissolved in EtOH and slowly added to the reaction solution. After stirring under reflux, the solvent was reduced by half. The residual dark red mixture was dissolved in chloroform and extracted with NH_4Cl solution. Recrystallization from diethyl ether yielded in pure orange product in high yields (56% th., Scheme 6).

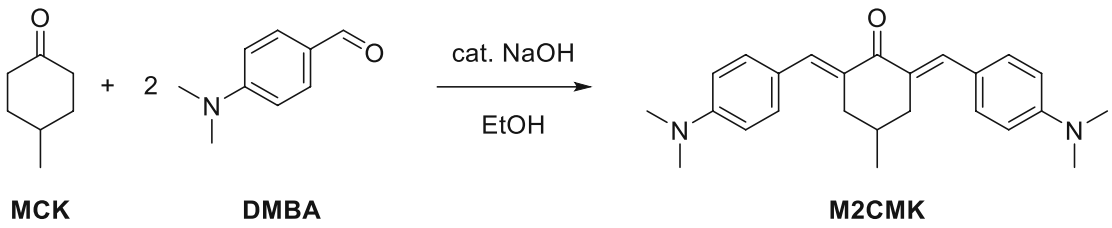

Scheme 6: Synthesis of state-of-the-art reference sensitizer (M2CMK).[153]

1.2.1.2 Testing

Formulations based on an acrylic monomer mixture (equimolar mixture of trimethylolpropane triacrylate (TTA) and ethoxylated trimethylolpropane triacrylate (ETA)) were prepared containing various molar ratios of sensitizer (M2CMK, 0.5-0.05 mM, Table 1) and co-initiator (BABO, 0.5-1.0 mM, Table 1). Furthermore, reference-formulations were prepared containing solely sensitizer and co-initiator to investigate monomer mixture-reactivity without the influence of either co-initiator or sensitizer. The co-initiator molecule benzaldehyde O-benzoyl oxime (BABO) was available from previous studies (Figure 16).[214]

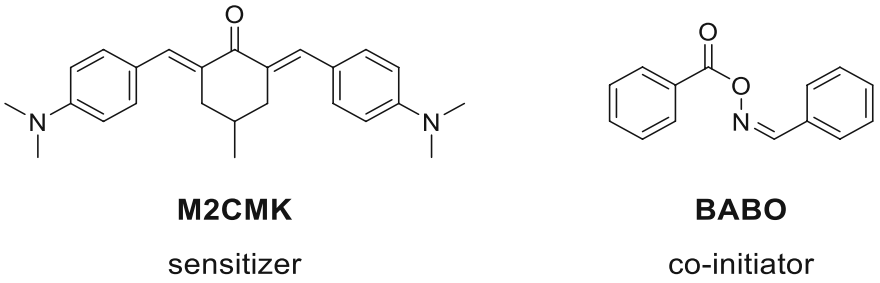

Figure 16: State-of-the-art sensitizer (M2CMK) and oxime ester co-initiator (BABO) were used in order to investigate reactivity of acrylic monomer mixtures (ETA:TTA) containing various molar concentrations of either compound.

Different experiments were performed, where the type of 3D printed object (single lines, Atomium, TU Wien Logo) was varied accordingly. First a thorough study on a broad range of concentrations was performed starting from a concentration of 0.5 mM M2CMK, commonly used for 2PIs. The sensitizer concentration was kept constant, whereas the co-initiator concentration was varied respectively (0.05 mM - 0.5 mM, Table 1). Two control formulations were prepared, where solely co-initiator (control 1) or sensitizer (control 2) was added to the acrylic monomer

Die approbierte gedruckte Originalversion dieser Dissertation ist an der TU Wien Bibliothek verfügbar.
The approved original version of this doctoral thesis is available in print at TU Wien Bibliothek.
TU Bibliothek Your knowledge hub WIEN

mixture. To investigate the limit of polymerization in further detail, additional formulations were prepared with reduced M2CMK concentration (0.1 mM). Selected formulations were structured using CAD files based on TU Wien Logos (Table 1, right). Since the long-term target of this study was the covalent coupling of co-initiator moieties to a sensitizer, and the attachment of OE moieties would in any case lead to an over-stoichiometric ratio of OE compared to sensitizer, under-stoichiometric ratios were not studied here.

Table 1: Overview on molar ratios between BABO and M2CMK and final concentrations (mM) for formulations in an equimolar acrylic monomer mixture (ETA:TTA).

	Single Line		Atomium		TU Wien Logo	
Molar ratio BABO:M2CMK	**BABO [mM]**	**M2CMK [mM]**	**BABO [mM]**	**M2CMK [mM]**	**BABO [mM]**	**M2CMK [mM]**
Control 1	0.50	-	0.50	-	1.00	-
Control 2	-	0.50	-	0.50	-	0.10
10:1	0.50	0.05	0.50	0.05	1.00	0.10
5:1	0.50	0.10	0.50	0.10	n.a.	
2:1	0.50	0.25	0.50	0.25	n.a.	
1:1	0.50	0.50	0.50	0.50	0.10	0.10

The polymerization threshold (P_{th}) was determined for each formulation. P_{th} is defined as the threshold power required to generate stable 3D structures.[215] In general, the tendency for complex 3D structures to collapse depends on the laser power and writing speed as a consequence of feature size.[216] These, amongst other factors guide the final mechanical strength of fabricated elements. Hence, different 3D structures were fabricated according to CAD-files to examine the P_{th} according to the composition of the formulation as well as type of CAD-model (Single-line, Atomium, TU Wien Logo, Figure 17). For clarification, the P_{th} of all formulations was assessed after post-processing. This chemical treatment is necessary to remove unreacted acrylic monomer mixture by rinsing the constructs with solvent (2-propanol). In general, post-processing techniques (chemical or thermal) can provide significant improvement in the spatial resolution of final printed constructs.[103] Besides post-processing techniques, structuring parameters, such as laser power, the layer spacing along z direction (dz), the line spacing in x-y direction (hatch) and writing speed are additional critical factors influencing microstructure-stability.[217] Within this study, the laser power was varied, keeping constant values for dz (0.4 µm), hatch (0.5 µm) and writing speed (100 mm s^{-1}).

Die approbierte gedruckte Originalversion dieser Dissertation ist an der TU Wien Bibliothek verfügbar.
The approved original version of this doctoral thesis is available in print at TU Wien Bibliothek.
TU Bibliothek Your knowledge hub WIEN

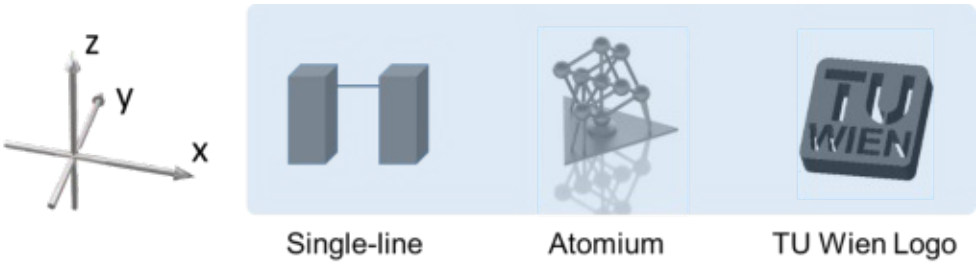

Figure 17: The polymerization threshold of acrylic monomer mixtures was determined according to CAD-files. Single lines between pillars (distance between pillars: 10 µm), Atomium (lateral length: 150 µm) and TU Wien Logo (100x100x100 µm).

A popular method to evaluate 2PA initiation efficiency of 2PIs is the single-line writing process, where parameters such as line width and laser power are used to quantify writing efficiency.[165] Generally, lines which are printed right next to previous printed lines are likely to stabilize each other resulting in a more stable final 3D construct and seemingly lower P_{th} e.g. as a consequence of oxygen depletion.[218] Instead of scanning the focus of the laser beam line-after-line, free hanging lines anchored between two pillars can be structured and used as sensitive measure to obtain P_{th} for each formulation. As soon as the first stable line is observed, whilst gradually increasing laser power, P_{th} is obtained. A schematic figure on how the P_{th} is obtained is depicted hereafter (Figure 18). Each pillar was printed with the same laser power (100 mW) only varying the laser power for single-lines along the y-axis. Furthermore, a constant writing speed for pillars and lines was maintained (100 mm s^{-1}). First, triplicates were structured (x-axis) varying laser power along the y-axis at increments of 10 mW. Secondly, triplicate single-lines were structured at increments of 2 mW for a detailed determination of the P_{th} (Figure 18). The P_{th} was defined to be the required laser power, where all three lines were stable.

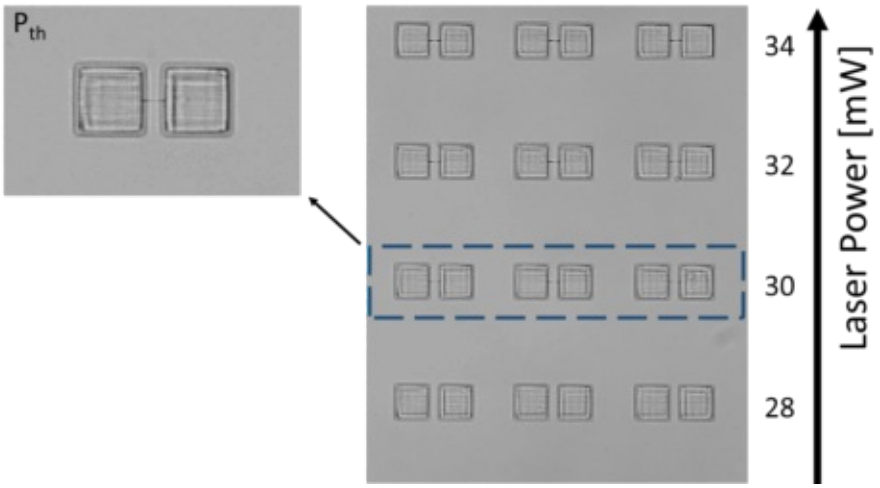

Figure 18: Determination of the polymerization threshold (P_{th}, dashed line) representing the laser power required where stable free hanging lines (triplicates) were structured between two pillars. A 2D-array is structured varying laser power along the y-axis at increments of 2 mW.

Die approbierte gedruckte Originalversion dieser Dissertation ist an der TU Wien Bibliothek verfügbar.
The approved original version of this doctoral thesis is available in print at TU Wien Bibliothek.

The laser was calibrated to two different wavelengths (Figure 19) in order to compare the structuring performance at 800 nm (commonly used for M2CMK) and the structuring performance at M2CMK's 2PA maximum (760 nm).[219]

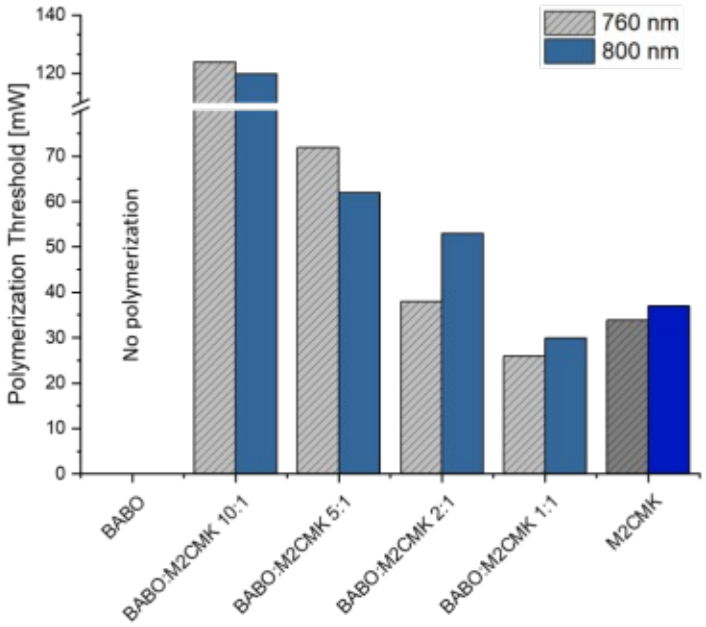

Figure 19: The polymerization threshold for each formulation was determined by structuring triplicates of single-lines in acrylic monomer mixtures (ETA:TTA). The structuring efficiency at two different wavelengths (760 and 800 nm) was investigated for formulations containing various molar ratios of BABO and M2CMK (10:1, 5:1, 2:1, 1:1) keeping a constant concentration of 0.5 mM M2CMK. Two reference formulations were prepared (BABO, M2CMK).

Overall, lowest P_{th} was obtained for formulations containing equimolar ratio of BABO and M2CMK (1:1). No polymerization was observed for control formulation 1 (BABO). Promising P_{th} was observed for control formulation 2 since M2CMK is known for its high 2PA at 760 nm.[219] Taking a closer look to the applied wavelength, lower P_{th} was observed for control formulation 2 at 760 nm compared to 800 nm (ΔP_{th} = 3 mW). This trend was additionally observed for formulations containing molar ratios of 1:1 and 2:1 (BABO:M2CMK). Interestingly, this tendency reversed (P_{th} at 760 nm > P_{th} at 800 nm) once the molar ratio of BABO was increased (5:1, 10:1). P_{th} values for all formulations are summarized in Table 7 (experimental part). The reversed trend might be caused by a shift of the absorption profile of the processed formulations, as soon as the concentration of BABO is varied. Since the overall formulation is a synergy of the 2PA of the individual matrix components (BABO, M2CMK, ETA, TTA), the local absorption maxima and consequently the probability of molecule excitation is proposed to be shifted when the concentration of the individual compounds are modified (1PA λ_{max}^{BABO} = 259 nm, 1PA λ_{max}^{M2CMK} = 432 nm, 2PA λ_{max}^{M2CMK} = 760 nm). Accordingly, 760 nm might be an effective irradiation wavelength for formulations based on (M2CMK) and BABO:M2CMK up to a 2:1 molar concentration. Further over-stoichiometric mixtures of BABO:M2CMK (5:1, 10:1) resulted in a loss of polymerization efficiency at 760 nm, leading to decreased P_{th} at 800 nm. Here, not only the

Die approbierte gedruckte Originalversion dieser Dissertation ist an der TU Wien Bibliothek verfügbar.
The approved original version of this doctoral thesis is available in print at TU Wien Bibliothek.
TU Bibliothek Your knowledge hub WIEN

wavelength, but also the molar ratio of the formulation plays a critical role for the polymerization efficiency. Excessive molar ratio of co-initiator seems to hinder radical polymerization. Since radical-quenching is a well-known limitation for radical polymerization,[74] and OEs tend to decompose upon irradiation, generating reactive radicals,[194] excessive amount of BABO (OE) might hinder the polymerization process due to recombination reactions.[220] However, there are multiple limiting factors determining the P_{th}, such as the applied laser parameters (wavelength, laser power, writing speed, layer spacing), as well as intrinsic limitations of the photoinitiation process (limited electron transfer between sensitizer and co-initiator or photoinduced back electron transfer, radical generation rate). Nevertheless, a more profound effect on P_{th} is proposed to be derived by the overall concentration of the sensitizer. Here, the molar ratio of co-initiator was increased by reducing the amount of sensitizer. Via this method, the limit of polymerization might have been reached, overruling the eventual beneficial effect of the co-initiator. Generally, the minimum concentration of sensitizer required for 2PP is ought to be determined before variation of single parameters and should be kept constant, while determining the effect of molar co-initiator concentrations.

Besides that the molar concentration of the matrix compounds, the type of microfabricated 3D structure majorly guides the fragility/collapse of manufactured parts (e.g. cumulative weight effects), not necessarily being a consequence of bad polymerization efficiency. Nevertheless, the observed trends of the reactivity of the acrylate-based formulation cannot be directly transferred to hydrogel systems, being a major part in this thesis. A thorough study on the origin of the P_{th} trends is necessary to fully understanding the observed process, which exceeded the scope of this thesis. Although, single-line writing is a powerful tool for a detailed investigation of the P_{th} of reactive monomer mixtures, the stability of complex 3D constructs might differ severely from the P_{th} observed via single-line writing. Decreased stability due to missing support-structures (or vice-versa) including cumulative weight effects can result in a collapse or layer-by-layer destabilization effects of 3D micro structures.[217] Therefore, the P_{th} of OE-based formulations was further investigated via the fabrication of complex 3D structures according to CAD-files (*Atomium*). Here, P_{th} was defined as the laser power required as soon as the first stable 3D structure was obtained. A depiction of collapsed and stable 3D structures can be found hereafter (Figure 20). To achieve consistent results, the wavelength was tuned according to M2CMK's absorption maximum (760 nm). Laser power was varied from 10 to 100 mW at increments of 10 mW along the x-axis keeping a constant writing speed of 100 mm s^{-1}.

Die approbierte gedruckte Originalversion dieser Dissertation ist an der TU Wien Bibliothek verfügbar.
The approved original version of this doctoral thesis is available in print at TU Wien Bibliothek.

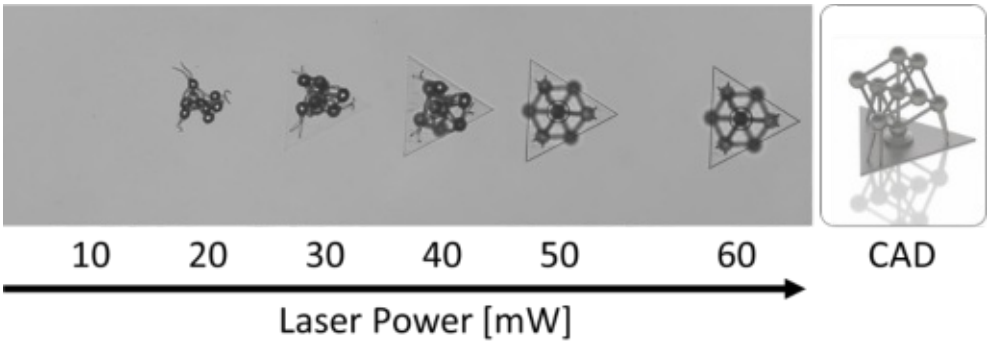

Figure 20: Microscope images of 3D structures (Atomium) fabricated with different laser powers (20-60 mW, Δ = 10 mW) in order to determine the polymerization threshold (50 mW for this case) (formulation: acrylic monomer mixture ETA:TTA containing 0.5 mM BABO and 0.5 mM M2CMK, structuring at 760 nm with parameters: dz= 0.4 µm, hatch = 0.5 µm, objective: 10x/(NA 0.4)

A detailed depiction of all observed P_{th} is depicted in Table 7 (experimental part). A comparable trend was observed concerning structure stability compared to the single-line writing experiment. Lowest P_{th} (50 mW) was observed for the formulation containing equimolar ratio of BABO and M2CMK (1:1). As soon as the molar concentration of BABO was increased, higher laser power was required to produce stable structures. Control formulation 2 (M2CMK) showed promising structuring performance (70 mW) compared to the formulation containing 2:1 molar ratio BABO:M2CMK (80 mW, Table 7).

To investigate the limit of polymerization, additional formulations were prepared with lower sensitizer concentration (0.1 mM M2CMK) compared to previously used concentration (0.5 mM). This time, a selected number of formulations were prepared to gain overview on monomer mixture-reactivity (molar ratios 1:1 and 10:1). This time, a constant sensitizer concentration was used (0.1 mM M2CMK) varying co-initiator concentrations accordingly (0.1 BABO and 1 mM BABO). Furthermore, reference formulations (control 1, control 2) without sensitizer or co-initiator were prepared. TU Wien Logos were fabricated according to CAD-files. The laser power was varied from 10 to 100 mW at increments of 10 mW along the x-axis keeping a constant writing speed of 100 mm s^{-1}.

Die approbierte gedruckte Originalversion dieser Dissertation ist an der TU Wien Bibliothek verfügbar.
The approved original version of this doctoral thesis is available in print at TU Wien Bibliothek.

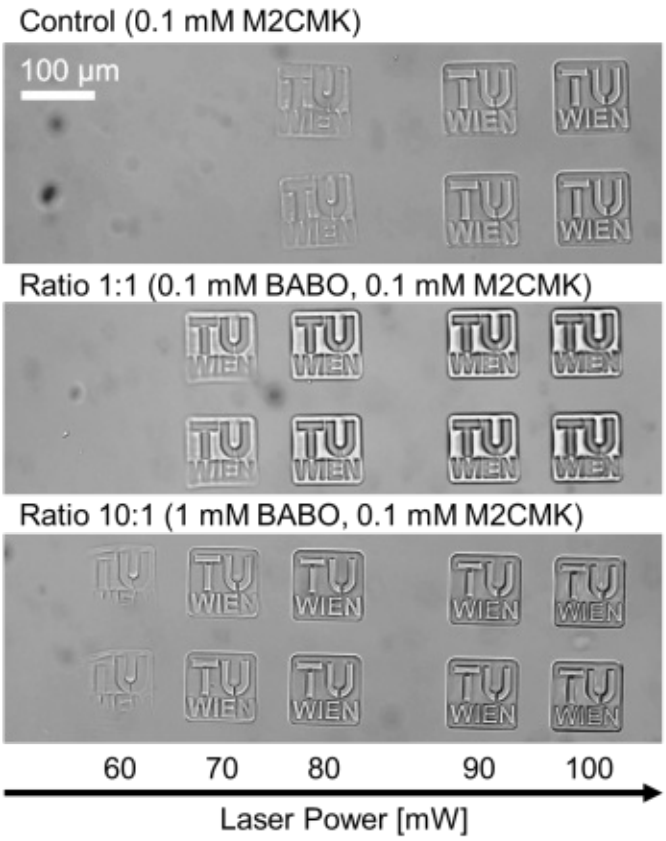

Figure 21: Brightfield-images of 2PP-fabricated TU Wien Logos in order to determine polymerization thresholds for each formulation. Formulations were prepared based on an acrylic monomer mixture ETA:TTA (1:1). Structuring parameters: dz= 0.4 µm, hatch = 0.5 µm, λ = 760 nm, Objective: 10x/0.4 NA

Here, lowest P_{th} (60 mW) was obtained for the formulation containing 10-fold molar excess of co-initiator (BABO:M2CMK 10:1, Figure 21, bottom). The reversed trend, contrary to what was observed during single-line writing (Figure 19), might be explained by the layer-by-layer stabilization effects, which were generated via the bottom-up structuring approach, hence building up a massive supporting structure to the above structured lines. Higher P_{th} (70 mW) was observed for the formulation containing equimolar ratio of sensitizer and co-initiator (Figure 21, middle), compared to the 10:1 molar ratio. Highest laser power (80 mW) was required for the reference formulation (0.1 mM M2CMK, Figure 21, top), whereas no polymerization was observed for reference formulation 1 (co-initiator, 0.1 mM BABO). A detailed list of all P_{th} values is depicted in Table 7 (experimental part). In conclusion, a minimum concentration of sensitizer is required to effectively initiate polymerization, also determined by the type of the monomer mixture. Here, a highly-potent 2PI was used and therefore, initiation even at relatively low concentrations was possible. Generally, the 2PI-concentration is a crucial factor when used in the presence of cells, as these compounds can show cytotoxicity to a certain extent.[221]

Overall, the preliminary investigation on a bimolecular system revealed no polymerization for control formulation 1, containing co-initiator (BABO), originating from the expected low 2PA-cross section of BABO (λ_{max} = 259 nm), exhibiting an absorption maximum far off the absorption region

Die approbierte gedruckte Originalversion dieser Dissertation ist an der TU Wien Bibliothek verfügbar.
The approved original version of this doctoral thesis is available in print at TU Wien Bibliothek.
TU Bibliothek Your knowledge hub WIEN

commonly required for 2PIs.[168,194] Based on these results, the sensitizer is a key performance indicator for an effective polymerization. In any case, a minimum limit for the sensitizer was necessary for this type of acrylic monomer mixture. Although, a moderate sensitizer-concentration was used for structuring the TU Wien Logos (0.1 mM), compared to the single-line writing experiment (0.05 - 0.5 mM), the polymerization containing excessive amount of BABO (10:1) proceeded at lower P_{th}, compared to the reference formulations (Figure 21). Generally, the fabrication method majorly influences the stability of the 3D construct and heavily determines the required sensitizer concentration. Although, free hanging single-lines are already fragile *per se*, complex 3D structures show additional instability due to cumulative weight effects.[217,222,223] Especially, hollow constructs are prone to collapse due to weak supporting structures and low layer-by-layer stabilization effects.[216] Therefore, higher laser powers are required, especially for porous *Atomium* structures. In general, the single-line writing process is a suitable approach to investigate structuring efficiency for acrylic monomer mixtures, however, final P_{th} need to be investigated for every type of monomer mixture as well as for every specific printed construct. Therefore, the comparison between the results of single-line writing and TU Wien Logo-structuring remains difficult.

In conclusion, promising results for the proposed concept were found based on the performed experiments on the bimolecular OE system using BABO as co-initiator in the presence of the state-of-the-art benzylidene cycloketone sensitizer. OE co-initiators were expected to decrease P_{th} of acrylic monomer mixtures compared to formulations containing pure sensitizer. This study supports the findings from previous experiments, where OE co-initiators were proposed to increase structuring efficiency for one-photon conditions.[194] Highly efficient 2PIs are needed in order to obtain high structuring efficiency while keeping P_{th} to a minimum. As already mentioned, the 2PI-concentration cannot be increased arbitrary because it critically influences cell viability.[221] Therefore, low-toxic 2PI molecules are required and in the same time low concentrations should be used for 2PP. To date, state-of-the-art concentrations used for 2PIs are located around 1 mM.[143] When 2PI-efficiency is increased accordingly, the 2PI concentration can be properly lowered, positively influencing cell viability. This supports the strategy to synthesize monomolecular 2PIs based on a sensitizer-moiety (M2CMK) with covalently coupled co-initiator molecules (OEs) with the goal to increase structuring efficiency.

Development of Monomolecular OE-2PIs

Since bimolecular systems exhibit intrinsic limitations, such as limited electron transfer between PI and co-initiator or photoinduced back electron transfer upon regeneration of the parent system, the initiation efficiency of 2PIs can be significantly decreased. Here, the synthesis of monomolecular 2PIs is described, replacing classical bi-molecular systems and merging the concept of an efficient benzylidene-sensitizer and co-initiator. Previous studies on OEs reported the effective photoinduced cleavage of N-O bonds for radical polymerization.[195] However, previously bimolecular mechanisms were examined for one-photon conditions (UV-Vis).

Die approbierte gedruckte Originalversion dieser Dissertation ist an der TU Wien Bibliothek verfügbar.
The approved original version of this doctoral thesis is available in print at TU Wien Bibliothek.
TU Bibliothek Your knowledge hub WIEN

Therefore, this thesis is focusing on the development of novel monomolecular 2PIs. For this, cross-conjugated compounds are required for an efficient absorption of light in the NIR region. Extensive research on benzylidene cycloketones showed that these types of chromophores offer promising performance during 2PP. Accordingly, 2PIs based on a benzylidene cycloketones core-structure should be covalently coupled to photocleavable OE derivatives. To introduce OE moieties, functional carbonyl groups are required offering the capability for modification. First, corresponding oximes are synthesized originating from ketones and aldehydes followed by acylation leading to oxime esters. The base-catalyzed o-acylation was widely used in literature, such as the pyridine-assisted acylation with acid chlorides.[224-226] Commonly, acid scavengers are needed to neutralize the formed acids. A straightforward synthesis approach was developed, starting from terminal carbonyl functionalities. Subsequent conversion to oximes and reaction with different acylation agents such as acid halides and -anhydrides should offer the path towards a broad range of OE-2PIs (Scheme 7).

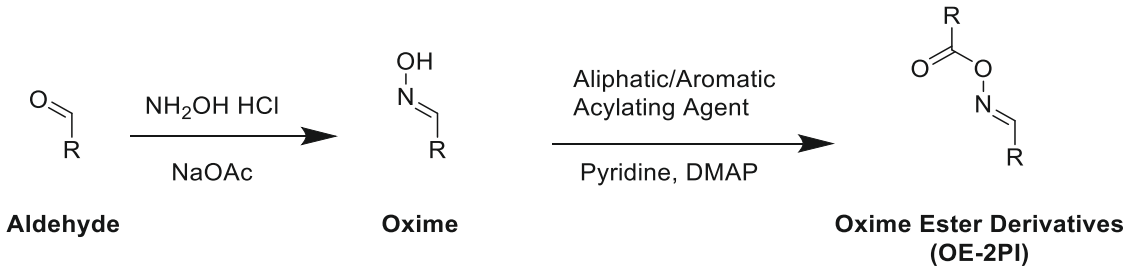

Scheme 7: Synthesis route towards oxime ester-based two-photon initiators.

Cyclic derivatives of inorganic acids provide the option to introduce ionizable functionalities. Carboxylate salts were already introduced to prepare water-soluble benzylidene cycloketones initiators.[165,227,228] Here, carboxylic- and sulfonic acid anhydrides were studied for this approach. Consequently, two classes of compounds are targeted: I) OEs with aromatic and aliphatic terminal groups and II) OEs with ionizable functionalities. To determine the required reaction conditions, model compounds should be synthesized. Low-m.w. molecules with mono- and difunctional terminal carbonyl groups are chosen (benzaldehyde (BA) and terephthalaldehyde (TA)). Via this, it was possible to define the required parameters to synthesize target 2PIs with enhanced π-conjugation. The synthesis was performed via aldol-condensations, following the above-mentioned strategy to covalently couple benzylidene cycloketones structures with photocleavable OE functionalities.[153] First, aromatic aldehydes are synthesized via Claisen-Schmidt condensation of TA and 4-methylcyclohexanone (MCK, Scheme 8).

Die approbierte gedruckte Originalversion dieser Dissertation ist an der TU Wien Bibliothek verfügbar.
The approved original version of this doctoral thesis is available in print at TU Wien Bibliothek.

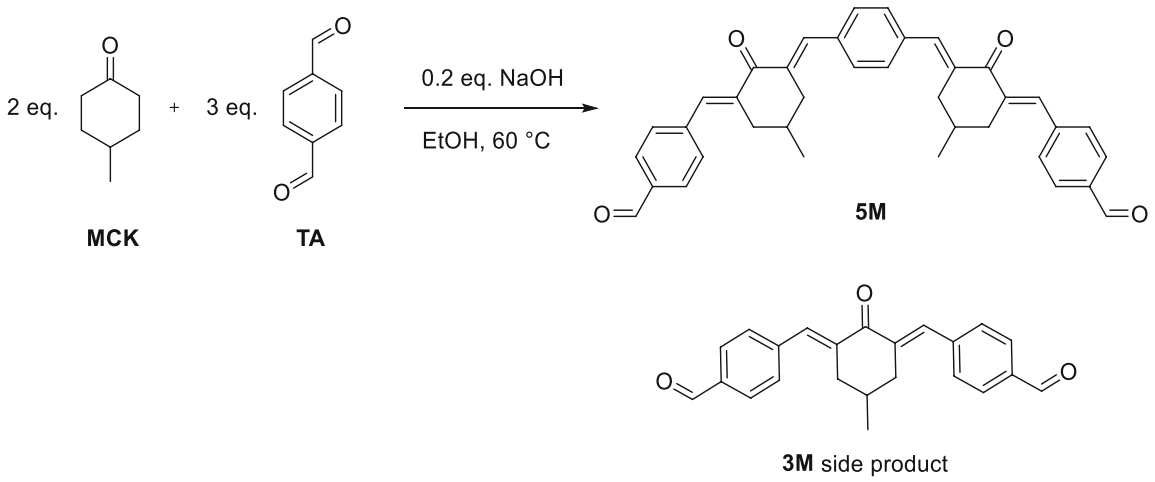

Scheme 8: Synthesis of a benzylidene-cycloketone core-structure (5M) via Claisen-Schmidt condensation of terephthalaldehyde (TA, 3 eq.) and methyl-cycloketone (MCK, 2 eq.). Catalytic amount of NaOH (0.2 eq.) is required to promote the base-catalyzed aldol condensation.

Two reaction products are formed (3M and 5M), where 5M can be easily separated via suction filtration, since 5M precipitates from the reaction solution. Additionally, several batches of 5M can be obtained via reduction of the mother liquor by half and storing the reaction solution for 24 h at 7°C. Residual starting material can be removed by washing the yellow precipitate extensively with hot EtOH.

The work-up of 3M showed several limitations. In contrast to 5M, 3M was not effectively separated neither by precipitation nor by extraction. Several attempts on the purification of 3M were performed but neither reversed- nor normal-phase column chromatography resulted in the desired product. Instead, several decomposition products were detected. In general, aromatic aldehydes are known to decompose under certain conditions such as competing reactions like Cannizzaro reactions (for carbonyl compounds with missing α-hydrogens). Especially in basic media, hydride transfer with additional TA molecules can lead to the formation of corresponding alcohols. However, the chance for crossed aldol reactions was reduced to a certain extent because only MCK can act as nucleophilic enol during aldol condensation and TA is not enolized due to missing α-hydrogens (Claisen-Schmidt condensation). Side products derived from aldol addition as well as retro-aldol reactions were not detected. It was observed that excessive amount of base (2.5 eq.) promotes Cannizzaro reaction products, highly undesirable for the scope of this thesis. A reduced amount of base (0.01 eq.) does not sufficiently lead to the formation of 5M within reasonable timeframes. An optimum amount of base (NaOH) was found to be 0.1 eq. As alternative, KOH can be used. According to Carothers an optimum ratio of 2:3 eq. (MCK:TA) was found to synthesize 5M in high purity and high yield (64% th.). A strategy to isolate 3M was neglected for this thesis. However, minimal amount of crude 3M was obtained via the extraction of the mother liquor with DCM and UV-Vis spectra of both compounds were measured (Figure 22).

Die approbierte gedruckte Originalversion dieser Dissertation ist an der TU Wien Bibliothek verfügbar.
The approved original version of this doctoral thesis is available in print at TU Wien Bibliothek.

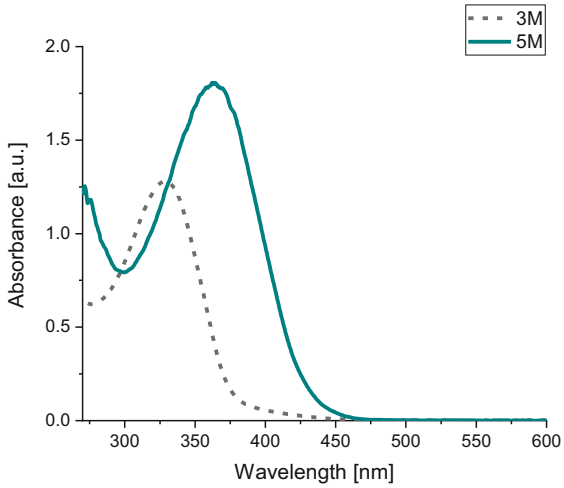

Figure 22: UV-Vis absorption spectra of 3M and 5M (0.03 mM in THF, λ_{max}^{3M} = 328 nm, ε_{max}^{3M} = 43,582 M^{-1} cm^{-1}) (λ_{max}^{5M} = 366 nm, ε_{max}^{5M} = 62,140 M^{-1} cm^{-1}). To visualize the enhanced molar extinction coefficient of 5M, the spectra are given in arbitrary units (a.u.).

The absorption maximum of 5M was shifted towards longer wavelength (λ_{max}^{5M} = 366 nm; ε_{max}^{5M} = 62,140 M^{-1} cm^{-1}) compared to 3M (λ_{max}^{3M} = 328 nm; ε_{max}^{3M} = 43,582 M^{-1} cm^{-1}). This bathochromic shift was indicative for a transition that occurs at lower energy[228] and was expected to derive from chromophores with extended cross-conjugation.[229] Consequently, 5M with its extended conjugation and bathochromic shifted absorption spectrum was expected to increase the chance for being an effective photosensitizer for 2PP compared to 3M. Besides the straightforward synthesis of 5M, the shifted absorption spectrum was an additional reason to focus on this compound for the development of novel 2PIs.

After synthesizing benzylidene cycloketones, the corresponding oximes were synthesized. In general, oximations are performed via treatment of the corresponding aldehydes with hydroxylamine salts.[230] The nucleophilic attack of the nitrogen of the hydroxylamine on the carbonyl-carbon leads to the formation of tetrahedral intermediates and a series of proton transfers and finally to the elimination of water. A classical method to effectively synthesize oximes, is the reaction of carbonyl compounds with $NH_2OH{\cdot}HCl$ in the presence of NaOAc, serving as buffer for the generated hydrochloric acid. Usually, this reaction is performed in alcoholic solutions, which was not applicable for 5M due to the low solubility of 5M in EtOH. Dioxane was chosen as alternative solvent. NaOAc had to be finely powdered to ensure dissolution in dioxane. 5M was transformed to the corresponding oxime (5MOx) using an excess of hydroxylamine salt (2.5 eq.) to assure full conversion of the aldehyde functionalities (Scheme 9).

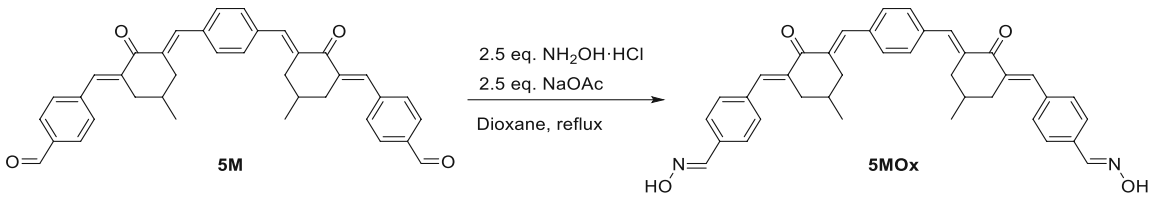

Scheme 9: Synthesis of 5MOx (Yield: 51% th.).

Die approbierte gedruckte Originalversion dieser Dissertation ist an der TU Wien Bibliothek verfügbar.
The approved original version of this doctoral thesis is available in print at TU Wien Bibliothek.
TU Bibliothek Your knowledge hub WIEN

Due to increased solubility in dioxane compared to THF, the synthesis was performed in dioxane in the presence of NaOAc (2.5 eq.) and $NH_2OH{\cdot}HCl$ (2.5 eq.). The reaction mixture was stirred under reflux overnight, while monitoring the reaction progress via TLC. 5MOx was isolated via dropwise addition of the reduced mother liquor onto a cooled solution of hydrochloric acid in water (10%). The precipitate was centrifuged off, dissolved in THF, and dried over Na_2SO_4. The pure product was obtained by removing the solvent in high vacuum (Yield: 51% th.). UV-Vis absorption spectra of 5M and 5MOx were measured and are depicted hereafter (Figure 23).

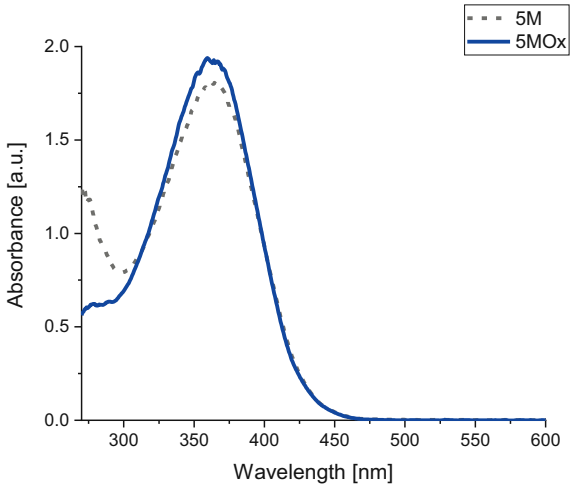

Figure 23: UV-Vis absorption spectra of 5M and 5MOx (0.05 mM in THF, λ_{max}^{5M} = 366 nm, ε_{max}^{5M} = 62,140 $M^{-1}\,cm^{-1}$ λ_{max}^{5MOx} = 360 nm, ε_{max}^{5MOx} = 68,780 $M^{-1}\,cm^{-1}$) are given in arbitrary units (a.u.) to visualize the differences in the absorption profile.

For the synthesis of 5M-derivatives, hydrolysis of oximes and restoration of the original aldehyde must be strictly avoided. In general, oximes are prone to decomposition upon extensive heating in the presence of (in)organic acids.[231] Furthermore, several side products can form for example hydrolysis to carbonyls, reduction to amines or hydroxylamines, oxidation to nitro compounds and the acid-/base catalyzed Beckmann rearrangement.[232] However, the synthesis of 5MOx was successful and no side products were observed at applied conditions. In general, the extraction of oximes should be performed at moderate temperatures in slightly acidic to neutral pH to avoid hydrolysis or rearrangement reactions. The required reaction conditions were first investigated using mono- and di-functional model compounds (benzaldehyde (BA) and terephthalaldehyde (TA)). Generally, reaction conditions were adjusted according to conditions found in literature.[197,233-236] Accordingly, corresponding oximes of BA and TA were synthesized using an excess of $NH_2OH{\cdot}HCl$ (2.2 eq) in the presence of NaOAc as buffer. The work-up for TA was performed according to the method applied for 5M, whereby, the work-up for BA had to be adjusted. Precipitation of BAOx in aqueous HCl solution could not be applied and therefore the product was extracted with 0.1 M aqueous HCl and saturated $NaHCO_3$. The organic phase (THF) was dried over Na_2SO_4 and the products were isolated either as clear oil (Yield: 70% th. BAOx) or white powder (Yield: 49% th. TAOx). The characteristic absorption profiles according to the respective chromophores are depicted in Figure 24.

Die approbierte gedruckte Originalversion dieser Dissertation ist an der TU Wien Bibliothek verfügbar.
The approved original version of this doctoral thesis is available in print at TU Wien Bibliothek.
TU Bibliothek Your knowledge hub WIEN

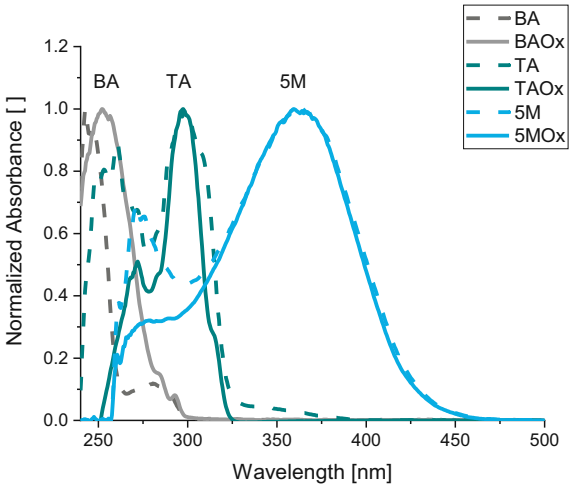

Figure 24: Normalized absorbance of BA, BAOx (grey), TA, TAOx (cyan), 5M, 5MOx (blue). UV-Vis spectra of model compounds and their corresponding oximes (λ_{max}^{BA} = 243 nm, λ_{max}^{BAOx} = 252 nm, λ_{max}^{TA} = 299 nm, λ_{max}^{TAOx} = 298 nm)

An overview on all absorption maxima as well as corresponding molar extinction coefficients (at λ_{max}) of available compounds is depicted in the conclusion section of this chapter (Table 3). Accordingly, a pool of compounds was now available for modification. After the successful synthesis of various functional oximes based on BA, TA and 5M, several OE target compounds were synthesized via selective acylation of the corresponding oximes. For this purpose, several acyl derivatives were chosen (Figure 25). Acid halides, such as benzoyl chloride (BC) and pivalic acid chloride (PAC) and cyclic organic acid anhydrides, like succinic anhydride (SA), 1,2,4-benzenetricarboxylic anhydride (BTCA) and 2-sulfobenzoic anhydride (SBA).

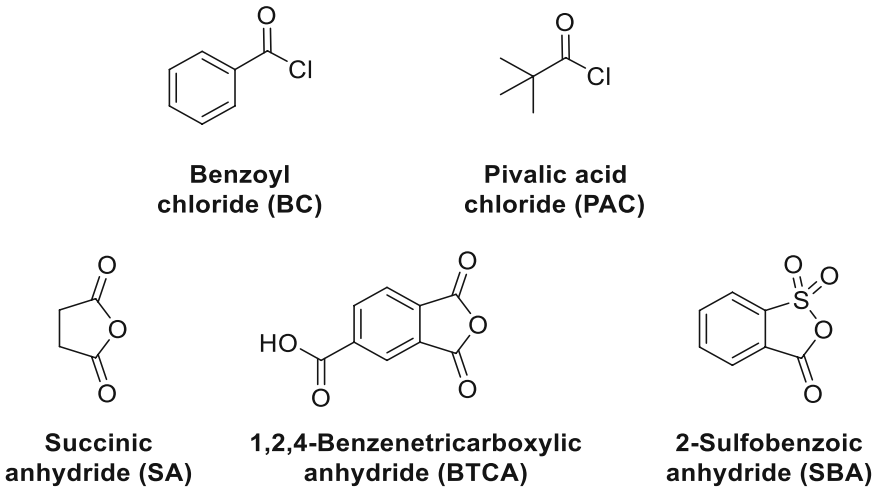

Figure 25: Acyl derivatives used for the synthesis of oxime ester 2PIs. Top: aromatic (BC) and aliphatic (PAC) acid chlorides. Bottom: Carboxylic- and sulfonic acid anhydrides (SA, BTCA, SBA) were used to introduce ionizable functionalities.

The mechanism of the acyl substitution proceeds via a nucleophilic attack of the oxime-oxygen on the carbonyl carbon of the acyl derivative. The formation of the tetrahedral intermediate and the subsequent elimination of the leaving group is the rate-determining step.[237] The acylation can be

Die approbierte gedruckte Originalversion dieser Dissertation ist an der TU Wien Bibliothek verfügbar.
The approved original version of this doctoral thesis is available in print at TU Wien Bibliothek.

performed under acid- or base-catalyzed conditions.[238] In this thesis, the base-catalyzed reaction was performed, which is proceeding via deprotonation of the oxime, further reacting acyl derivatives under formation of tetrahedral intermediates. Subsequent, elimination of the leaving group and restoration of the carbon-oxygen double bond results in the desired ester (Scheme 10).

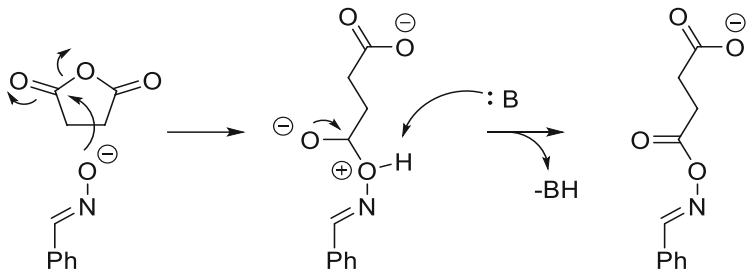

Scheme 10: Mechanism of the base-catalyzed acylation of oximes.

The reaction occurs in two distinct stages and involves an addition- and elimination reaction, where the leaving group is either released (HCl in the case of acyl chlorides) or remains covalently bound when cyclic anhydrides are used. The reactivity of acyl derivatives is determined by their acidity, which relates to its ability to eliminate the leaving group.[237] In anhydrides the donation of electrons to one carbonyl group is in competition with the donation of electrons to the second carbonyl group. Thus, anhydrides are less reactive in comparison to acyl halides. Acid chlorides are more reactive since the partial positive charge is less resonance stabilized by the halogen. Although acid anhydrides are less reactive than acid chlorides, they are still very active acylation agents.[239] The reaction conditions need to be adjusted according to the partial positive charge (δ+) of the carbon and according to the pk_a values of the conjugated acids. The introduction of inorganic acid derivatives (carboxylate-/sulfonate moieties) enables the liberation of ionizable groups, favorable for the preparation of water-soluble derivatives. Furthermore, aliphatic- (SA, PCA) and aromatic substituents (SBA, BTCA, BC) can be introduced to adjust the electronical properties of the respective chromophores (Figure 26).

Die approbierte gedruckte Originalversion dieser Dissertation ist an der TU Wien Bibliothek verfügbar.
The approved original version of this doctoral thesis is available in print at TU Wien Bibliothek.

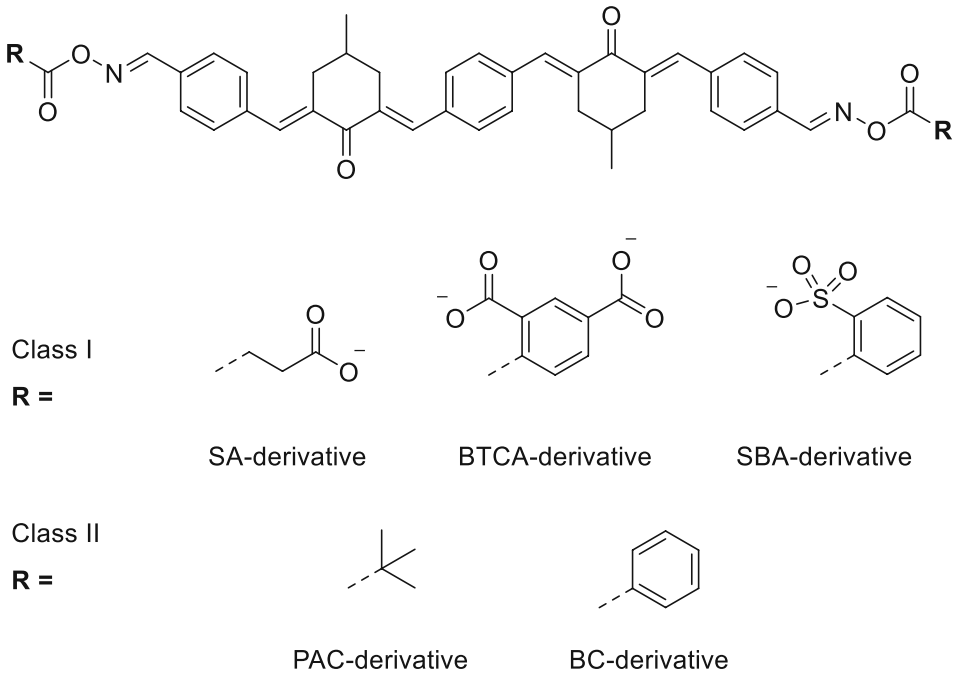

Figure 26: Target compounds based on a 5-membered chromophore (5M), which was synthesized previously via classical aldol condensation. Terminal aldehyde functionalities of 5M were first transformed into oximes and subsequently reacted with various acylation agents resulting in the desired OE-2PIs. Carboxylate- and sulfonate derivatives were synthesized via a selective ring-opening of anhydrides (Class I). Non-ionizable OE-2PIs (Class II) were synthesized via the reaction with acid halides.

First, the reaction conditions were investigated using the previously synthesized model compounds (BAOx, TAOx). Multiple attempts of applying TEA as base failed during the synthesis of OE-derivatives via various aliphatic and aromatic acylation agents (PAC, BC, SA, BTCA, SBA) and (Scheme 11). Since primarily aldehyde- or oxime starting materials were isolated, TEA was observed to be unreactive towards the applied coupling agents.

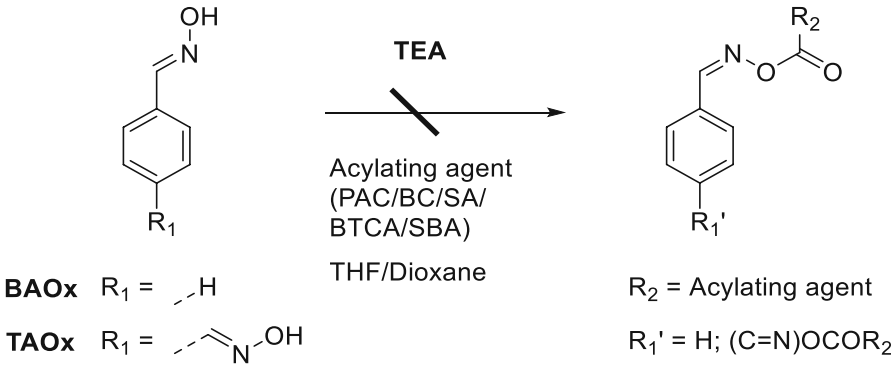

Scheme 11: Failed attempt of using TEA for the acylation of oximes (in case of BAOx: 1 eq. TEA, 1 eq. acylation agent in THF; in case of TAOx: 2 eq. TEA and 2 eq. acylation agent in dioxane).

Instead, a strong base (pyridine) was applied and successfully led to the synthesis of various OE-derivatives (Scheme 12 -Scheme 22). To avoid partial conversion of the oximes, the amount of acylation agent was increased (Δ = 0.2 eq) compared to the previously used equimolar ratio between oxime and coupling agent, in the same time increasing the amount of pyridine

Die approbierte gedruckte Originalversion dieser Dissertation ist an der TU Wien Bibliothek verfügbar.
The approved original version of this doctoral thesis is available in print at TU Wien Bibliothek.

(Δ = 0.4 eq.), to ensure full scavenging of any freed acids. To enhance the reactivity of anhydrides, the application of 4-(dimethylamino)pyridine (DMAP) was investigated. In general, amino pyridines, such as DMAP are especially effective catalysts for the acylation of carbonyl compounds as well as for the formation of sterically hindered esters (Steglich esterification).[240] Compared to pyridine, the nucleophilic nature of the nitrogen can be reinforced by the introduction of the dimethyl amino group of DMAP.[241] Instead of using pyridine as solvent, which can lead to unwanted side-products, the application of DMAP was used. Consequently, the amount of pyridine can be reduced while increasing the reactivity of acylation catalysts. The reaction with anhydrides proceed via a transformation into their tetrahedral intermediates upon attack of DMAP, hence increasing their electrophilicity.[242] Subsequent restoration of the carbonyl functionality and elimination of a carboxylate ion makes the anhydride more susceptible towards nucleophilic attack than the original anhydride. In a final step, the attack of the oxime gives another tetrahedral intermediate, leading to the restoration of DMAP upon elimination of the leaving group. Accordingly, esterification of the oximes (TAOx, BAOx, 5MOx) was performed using catalytic amount of DMAP (0.1 eq.) as activating agent and pyridine as auxiliary base. First, the acylation of BAOx and TAOx was investigated using BC (Scheme 12, Scheme 13).

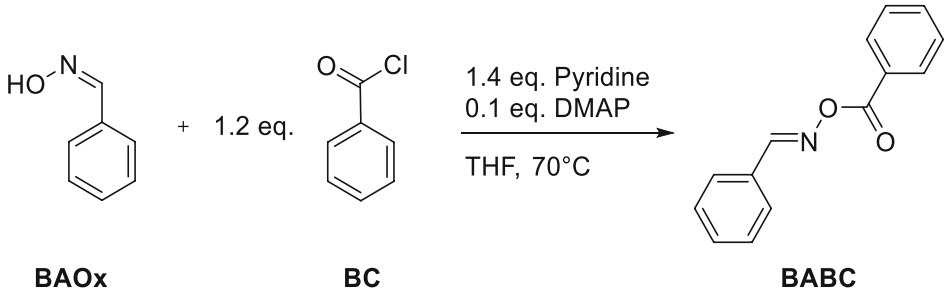

Scheme 12: Synthesis of BABC via BAOx and benzoyl chloride (BC) in THF.

The reactions described here were performed in anhydrous solvents under inert gas (Ar) to prevent the hydrolysis of the acylation agents. The general procedure is mentioned hereafter, with slight changes mentioned for each individual product. The oximes were dissolved in the respective solvents (listed in Table 2) and combined with anhydrous distilled pyridine. Due to the limited solubility of TAOx (and 5MOx) in THF, these reactions were performed in dioxane. The reaction mixture was then cooled to 15°C (considering the melting point of dioxane), gradually adding acid chloride/anhydride at a slight excess regarding oxime functional groups (1.2 or 2.2 eq.) and finally, DMAP as activating agent (0.1 eq.). Immediately, upon addition of acid chlorides (BC, PAC), the formation of a white precipitate (pyridine-chloride salt) can be observed. The mixture was refluxed overnight, controlling the reaction progress via TLC (PE:EE). Upon ensuring complete conversion of the oximes, the reaction mixture was allowed to cool to room temperature and the volume was reduced by half by evaporation of the solvent. Any precipitate was separated from the reaction mixture and analyzed separately. The mother liquor was then extracted with 1M HCl (BABC, BAPAC) or precipitated in 0.5M HCl (TA- & 5M-derivatives) obtaining the products as liquids (BAPAC) or solids (BABC, TAPAC, TASA, TASBA, 5MBC, 5MPAC, 5MSA, 5MSBA). Since BAPAC

Die approbierte gedruckte Originalversion dieser Dissertation ist an der TU Wien Bibliothek verfügbar.
The approved original version of this doctoral thesis is available in print at TU Wien Bibliothek.
TU Bibliothek Your knowledge hub WIEN

is liquid *per se*, a precipitation approach was not suitable. Here, the mother liquor was reduced to a minimum after separating the precipitated pyridine-chloride salt from the reaction solution. The yellow liquid was dissolved in DCM, extracted with 1M HCl and the collected organic phases dried over Na_2SO_4. The extraction with saturated sodium bicarbonate was examined, however resulted in the decomposition of the products (restoration of oximes). Precipitation of the target compounds was a convenient method to remove residual base and acylation agents from the reaction mixtures. Residual water derived from the precipitation in aqueous HCl can be removed by redissolving the product in the appropriate solvent (see Table 2) and drying over Na_2SO_4. Recrystallization from EA gave the desired products (yields see Table 2).

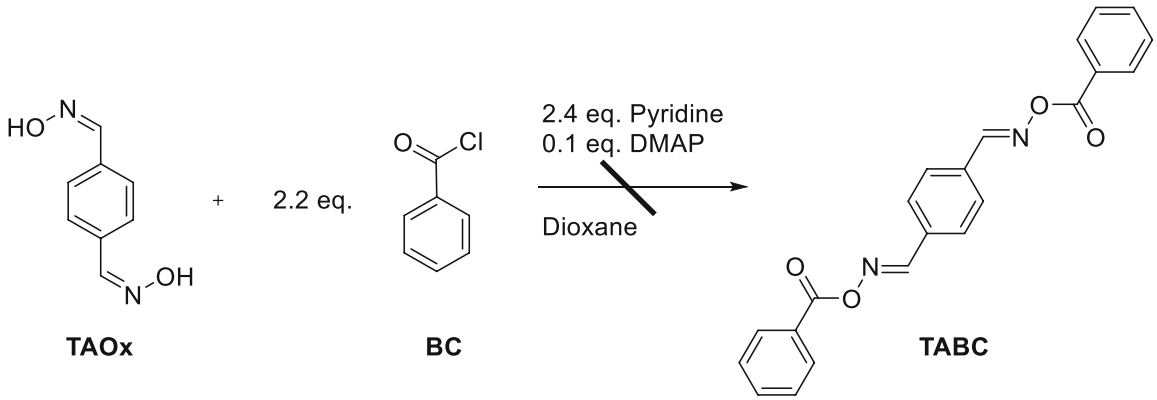

Scheme 13: Failed attempt of synthesizing TABC.

Several trials of synthesizing TABC failed, since the obtained solid was insoluble in many common solvents ($CHCl_3$, DCM, DMSO, benzene, toluene, D_2O, DMF, EA, PE, diethyl ether, ACN, THF, acetone, Scheme 13) presumably due to extensive π-stacking of the aromatic moieties.[243] Subsequently, the model compounds (BAOx, TAOx) were coupled to the aliphatic acylation agent (PAC, Scheme 14, Scheme 15).

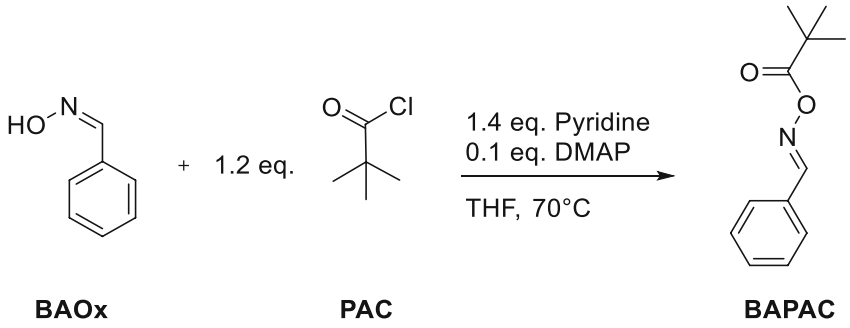

Scheme 14: Synthesis of BAPAC via acylation of BAOx using pivalic acid chloride (PAC).

Die approbierte gedruckte Originalversion dieser Dissertation ist an der TU Wien Bibliothek verfügbar.
The approved original version of this doctoral thesis is available in print at TU Wien Bibliothek.

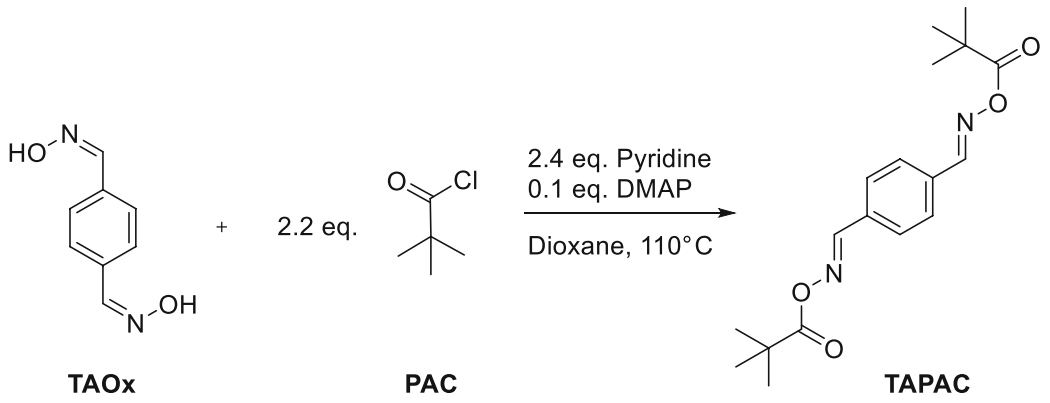

Scheme 15: Synthesis of TAPAC.

Both model compounds (BAPAC, TAPAC) were successfully synthesized according to the previously described method. BAOx was left to react with PAC in THF to obtain the product as colorless liquid at a yield of 46% th. TAPAC was synthesized by reaction of TAOx with PAC in dioxane obtaining the product as white solid. Here, multiple purification steps were required and resulted in a moderate yield (10% th.). Upon successful examination of the reaction conditions using the model compounds (BAOx, TAOx), the anhydrides (SA, SBA) were exclusively coupled to TAOx (Scheme 16, Scheme 17) (and 5MOx Scheme 21, Scheme 22), while excluding BAOx due to the structural resemblance of TA- to 5M-derivatives and the straightforward isolation of TA-derivatives (precipitation).

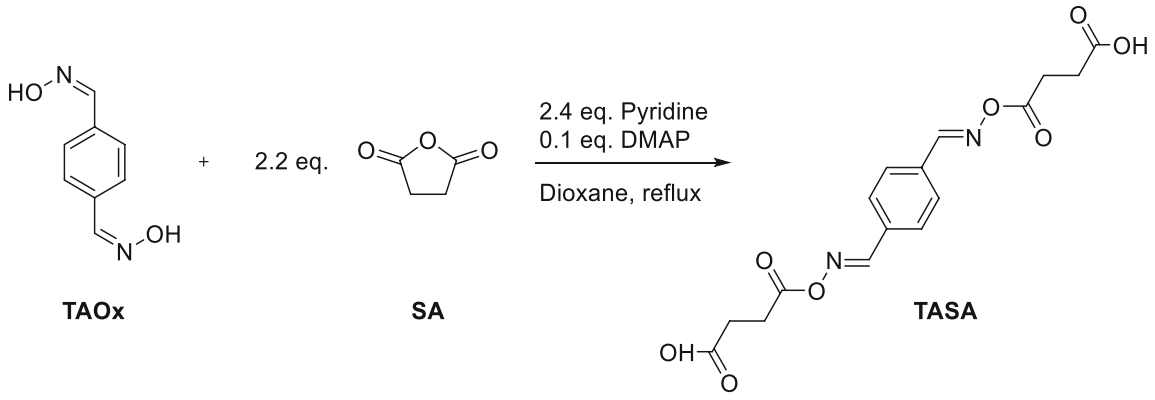

Scheme 16: Synthesis of TASA.

Die approbierte gedruckte Originalversion dieser Dissertation ist an der TU Wien Bibliothek verfügbar.
The approved original version of this doctoral thesis is available in print at TU Wien Bibliothek.

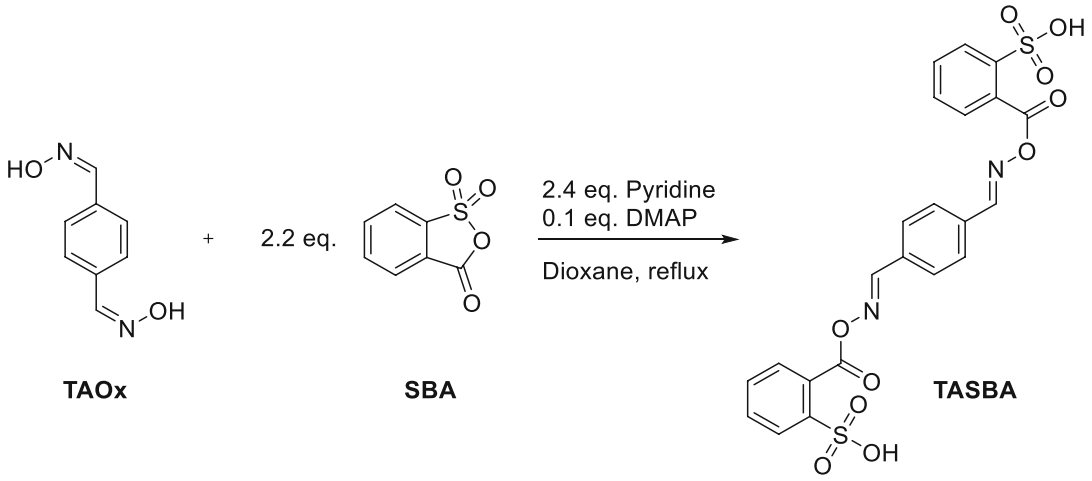

Scheme 17: Synthesis of TASBA.

The anhydrides were successfully coupled to TAOx with reasonable yields (32% th. TASA, 43% th. TASBA). The nucleophilic attack of the oxime occurred at the carbonyl site of SBA, since the carbonyl peak of the product (TASBA) was observed via ^{13}C NMR spectroscopy (166.00 ppm). In general, reactions performed at room temperature did not result in formation of the desired products within a reasonable timeframe. Therefore, all reactions were carried out under reflux to increase reaction kinetics. A general trend was observable regarding reaction speed for various acylation agents. Acid chlorides (BC, PAC) exhibited increased reaction rates (24 h) compared to decreased reaction rates for acid anhydrides (SA, SBA. 48 h - 4 d), derived by the enhanced reactivity of acid chlorides.[239] The acylation of TAOx (and later 5MOx) using the benzenetricarboxylic anhydride (BTCA) failed multiple times, although the reaction was expected to be comparable to previously applied methods (Scheme 18). Presumably, the nucleophilicity of the oximes was not sufficient, since primarily aldehyde- or oxime starting materials were isolated here.[244-246].

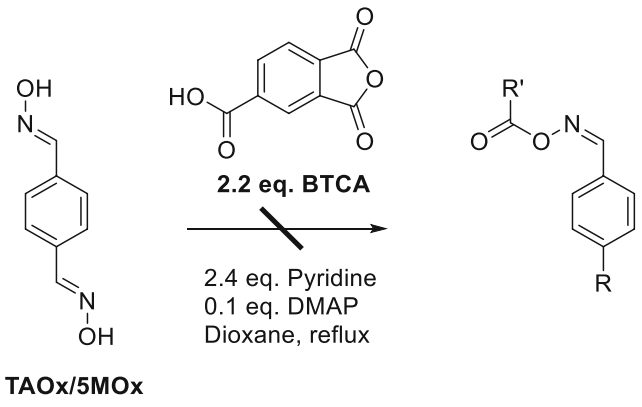

Scheme 18: Failed attempt of synthesizing BTCA-derivatives of the respective oximes (TAOx, 5MOx).

The synthesis of the 5M derivatives (5MBC, 5MPAC, 5MSA, 5MSBA) was performed in dioxane using 1 eq. of 5MOx, 2.2 eq. acylation agent (BC/PAC/SA/SBA), 2.4 eq. pyridine and 0.1 eq. DMAP (Scheme 19 – Scheme 22).

Die approbierte gedruckte Originalversion dieser Dissertation ist an der TU Wien Bibliothek verfügbar.
The approved original version of this doctoral thesis is available in print at TU Wien Bibliothek.

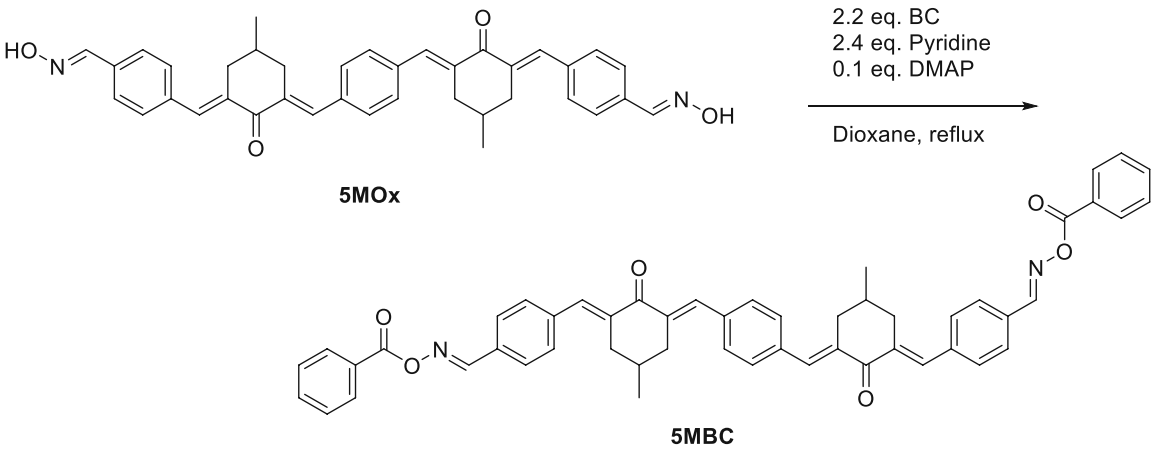

Scheme 19: Synthesis of 5MBC via acylation of 5MOx using benzoyl chloride (BC).

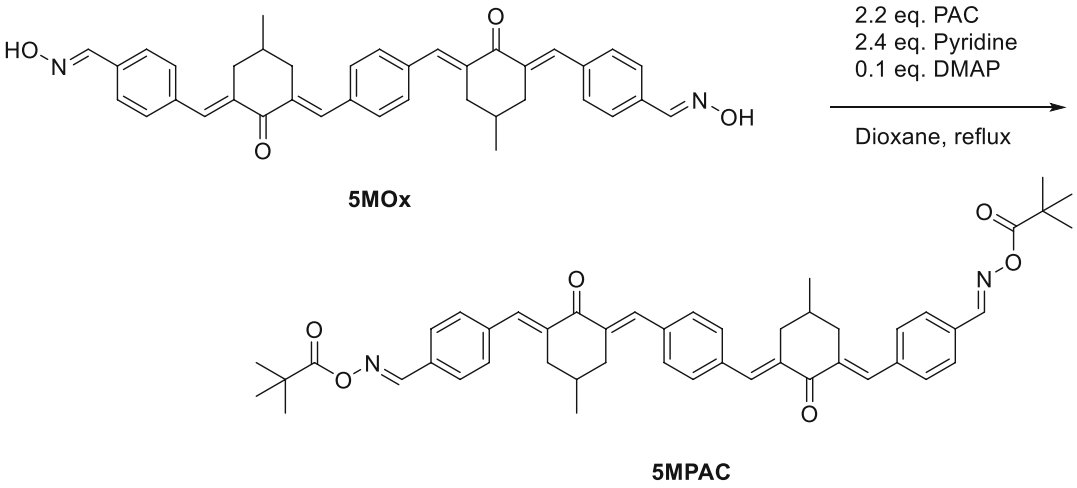

Scheme 20: Synthesis of 5MPAC via acylation of 5MOx using pivalic acid chloride (PAC).

The synthesis of 5MBC and 5MPAC each time resulted in the precipitation of the pyridine chloride salt, which was separated upon complete conversion of the oximes. The mother liquor of the following 5M-derivatives (5MBC, 5MPAC, 5MSA) exhibited a bright red color and the products were obtained upon precipitation from 0.5 M HCl. After precipitation, the products were dissolved in DCM (5MBC, 5MPAC) or THF (5MSA), died over Na_2SO_4 and the solvent evaporated. The solids (5MBC, 5MPAC, 5MSA) were recrystallized from EA obtaining the products as orange crystals (Yields: Table 2). All products were confirmed via ^{1}H- and ^{13}C NMR spectroscopy and HR-MS measurements (ESI^+). 5MBC and 5MPAC were fully ionizable and detected as $[M+H]^+$ adducts. Contrary to the previously described 5M-derivatives, the isolation method for 5MSBA had to be adjusted, since a dark red oily organic phase formed at the bottom of the reaction flask upon proceeding reaction time (Scheme 22).

Die approbierte gedruckte Originalversion dieser Dissertation ist an der TU Wien Bibliothek verfügbar.
The approved original version of this doctoral thesis is available in print at TU Wien Bibliothek.

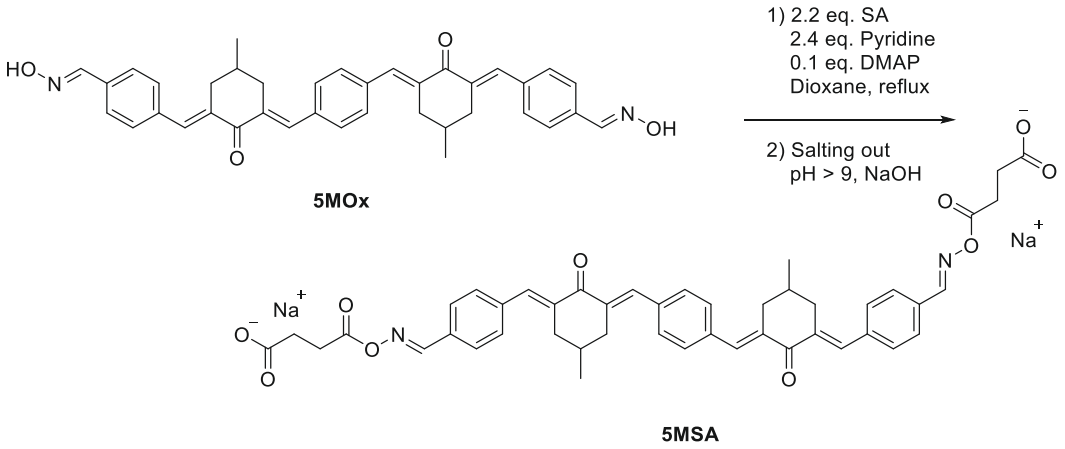

Scheme 21: Synthesis of 5MSA via acylation of 5MOx using succinic acid anhydride (SA) in the presence of pyridine (2.4 eq.) and DMAP (0.1 eq.) as activating agent.

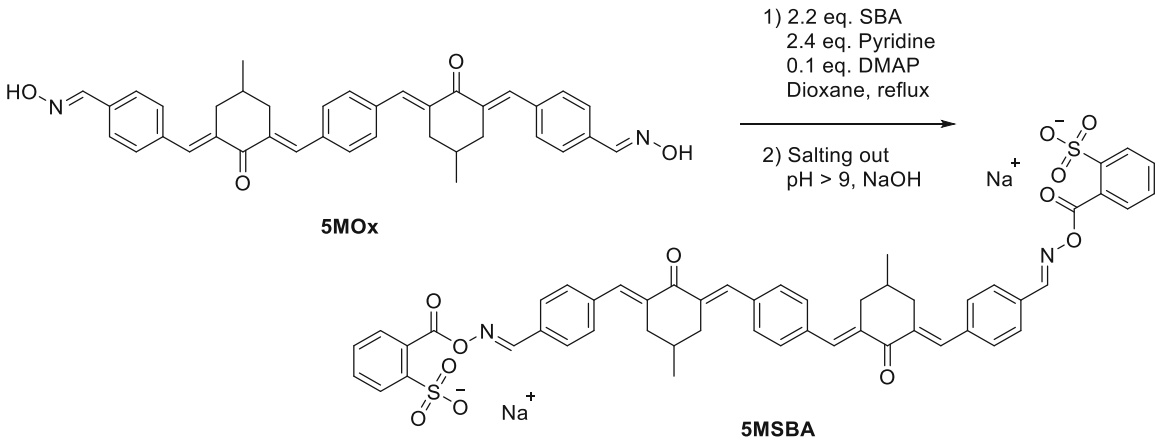

Scheme 22: Synthesis of 5MSBA via acylation of 5MOx using sulfobenzoic anhydride (SBA) in the presence of pyridine (2.4 eq.) and DMAP (0.1 eq.) as activating agent.

The synthesis of the ionizable derivatives (5MSA, 5MSBA) was performed as follows. The separation of 5MSA from the reaction mixture followed the method described above (precipitation in 0.5 M HCl). The work-up for 5MSBA however had to be adjusted accordingly, since a red oily phase formed at the bottom of the flask during the reaction. The red oily residue was separated from the reaction mixture via decantation, dissolved in DMF and slowly added to a stirred acidic aqueous solution (0.5 M HCl). A spongy precipitate was obtained upon moderate centrifugation (2200 rpm, 3 min). Extensive centrifugation (5000 rpm, >3 min) can lead to the formation of solid aggregates which are difficult to dissolve. The red precipitate was redissolved in DMF, dried over Na_2SO_4 and the solvent evaporated in vacuo. The product was confirmed via ^{1}H- and ^{13}C NMR spectroscopy. The nucleophilic attack of the oxime occurred at the carbonyl site of SBA, since the carbonyl peak of the product (5MSBA) was observed via ^{13}C NMR spectroscopy (169.26 ppm). Both ionizable derivatives (5MSA, 5MSBA) were isolated as salts to enhance the water solubility of the synthesized 2PIs. The salting-out approach of both products was performed by suspending the corresponding acids in distilled water. The aqueous suspensions were vigorously stirred in brown glass vials and aqueous sodium hydroxide solution (0.5 M) was slowly

Die approbierte gedruckte Originalversion dieser Dissertation ist an der TU Wien Bibliothek verfügbar.
The approved original version of this doctoral thesis is available in print at TU Wien Bibliothek.
TU Bibliothek Your knowledge hub WIEN

added until a pH of 9 was reached. For 5MSA, a few drops of THF were added, to increase phase transfer into the aqueous solution. The mixtures were vigorously stirred at room temperature multiple days (3d). Once, a color change of the aqueous phase from colorless to orange was observed, the remaining solids were separated by centrifugation and the aqueous phase was freeze-dried at 0.01 mbar. Extensive cooling of the aqueous solutions and storage of the solution for 7 days at 7°C was not sufficient to precipitate the desired products from aqueous medium. HR-MS measurements (ESI^+) of 5MSA and 5MSBA were performed, whereas higher fragmentation voltage was required (180 V) compared to the previously applied voltage (100 V for the ionization of 5MBC and 5MPAC). Although the products were confirmed via ^1H- and ^{13}C NMR spectroscopy, HR-MS measurements resulted in the one-sided fragments. The one-side fragmented species probably derive from a decomposition during the salt formation in basic aqueous media, since basic solutions were often found to lead to a partial decomposition of OE-derivatives. The extraction of the organic phase using $NaHCO_3$ led to a partial loss of the desired products. Presumably, rearrangement or decomposition to amides or cyanoformates occurred in the presence of excessive amount of base.[247,248] In general, column chromatography (normal- and reversed phase) was found to be an ineffective method to separate target compounds from side products, since precipitation in acidic media and extraction was found to be straightforward. Since, the conversion of the oximes could be monitored and the target compounds were confirmed via ^1H and ^{13}C NMR spectroscopy before preparation of the salts, the purity was found to be sufficient to investigate their performance during 2PP. The performance of the water-soluble derivatives (5MSA, 5MSBA) were first tested towards their performance during steady-state photolysis experiments (1PA) and secondly in hydrogel matrices using 2PP. Since biological-based systems require water-soluble 2PIs, the investigation of the organo-soluble chromophores (5MBC and 5MPAC) was terminated here. Solubilities and yields of the synthesized compounds are summarized in Table 2.

Die approbierte gedruckte Originalversion dieser Dissertation ist an der TU Wien Bibliothek verfügbar.
The approved original version of this doctoral thesis is available in print at TU Wien Bibliothek.

*Table 2: Overview on the performed experimental conditions of the synthesis routes and available initiators. All reactions were performed with oximes (based on either BA, TA or 5M) as starting materials, various aliphatic- (PAC, SA) and aromatic acyl derivatives (BC, SBA), in the presence of pyridine and catalytic amount of DMAP. Model reactions using BAOx were performed in THF, and target compounds based on TAOx and 5MOx were performed in dioxane. Ionizable target compounds (5MSA, 5MSBA) were transformed into their water-soluble sodium salts via salting-out. *Solubilities are given for the conditions during synthesis (THF, dioxane) and during work-up (DCM, THF, DMF, H_2O).*

Target compounds	**Yields (% th.)**	**Solubilities***	**Water-soluble salts available**
5M	64	DCM, THF	×
5MOx	51	Dioxane	×
5MBC	33	DCM, Dioxane	×
5MPAC	64	DCM, Dioxane	×
5MSA	24	THF, Dioxane, H_2O	✓
5MSBA	25	THF, Dioxane, DMF, H_2O	✓
Model reactions			
BABC	34	THF	×
BAPAC	46	THF	×
TAPAC	10	Dioxane	×
TASA	32	Dioxane	×
TASBA	43	Dioxane	×

Die approbierte gedruckte Originalversion dieser Dissertation ist an der TU Wien Bibliothek verfügbar.
The approved original version of this doctoral thesis is available in print at TU Wien Bibliothek.

1.3 Steady-State Photolysis of Oxime Ester-2PIs

UV-Vis absorption spectra of the synthesized water-soluble derivatives (5MSA, 5MSBA) were recorded, while irradiating solutions of the novel 5M-derivatives with LED light in order to investigate whether the hypothesis of OE-cleavage can be supported upon inducing a photochemical trigger. Here, an extensive photoreactor study including NMR and HPLC studies was not conducted (similar to section 2.3) due to the small quantity of analytes. Therefore, a steady-state photolysis was performed, irradiating 2PI stock solutions in quartz-cuvettes while measuring the UV-Vis absorption profiles during LED irradiation.

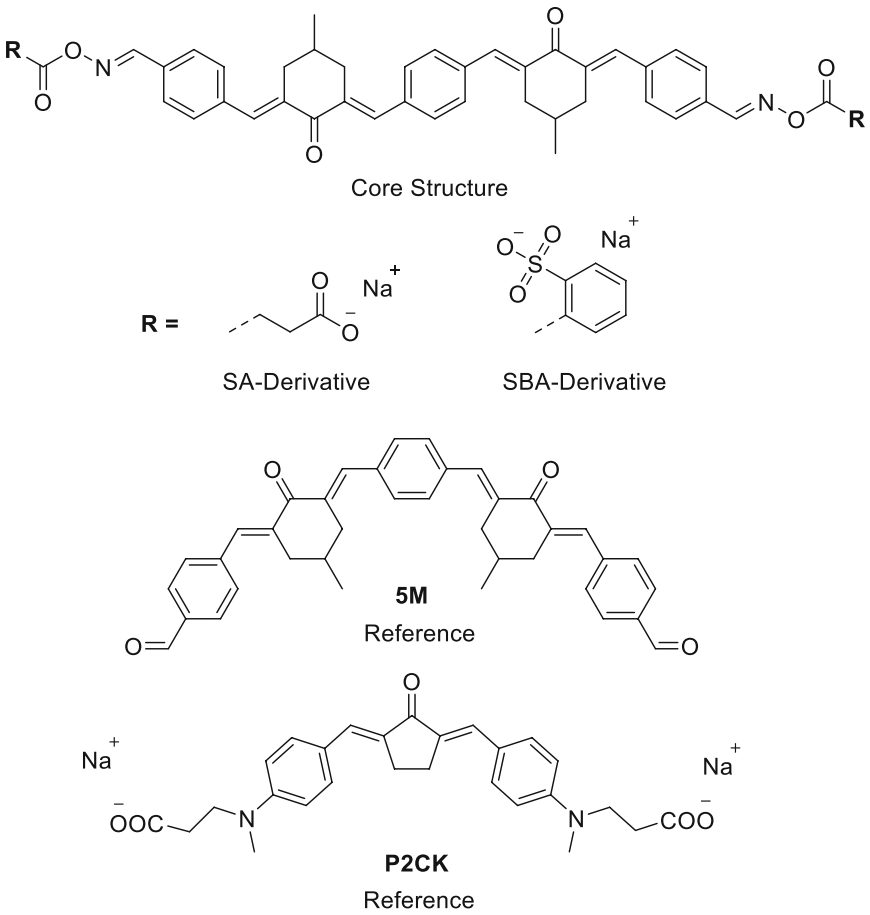

Figure 27: UV-Vis absorption spectra were measured upon irradiation with LED light of 5M derivatives (5MSA, 5MSBA) in comparison to the reference chromophores (5M, P2CK).

On the one hand, the organo-soluble precursor molecule (5M) and on the other hand a state-of-the-art 2PI (P2CK) were examined as references. Since the synthesized derivatives (5MBC, 5MPAC) are not water-soluble, and were primarily synthesized in order to set the experimental conditions for the synthesis of the water-soluble derivatives, the photochemical characterization of the compounds was not target of this study. 2PI stock solutions (0.02 mM) were prepared and transferred into quartz-cuvettes and the solutions were irradiated using LED light for up to 60 min. Irradiation intensities of 100 mW cm^{-2} were applied to the 2PI solutions at a distance of 1 cm from the LED-lens. Since the absorption spectra of the 5M-derivatives are overlapping with the 365 nm

Die approbierte gedruckte Originalversion dieser Dissertation ist an der TU Wien Bibliothek verfügbar.
The approved original version of this doctoral thesis is available in print at TU Wien Bibliothek.

LED and the spectrum of P2CK with 460 nm, the irradiation source was chosen accordingly. In contrast to the water-soluble derivatives (P2CK, 5M-derivatives), which were prepared in PBS the organo-soluble reference (5M) was dissolved in THF. Since hydrogen abstraction can occur from solvents such as THF, being in competition with the photochemical induced electron transfer, the experiment of 5M was repeated using DMSO. Both solutions exhibited a similar behavior, therefore it was assumed that the used solvents (THF, DMSO) do not contribute significantly to the photochemical behavior of 5M. The UV-Vis absorption spectra of the reference compounds are depicted below (Figure 28).

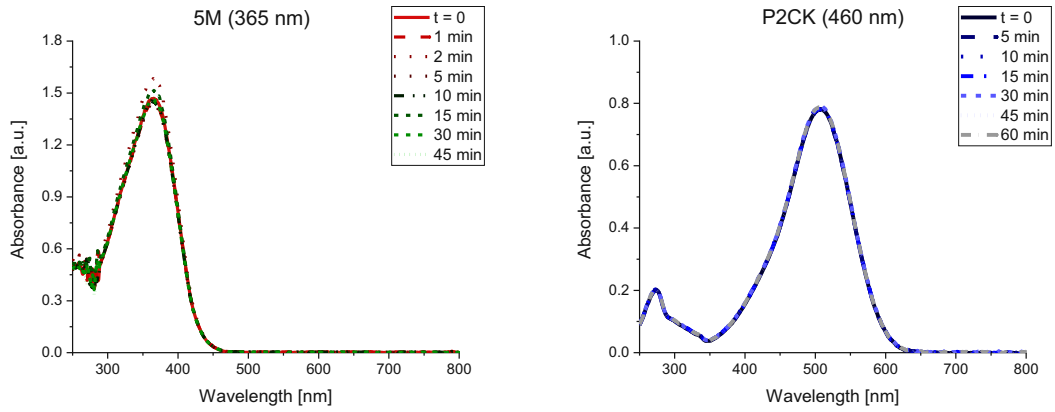

Figure 28: UV-Vis absorption spectra (arbitrary units) of the reference 2PIs (P2CK, 5M) upon irradiation with 365 nm LED light (0.04 mM 5M, THF) or 460 nm LED light (0.02 mM P2CK, PBS).

No change in absorbance was observed for the reference compounds (5M, P2CK) upon irradiation with LED light. Subsequently, UV-Vis absorption spectra of the novel 2PIs (5MSA, 5MSBA) were recorded using 365 nm (Figure 29).

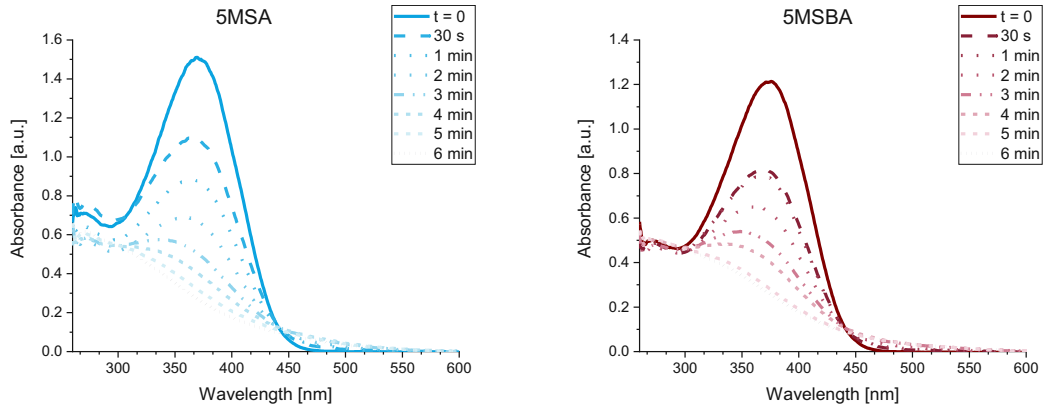

Figure 29: Absorption spectra (arbitrary units) of the novel 5M derivatives (5MSA, 5MSBA) measured upon irradiation with LED light (365 nm).

In contrast to the reference compounds (5M, P2CK), photobleaching was reported for all tested 5M-derivatives. The local absorption maxima of the 5M-derivatives (5MSA, 5MSBA) significantly decreased upon increasing irradiation time (365 nm). After 6 minutes, the absorption band of all derivatives converged to a minimum, resulting in a decomposition of the chromophore. The

Die approbierte gedruckte Originalversion dieser Dissertation ist an der TU Wien Bibliothek verfügbar.
The approved original version of this doctoral thesis is available in print at TU Wien Bibliothek.
TU Bibliothek Your knowledge hub WIEN

decomposition could be additionally observed visually, since the 2PI solutions completely lost their intensive yellow color upon irradiation. 5M exhibited an intense absorption band around 366 nm and cleavage of OE moieties was proposed to result in a restoration of the parent system (5M). Since, irradiation of the derivatives resulted in a complete loss of the absorption maxima, the photoexcitation must follow another mechanism. Since the overlap between emission band of the LED (365 nm) and the absorption maxima of the OE-2PIs (Table 3) is adjusted to be greatest possible, the energy-input seems to be sufficient to initiate a decomposition of the chromophore, accompanied by an abrupt loss of absorbance band. In contrast to the reference molecules (5M, P2CK), which do not exhibit photolabile moieties (OEs), the observed photobleaching behavior is expected to be caused as a consequence of introducing OE functionalities. Photobleaching, which is especially desired in dental applications, is often described as a consequence of α-cleavage from a visible light chromophore, specifically the loss of conjugation length might be a consequence of a fragmentation reaction and can be studied via the electronic transitions of the chromophore.[249-251] Similarly, OE-2PIs can undergo homolytic N-O bond cleavage, which can consequently lead to a decomposition of the chromophore. The rapid decrease of absorbance (after 6 min) might be an additionally promoted by the kinetic driving force of decarboxylation. Since the type of substituent are generally influencing the absorbance band of a chromophore, the synthesized chromophores show minimally red-shifted absorption maxima (Table 3). However, the shift was expected to be more profound for the SBA-derivative, since the delocalized π-systems is extended upon introducing an aromatic moiety. The red-shift of the absorption maxima of the derivatives were rated accordingly (Table 3).

Table 3: Overview on local UV-Vis absorption maxima (λ_{max}) before irradiation and maximum molar extinction coefficients (ε_{max}) of selected 2PIs.

	λ_{max} [nm]	ε_{max} [M^{-1} cm^{-1}]
5M	366	62,140
5MSA	370	68,714
5MSBA	376	66,591
P2CK	508	39,100

Since the UV-Vis absorption of radiation usually corresponds to the electronical transition between molecular orbitals, the substituent plays a fundamental role regarding the electronical structure of the 2PI. For 5M-derivatives the electron withdrawing carboxylic- and sulfonic acid groups might additionally affect the chromophore, resulting in a shift of the transition band. The photobleaching observed for OE-2PIs might be explained by following hypothesis. Since a simple OE-cleavage would result in the restoration of the original 5M-absorption profile (Scheme 23) and the absorption profile is completely lost upon irradiation (photobleaching), a complete destruction of the parent chromophore system is more likely. The proposed photochemical mechanism involves an initial cleavage of the N-O bond, producing a transition state iminyl- and acyloxy radical pair (Scheme 23), which would then undergo decarboxylation followed by a radical pair recombination to produce the corresponding imine. The generated acidic media, could

Die approbierte gedruckte Originalversion dieser Dissertation ist an der TU Wien Bibliothek verfügbar.
The approved original version of this doctoral thesis is available in print at TU Wien Bibliothek.
TU Bibliothek Your knowledge hub WIEN

possibly result in a hydrolysis to of the imine restoring the parent 5M chromophore.[207,252] The freed amines could then undergo Michael-Addition onto the chromophore resulting in a destruction of conjugation upon loss of the absorption maxima.

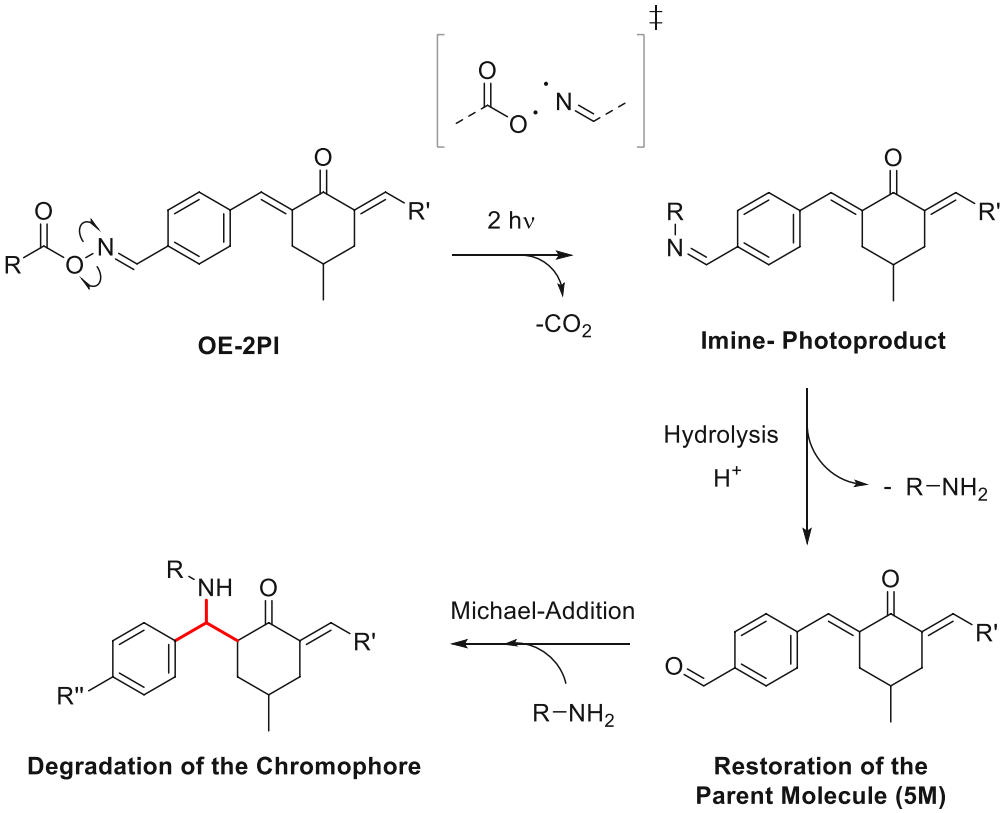

Scheme 23: Proposed mechanism of OE-cleavage upon excitation and the corresponding photodegradation of the chromophore. OE-cleavage proceeds via phototriggered N-O bond scission, forming intermediate iminyl-/acyloxy-radical pairs, followed by a decarboxylation releasing the corresponding imine photoproduct. Hydrolysis in acidic media would result in the restoration of the parent (5M) molecule[252] however, nucleophilic attack of the freed amines would lead to a complete or partial degradation of the chromophore (Michael-Addition).[253-256]

The Michael-Addition of α,β-unsaturated ketones with β-di-carbonyl compounds is a well-established topic.[257,258] However, besides the classical metal-catalyzed reactions,[259-261] various reports of Michael-Additions under metal-free conditions were found in literature including thia-[262-265] and aza-Michael-Additions.[253-256] A broad spectrum of systematic studies on O-acyl oximes are available in literature including photochemical induced rearrangement-, fragmentation-, isomerization- and cyclization mechanisms[63,266-272] along with studies on the photochemistry of the carbon-nitrogen double bond.[273] The well-established Fries-rearrangement may also be in strong competition with the photoinduced decarboxylation mechanism of OEs.[103] Studies have shown that the active photodissociative character of the N-O bond was enhanced, if the electronic structure is localized at the cleavable moiety and not delocalized across the molecule.[136] Furthermore, OEs have been studied to be efficient precursors for the construction of benzyl C-O and C-N bonds. Under visible light catalysis, substrates were coupled to primary and secondary alcohols, amines and amides.[209,274] A study suggests photoisomerization of benzylic OEs as major pathway, whereas photodecomposition being a minor process.[190] Furthermore, oxime

Die approbierte gedruckte Originalversion dieser Dissertation ist an der TU Wien Bibliothek verfügbar.
The approved original version of this doctoral thesis is available in print at TU Wien Bibliothek.
TU Bibliothek Your knowledge hub WIEN

carbamates were studied towards their capability to photodissociate by scission of their N–O bond. The resulting iminyl radicals were found to be able to proceed through a radical cyclization mechanism onto the adjacent aromatic ring.[275] A thorough study on the photochemical behavior of 5M-derivatives might be necessary to understand the mechanistic behavior and to draw profound conclusions on their photolabile behavior. Quantum mechanical calculations could give further evidence here. A detailed elucidation of the mechanism of 5M-derivatives remains a cumbersome task, exceeding the scope of this thesis. Moreover, the behavior upon one-photon excitation (UV-Vis) cannot be transferred to two-photon conditions (IR). Since the application of the 5M-derivatives as 2PIs is of major interest for this thesis, the implementation of the derivatives was studied in subsequent section using 2PP.

1.4 Two-Photon Polymerization of Oxime Ester-2PIs

The processing window of the novel 2PIs was determined via a parametric study on laser power and writing speed. Hydrogel formulations were prepared in order to assess the polymerization threshold (P_{th}) of the novel 2PIs (5MSA, 5MSBA). Due to insufficient polymerization of poly(ethylene glycol) diacrylate (no polymerization for PEG4600DA, 15 wt%, 400 mW, 2 mM 2PI), formulations were prepared based on GelMA (DS95%, 15 wt%, 2 mM 2PI). A state-of-the-art cycloketone 2PI was used as reference (P2CK). Due to insufficient laser alignment at 700 and 900 nm and laser maintenance, this study was performed at 800 nm. The processing window is related to the applied laser power in combination with the writing speed. The serial testing of both parameters is given hereafter (parameter array TU Wien Logos). First, the P_{th} for a broad range of laser powers (400 mW-10 mW, Δ = -50 mW) and writing speeds (200-1000 mm s^{-1}) was determined (not depicted). After the approximation, a detailed study on the P_{th} was performed using adjusted laser settings (400-220 mW, Δ = -20 mW, Figure 30).

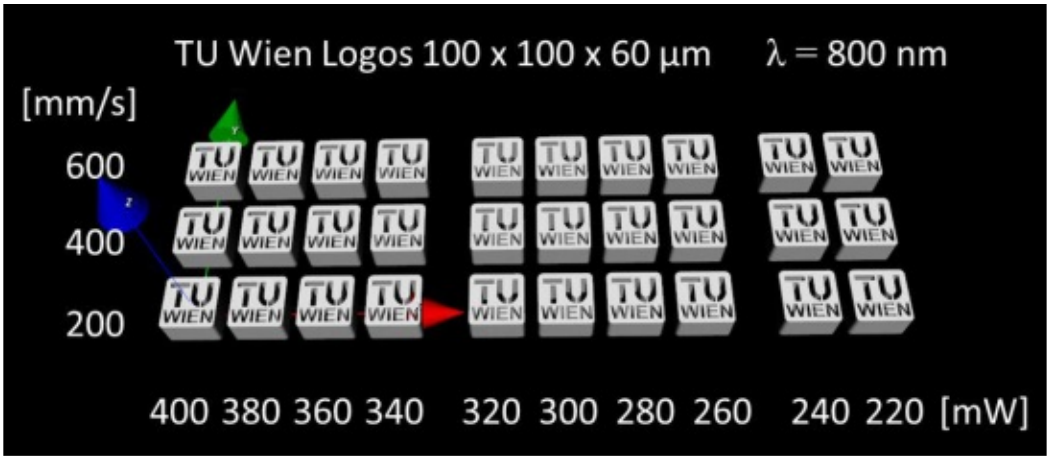

Figure 30: 2D Array of TU Wien Logos printed at 800 nm varying the laser power (400-220 mW) and writing speed (200-600 mm s^{-1}).

After 2PP processing, the formulations were immersed in PBS and incubated for 15 min at 37°C, assuring the removal of unpolymerized gelatin (post-processing). The hydrogels were imaged in

Die approbierte gedruckte Originalversion dieser Dissertation ist an der TU Wien Bibliothek verfügbar.
The approved original version of this doctoral thesis is available in print at TU Wien Bibliothek.

the brightfield (Figure 31, Figure 32) and via laser scanning microscopy (LSM700, channel 555 nm, Figure 34).

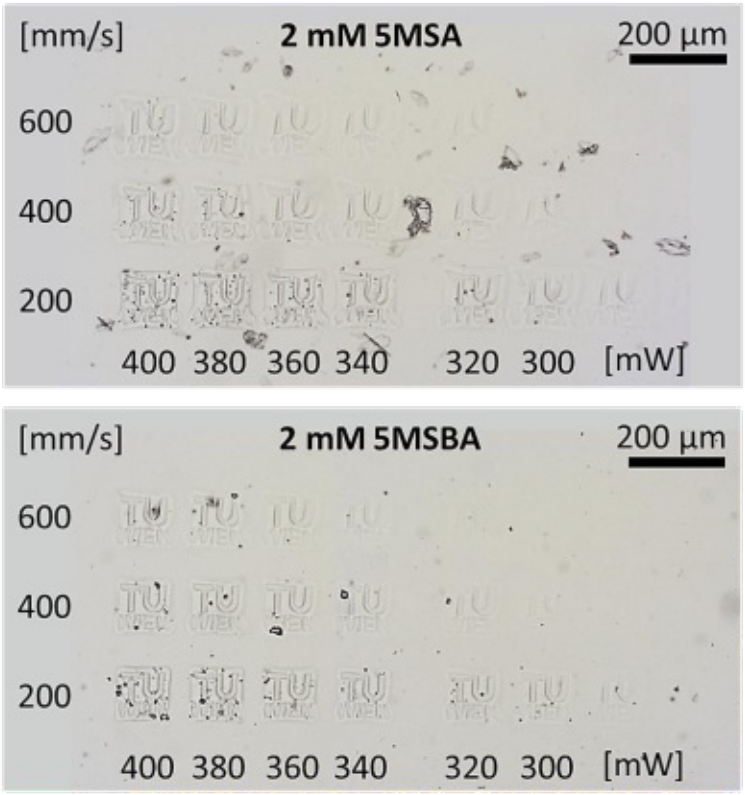

Figure 31: Brightfield images of 2PP-processed and post-processed hydrogels containing 15 wt% GELMA (DS95%) and different 2PIs (2 mM 5MSA, 5MSBA). 2D arrays of TU Wien Logos were printed in order to investigate the polymerization threshold.

Stable hydrogel structures were fabricated with average laser powers of 400 mW and writing speed of 200 mm s^{-1}. However, compared to the reference formulation (P2CK) relative high laser power was required in order to produce stable structures. For the reference formulation based on P2CK, stable cubes were fabricated down to 80 mW (Figure 32).

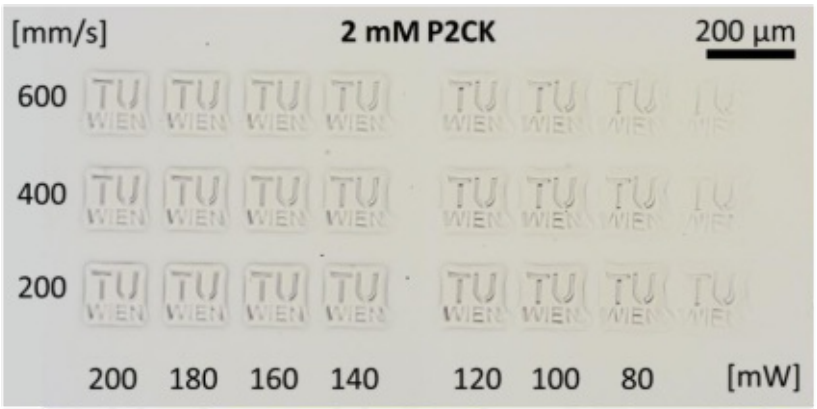

Figure 32: Brightfield image of 2PP-fabricated and post-processed hydrogel structures based on the reference formulation (2 mM P2CK, 15 wt% GELMA, DS95%).

Die approbierte gedruckte Originalversion dieser Dissertation ist an der TU Wien Bibliothek verfügbar.
The approved original version of this doctoral thesis is available in print at TU Wien Bibliothek.

Contrary to the reference formulation, bubble formation was observed during processing for OE-formulations (arrows, Figure 33). After post-processing (removal of unpolymerized gelatin), bubbles captured within the hydrogel constructs still were observed in the brightfield as dark spots (Figure 31). No bubbles were observed for the reference formulation when structured with the same laser power.

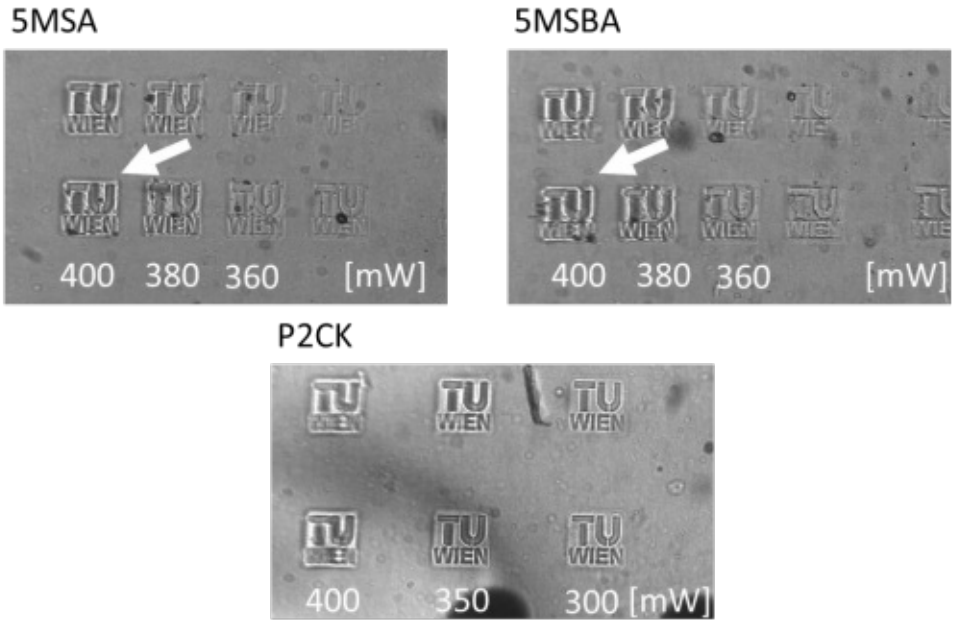

Figure 33: Bubble formation was observed for high laser powers and low writing speeds for the OE-derivatives (marked with arrows). No bubble formation was observed for the formulation based on the reference 2PI (P2CK).

3D structures, fabricated with low writing speed (200 mm s^{-1}) and high average laser power (400 mW) exhibited a higher tendency for bubble formation. This observation might be an indication for the release of gaseous CO_2 derived from OE-cleavage, as proposed in chapter 1.1. However, thermal decomposition (evaporation of water) might also induce bubble formation as a consequence from a high energy-intake in combination with relative low writing speed.[276] Still, the reference formulation (P2CK) did not exhibit such behavior, even if processed with the same energy-intake (not shown). In general, similar P_{th} were observed for the tested OE-formulations. In principle, hydrogels structured in the presence of 5MSA seemed to be more fragile compared to formulation based on 5MSBA, since they were washed away after the second post-processing treatment. However, the washing process (performed via pipette) significantly influences hydrogel stability. Although, modified µ-dishes were used, which should ensure hydrogel attachment, thorough washing might induce hydrogel-erosion. Fluorescence signals were exclusively observed for hydrogel constructs printed in the presence of P2CK and no fluorescence was detected for hydrogels involving 5M-derivatives (5MSA, 5MSBA, Figure 34).

Die approbierte gedruckte Originalversion dieser Dissertation ist an der TU Wien Bibliothek verfügbar.
The approved original version of this doctoral thesis is available in print at TU Wien Bibliothek.

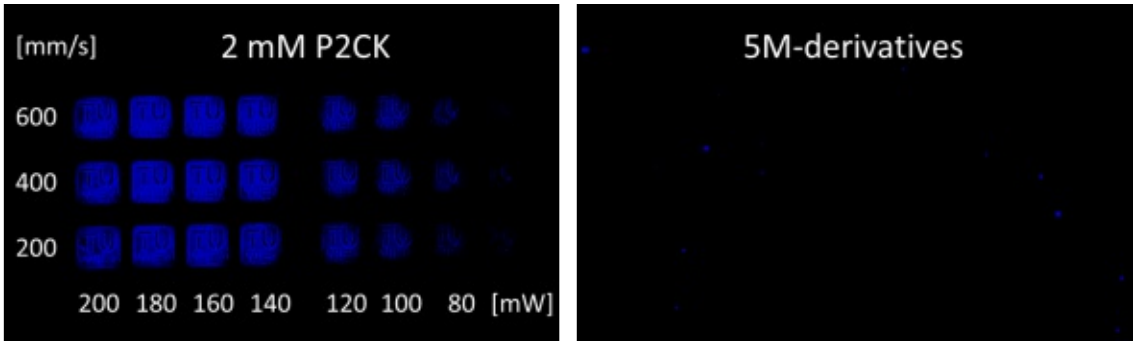

Figure 34: Confocal laser scanning microscopy images of hydrogel constructs fabricated via 2PP (GelMA 15 wt%, 95% DS, 2 mM P2CK: left). No fluorescence signals could be detected for hydrogel constructs fabricated in the presence of 5M-derivatives (5MSA, 5MSBA).

Despite the structural resemblance of 5M-derivatives with P2CK (cycloketone-core structure combined with an extended aromatic π-system), fluorescence quantum yield is a complex mechanism and depends on multiple structural and micro-environmental factors.[277] Commonly, fluorescence of 2PIs is not desired, however the handling of P2CK during confocal imaging is pleasing, since bright fluorescence can be observed. To possibly increase fluorescence signals of OE-derivatives, an increased concentration might be necessary (> 2mM), which would provide the opportunity to possibly decrease P_{th} during processing. An overview on observed threshold values is given hereafter (Figure 35).

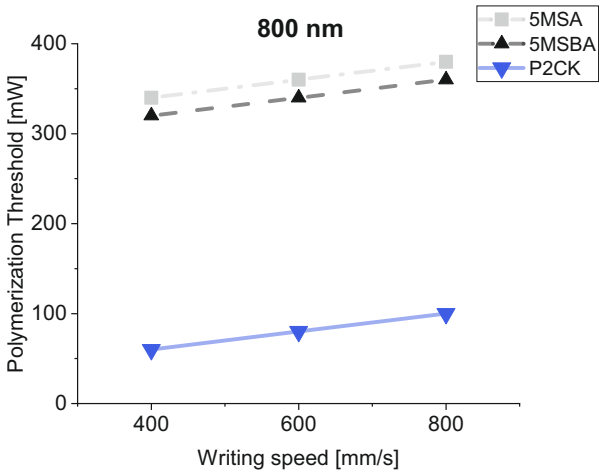

Figure 35: Polymerization threshold of each hydrogel formulation at various writing speeds (2 mM 5MSA, 5MSBA, reference P2CK, GelMA DS 95%, 15 wt% macromer content).

Lowest P_{th} was observed for formulations based on P2CK. The common trend of increasing threshold along with increasing writing speed was observed for all tested formulations. Since hydrogel formulations based on P2CK are well-established, extended data on experimental conditions (2PP structuring parameters) as well as average 2PA-cross section values on P2CK are available (white-light continuum z-scan: 180 GM at 800 nm). The set-up of the optimum 2PP structuring parameters for novel 2PI systems is of crucial importance and usually is a cumbersome task in order to produce stable micro-structures. Therefore, preliminary z-scan measurements

Die approbierte gedruckte Originalversion dieser Dissertation ist an der TU Wien Bibliothek verfügbar.
The approved original version of this doctoral thesis is available in print at TU Wien Bibliothek.
TU Bibliothek Your knowledge hub WIEN

would be necessary in order to obtain information on the 2PA-cross section for each wavelength. Besides the 2PA-cross section, the processing window is additionally influenced by the applied structuring parameters. The stability of final 3D constructs majorly depends on the slicing distance (layer spacing in z-direction) and the line spacing in x-y direction (hatch). Since the product of the applied writing speed and average laser power is yielding the laser dosage exposed to a focal volume, an increased focal overlap can on the one hand enhance polymerization efficiency (decreasing P_{th}) or on the other hand induce overexposure of the material (Figure 36).

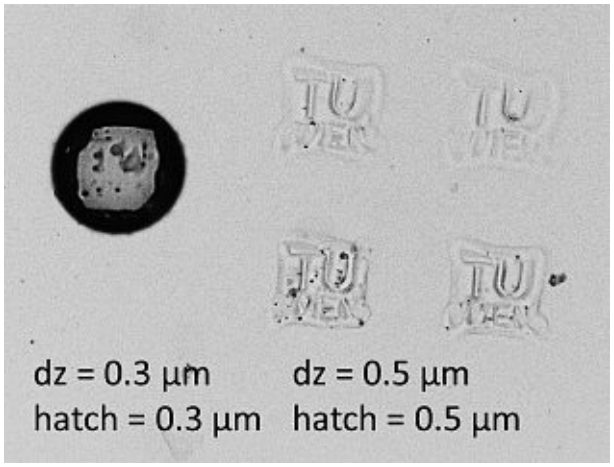

Figure 36: Brightfield images of 3D hydrogel constructs fabricated with either reduced (left) or increased (right) line- and layer spacing, risking overexposure of the material due to excessive focal overlap of the laser.

How many times every voxel is exposed to the laser can be adjusted with the applied layer- and line spacing. Here, it should be noted that the voxel size itself heavily depends on the numerical aperture of the objective, which means that a change of objective, should inevitably lead to a readjustment of laser settings (dz, hatch). Layer- and line-spacing may vary significantly, depending on objective, printed object (cube, TU Wien Logo) and the laser scan mode (e.g. pixel line). By decreasing the slicing distance in x-y and z-direction, every crosslinked voxel is exposed each time within a single layer and even more often with every layer above and underneath. Setting the accurate line- and layer spacing maintains to be a time-consuming task, even more if the optical properties of the novel formulations are unknown.

Nevertheless, the synthesized 2PIs were successfully examined via 2PP and hydrogel constructs with high-resolution were fabricated. Due to laser maintenance, a comprehensive study on a wavelength-dependent behavior of OE-derivatives could not be performed. While data on 2PA cross sections of the novel 2PIs are still missing, extended characteristic data would be necessary in order to apply the wavelength of maximum absorbance for each derivative. With the possibility of a tunable laser (700-900 nm), an extended study could be performed aiming to decrease P_{th} necessary for future cell-encapsulation experiments. Furthermore, the observed bubble formation at relative low writing speed and high average laser power could be interpreted as indication for OE-cleavage, similar to the decarboxylation mechanism investigated in literature.[141] Photodecomposition of OEs proceeds predominantly via N-O bond cleavage and the subsequent

Die approbierte gedruckte Originalversion dieser Dissertation ist an der TU Wien Bibliothek verfügbar.
The approved original version of this doctoral thesis is available in print at TU Wien Bibliothek.
TU Bibliothek Your knowledge hub WIEN

rapid decarboxylation of the corresponding acyloxy radicals.[191] Studies showed that the excited triplet states in any case play a vital role in the photodecomposition of oxime esters.[140] While monitoring the decomposition of OEs upon sensitization with various sensitizers (benzophenone, xanthone, acetonaphthone, benzil, fluorenone), researchers found a decreased chance for OE-decomposition for decreased triplet energies of the sensitizers. Electron spin resonance- (ESR) and photo-CIDNP experiments revealed knowledge on the excited triplet states, being close to their ketone parent system and abundant in π-π* character. However, another study showed that both, photoisomerization and/or photodecomposition can occur, depending on the substituent of the derivatives.[190] For aryl-derivatives, photoisomerization is proposed to be the major process, whereas photodecomposition is suggested to be the main pathway for alkyl-derivatives.

1.5 Conclusion

This thesis was aiming to develop novel water-soluble two-photon initiators (2PIs) for biomedical applications. Since current state of the art cycloketone based 2PIs are lacking biocompatibility, a novel approach was developed by introducing photolabile moieties (oxime esters, OE). The irreversible OE-cleavage upon irradiation, promoted by the kinetic driving force of decarboxylation should lower the generation of radical oxygen species, which can be one of the predominant causes of photodamage. However, besides lower excited triplet-state lifetimes (by OE-cleavage) sufficient radical generation rate is necessary for two-photon induced radical polymerization (2PP). Accordingly, a novel approach was followed to covalently couple photolabile OE functionalities to an extended aromatic chromophore. The performance of OEs in the presence of a well-established sensitizer (M2CMK) was investigated first using 2PP. A thorough study was performed, determining the polymerization threshold of acrylic monomer mixtures (ETA:TTA) containing various molar ratios of a bimolecular initiator system (Figure 37). The optimum molar ratio (1:1) between OE and sensitizer was found, paving the way towards the synthesis of a monomolecular OE-2PIs.

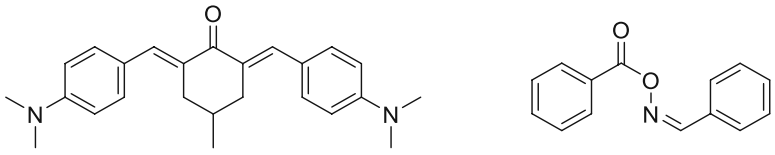

M2CMK Sensitizer

BABO Co-initiator

Figure 37: Preliminary tests were performed to investigate the two-photon initiation efficiency of a bimolecular oxime ester system.

Additionally, over-stoichiometric ratio (5:1, 10:1) of BABO:M2CMK were found to hinder radical polymerization, while increasing polymerization thresholds of the tested formulations. Since bimolecular initiator systems itself exhibit intrinsic limitations, such as reduced electron transfer between PI and co-initiator or upon regeneration of the parent system (back electron transfer) the synthesis of monomolecular 2PIs was the major goal of this thesis. A classical

Die approbierte gedruckte Originalversion dieser Dissertation ist an der TU Wien Bibliothek verfügbar.
The approved original version of this doctoral thesis is available in print at TU Wien Bibliothek.
TU Bibliothek Your knowledge hub WIEN

aldol-condensation was established as powerful tool to couple commercially available cycloketones with aldehydes, to increase the size of the chromophore. Being aware of the challenging acylation of an extended conjugated chromophore the reaction conditions were first investigated for simple model compounds (benzaldehyde, terephthalaldehyde TA). Several O-acylated oximes were prepared by first synthesizing extended aromatic aldehydes (5M) via classical Claisen-Schmidt condensation of TA and 4-methylcyclohexanone. However, the hypothesized synthesis route towards the 3-membered chromophore (3M) showed several limitations. Therefore, the isolation of the 5-membered aldehyde (5M) was a major focus. Furthermore, a higher molar extinction coefficient compared to 3M additionally confirmed this approach. Subsequently, the corresponding oximes were prepared by treating the terminal aldehydes with hydroxylamine hydrochloride in the presence of sodium acetate. Target compounds were synthesized via O-acylation of the respective oximes, including various substituents via acid chlorides (pivalic acid chloride, benzoyl chloride) and -anhydrides (succinic anhydride, sulfobenzoic anhydride, Figure 38).

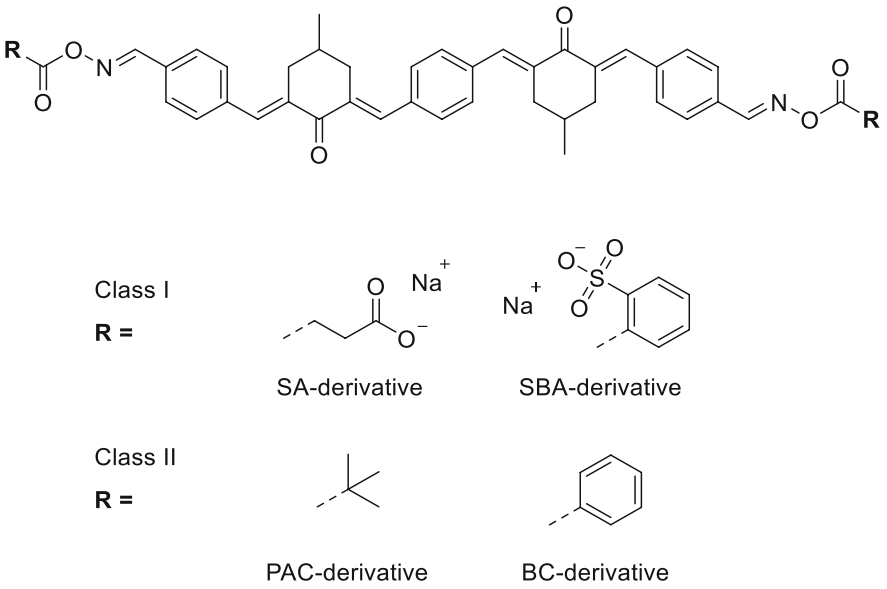

Figure 38: Synthesized monomolecular 2PIs based on an extended aromatic (5M) chromophore and attached photolabile OE-functionalities.

The synthesis was optimized using pyridine as base and DMAP (0.1 eq.) as catalyst. The organo-soluble derivatives (5MPAC, 5MBC) were successfully obtained via precipitation of the reduced mother liquor in aqueous HCl. The water-soluble ionizable derivatives (5MSA, 5MSBA) were obtained, via freeze-drying upon dissolution of the respective acids in alkaline aqueous media (pH=9). The electronic structure of the novel 2PIs was significantly influenced upon introducing additional functional groups, while increasing the conjugation length, resulting in bathochromic shifted absorption maxima compared to the starting material 5M ($\Delta\lambda_{max}$ ~ 10 nm). The novel water-soluble 2PIs (5MSA, 5MSBA) were investigated via steady-state photolysis experiments (using LED light) and compared to state-of the art cycloketone 2PI (P2CK) as well as to their organo-soluble precursor (5M).

Die approbierte gedruckte Originalversion dieser Dissertation ist an der TU Wien Bibliothek verfügbar.
The approved original version of this doctoral thesis is available in print at TU Wien Bibliothek.
TU Bibliothek Your knowledge hub WIEN

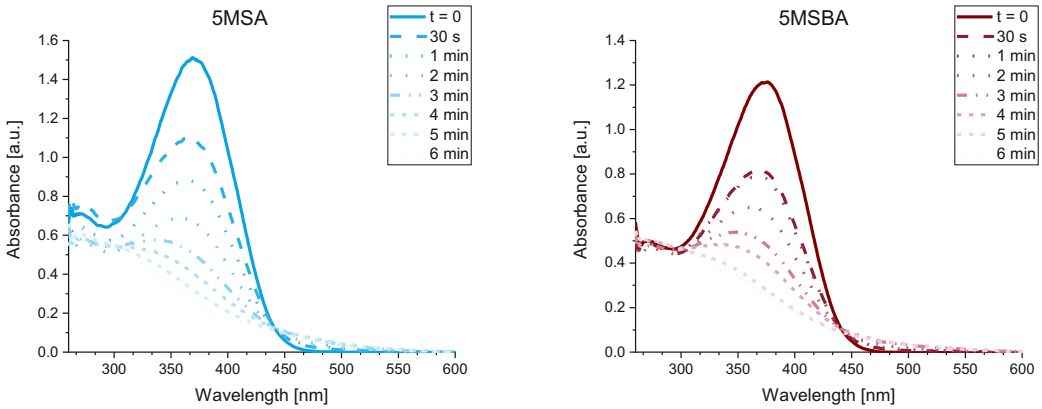

Figure 39: Photobleaching was observed upon irradiating 2PI solutions with 365 nm LED light.

In contrast to the reference chromophores (5M, P2CK), photobleaching was observed for the tested 2PIs (5MSA, 5MSBA, Figure 39). The photobleaching was proposed to be a consequence of OE-cleavage upon the loss of conjugation length and the decomposition of the chromophores. The conformational change and the reduced chance for π-π* electronical transitions are often accompanied by a considerable loss of absorbance. The photobleaching was proposed to be a consequence of OE-cleavage, subsequent hydrolysis of the imine photoproduct, where the freed amines could possibly undergo Michael-Addition onto the chromophore. In conclusion, a library of novel OE-2PIs was synthesized and tested towards their performance during 2PP. The polymerization threshold for OE-2PIs was investigated in methacrylate-modified gelatin hydrogels and compared to the state-of-the-art 2PI (P2CK). However, relatively high polymerization thresholds were observed for the novel OE-2PIs. Since the 2PA-cross section of the novel 2PIs have not been measured yet, it is difficult to find the optimum laser settings. Generally speaking, the 1PA spectrum of a sensitizer is not a straightforward guide for selecting the most efficient excitation wavelength for 2PP. This study was performed at 800 nm, being close to the maximum 2PA-cross section of P2CK (830 nm). A separate study would be required, investigating the optimum experimental set-up (laser wavelength, structuring parameters) of the novel OE-2PIs.

Die approbierte gedruckte Originalversion dieser Dissertation ist an der TU Wien Bibliothek verfügbar.
The approved original version of this doctoral thesis is available in print at TU Wien Bibliothek.

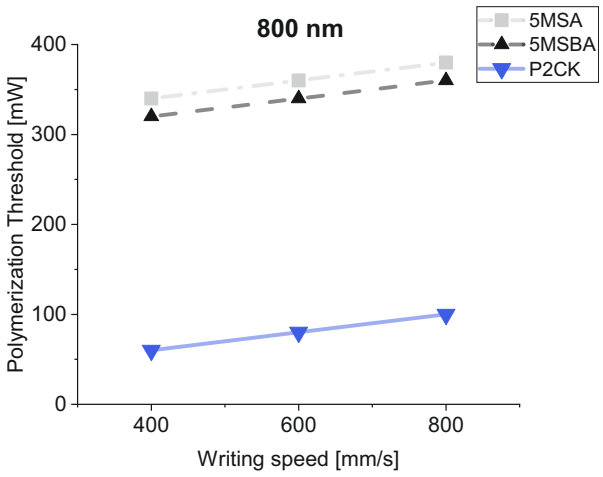

Figure 40: Polymerization threshold determined for novel 2PIs (5MSA, 5MSBA) via two-photon polymerization at 800 nm using gelatin hydrogels (15 wt% GelMA) compared to the reference (P2CK).

Still, the proposed photolabile OE-cleavage mechanism could be observed during 2PP since an extensive amount of bubble formation was observed during printing, which was not observed for the reference 2PI (P2CK). The observations are in accordance to the bubble formation mentioned from previous studies, which were proposed to be a consequence of photocleavage.[164] Similar to the proposed N_2 elimination upon irradiation, the observed bubble formation can be taken as indication for the release of gaseous CO_2 as a consequence of OE-cleavage.

Die approbierte gedruckte Originalversion dieser Dissertation ist an der TU Wien Bibliothek verfügbar.
The approved original version of this doctoral thesis is available in print at TU Wien Bibliothek.

2 Two-Photon Initiators based on Azosulfonates

2.1 State-of-the-Art Azosulfonates

Azo-compounds are an important class of molecules with significant optical switching properties and wide-spread applications.[278-280] The development of azo-compounds flourished, since the introduction of the well-established free radical initiator 2,2'-azobisisobutyronitrile in 1896.[281] Especially, the photochemical trigger has opened new pathways for the development of functional materials. Pioneering applications in biological systems were reported in the late 1970s.[282] The diagnostic value of azobenzene-modified lipids was examined towards their ability to selectively penetrate through membranes, controlled via light.[283] Furthermore, photoswitchable supramolecular hydrogels were developed formed by cyclodextrins and azobenzene polymers.[284] The characteristic photoisomerization of azobenzenes between the extended (trans) and the compact (cis) conformations was also used to study conformational preferences of protein fragments.[285,286] Furthermore, ion channels of eukaryotic cells were precisely controlled via light, enabling the specific targeting of K^+ channels.[287] Many applications in the field of optics and photonics were already described such as dye-sensitized solar cells and optical data storage.[288,289] The wide application potential of azo-motifs was recently summarized in a review (Figure 41).[290]

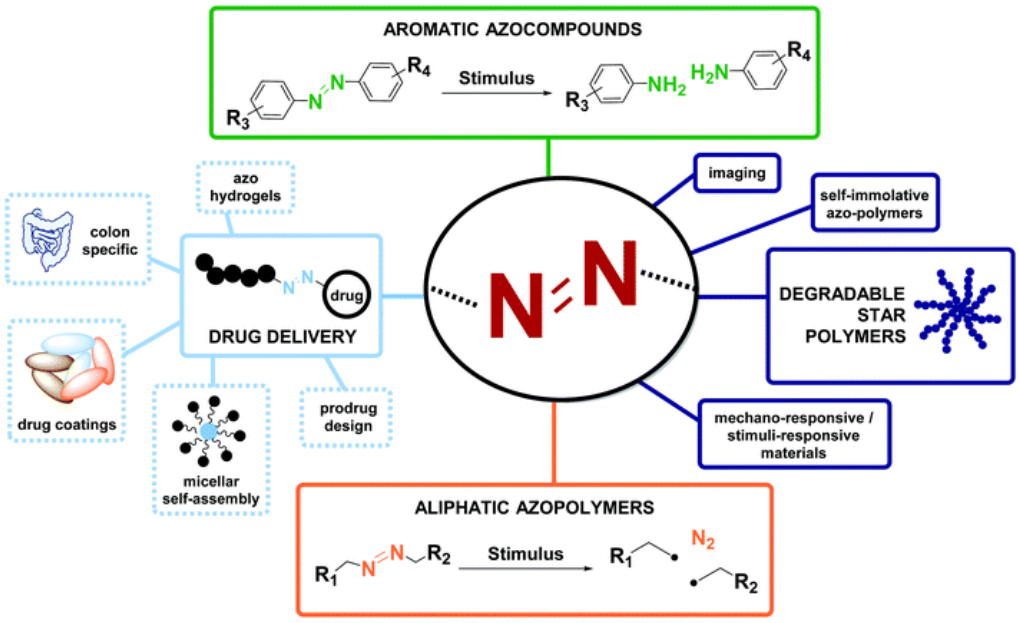

Figure 41: The application potential of azo-containing compounds.[290]

A broad variety of commercially available thermo-, photo- and mechano-responsive azo-derivatives are accessible nowadays. Especially, the photochemical trigger was of interest for this thesis, since the focus of this thesis was the development of photolabile 2PIs. Azo-compounds are able to consume UV-light due to electronical transitions, which result from the sp^3 hybridization of the nitrogen lone pair orbitals.[291] The lowest energy transition ($n \rightarrow \pi^*$) is a

Die approbierte gedruckte Originalversion dieser Dissertation ist an der TU Wien Bibliothek verfügbar.
The approved original version of this doctoral thesis is available in print at TU Wien Bibliothek.
TU Bibliothek Your knowledge hub WIEN

consequence of the strong interaction between the non-bonding and bonding nitrogen orbitals. Azo bonds can exist in two geometrical isomers, the trans-(E) and cis (Z) species, due to the trigonal planar geometry derived from the sp^2 hybridization of the nitrogen atoms. The strong tendency of the azo-motif to dissociate proceeds mainly via two major mechanisms.[292-294] On the one hand, the azo-motif can decompose via a concerted mechanism including the simultaneous dissociation of the two C-N bonds ($\Delta H \sim 460 \cdot mol^{-1}$).[295] On the other hand, one C-N bond can decompose (non-concerted) pursued by a fast decomposition of the unstable R-N_2· radical (Scheme 24).

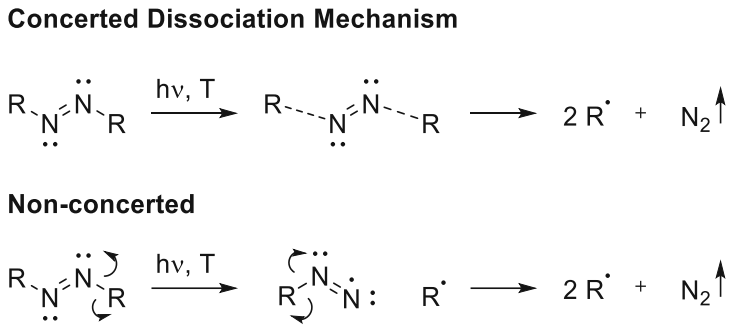

Scheme 24: Two major pathways for the decomposition of excited state azo-molecules.[292-294] The C-N bond can either decompose in a concerted mechanism, which is energetically preferred (above). However, dissociation can also occur via one C-N bond, followed by a fast decomposition of unstable radical intermediates (R-N_2·).

Theoretical calculations revealed that the concerted cleaving mechanism is energetically preferred, although noticing that the dissociation of unsymmetrical azo compounds depends on the structure of R· radicals and their dissociation rate constants. Additionally, photoisomerization seems to play a critical role in the decomposition mechanism, since acyclic cis-azoalkanes, which are produced by irradiation of the trans isomers, are of higher energy and lose nitrogen more readily than trans-azoalkanes.[296] Due to their efficient dissociation mechanism, driven by the release of gaseous nitrogen, azo compounds were already widely studied as free radical initiators. A detailed list of available azo-initiators can be found in literature.[297]

Especially, the photochemically-, electrochemically and thermally initiated decomposition of azosulfonates (AS) was soon reported.[298] The stability of AS and their radical products were observed in detail amongst many other azo compounds (azophosphonates, azosulfones, azosulfides, triazenes, penta- and hexazadienes, diazonium salts). Electron paramagnetic resonance spin trapping experiments revealed the decomposition of AS into their corresponding substituted aryl- and ·SO_3^- radical adducts. Interestingly, water-soluble AS's decompose not only photolytically into aryl- and sulfite radicals, but can simultaneously trap radicals to form spin-adducts (hydrogen abstraction from photochemically activated complexes with solvents leading to R-C_6H_4-NH-N· SO_3^-). Additionally, AS compounds were already applied for radical polymerization together with acrylic monomers.[299,300] Hence, AS are especially promising candidates for the development of photocleavable 2PIs. Key factors in the development of novel 2PIs are the fine-tuning of intramolecular charge-transfer, conjugation length and coplanarity.[301]

Die approbierte gedruckte Originalversion dieser Dissertation ist an der TU Wien Bibliothek verfügbar.
The approved original version of this doctoral thesis is available in print at TU Wien Bibliothek.

Due to the limited availability of 2PIs with enhanced σ_{2PA} in the region around 900 nm, there is a strong demand for novel 2PIs with bathochromic shifted absorption maxima. In general, the absorption profile, -coefficient and charge separation can be guided via the introduction of conjugated chromophores as well as via the attachment of electron donating/-accepting substituents. Recently, diazosulfonates were introduced as efficient 2PIs for direct cell encapsulation.[164] Although, stilbenes show relatively small π-conjugation, commonly associated with low σ_{2PA}, dendritic stilbenes were proven to exhibit enhanced σ_{2PA} with increasing numbers of stilbene moieties.[302] Especially, tetrapotassium salts of stilbenes were prepared in order to attach strong hydrophilic sulfonate moieties, hence increasing water-solubility (Figure 42).

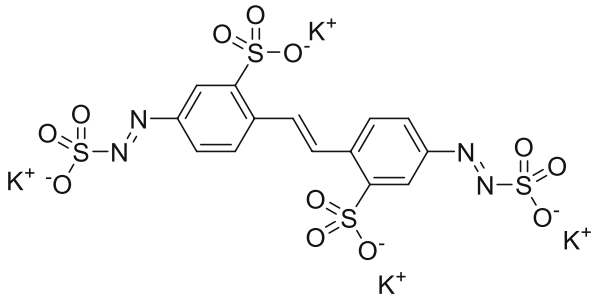

Figure 42: Azosulfonate-based 2PI used for direct cell encapsulation.[164]

Water-solubility is a crucial factor guiding the successful application of 2PIs in aqueous systems. Simple water-soluble, commercially available dyes, such as xanthene derivatives (rose bengal, eosin Y, rhodamine B and erythrosine) were already used as 2PIs in order to fabricate 3D objects.[154,303,304] In general, a variety of two-photon active dyes was already described in literature.[301] Especially, azo dyes have attracted researchers, since they are the largest group among organic pigments.[305] Combined with their ability to be modified towards AS, azo dyes are highly promising candidates for the development of photolabile 2PIs. For this thesis, compounds with absorption maxima (λ_{max}) close to 400-500 nm are preferred, to enhance the σ_{2PA} in the far-IR.[120]

2.2 Synthesis of Azosulfonate-based Two-Photon Initiators

This thesis is focusing on the development of novel 2PIs based on azo dyes. In general, azo compounds are belonging to the water hazard classification 3 (highly dangerous for aquatic ecosystem) and must be always separately treated as wastewater. The majority of azo dyes commonly consist of poorly water-soluble organic compounds. However, strong hydrophilic functional groups enhance water-solubility of conjugated aromatic chromophores. Aromatic sulfonate groups in general are widely used in order to increase water-solubility due to the advantage of being negatively charged in aqueous solution over a broad range of pH.[306,307] The photochemical radical decomposition mechanism of azosulfonates (AS) was already described in literature, which is proceeding via homolytic C-N bond cleavage under release of gaseous nitrogen

Die approbierte gedruckte Originalversion dieser Dissertation ist an der TU Wien Bibliothek verfügbar.
The approved original version of this doctoral thesis is available in print at TU Wien Bibliothek.
TU Bibliothek Your knowledge hub WIEN

and the formation of the corresponding aryl- and sulfonyl-based radicals.[298,308] Driven by the knowledge of previous studies, where AS-2PIs were studied as biocompatible alternatives for 2PP cell encapsulation experiments,[164] a major focus of this thesis was the development of novel AS-2PIs for radical photopolymerization. For a straightforward synthesis approach, commercially available azo dyes should be used as starting materials. In general, di-azo compounds are synthesized via electrophilic substitution of aryl diazonium cations with aromatic coupling agents. Diazonium salts are weak electrophiles readily reacting with electron rich species, such as substituted arenes. However, instead of coupling diazonium salts with aromatic moieties, here, sulfite ions are used as coupling agents. First, diazotization of aromatic amines in the presence of $NaNO_2$ in strongly acidic aqueous solution leads to the formation of diazonium salts in situ.[309] Since this reaction is pH dependent the acid is necessary to liberate nitrous acid from $NaNO_2$ (Scheme 25).[310]

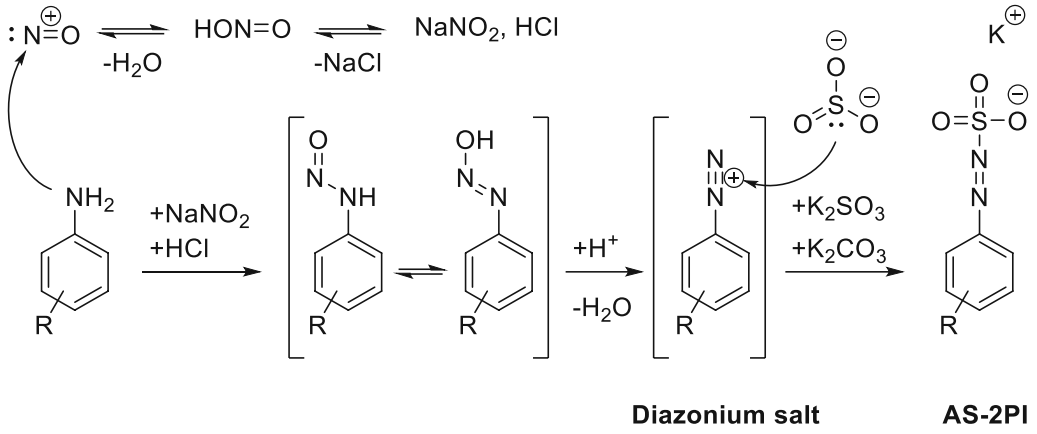

Scheme 25: Synthesis of azosulfonate-based 2PIs (AS-2PI) via diazotization of aromatic amines followed by an azo-coupling of the diazonium salts with sulfites.

The stability of diazonium salts is strongly influenced by the type counterion, therefore they are usually not isolated but directly converted to AS-derivatives as intermediates in a one-pot procedure.[310] In the second step, the nucleophilic addition of sulfites leads to the formation of AS-2PIs. Nowadays, chromophores with efficient 2PP structuring properties in the region of 900 nm are desired. Therefore, precursor molecules with enhanced UV-Vis absorption properties above 400 nm are required. Literature research on commercially available, water-soluble azo dyes was performed and revealed a number of promising compounds (Table 4).

Die approbierte gedruckte Originalversion dieser Dissertation ist an der TU Wien Bibliothek verfügbar.
The approved original version of this doctoral thesis is available in print at TU Wien Bibliothek.

Table 4: Commercially available water-soluble azo dyes with amino groups available for functionalization.

Azo dye	λ_{max} [nm]	CAS Number
Disperse Black 9	461	20721-50-0
Direct Blue 15	592	2429-74-5
Congo Red	498	14684-01-6
Evans-Blue	590	314-13-6
Bismarck Brown Y	465	10114-58-6
Bismarck Brown R	465	5421-66-9
Naphthol Blue Black	618	1064-48-8
Reactive Black 5	597	17095-24-8
Trypan Blue	590	72-57-1

Bismarck Brown Y (BB) and Congo Red (CR) were chosen as suitable compounds for the development of AS-2PIs. The terminal aromatic amines should be modified according to the above-mentioned synthesis strategy (Scheme 25, Figure 43).

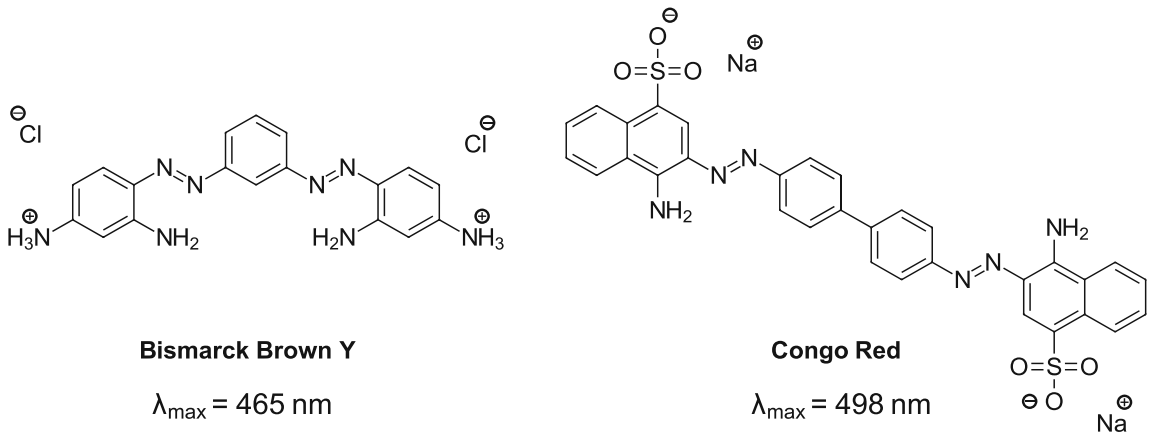

Figure 43: Commercially available azo dyes Bismarck Brown Y and Congo Red serving as starting materials for the development of novel 2PIs.

Both azo dyes were first introduced at the end of the 19th century and have been widely used in cotton-dyeing.[311] The dying process usually consists of ionic adhesion of anionic dyes to cationic proteins of wool. However, BB is classified as cationic di-azo dye, usually consisting of a mixture of oligomers, which is mostly applied on dyeing of polyester and acrylic fibers.[312] The characteristic absorption spectra of CR and BB were recorded via UV-Vis measurements (Figure 44).

Die approbierte gedruckte Originalversion dieser Dissertation ist an der TU Wien Bibliothek verfügbar.
The approved original version of this doctoral thesis is available in print at TU Wien Bibliothek.

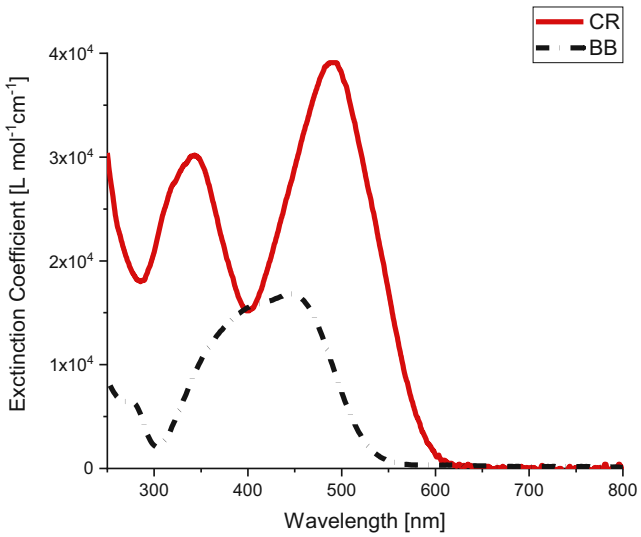

Figure 44: Maximum molar extinction coefficients of CR and BB in PBS (10 µM). ε^{CR} = 39,100 M^{-1} cm^{-1}, ε^{BB} = 16,820 M^{-1} cm^{-1} and local absorption maxima for CR: $\lambda_{max,1}$ = 498 nm, $\lambda_{max,2}$ = 341 nm and BB: λ_{max} = 446 nm.

A remarkable difference in calculated molar extinction coefficients was observed. CR showed significantly higher ε at λ_{max} (39,100 M^{-1} cm^{-1}) compared to BB at λ_{max} (16,820 M^{-1} cm^{-1}). BB and CR should be used to synthesize 2PIs based on these chromophores following proposed approach. Diazotization of terminal amino groups and subsequent coupling with sulfite ions should be performed. First, the synthesis of Azo-BB was performed using parameters mentioned in literature (Scheme 26).[164]

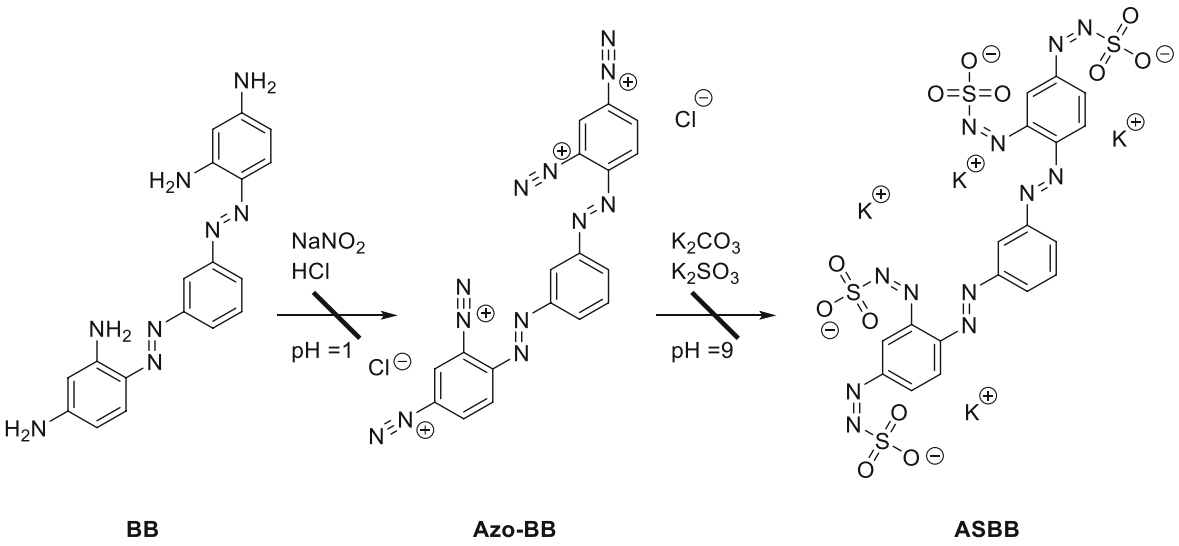

Scheme 26: Failed synthesis approach for the modification of Bismarck Brown Y (BB). Diazotization of aromatic amines and subsequent coupling to sulfites did not lead to the formation of azosulfonate Bismarck Brown Y (ASBB).

BB was purchased as certified stain, commonly used in for biological staining processes. However, BB is proposed having a dye content of 50%, which included laborious procedures to obtain the starting material in sufficient purity. Commonly, BB is synthesized via the treatment of m-phenylenediamine with nitrite in acidic solution.[311-313] The final products usually consist of

Die approbierte gedruckte Originalversion dieser Dissertation ist an der TU Wien Bibliothek verfügbar.
The approved original version of this doctoral thesis is available in print at TU Wien Bibliothek.
TU Bibliothek Your knowledge hub WIEN

mixtures of mono-azo, di-azo, and poly-azo dyes. The industrial synthesis includes a salting-out mechanism immediately after dye-formation in the presence of sodium chloride. However, the formation of poly-azo dyes can rarely be prevented. Azo dyes in general exhibit a high tendency to form H-bonds, electrostatic- and hydrophobic interactions as well as van der Waals forces, leading to self-aggregated dimers and higher aggregates.[305] Likewise, the formation of water-insoluble dye aggregates complicated the synthesis process here. Principally, BB is of interest for the development of 2PIs but the limited dye content (50%) of the technical product and the time-consuming purification was not suitable for a systematic study being outside of the scope of this thesis. Therefore, the modification of CR was performed instead, according to the proposed mechanism (Scheme 27).

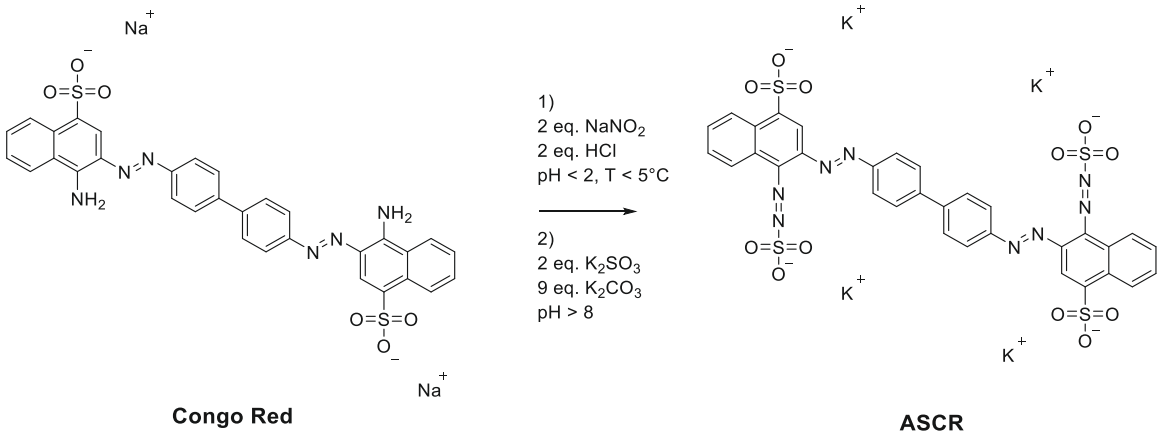

Congo Red **ASCR**

Scheme 27: Synthesis of ASCR via diazotization (1) of commercially available Congo Red (CR) in acidic media and subsequent azo coupling with sulfites in basic media (2).

At first, the commercially available CR was recrystallized in hot purified water (5% solution) to avoid extensive agglomeration during synthesis. Sonication (40°C) can facilitate solvation of the azo dye reducing the extended π-stacking behavior of CR. Upon removal of undissolved agglomerates, the red aqueous solution was left to recrystallize at 7°C for 4d. For diazotization, a strong acid (HCl) was necessary to liberate nitrous acid from $NaNO_2$ in situ. Subsequent, protonation and elimination of water provides the reactive intermediate (nitrosonium ion, NO^+).[314] Therefore, a diluted solution of the recrystallized CR (1 g/L) was prepared. The CR was then cooled to 7°C and added to the extensively stirred solution of nitrous acid. Diazotization of the aromatic amines was proceeded overnight at a constant temperature of <5°C. The pH was accurately monitored (pH 1), since strong basic conditions can promote the formation of diazohydroxide, further dissociating into diazotate ions inhibiting the coupling reaction.[309] The formation of diazonium salts was monitored via selective staining the amino groups of CR via TLC (anisaldehyde- and cerium molybdate stain). A one-step approach was implemented since the attempted isolation of the diazonium salt failed multiple times. The intermediate diazonium salt was coupled to sulfites by slowly adding the cooled reaction solution to a cooled alkaline aqueous solution of K_2SO_3 and K_2CO_3.[315-319] The reaction solution was vigorously stirred for 8 h (23 °C), while monitoring the pH necessary for coupling (pH >8). The isolation of ASCR salt was performed via

Die approbierte gedruckte Originalversion dieser Dissertation ist an der TU Wien Bibliothek verfügbar.
The approved original version of this doctoral thesis is available in print at TU Wien Bibliothek.
TU Bibliothek Your knowledge hub WIEN

salting-out. Here, pH and the concentration of the analyte (> 20 wt%) as well as high salt concentrations are crucial (> 30 g/L) for an effective salting-out approach.[320-322] The isolation and precipitation of ASCR by simple cooling the reaction solution (7°C) was not successful neither was the process of freeze-drying. The high pka (~ 7) of the sulfonic acids might have prevented the crystallization. Furthermore, precipitation in the presence of NaCl as suggested by literature neither was successful.[234] The successful salting-out of ASCR was performed at high sample concentrations (25 wt%), separating any solids before cooling the solution (7 °C) for multiple days in the presence of high salt concentrations (9 eq. K_2CO_3). The obtained olive-green solids were separated via suction filtration and washed with minimum amount of purified water. Recrystallization from purified water resulted in the pure product (30% th.). The sodium adduct ($C_{32}H_{18}K_4N_8NaO_{12}S_4^+$) of the ASCR molecular peak was confirmed via HR-MS (ESI^+). The azo-sulfonate fragment ($C_{22}H_{17}N_5NaO_6S_2^+$) was confirmed via LC-MS by detecting the exact mass (534.05 g/mol) using a reversed phase column with a covalently modified pentafluoro phenyl phase (C18-PFP, eluent: MeOH with 0.1% TFA). Additionally, AT-IR spectra (KBr window) of ASCR were measured and compared to molecular vibrations recorded for CR and compared to vibrations of azo dyes presented in literature.[323-326] Transmission spectra of ASCR and CR enabled the observation of the characteristic C-N stretching vibrations (1350 cm^{-1}), C=C conjugated aryl vibrations (1600 cm^{-1}) and the C-H stretching vibrations of aryl protons (2900 cm^{-1}). The dominant stretching frequency of the amino groups of CR (3470 cm^{-1}) is overlapping with the stretching vibrations of the OH groups of ASCR derivatives. Therefore, the introduced azo-groups of ASCR were confirmed by the additional N=N stretching frequencies at 1495 cm^{-1}. Finally, the successful synthesis of ASCR was verified by HR-MS measurements in ultrapure water. The sodium adduct of ASCR was confirmed using ESI+ ionization mode. UV-Vis spectra of ASCR were measured and compared to the absorption of the starting material (CR, Figure 45).

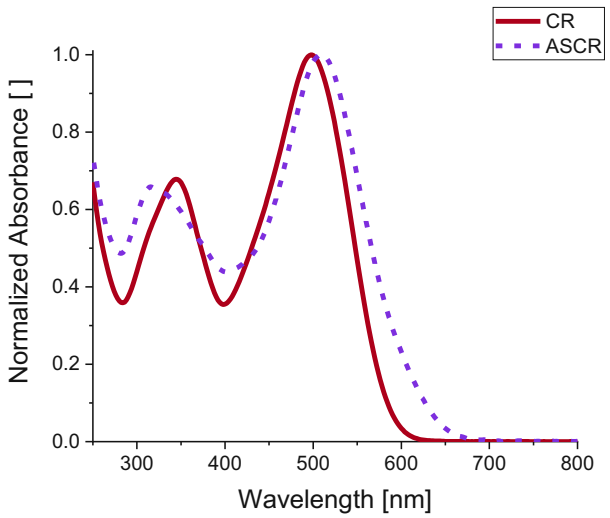

Figure 45: UV-Vis spectra of CR (λ_{max} = 498 nm) and the azo-sulfonate derivative (ASCR, λ_{max} = 510 nm). Maximum molar extinction coefficients for CR (ε_{max} = 121,920 $M^{-1}cm^{-1}$) and for ASCR (ε_{max} = 89,606 $M^{-1}cm^{-1}$) were calculated accordingly.

Die approbierte gedruckte Originalversion dieser Dissertation ist an der TU Wien Bibliothek verfügbar.
The approved original version of this doctoral thesis is available in print at TU Wien Bibliothek.
TU Bibliothek Your knowledge hub WIEN

Two local absorption bands were observed (350 nm, 500 nm), assigned to the distinct electronic transitions (π-π*) of the respective polycyclic moieties (biphenyl- and naphthalin moiety). Upon modification, a bathochromic shift of the absorption maximum (Δ = 12 nm ASCR vs CR) was observed, similar to the modification of DAS (Δ = 31 nm), proposed to be derived by the introduction of the flanking azosulfonate moieties (electronic acceptors).[164] Since CR is especially prone to form water-insoluble dye-aggregates, low sample concentrations and sonication are required to obtain spectra with sufficient resolution. Additionally, the hydrophobic biphenyl moiety as well as intramolecular hydrogen bonding between amino- and azobenzene functionality often results in colloidal solutions of CR suppressing the signal to noise ratio.[327,328] Although, multiple attempts were made to record ^{13}C-spectra in order to monitor the conversion of the carbon adjacent to the amino groups of CR, insufficient signal to noise ratio was obtained. Still, downfield-shifted signals of the aromatic protons of the naphthalene moiety and missing amino signals were observed for recorded ASCR spectra.

For the characterization of the novel 2PI (ASCR), the reference 2PI (DAS) was additionally synthesized via diazotization of the commercially available starting material 4,4'-diamino-2,2'-stilbenedisulfonic acid (DADS, Scheme 28).[164]

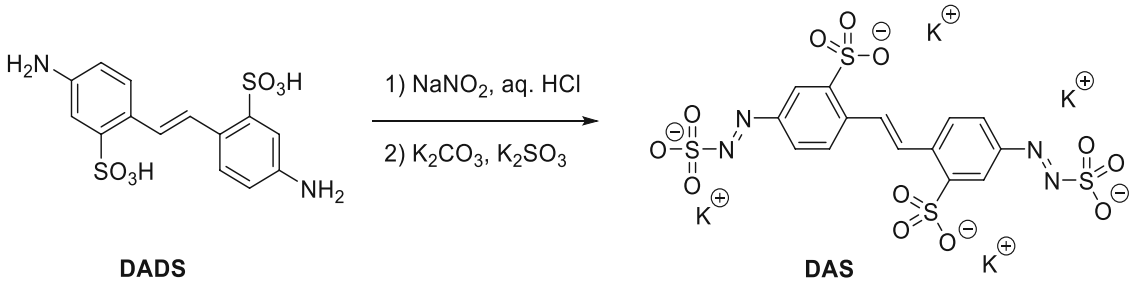

Scheme 28: Synthesis of the water-soluble state-of-the art reference 2PI (DAS).

2.3 Characterization of Azosulfonate-2PIs

2.3.1 Photoreactor Studies

To investigate the photochemical behavior of the novel azo-based 2PI (ASCR) photoreactor studies were performed. As reference material, the state-of-the-art 2PI (DAS) and the commercially available starting materials (CR, DADS) were examined additionally (Figure 46).

Die approbierte gedruckte Originalversion dieser Dissertation ist an der TU Wien Bibliothek verfügbar.
The approved original version of this doctoral thesis is available in print at TU Wien Bibliothek.

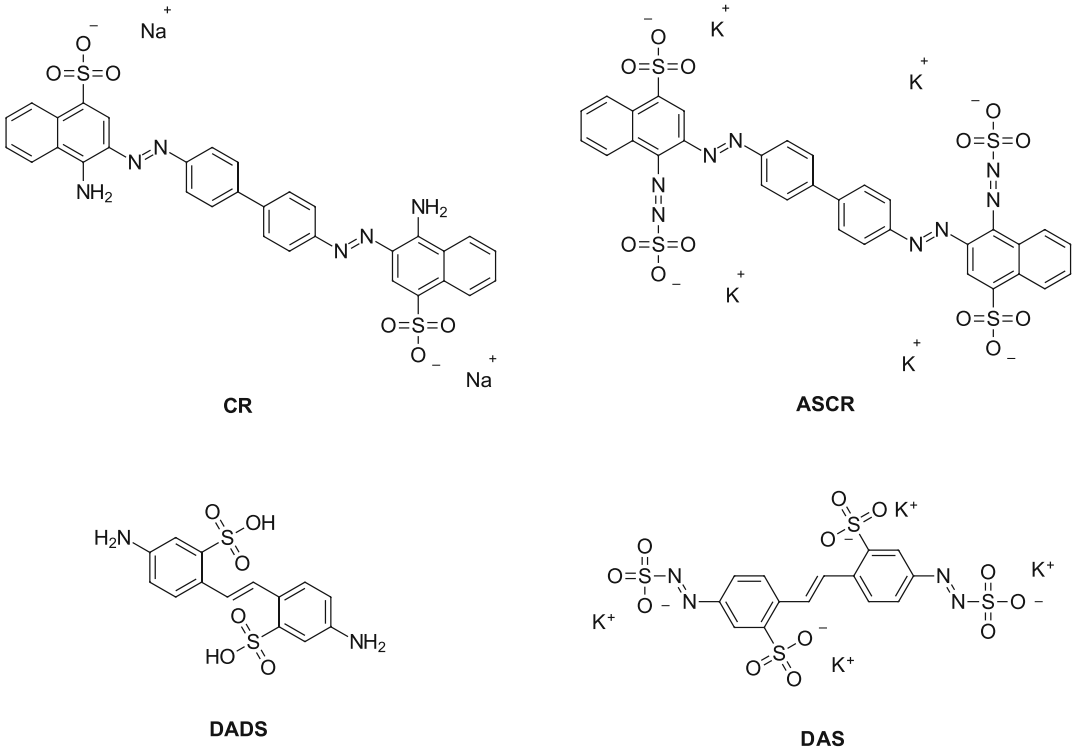

Figure 46: Molecular structures of azo-sulfonate based 2PIs (ASCR, DAS) and the corresponding starting materials (CR and DADS).

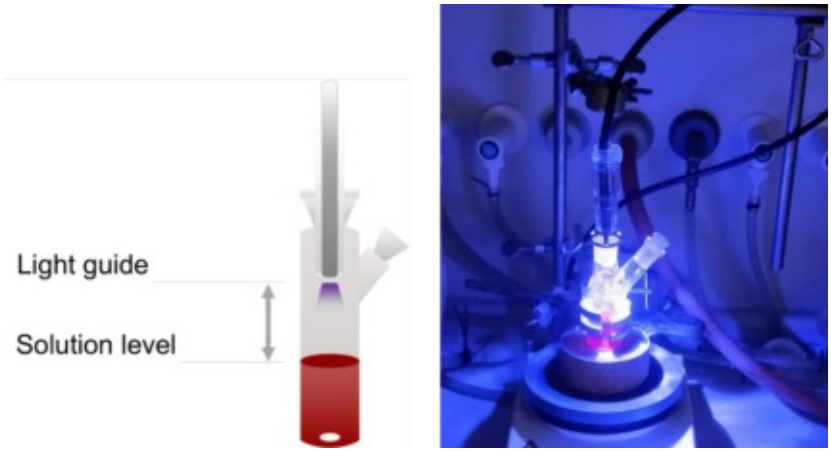

Figure 47: Photoreactor studies were performed in a two-necked flask, which was equipped with a quartz adapter coupled to a lightguide. Samples were collected before and during irradiation with LED light (365 nm, 460 nm) at defined intervals.

A two-necked photoreactor flask containing a stirred solution of 2PI (1 mM in 20 mL PBS) was irradiated with LED light (365 nm, 460 nm) from the top (Figure 47). The LED heads were connected to a controller and a lightguide, which was coupled to a quartz adapter at the photoreactor. Irradiation intensities at the solution level were set to 100 mW cm^{-2} (corresponding to 290 mW cm^{-2} behind the quartz adapter for 365 nm and 350 mW cm^{-2} for 460 nm). The distance between the solution level inside of the photoreactor and the lightguide immersed into a quartz adapter was 1 cm. UV-Vis spectra before irradiation (t = 0) and the corresponding absorption maxima of each 2PI are given in Figure 48.

Die approbierte gedruckte Originalversion dieser Dissertation ist an der TU Wien Bibliothek verfügbar.
The approved original version of this doctoral thesis is available in print at TU Wien Bibliothek.

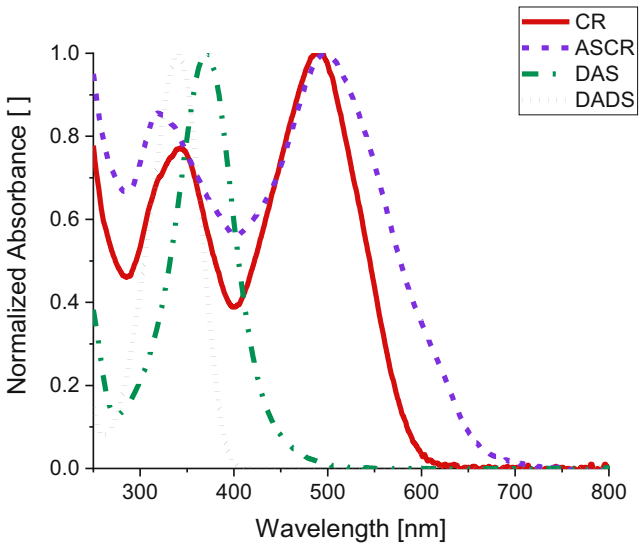

Figure 48: Normalized UV-Vis absorption spectra of selected 2PIs in PBS (0.04 mM ASCR, DAS, DADS and 0.01 mM CR) and their absorption maxima ($\lambda_{max}^{(CR)}$ = 498 nm, $\lambda_{max}^{(ASCR)}$ = 510 nm, $\lambda_{max}^{(DADS)}$ = 341 nm, $\lambda_{max}^{(DAS)}$ = 372 nm) before irradiation.

At defined intervals (0 min, 5 min, 10 min, 15 min, 30 min, 45 min, 60 min) samples (300 µL) were collected in brown glass vials and diluted with PBS in order to maintain linearity of Lambert-Beer's law at the photometer (final concentration: 0.01 mM for CR, 0.04 mM for ASCR, DAS and DADS). Molar extinction coefficients are given in Table 10. UV-Vis spectra were recorded measuring PBS as background spectra (Figure 49, Figure 50).

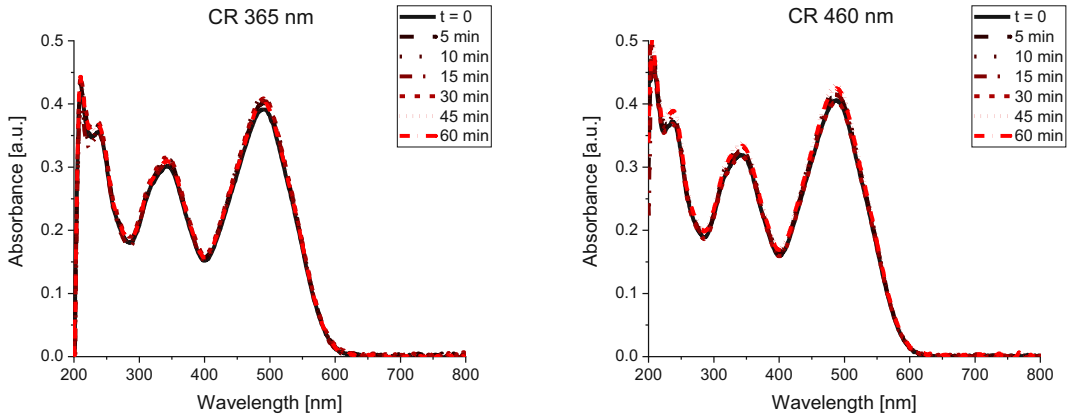

Figure 49: CR before (t=0) and during irradiation with LED light (365 and 460 nm) for up to 60 min (0.01 mM in PBS). CR is showing an additional local absorbance band at $\lambda_2^{(local)}$ = 346 nm, besides the absorption maximum at $\lambda_{max}^{(CR)}$ = 498 nm.

Die approbierte gedruckte Originalversion dieser Dissertation ist an der TU Wien Bibliothek verfügbar.
The approved original version of this doctoral thesis is available in print at TU Wien Bibliothek.

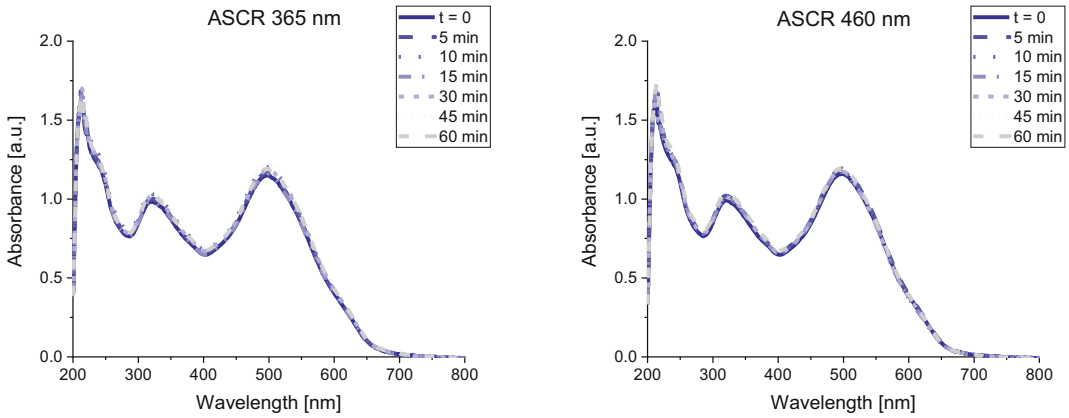

Figure 50: ASCR before irradiation with 365 nm and 460 nm (t=0) and upon irradiation up to 60 min (0.04 mM in PBS). ASCR is showing an additional local absorbance band at $\lambda_2^{(local)}$ = 342 nm, besides the absorption maximum at $\lambda_{max}^{(ASCR)}$ = 510 nm.

First, 460 nm LED light was used due to the effective overlap between extinction source and absorption profile of CR and ASCR. However, no photobleaching of CR and ASCR was observed. To investigate the effect of the irradiation source, both solutions were prepared once more and irradiated using 365 nm LED light. Neither by adjustment of the controller to the maximum irradiation intensity (200 mW cm^{-2} for 365 nm and 240 mW cm^{-2} for 460 nm, 1 cm distance from the quartz adapter) nor heating of the sample could enable a photobleaching effect of the 2PI solutions.

Subsequently, UV-Vis spectra of the state-of-the-art 2PI system (DAS) and the corresponding starting material (DADS) were recorded before and upon irradiation with LED light. Due to the characteristic absorption profile of DAS (371 nm) and DADS (341 nm), the irradiation source was chosen accordingly (365 nm). Additional samples (300 µL each) with a narrower interval were collected (0 min, 10 s, 30 s, 1 min, 5 min, 10 min, 15 min, 30 min, 45 min, 60 min, Figure 51).

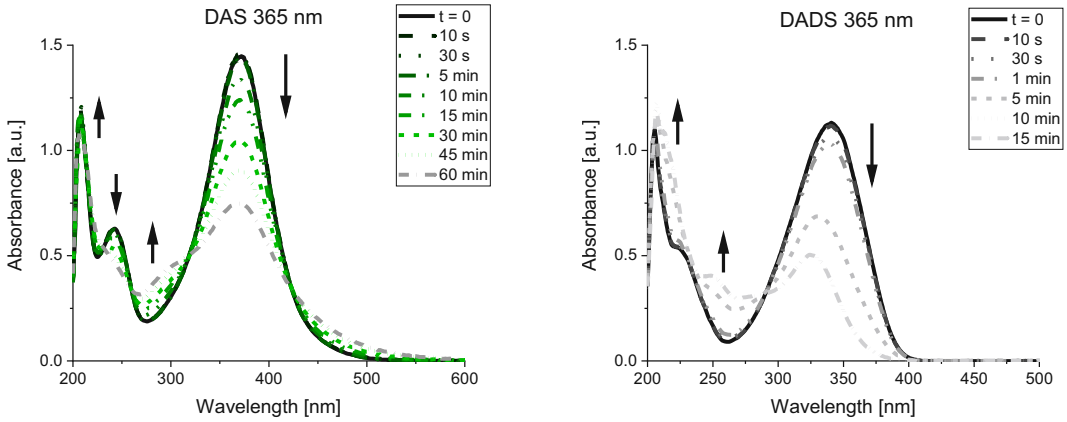

Figure 51: Photoisomerization of DAS and DADS upon irradiation with LED light (365 nm, 0.04 mM in PBS).

Contrary to what was expected, photobleaching was observed for both compounds (DAS, DADS) upon irradiation. As previously proposed in literature, photobleaching was assumed to be derived by the cleavage of terminal azosulfonate groups.[164] However, the missing terminal

Die approbierte gedruckte Originalversion dieser Dissertation ist an der TU Wien Bibliothek verfügbar.
The approved original version of this doctoral thesis is available in print at TU Wien Bibliothek.
TU Bibliothek Your knowledge hub WIEN

azo-functionalities of the starting material (DADS) might arise the assumption that photobleaching is more likely to be derived from a photoisomerization of the stilbene moiety (Figure 46). Previous studies attempted to elucidate the photoinitiation mechanism of DAS via laser flash photolysis (LFP) and chemically induced dynamic nuclear polarization (CIDNP), however never including the starting material (DADS).[329] Besides that, an attempt was made to investigate the reason for the improved cytocompatibility of DAS compared to P2CK via singlet oxygen luminescence measurements, but no full elucidation of the mechanism was achieved.[164]

Stilbenes, azobenzenes and rotaxanes are the most widespread photochromes and their photoisomerization mechanism has become widely appreciated for the application as spatiotemporal control in biology and for photonic molecular switches.[70,106,282,311,330-334] A comprehensive review on the kinetics and mechanism of the thermal (and photochemical) decomposition of azo-derivatives can be found in literature.[296] Interestingly, two-photon induced photoisomerization of azobenzenes has also been reported.[335,336] Due to the conformational twist derived from the steric hindrance, the absorption band significantly decreases, upon conformational change from trans to cis (Scheme 29). Consequently, the electronical structure changes significantly and the absorption band decreases.

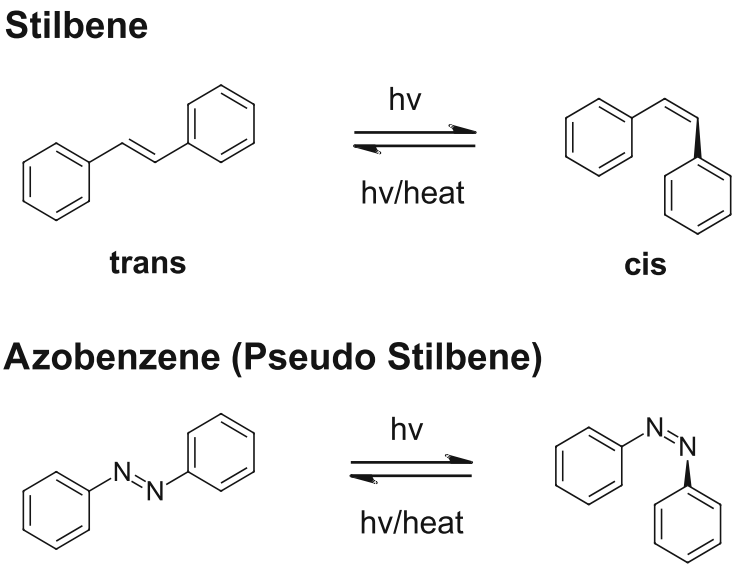

Scheme 29: Photoisomerization (trans→cis) of stilbene and azobenzene upon irradiation with UV light.[280]

The different isomers, steric effects and their electronic transitions can be monitored by UV-Vis spectroscopy. For the most effective overlap of the π-orbitals a co-planar structure is required. The sterically more restricted cis-isomers are less planar than the non-hindered trans-isomers. Therefore, the π-π* transition of electrons is facilitated in a planar molecule (trans) where the overlap of the π-orbitals occurs more easily. The absorption maximum of the trans isomer (corresponding to the π-π* transition) usually appears around 320 nm. The chance for π-π* transition in cis-stilbene is lowered due to the steric effects and decreased coplanarity hence, the absorption band decreases (Scheme 29).[337] A related mechanism is proposed for DAS and DADS.

Die approbierte gedruckte Originalversion dieser Dissertation ist an der TU Wien Bibliothek verfügbar.
The approved original version of this doctoral thesis is available in print at TU Wien Bibliothek.
TU Bibliothek Your knowledge hub WIEN

Nevertheless, a detailed picture on the photoisomerization of stilbenes is complicated by the presence of multiple electronic states and multiple intramolecular degrees of freedom. Commonly, the bond order of the ethylene moiety is reduced upon excitation. Subsequent twisting about the ethylene bond is enabled during the excited-state lifetime. Especially for asymmetrically substituted stilbenes (electron-donor and -acceptor groups) where intramolecular charge transfer is possible.[338]

Similar to stilbenes, azobenzenes can also experience a twisting motion including an internal charge transfer state, whereupon the spectral characteristics of azobenzenes are related to the pseudo stilbene type.[280] Accordingly, the twisted internal charge-transfer (TICT) can be observed via fluorescence emission spectra.[280,339] Since the central azo-motifs of CR and ASCR are differing from the electronic structure of azobenzenes (adjacent biphenyl- and a naphthalene moieties), the proposed isomerization and/or an eventual photodecomposition mechanism might vary distinctively. This would explain the missing photoisomerization of CR and ASCR, which was neither observed for 365 nm nor for 460 nm irradiation (Figure 49, Figure 50). The naphthalene as well as central biphenyl moieties of CR and ASCR, seem to influence the electrochemical properties of CR and ASCR. The simple comparison of CR and ASCR with the basic azobenzene photo switching mechanism is misleading.

To study the reversibility of the DAS photoisomerization, additional photoreactor experiments were performed. For this purpose, the 2PI stock solution (Figure 52, t=0) was first irradiated with 365 nm LED, to induce trans→cis isomerization (Figure 52, 60 min 365 nm) and second with 460 nm for 60 min to attempt a restoration of the trans-isomer of DAS (cis→trans isomerization).

Die approbierte gedruckte Originalversion dieser Dissertation ist an der TU Wien Bibliothek verfügbar.
The approved original version of this doctoral thesis is available in print at TU Wien Bibliothek.

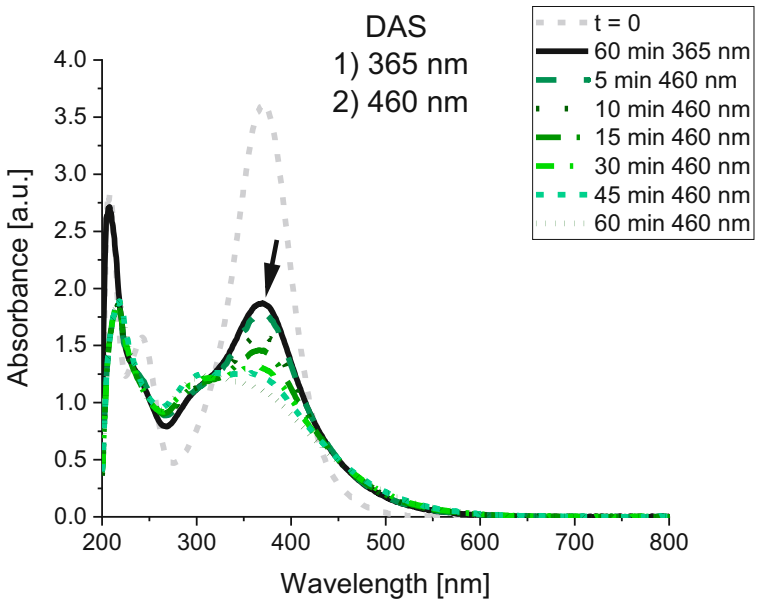

Figure 52: Failed attempt to invert the photoisomerization of DAS. The initial absorption profile of DAS (without irradiation) at the beginning of the photoreactor experiment is depicted in grey (dashed line, t=0). DAS solution was first irradiated with 365 nm for 60 min (1) to induce trans→cis isomerization. Secondly, the same solution was irradiated with 460 nm (2) to attempt an induction of cis→trans isomerization, which would be represented by an increase in absorption. However, a decrease of the absorption band was observed.

Photobleaching was observed upon irradiation with 365 nm (Figure 52). However, irradiation with 460 nm led to an additional decrease of the absorption band, previously reported. As an alternative irradiation source, 400 nm LED was used in order to induce cis→trans isomerization, but neither of both irradiation sources (460 and 400 nm) resulted in a restorage of the original DAS spectrum (t=0, trans-isomer, Figure 51). Additionally, the solution irradiated with LED light (solution B) was compared to a DAS stock solution, which was prepared under UV protection (solution A) and exposed to sunlight (Figure 53). UV-Vis spectra of both solutions were measured (24 h) and both exhibit comparable UV-Vis absorbance. To investigate dark-relaxation, both solutions were stored in the dark for 7 days but no reversible photoisomerization was observed.

Die approbierte gedruckte Originalversion dieser Dissertation ist an der TU Wien Bibliothek verfügbar.
The approved original version of this doctoral thesis is available in print at TU Wien Bibliothek.

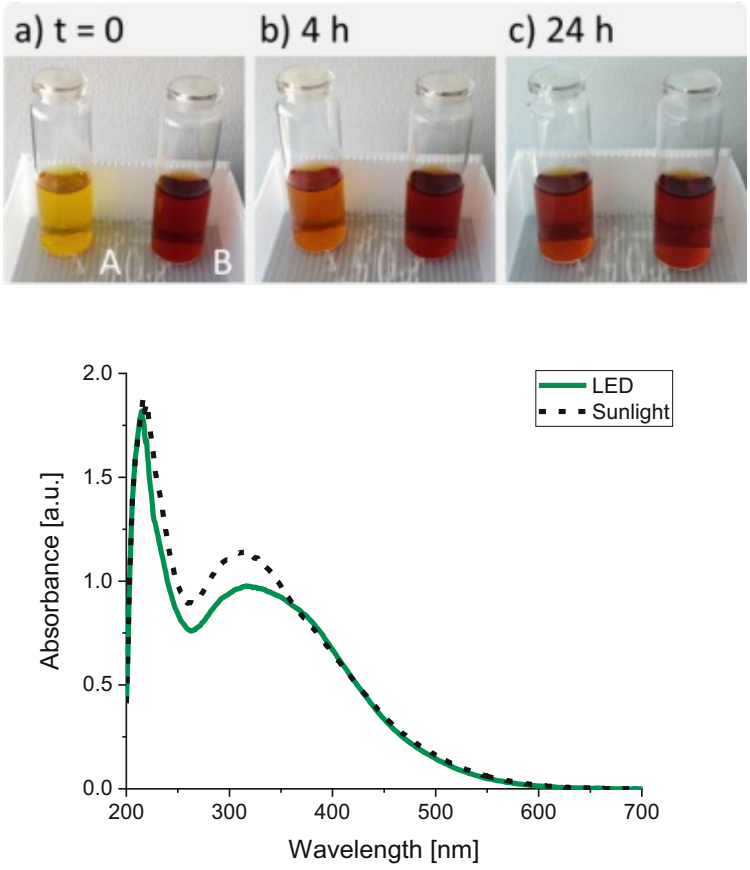

Figure 53: Two types of DAS solutions (1 mM, PBS) were exposed to sunlight for 24 h. Solution A was prepared for this experiment under UV-protection and flask B was examined as reference (solution after exposure to 365 nm LED light).

In previous studies, gas formation (N_2) was proposed as indication for homolytic bond cleavage of DAS, but this could not be confirmed during the performed experiments. Still, bubble formation during 2PP will be discussed in more detail in previous section (2.4 Two-Photon Polymerization of Azosulfonate-2PIs).

Die approbierte gedruckte Originalversion dieser Dissertation ist an der TU Wien Bibliothek verfügbar.
The approved original version of this doctoral thesis is available in print at TU Wien Bibliothek.

2.3.2 NMR Study of Photoproducts

To investigate possible photoproducts and for a detailed investigation of the photoisomerization mechanism of the stilbene-based molecules (DADS, DAS), photoreactor samples were freeze-dried and analyzed via NMR spectroscopy (600 MHz, D_2O). Spectra of the starting materials were recorded separately (Figure 54, Figure 55).

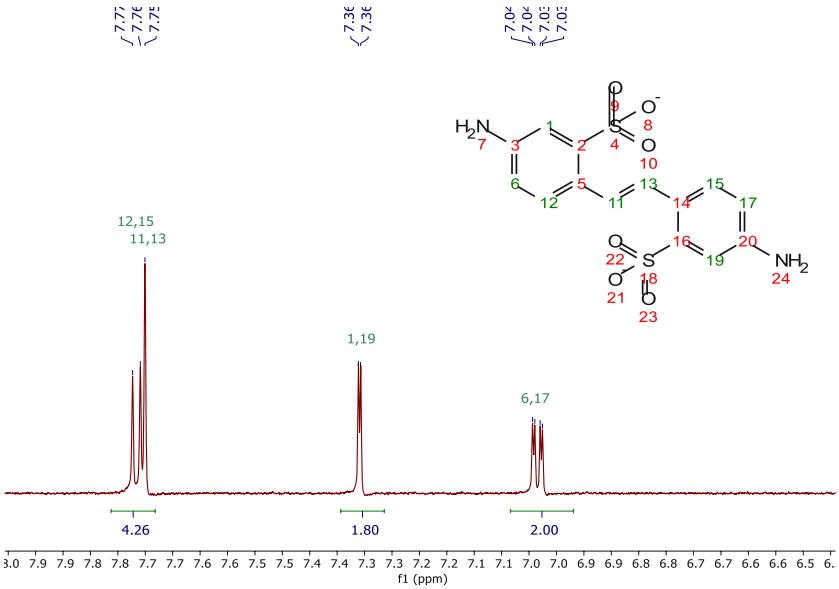

Figure 54: ^{1}H-NMR of DADS before irradiation (600 MHz, D_2O) δ 7.76 (d, J = 8.4 Hz, 2H), 7.75 (s, 2H), 7.36 (d, J = 2.5 Hz, 2H), 7.03 (dd, J = 8.4, 2.5 Hz, 2H).

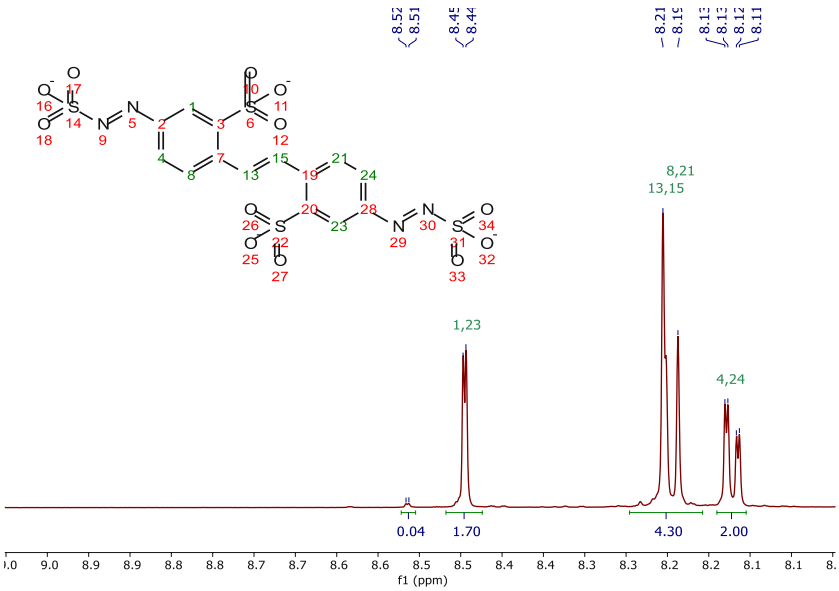

Figure 55: ^{1}H-NMR of DAS before irradiation (600 MHz, deuterium oxide) δ 8.45 (dd, J = 2.1, 0.5 Hz, 2H), 8.21 (s, 2H), 8.19 (d, 2H), 8.12 (dd, J = 8.3, 2.2 Hz, 2H).

The singlet at 7.75 ppm (DADS, Figure 54) and at 8.21 ppm (DAS, Figure 55) can be assigned to the central ethylene moiety of the chromophores. In each case, the singlet peak is overlapping with

Die approbierte gedruckte Originalversion dieser Dissertation ist an der TU Wien Bibliothek verfügbar.
The approved original version of this doctoral thesis is available in print at TU Wien Bibliothek.

the doublet of the corresponding protons of the aromatic ring. The ^{1}H-NMR spectra of each photoreactor sample were summarized for DADS (Figure 56) and for DAS (Figure 57).

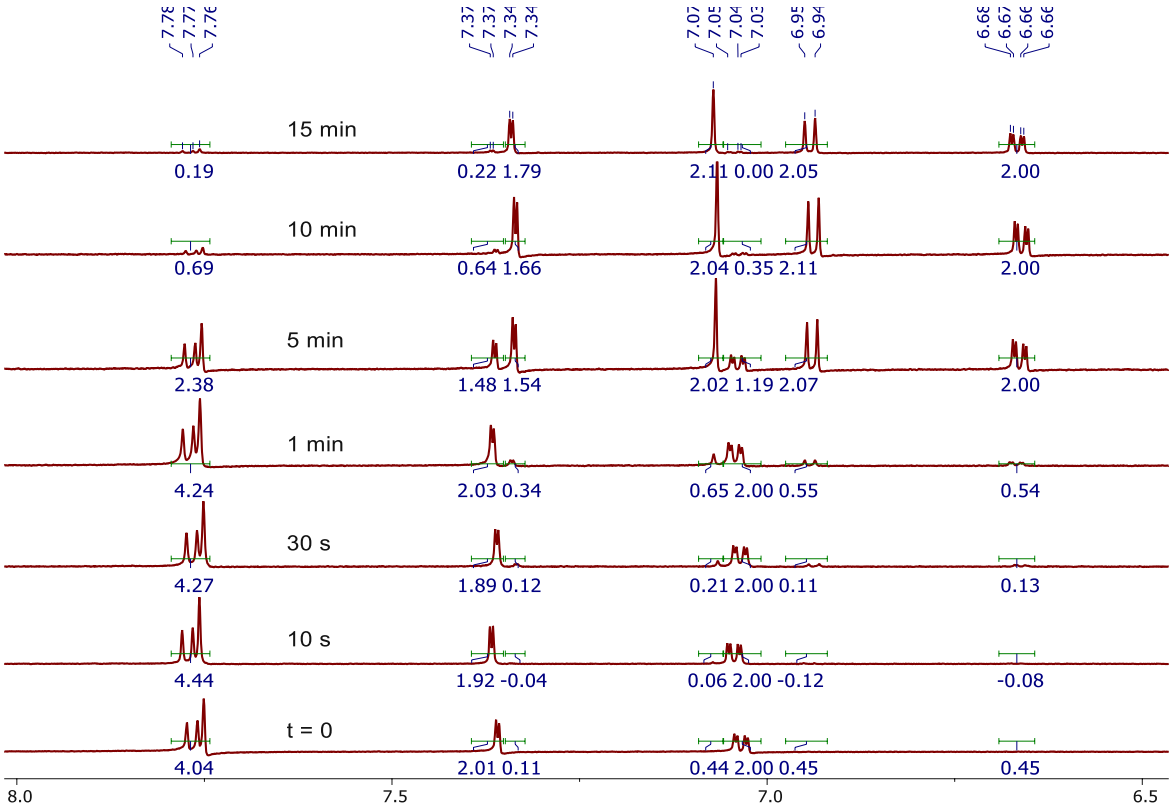

Figure 56: ^{1}H-NMR spectra of DADS photoreactor samples (600 MHz, deuterium oxide). Upon irradiation (15 min) with 365 nm, peaks are shifted up field (shielded). As reference, the peak (dd) at 6.67 ppm was used for calibration for the samples taken at 5 – 15 min and the peak (dd) at 7.04 ppm for the samples taken at 0 - 1 min.

As proposed, the trans→cis isomerization of DADS could be confirmed via ^{1}H-NMR spectroscopy and was studied in detail over time. Owing to a low sample concentration, ^{13}C-NMR spectra could not be measured. Commonly, the distinct vicinal coupling constant across the ethylene moiety ($^{3}J_{HH}$) can be used to distinguish between trans- and cis-isomer. However, due to the symmetry of both compounds (DADS, DAS) and the chemical equivalence of the protons, the Karplus equation could not be applied here. Still, a considerable shift was observed, which can be attributed to the trans→cis isomerization of DADS. A detailed depiction of the spectra before and after irradiation, including all coupling constant is given in the experimental section (Figure 100). After successful analysis of DADS, the photoreactor samples of DAS were measured (Figure 57).

Die approbierte gedruckte Originalversion dieser Dissertation ist an der TU Wien Bibliothek verfügbar.
The approved original version of this doctoral thesis is available in print at TU Wien Bibliothek.

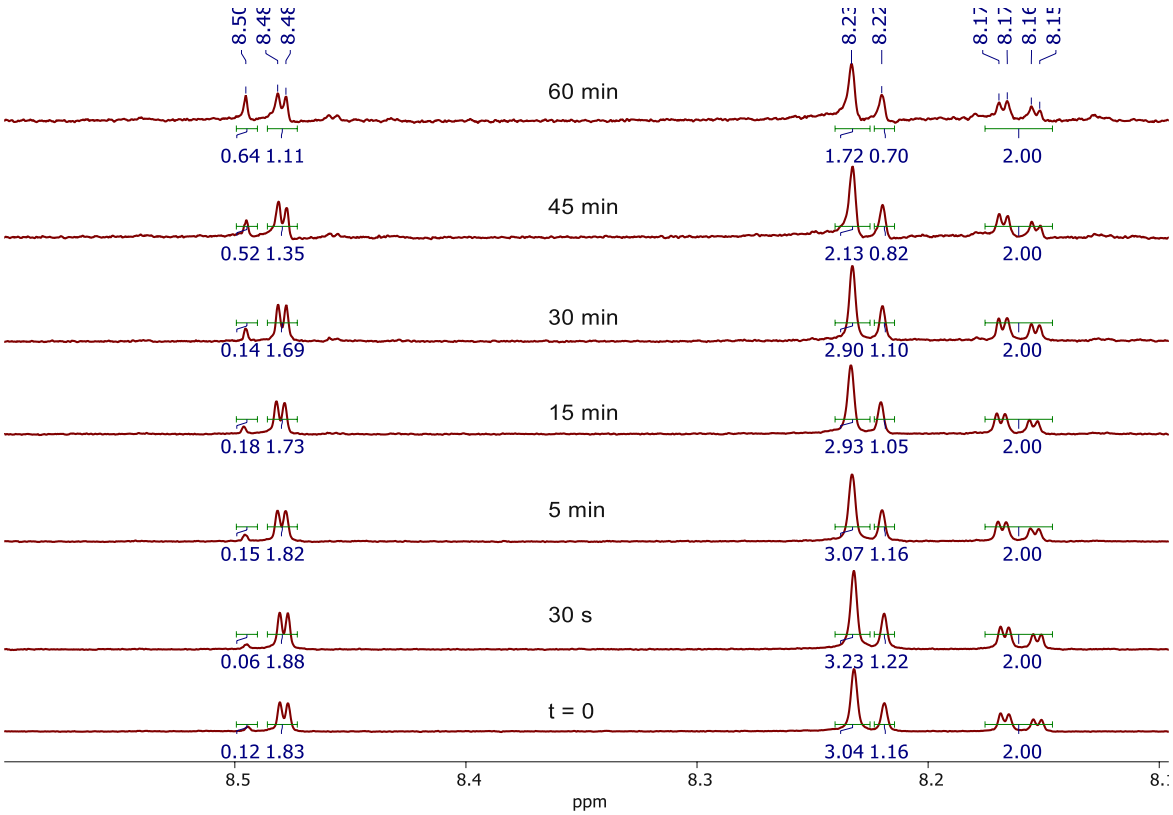

Figure 57: ^{1}H-NMR spectra of DAS photoreactor samples (600 MHz, deuterium oxide). δ 8.50 (s), 8.48 (d, J = 2.1 Hz, 2H), 8.23 (s, 2H), 8.22 (d, 2H), 8.16 (dd, J = 8.4, 2.2 Hz, 2H).

For DAS samples, no significant peak-shift as well as no significant change in coupling constants was observed upon irradiation (Figure 57). A detailed depiction of ^{1}H-NMR spectra before (t = 0) and after irradiation for 60 min is given hereafter (Figure 58). Contrary to the expected photoisomerization of DAS, no such mechanism could be confirmed. A general decrease of signal-intensity was observed. However, neither a distinct peak-shift, nor the generation of additional peaks of any possible photoproducts was detected.

Die approbierte gedruckte Originalversion dieser Dissertation ist an der TU Wien Bibliothek verfügbar.
The approved original version of this doctoral thesis is available in print at TU Wien Bibliothek.

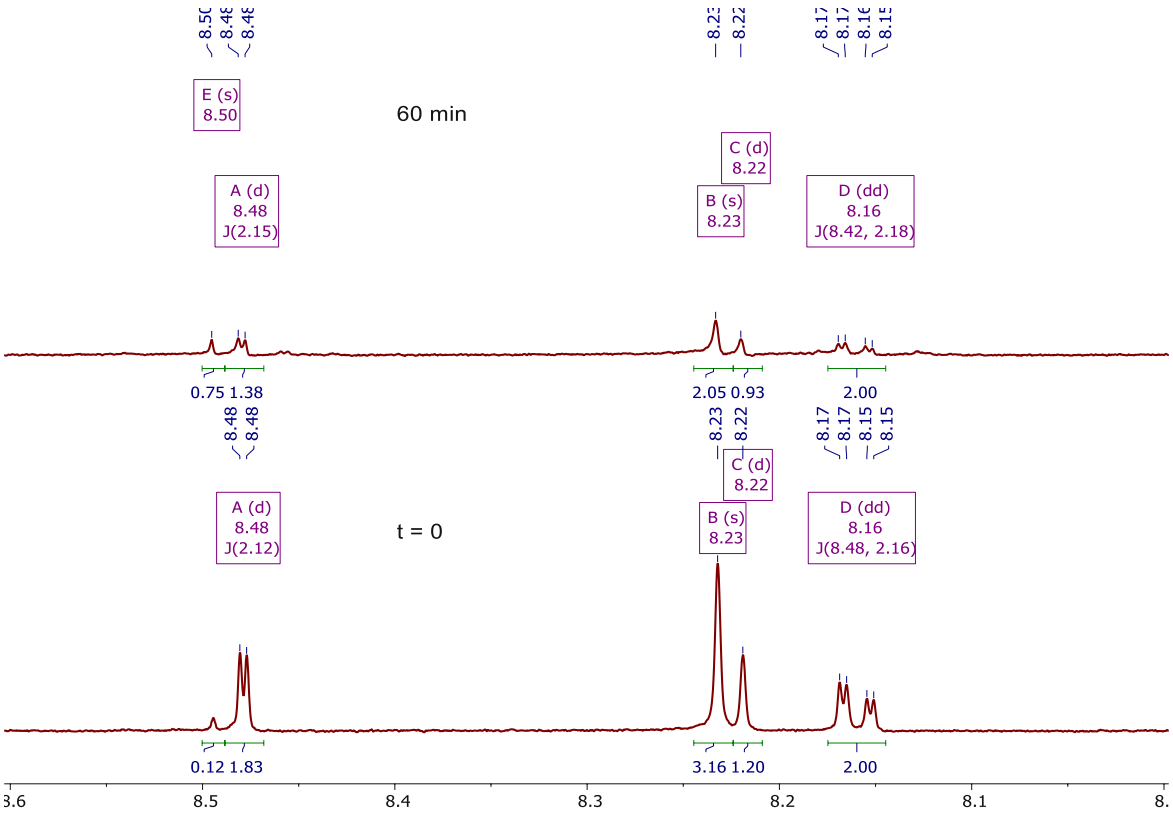

Figure 58: [1]H-NMR spectra (equal scaling) of DAS photoreactor samples before (t = 0, bottom) and upon irradiation with 365 nm LED light (60 min, top). An overall decrease in peak-intensity was observed over time and the integral of peak E (8.50 ppm) was increasing and the integral of peak B (8.23 ppm) was decreasing upon irradiation.

A higher relative intensity (∫0.12) was observed for peak E (t=0, Figure 58, s, 8.50 ppm), compared to the freshly prepared sample spectrum (Figure 55, ∫0.04). Up until now, the evolution of this peak is not clear and could not be assigned to any proton of DAS, since the integral values of the remaining peaks can be distinctively assigned to each proton of the chromophore (Figure 55). Furthermore, all samples were exclusively prepared in the dark and the spectrum was measured in brown-glass NMR tubes. However, the spectrum seems to change over time, which is interpreted as degradation of DAS in solution (D_2O). Besides the relative increase of peak E (s, 8.50 ppm), a relative decrease of the peak assigned to the ethylene moiety (peak B, s, 8.23 ppm) was observed. At all times, the spectrum was calibrated to the aromatic protons (dd, 8.16 ppm, peak D). Still, an interpretation of these peaks remains inconclusive, since with decreasing peak-intensity over time the calibration to the reference (aromatic protons at 8.16 ppm) becomes less significant, due to a decreasing signal-to-noise ratio. Neither photocleavage could be confirmed, since the multiplicity of the aromatic peaks is not changing, nor a photoisomerization mechanism was proven, since the relevant shift of the signals was not observed (as seen for DADS, Figure 56). Still, based on the observations made from UV-Vis measurements, a change of DAS' electronic status must be evident. To detect any photoproducts which are emerging upon cleavage of the azosulfonate-moiety, HPLC studies were performed additionally.

Die approbierte gedruckte Originalversion dieser Dissertation ist an der TU Wien Bibliothek verfügbar.
The approved original version of this doctoral thesis is available in print at TU Wien Bibliothek.
TU Bibliothek Your knowledge hub WIEN

2.3.3 HPLC Study of Photoproducts

To investigate photoproducts derived from a photodecomposition or -isomerization HPLC measurements of the chromophores (DAS, DADS) were performed. The matrix compounds were separated according to their retention time and affinity to a phenyl-modified stationary phase (mobile phase MeOH:H_2O 10:90). HPLC signals were recorded using an UV detector (350 nm) tuned to the absorption maxima of the analytes (Figure 59).

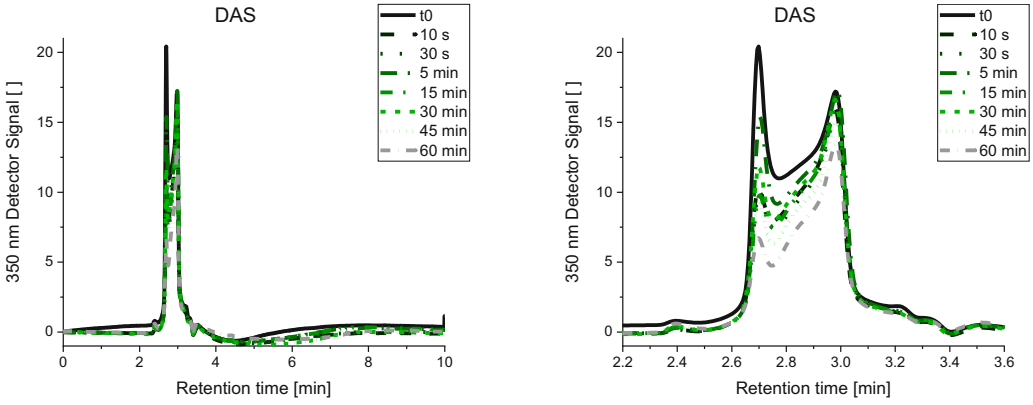

Figure 59: HPLC measurements of DAS photoreactor samples were performed (left). The peaks are depicted in a detailed section on the right (retention time: 2.2-3.6 min). The cis-isomer of DAS is proposed to be represented by the peak with shorter retention time (2.7 min) and the trans-isomer by the peak with longer retention time (3.0 min) according to the interaction rate with the stationary phase.[340]

Contrary to what was expected, two isolated peaks were detected for all DAS samples (including t0), representing two different molecules with varying affinity to the stationary phase. Generally, reversed-[341] and normal-phase columns[342] are used to separate the stilbene isomers.[343] Additionally, phenyl-modified reversed stationary phases with a methanol-water eluent are published as appropriate method to effectively separate aromatic hydrocarbons.[344] The separation method (stationary- & mobile phase) was tuned towards a high-resolution elution spectrum (varying the ratio of the mobile phase solvents), however a full separation of the peaks could not be achieved and best results were obtained using the phenyl-modified stationary phase with the above-mentioned eluent (MeOH:H_2O, 10:90). In case of a photodecomposition of DAS, aromatic photoproducts with increased affinity to the stationary phase (longer retention times) were expected, as a consequence of C-N bond cleavage and release of gaseous nitrogen (Figure 60, bottom left). The proposed photoisomerization products of DAS and DADS are depicted for comparison (Figure 60).

Die approbierte gedruckte Originalversion dieser Dissertation ist an der TU Wien Bibliothek verfügbar.
The approved original version of this doctoral thesis is available in print at TU Wien Bibliothek.

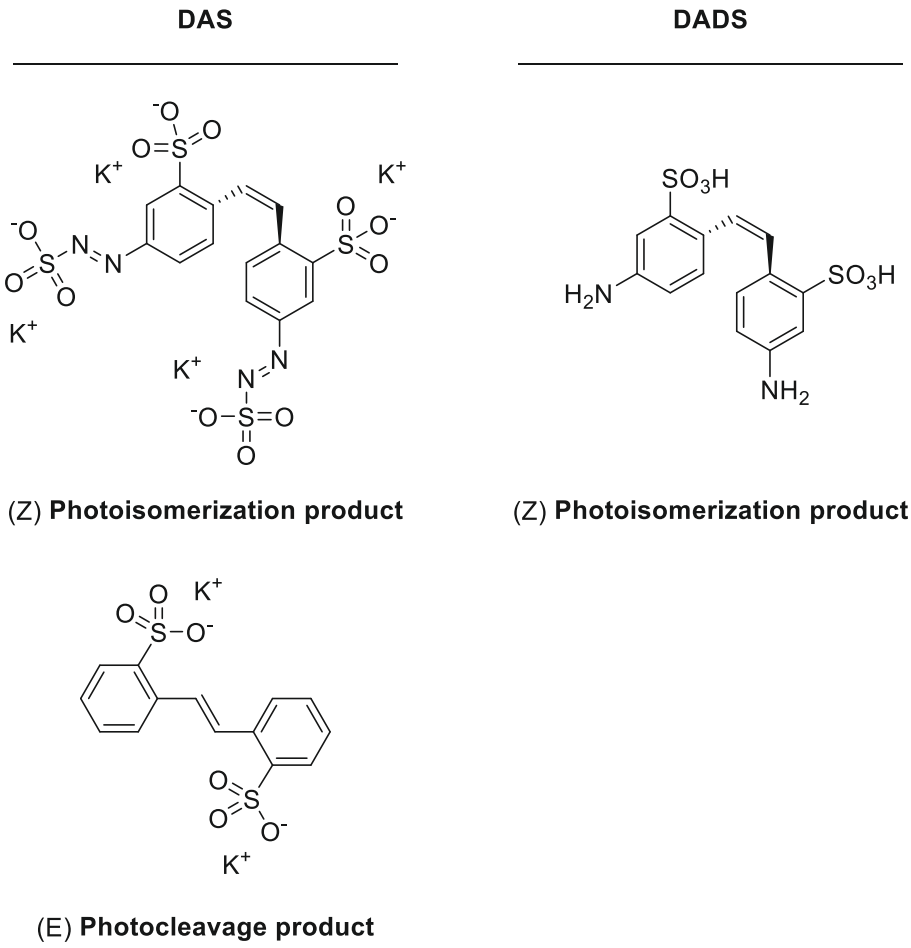

Figure 60: Possible analyte-photoproducts: Photocleavage of DAS (bottom, left) would lead to the loss of gaseous nitrogen and the generation of trans-species indicated as (E) photocleavage product. Photoisomerization would generate a conformational twist about the ethylene moiety, leading to a (Z) photoisomerization product (cis isomer). Since DADS does not exhibit photocleavable azosulfonate moieties, photoisomerization solely was expected here (DADS cis isomer, right).

Since photoproducts derived from a DAS-decomposition were not detected (E) photocleavage products), photoisomerization was suggested (Z) photoisomerization products). The proposed trans-isomer of DAS was associated to the peak with longer retention times (2.7 min), because the phenomenon of the elution order mainly results from the more planar molecular geometry of trans- vs. cis-isomer.[340] Therefore, the trans-isomer must exhibit a stronger interaction rate with the phenyl-modified stationary phase, resulting in a longer retention time, while the sterically more bulky cis-stilbene is geometrically more difficult to interact with the stationary phase. To compare these measurements with the retention profile of the starting material, DAS was measured additionally (prepared immediately before HPLC measurement without irradiation, Figure 61, left). For a comparison, the DADS elution spectrum before irradiation is given (Figure 61, right).

Die approbierte gedruckte Originalversion dieser Dissertation ist an der TU Wien Bibliothek verfügbar.
The approved original version of this doctoral thesis is available in print at TU Wien Bibliothek.

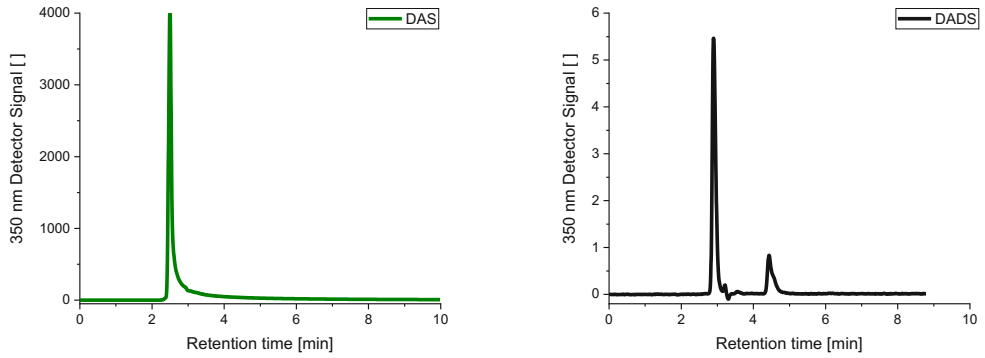

Figure 61: HPLC measurements of the analytes (DAS, DADS) were performed without irradiation.

Contrary to the photoreactor samples, one signal was detected for DAS (2.5 min, Figure 61, left), excluding the presence of impurities in the initial sample. Consequently, the two peaks of the photoreactor samples are either likely to be derived from the irradiation during the LED-experiment, or derived from the sample preparation. To clarify the method of sample preparation, the aliquots of the photoreactor solution were used both, for NMR- and HPLC studies (photoreactor – lyophilization - NMR study - lyophilization - HPLC study). This led to relatively long sample preparation time until the HPLC measurements were performed (3 days), which could have led to additional decomposition of the analytes, although the specimen were kept in brown-glass vials at all times to avoid any additional decomposition reactions. Still, there was a trend observable via HPLC over proceeding photoreactor time regarding the relative integration area of each peak (see DAS Figure 59 and Figure 63). Decreasing peak areas for the peak with shorter retention time (2.7 min, DAS cis-isomers) were accompanied by a relative increase of the peak areas at 3.0 min (DAS trans-isomers). This effect was contradictory to what was expected. Commonly, trans-isomers of stilbenes are the thermodynamically more stable state at reasonable temperatures.[345] Therefore, the peaks associated to the trans-isomers of DAS (longer retention times) were expected to decrease over time. Although, a shift between the two isomeric species was confirmed upon proceeding irradiation time, the opposite effect was observed. A full list of retention times for each sample is given in the experimental section (Table 11). To compare these results with the results of DADS, elution spectra were recorded (Figure 62).

Die approbierte gedruckte Originalversion dieser Dissertation ist an der TU Wien Bibliothek verfügbar.
The approved original version of this doctoral thesis is available in print at TU Wien Bibliothek.

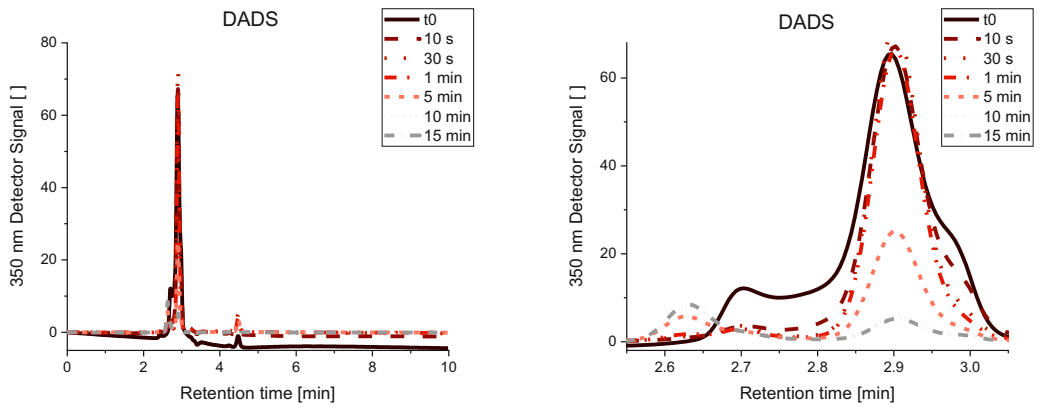

Figure 62: HPLC measurements of DADS photoreactor samples were performed (left). A detailed section of the relevant peaks is given on the right.

Similar to the previous experiment, multiple peaks were again observed for the t0-sample, which were not confirmed when the initial sample was prepared immediately before HPLC measurement (Figure 61). Particularly, two regions were in focus (2.6-2.7 min and 2.9 min), where a significant shift of the integration areas was observed (see Figure 63). However, additional signals were observed for all samples, which were confirmed to be present in the starting material (18% impurity at 4.4 min, Figure 61, right). To identify the impurity of DADS, further NMR experiments were performed. The addition of 1vol.% NaOD (sample in D_2O) was found to improve the resolution of the amphoteric DADS, however the impurity could not be specified (see experimental section: Figure 102). Nevertheless, the transformation between the stereoisomers (as already suggested via NMR measurements for DADS) was monitored in detail via plotting the peak integration areas over time (Figure 63, right). The peak integration areas of the DAS elution spectra were depicted additionally (Figure 63, left). The peak numbering was classified according to the peak retention time (lower number for shorter retention time).

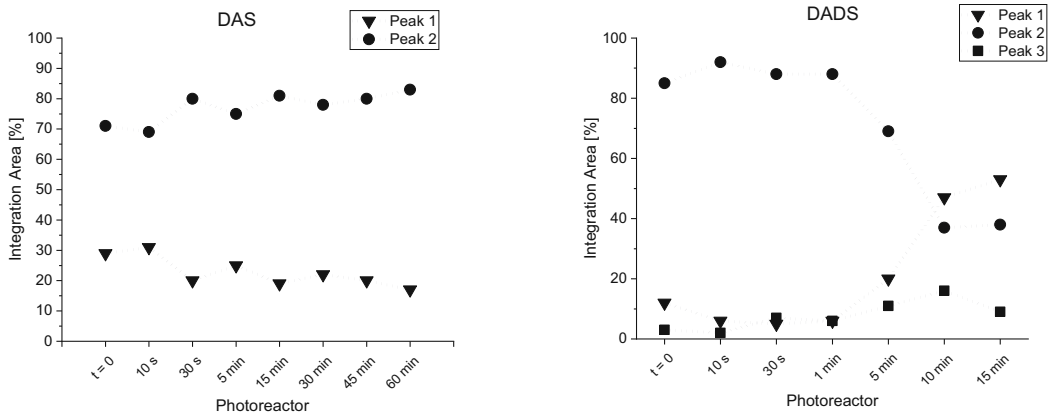

Figure 63: The integration areas of each peak were calculated and plotted against the reaction time during photoreactor experiment (peak 1: cis-isomers, peak 2: trans-isomers, peak 3: DADS impurity). HPLC measurements were performed using a phenyl-modified reversed phase column (mobile phase MeOH:H_2O, 10:90, UV detector at 350 nm).

For DADS on the one hand (Figure 63, right), decreasing peak areas of the trans-isomer (peak 2, 2.90 min) were accompanied as expected by a relative increase of peak areas of the cis-isomer

Die approbierte gedruckte Originalversion dieser Dissertation ist an der TU Wien Bibliothek verfügbar.
The approved original version of this doctoral thesis is available in print at TU Wien Bibliothek.
TU Bibliothek Your knowledge hub WIEN

(peak 1, 2.63 min). Again, a stronger interaction rate with the phenyl-modified stationary phase was expected for trans-isomers (longer retention times), compared to the sterically bulkier cis-stilbene with shorter retention times. The additional signals (Peak 3, 4.4 min) were not interpreted as photoproduct, since it is already present in the starting material, and the relative peak area moderately changes over the course of the photoreactor study. For DAS on the other hand, a contrary effect was observed. Again, an increased interaction of the trans-isomer with the stationary phase was expected, which would correspond to longer retention times. However, an increase of the trans-isomers (peak 2, 3.0 min) was detected, accompanied by a relative decrease of the cis-isomers (peak 1, 2.7 min).

In conclusion, the hypothesis of the previous NMR study (photoinduced trans→cis isomerization) was confirmed for DADS. The conversion between the trans- and cis-isomers of DADS can be effectively monitored via NMR as well as via HPLC. However, the moderate shift of peak integration areas of DAS and the missing detection of aromatic (E) photocleavage products, could not lead to a proof for photocleavage. Additionally, the relative low resolution of the DAS elution spectrum could have led to possible errors during peak integration. Consequently, neither photocleavage- nor photoisomerization products were confirmed for DAS. For both compounds (DAS, DADS) two signals were detected for the initial samples (t_0), supporting the assumption that the sample preparation (over the course of days) led to additional dark-decomposition before irradiation of the samples via LED light. Although, a constant shift between stereoisomers was observable for both analytes (DADS, DAS), the proposed photoisomerization could solely be confirmed for the reference compound (DADS). The performed measurements can be taken as indication for DAS photoisomerization, however the mechanism of DAS upon irradiation could not be elucidated in full detail.

Nevertheless, this section up until now offered a full study on the state-of the art 2PIs and novel synthesized/commercially available photosensitizers (ASCR, CR, DAS, DADS). Besides the photodriven change in stereochemistry/-decomposition, the 2PA-cross section is an additional parameter necessary to be studied for the successful application of the chromophores for 2PP.

2.3.4 Z-Scan Measurements

The 2PA-cross section of each 2PI can be investigated via measuring the 2PA of 2PI-solutions at different wavelengths (z-scan). In contrast to the commonly used white light continuum z-scan, which requires a complicated optical set-up, a fully automated z-scan set-up was developed by co-workers.[346] This alternative approach offers the possibility to use fs-laser oscillators as excitation source. Furthermore, this setup allows direct comparison between the z-scan results and 2PP experiments, as the same high repetition rate lasers are used for 2PP as well as for z-scan. Due to the tunability of the wavelength range from the visible to the NIR, a complete 2PA-cross section spectrum (3 measurements per wavelength in 10 nm steps) can be obtained. Z-scan measurements of CR were performed in PBS at different concentrations. The solvation of CR in

Die approbierte gedruckte Originalversion dieser Dissertation ist an der TU Wien Bibliothek verfügbar.
The approved original version of this doctoral thesis is available in print at TU Wien Bibliothek.
TU Bibliothek Your knowledge hub WIEN

aqueous media often requires sonication and remains a cumbersome task, during experimental preparation. Even more, colloidal solutions can be observed, when preparing concentrations above 1 mM (also observed for Rhodamine-B samples). Nevertheless, via incubation for 10 h at 37°C and extensive sonication (30 min), a 2 mM CR solution was prepared and the 2PA-cross section at different wavelengths (700 – 940 nm) was measured by Franziska Gantner (E308, Figure 64).

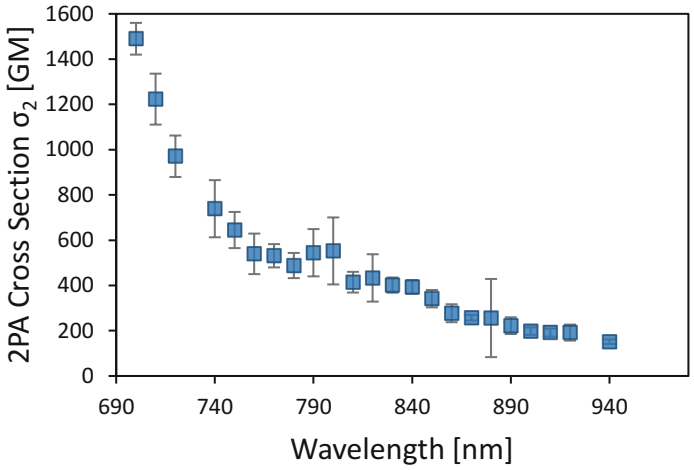

Figure 64: Mean values of the two-photon absorption (2PA) cross section (σ_2) of CR (2 mM, PBS) determined via z-scan at various wavelengths. CR exhibits comparably high σ_2 at 800 nm compared to state-of-the-art 2PIs (P2CK: 140 GM, DAS: 40 GM, CR: 600 GM).

Mean values for σ^{2PA} are depicted in the experimental section (Table 12). 2PA-cross sections of ASCR were not be performed, since the setup required maintenance. CR exhibited extraordinarily high σ^{2PA} values across the measured wavelength region (σ^{2PA}_{max} = 1490 GM at 700 nm), overruling many state of the art 2PIs (180 GM P2CK at 800 nm, 90 GM DAS at 720 nm).[165,347]

2.4 Two-Photon Polymerization of Azosulfonate-2PIs

To investigate the performance of the novel 2PIs (ASCR, CR), the processing window of hydrogel formulations was determined via 2PP. The processing window is related to the applied laser power in combination with the writing speed and was assessed via a serial test of both parameters. Formulations based on GelMA (DS95%) were prepared with a macromer concentration of 10 wt%, each containing 2 mM 2PI. Reference formulations were prepared, containing an azo-sulfonate 2PI (DAS) and a cyclo-ketone based 2PI (P2CK). The formulations were transferred to methacrylate-modified µ-dishes (glass surfaces were treated with 3-(trimethoxysilyl)propyl methacrylate)[348] and processed immediately. The polymerization threshold (P_{th}) was determined with variation of the laser power (x-axis) and writing speed (y-axis). The laser was calibrated to various wavelengths before each experiment (725, 800 and 900 nm, Figure 65). 725 nm was used for this study since pulse-broadening was observed at (the commonly applied wavelength) 700 – 720 nm.

Die approbierte gedruckte Originalversion dieser Dissertation ist an der TU Wien Bibliothek verfügbar.
The approved original version of this doctoral thesis is available in print at TU Wien Bibliothek.
TU Bibliothek Your knowledge hub WIEN

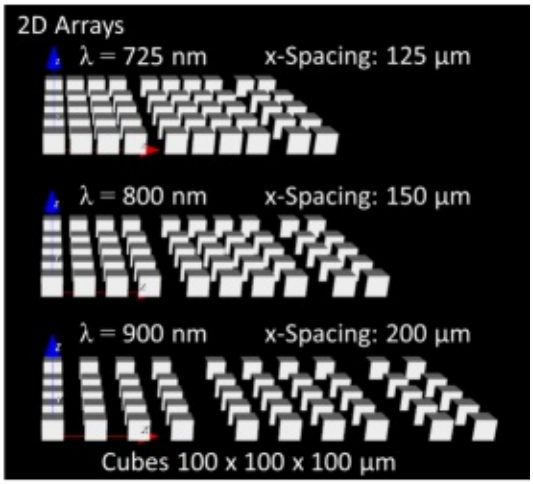

Figure 65: 2D Array of cubes printed at different wavelength (725, 800, 900 nm) with varying laser power (200-10 mW) and writing speed (200-1000 mm s^{-1}) The spacing between the cubes was varied according to the applied wavelength.

After 2PP processing, the formulations were immersed in PBS and incubated for 15 min at 37°C, assuring the removal of unpolymerized gelatin (post-processing). The dish was re-immersed in PBS and imaged via laser scanning microscopy (LSM700, channel 555 nm, Figure 66).

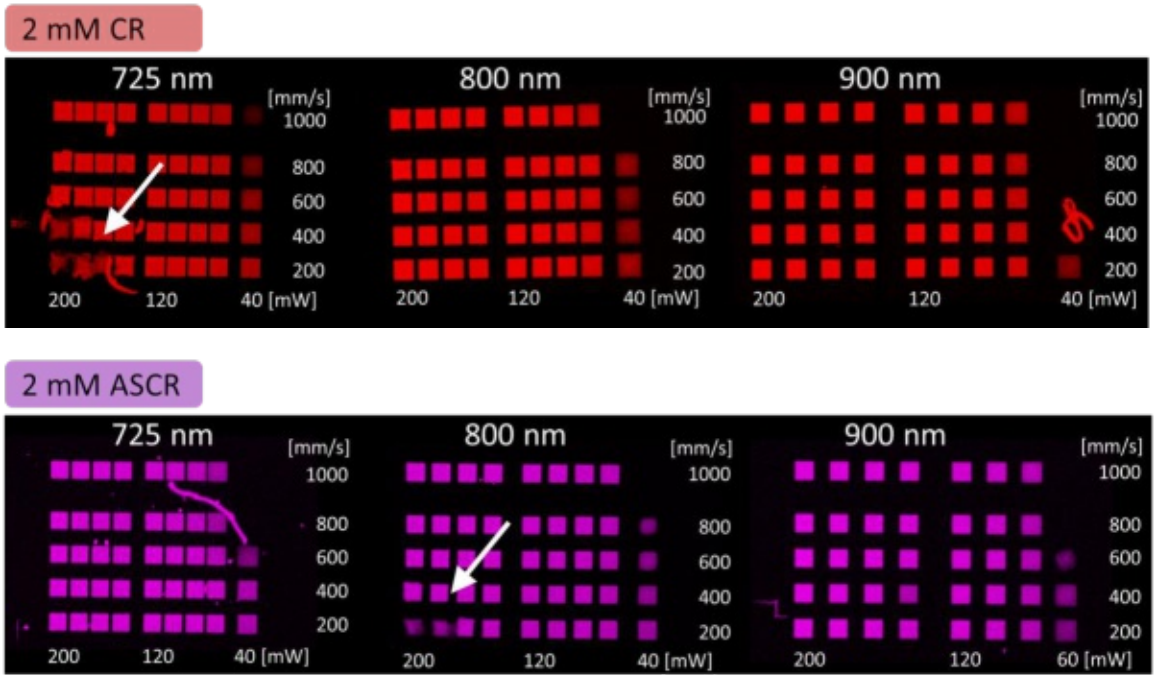

Figure 66: Laser scanning microscopy images of hydrogel constructs fabricated via 2PP of formulations based on GelMA (10 wt%, 95% DS) 2 mM CR (top) and 2 mM ASCR (bottom) at various wavelengths (725, 800, 900 nm). Arrows are marking a wavelength-dependent laser-ablation.

Promising results were observed at all applied wavelengths for the formulations containing CR and ASCR. Highly-resolved cubes were structured for all applied wavelengths (725, 800, 900 nm). Furthermore, sharp-edged cubes were processed using comparable low laser power (60 mW) and high writing speed (1000 mm s^{-1}). Superior performance (lowest P_{th} of all tested formulations) was observed for cubes structured with 725 nm (CR) and 800 nm (ASCR). For both 2PIs (CR and ASCR),

Die approbierte gedruckte Originalversion dieser Dissertation ist an der TU Wien Bibliothek verfügbar.
The approved original version of this doctoral thesis is available in print at TU Wien Bibliothek.
TU Bibliothek Your knowledge hub WIEN

a wavelength-dependent laser-ablation at comparable low writing speeds (200-400 mm s^{-1}) and high laser powers (200-160 mW) was observed for the applied laser settings (marked with arrows, Figure 66). Two-photon mediated laser ablation is a process described as the demanded subtractive 3D microfabrication of polymers.[349-353] In order to exclude any error derived from an uneven sample, the array was structured multiple times at different positions but laser ablation was observed for all cases. Hydrogel attachment onto the methacrylate-modified µ-dish was ensured, by starting the job 20 µm below the glass surface (zero z-position). Further investigation on the laser-ablation behavior was performed via a double exposure of the hydrogel formulation (cube-in-cube experiment), described in the following section (Figure 71). In summary, a wavelength-dependent behavior (laser-ablation) was observed for 725 nm (CR) and 800 nm (ASCR), which is supposed to derive from the extraordinarily high 2PA-cross section of the CR-chromophore and its modification. In some cases, 2PP in the presence of highly reactive 2PIs in combination with harsh structuring conditions can sometimes lead to hydrolysis/ablation of the hydrogel matrix.[354] As reference materials, hydrogel formulations based on DAS and P2CK were processed and imaged via LSM (Figure 67).

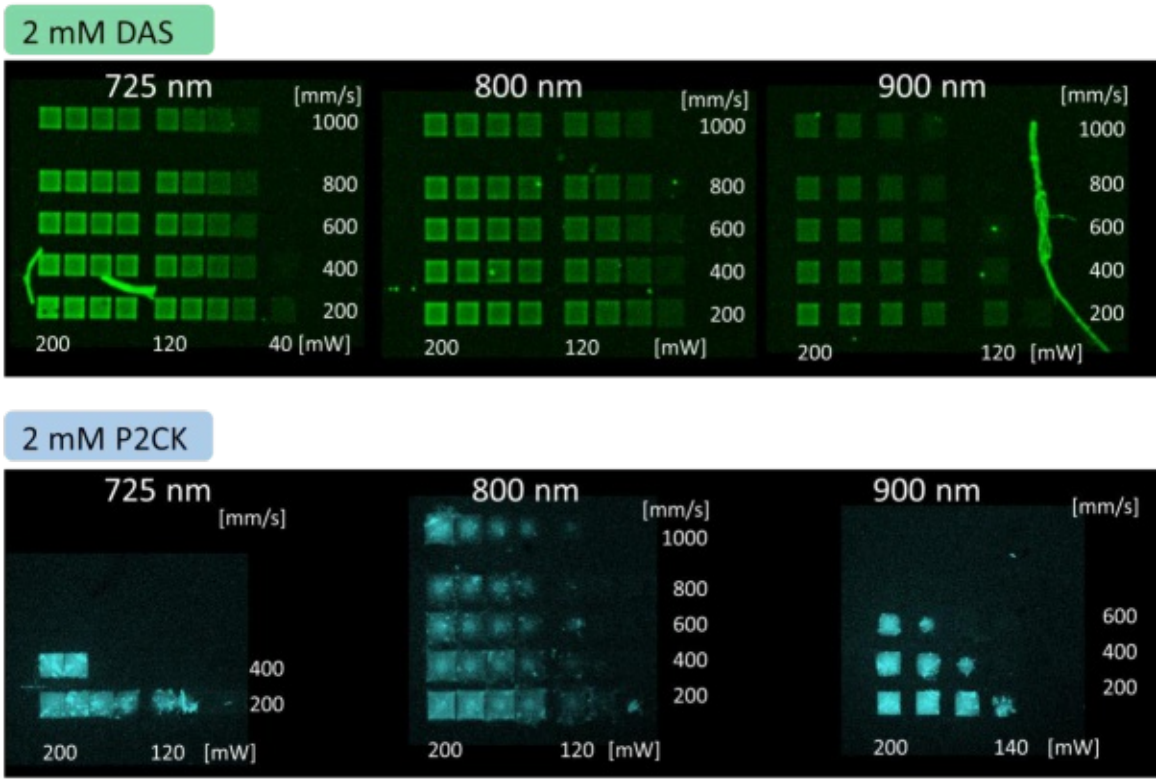

Figure 67: LSM images of formulations based on GelMA (10 wt%, 95% DS) containing 2 mM DAS (top) and 2 mM P2CK (bottom) at various wavelength (725, 800, 900 nm).

The performance of DAS (2 mM) at 800 nm correspond to the results published in literature.[164] P_{th} values of 60 mW at 200 mm s^{-1} and 70 mW at 1000 mm s^{-1} were observed for this study (Figure 67). Cubes with high resolution were observed for all applied wavelength, rating the structuring performance according to following order: 725>800>900 nm, which corresponds to the mean 2PA-cross section values based on z-scan measurements published in literature. Furthermore,

Die approbierte gedruckte Originalversion dieser Dissertation ist an der TU Wien Bibliothek verfügbar.
The approved original version of this doctoral thesis is available in print at TU Wien Bibliothek.
TU Bibliothek Your knowledge hub WIEN

bubble-formation was observed at 725 nm at low writing speed (200 mm s^{-1}) and high laser power (200-160 mW), being an indication for azo-bond cleavage. The precipitation of P2CK in gelatin-based hydrogel formulations, which was observed for this experiment is known from previous experiments but usually can be prevented for short-term experiments (<30 min). As a consequence of P2CK-precipitation, poorly stable cubes and relatively high P_{th} were observed at the applied settings (Figure 67). Microfabrication at 725 and 900 nm was aborted, since cubes were hardly visible during processing. Although, the formulation based on P2CK was prepared and processed right before the experiment, relatively long fabrication times (>30 min) resulted in fragile 3D cubes as a consequence of P2CK-precipitation.

Variation of Structuring Parameters

To further investigate the hydrogel ablation effect, observed for formulations based on CR and ASCR (Figure 66), the 2PP structuring parameters were adjusted, while keeping laser power and writing speed constant. This approach was chosen in order to assess, whether disintegration of hydrogels can be circumvented, especially for cubes structured with low writing speed (200 mm s^{-1}) and relatively high laser power (200 mW, Figure 68).

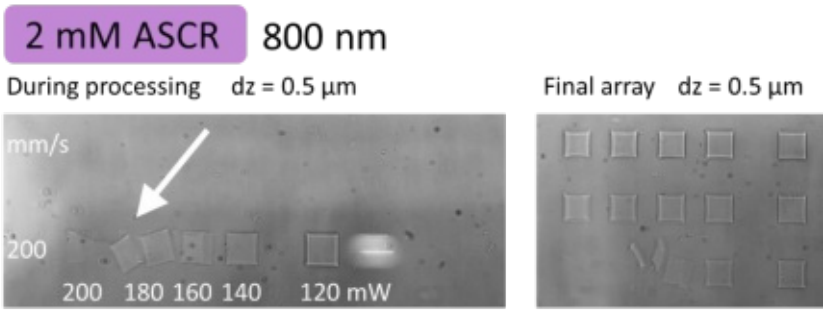

Figure 68: Hydrogel ablation was observed during processing in the presence of ASCR (above) and CR (not depicted), especially for hydrogel cubes structured with an average laser power of 200 mW and writing speed of 200 mm s^{-1}.

Since the product of the applied writing speed and average laser power is providing the laser dosage exposed to a focal volume, exaggerated focal overlap can on the one hand enhance polymerization efficiency (decrease P_{th}) on the other hand however, can induce overexposure of the material (see previous chapter 1.4, Figure 36). The quantity, how often each voxel is exposed to the laser can be adjusted by the structuring parameter. Worth noticing, that the voxel dimension heavily depends on the numerical aperture of the objective. Since optical aberrations can increase the focal spot size along z-direction, the layer spacing (dz) was the parameter of choice to be increased from 0.5 µm to 1 µm. One further advantage is the reduced processing time, when increasing the layer spacing. At all times, it was made sure to start the structuring process (zero z-position) 20 µm below the glass surface of the substrate, in order to ensure full attachment of the hydrogel. In order to investigate the effect of structuring parameter on the cube-stability, an array was printed, increasing laser power increment (Δ – 40 mW, x-axis) while increasing the layer spacing to 1 µm (Figure 69).

Die approbierte gedruckte Originalversion dieser Dissertation ist an der TU Wien Bibliothek verfügbar.
The approved original version of this doctoral thesis is available in print at TU Wien Bibliothek.
TU Bibliothek Your knowledge hub WIEN

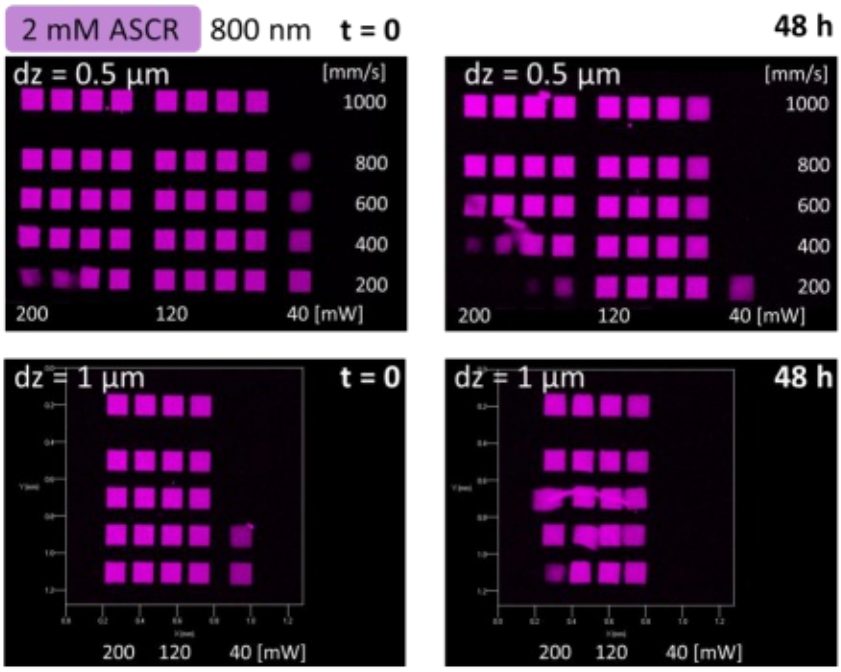

Figure 69: Hydrogel-ablation, observed for cubes structured with layer spacing of 0.5 µm (above) could be successfully reduced to a large extent by structuring cubes with increased layer spacing (dz = 1 µm, below). Especially, after incubation in PBS (48 h) disintegration of hydrogels was observed for cubes structured with low writing speed (200-400 mm s^{-1}) and high laser power (200-160 mW) and a layer spacing of 0.5 µm. Hydrogel formulations were based on 10 wt% GelMA95, 2 mM ASCR.

After structuring, the stability of the cubes structured with high laser power and low writing speed increased significantly (Figure 69, t = 0). No hydrogel ablation was observed during LSM-imaging. After incubation in PBS (48 h) one part of the array seems to show increased swellability and floating of cubes was observed. Taking a closer look to P_{th} after structuring, comparable values were obtained for cubes structured with increased layer spacing (40 mW, 400 mm s^{-1}) compared to those structured with reduced hatching (40 mW, 800 mm s^{-1}). As a consequence of hydrogel swelling, P_{th} was increased for both formulations accordingly. To sum up, hydrogel-ablation was successfully reduced by adjusting the appropriate laser settings (dz). By increasing the slicing distance in z-direction, the exposure-time per voxel per layer was successfully reduced. Presumably, ASCR exhibits similar exceptional 2PA-cross sections, compared to those observed for CR (Figure 64). Since hydrogels in general are prone to a high degree of swelling, the swelling was investigated for CR and ASCR accordingly (48 h, PBS, Figure 70).

Die approbierte gedruckte Originalversion dieser Dissertation ist an der TU Wien Bibliothek verfügbar.
The approved original version of this doctoral thesis is available in print at TU Wien Bibliothek.

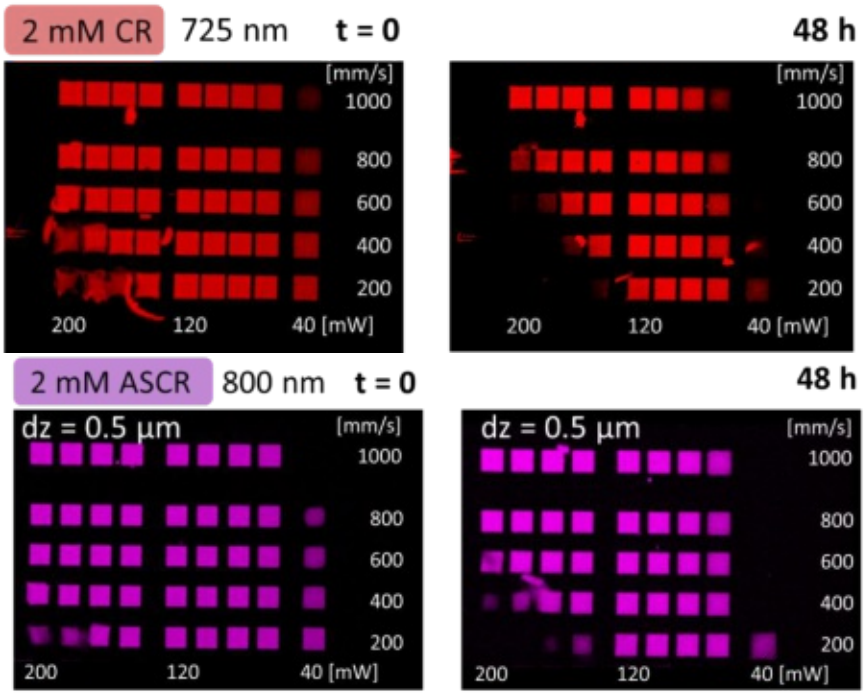

Figure 70: Hydrogel erosion was observed for cubes structured with laser powers (200-140 mW) and writing speeds (200-600 mm s^{-1}) in the presence of CR (725 nm) and ASCR (800 nm), especially after incubation for 48h at 37°C in PBS.

As expected, hydrogel erosion was observed for both arrays (CR 725 nm, ASCR, 800 nm) at both ends of the array (below P_{th} as well as at low writing speed and high laser power), with increased extent after incubation for 48h at 37°C.

An additional experiment was performed in order to investigate, whether laser-ablation can be observed on a large scale (z = 400 µm). First, a cube (400x400x400 µm) was structured with increased layer spacing (1 µm) and comparable low laser power (140 mW) and high writing speed (600 mm s^{-1}). Second, another cube was structured (double exposure) at the corner of the first cube (200x200x400 µm) in order to induce a hydrogel cleavage. For the second cube, the layer spacing was reduced to 0.5 µm. The laser was calibrated to 725 nm for CR and 800 nm for ASCR (Figure 71).

Die approbierte gedruckte Originalversion dieser Dissertation ist an der TU Wien Bibliothek verfügbar.
The approved original version of this doctoral thesis is available in print at TU Wien Bibliothek.

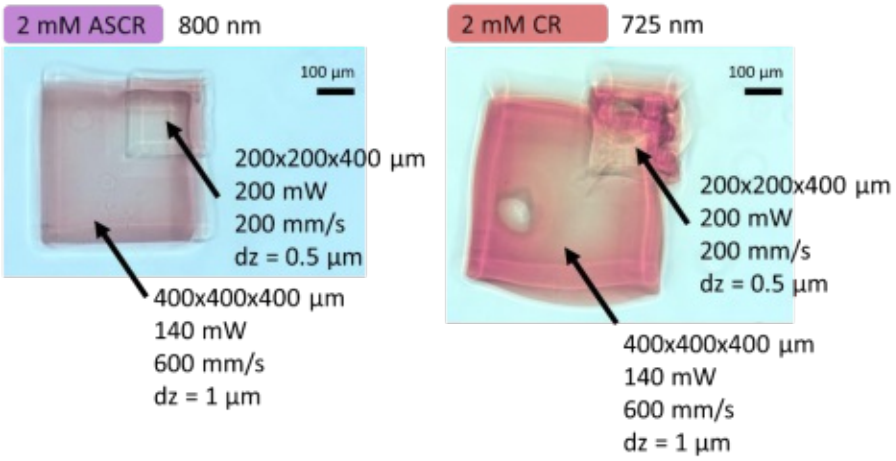

Figure 71: Double exposure of cubes with varying layer- spacing (dz) and energy intake (laser power, writing speed). The cube-overlap was intended in order to deliberately induce hydrogel ablation at the corner.

The cubes processed in the presence of CR exhibited a higher degree of swelling compared to ASCR (Figure 71). At first, no hydrogel erosion was observed along the z-axis while imaging in the brightfield however, after incubation for 48h in PBS, one part of the hydrogel structure was washed away (LSM imaging, CR, z = 60 µm, Figure 72).

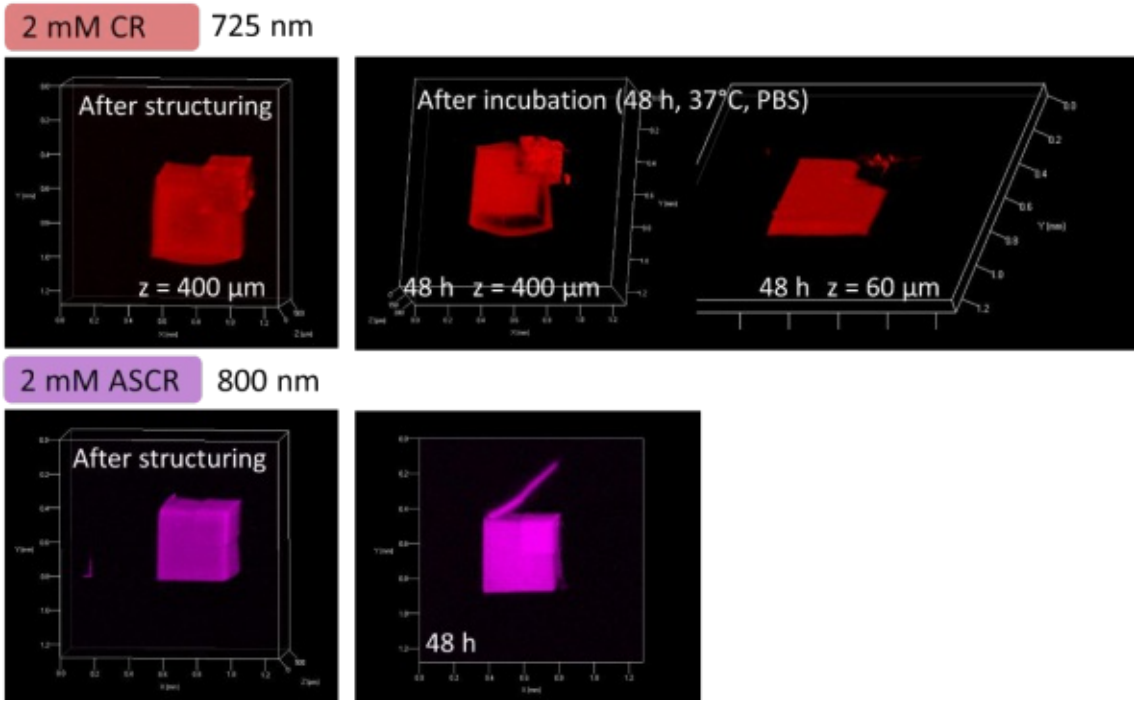

Figure 72: Hydrogel-erosion was observed for the cube structured in the presence of CR at the first 60 µm above the glass surface (top). At a higher z-position, the smaller cube (dz = 0.5 µm) is still attached on the top part of the larger cube.

Whenever wavelength-dependency of 2PIs is described, it is of major importance to first assess the dependency between the applied wavelength and the laser peak intensity. The laser exposure of a photosensitive formulation is commonly calibrated to a given wavelength using a laser power meter. However, whenever formulations are fabricated and compared at different wavelengths, the varying peak intensity of the pulsed laser beam (given at the focal spot) must be considered.

Die approbierte gedruckte Originalversion dieser Dissertation ist an der TU Wien Bibliothek verfügbar.
The approved original version of this doctoral thesis is available in print at TU Wien Bibliothek.
TU Bibliothek Your knowledge hub WIEN

Consequently, the peak intensity at each wavelength must be calculated before comparing the performance of different 2PIs at different wavelengths. As a simplification, the focal spot size is assumed as Gaussian function.[126] At a given average laser power ($\bar{P}$ [mW]), the peak intensity (I_{Peak}) can be calculated for every wavelength using (equation 1) and the correction factor (0.88). The peak intensity (I_{Peak}) is dependent on the average laser power ($\bar{P}$), numerical aperture of the objective (NA), repetition rate (R: 80 MHz), pulse length (τ) and the applied wavelength (λ).

Equation $$I_{Peak} \cong 0.88 \frac{\bar{P}\pi(NA)^2}{R\tau\lambda^2} \quad (1)$$

Consequently, each peak intensity can be calculated upon consideration of the respective pulse duration (725 nm: ~90 fs, 800 nm: ~70 fs). The peak intensity at 725 nm is calculated as I_{Peak} = 23 TW cm^{-2} (CR) and 25 TW cm^{-2} at 800 nm (ASCR), for a cube structured with an average laser power of 200 mW. Consequently, ASCR is exposed to a higher energy rate compared to CR (ΔI_{Peak}~ 2 TW cm^{-2}). It seems that the observed hydrogel-ablation, which was solely observed for CR might be majorly influenced by the extraordinarily high 2PA-cross section of CR (970 GM at 720 nm). The z-scan of ASCR was not performed, since the set-up required maintenance. Values for the 2PA cross section of P2CK (176 GM at 800 nm, WLC) and the 2PA cross section of DAS (~20 GM at 800 and ~60 GM at 725 nm) are published in literature.[165,346]

*Table 5: Overview on the structuring performance of tested formulations. Furthermore, literature values are given for the 2PA cross section (σ_{2PA}) for each applied wavelength (725, 800 900 nm) and the proposed wavelength, where maximum 2PA cross section (σ_{2PA}^{max}) was observed based on z-scan data. White light continuum z-scan (WLC) was performed for P2CK, indicated by *. Precipitation of P2CK was observed, marked by ~.*

2PI	Applied λ [nm]	Performance at applied λ	Literature σ_{2PA} at applied λ [GM]	Proposed λ [nm] for σ_{2PA}^{max} based on literature
DAS	725	✓	80	
	800	✓	20	700 (90 GM)
	900	✓	10	
P2CK	725	~	50*	
	800	~	180*	830 (180 GM)*
	900	~	60*	
CR	725	✓	970	
	800	✓	550	700 (1490 GM)
	900	✓	200	
ASCR	725	✓	no data	
	800	✓	no data	no data
	900	✓	no data	

Since photodegradation could not be proven for ASCR and CR within this study, a photosensitizing mechanism is hypothesized instead. A sensitizing mechanism of CR was already proposed in literature.[355,356] In conclusion, outstanding performance (low P_{th}) was observed for CR (40 mW, 800 mm s^{-1} at 725 and 800 nm) and ASCR (60 mW, 800 mm s^{-1}at 725, 800, 900 nm) compared to state-of-the-art 2PIs (DAS, P2CK, see Figure 66, Figure 67). It was observed, that laser-ablation is possible in gelatin hydrogels in the presence of ASCR (800 nm) and CR (725 nm), especially for harsh structuring parameters (dz = 0.5 µm, hatch = 0.5 µm). Hydrogel-ablation was successfully

Die approbierte gedruckte Originalversion dieser Dissertation ist an der TU Wien Bibliothek verfügbar.
The approved original version of this doctoral thesis is available in print at TU Wien Bibliothek.
TU Bibliothek Your knowledge hub WIEN

reduced, by increasing the layer spacing accordingly. Overall, promising performance (low P_{th}) of the novel 2PIs were observed compared to the state-of-the-art 2PIs (P2CK, DAS), especially at long-wavelength applications (800, 900 nm, Figure 73).

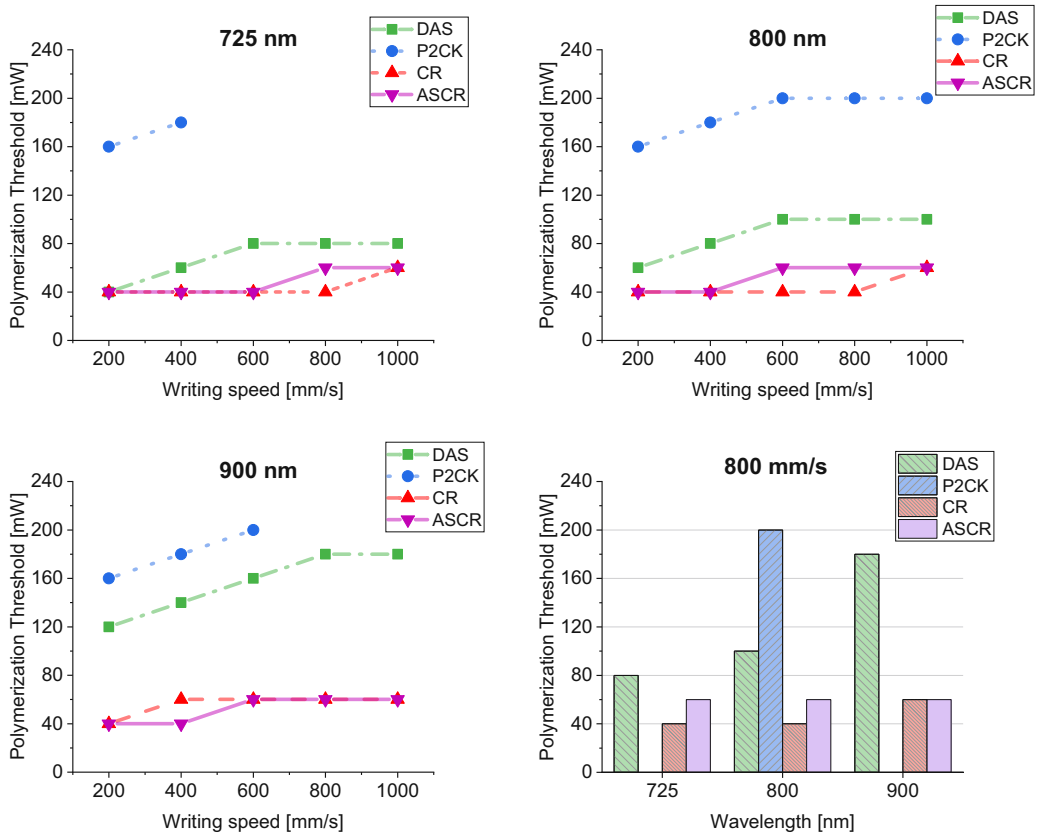

Figure 73: Polymerization Threshold (P_{th}) of the investigated 2PIs (DAS, P2CK, CR, ASCR, 2 mM) in GelMA95 hydrogels (10 wt% macromer content) according to the applied wavelength (725, 800, 900 nm). For comparison, the P_{th} of each formulation at 800 mm s^{-1} is additionally given as bar chart. P2CK is not given for 725 and 900 nm, since the structuring was prematurely aborted due to P2CK-precipitation.

Lowest P_{th} was observed for CR and ASCR, outpacing by far the P_{th} of DAS and P2CK. The outstanding performance of CR is in accordance to its exceptional high 2PA-cross section observed via z-scan (Table 12). Despite its lower 2PA-cross section (Table 5), DAS is an efficient 2PI for a broad range of wavelengths (700-900 nm) however, the contribution of its photoisomerization towards 2PP requires further investigation.

Die approbierte gedruckte Originalversion dieser Dissertation ist an der TU Wien Bibliothek verfügbar.
The approved original version of this doctoral thesis is available in print at TU Wien Bibliothek.

2.5 Biocompatibility Studies

2.5.1 Metabolic Activity

Besides the use of azo-compounds as dyeing agent in textile industry, the greatest use of CR is mentioned to be in biology and histochemistry (e.g. as staining agent in Alzheimer disease research, since it is associating to amyloid proteins enabling the detection of peptide-deposition in living patients).[357-360] CR was proposed to exhibit a lower affinity to perfuse the blood brain barrier at physiological pH compared to its carboxylic acid counterparts.[355,356,361-368] However, the international agency for research on cancer is warning of lipophilic primary aromatic amines and the possibility that carcinogenicity can arise upon reductive cleavage of azo dyes.[369] Still, aromatic amines are essential precursors for the formation of azo dyes, the largest family of synthetic dyes.[370,371] Especially, the amount of dyes released into the environment during their application as dyes is concerning.[372] For 2PP, usually low 2PI concentrations are required (1 mM) however, a study on the biocompatibility of 2PIs is inevitable for future cell encapsulation experiments. Here, the metabolic activity was used as indirect measure of cytotoxicity and the novel 2PIs (CR, ASCR) were tested using PrestoBlue® viability assay in comparison to reference 2PI (DAS). Cell-lines with different sensitivity were used (mouse fibroblasts L929, human umbilical vein endothelial cells - HUVECs, adipose-derived stem cells - ASCs). In a preliminary experiment, the cells were cultivated and exposed to various concentrations of ASCR, CR and DAS (2, 1, 0.5 mM). The control group was cultivated in cell medium (DMEM, Figure 74 - Figure 76).

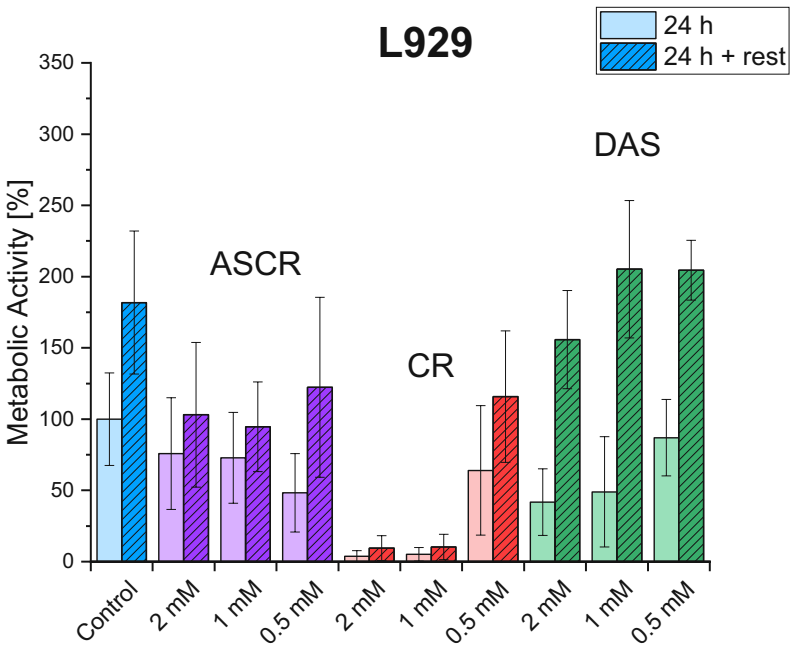

Figure 74: PrestoBlue® assay of mouse fibroblasts (L929) exposed to different concentrations of 2PI (2 mM, 1 mM, 0.5 mM, CR, ASCR, DAS). The control group was cultivated in cell medium. The metabolic activity of the cells was repeatingly assessed after an additional resting period (24 h + rest, medium exchange).

Die approbierte gedruckte Originalversion dieser Dissertation ist an der TU Wien Bibliothek verfügbar.
The approved original version of this doctoral thesis is available in print at TU Wien Bibliothek.

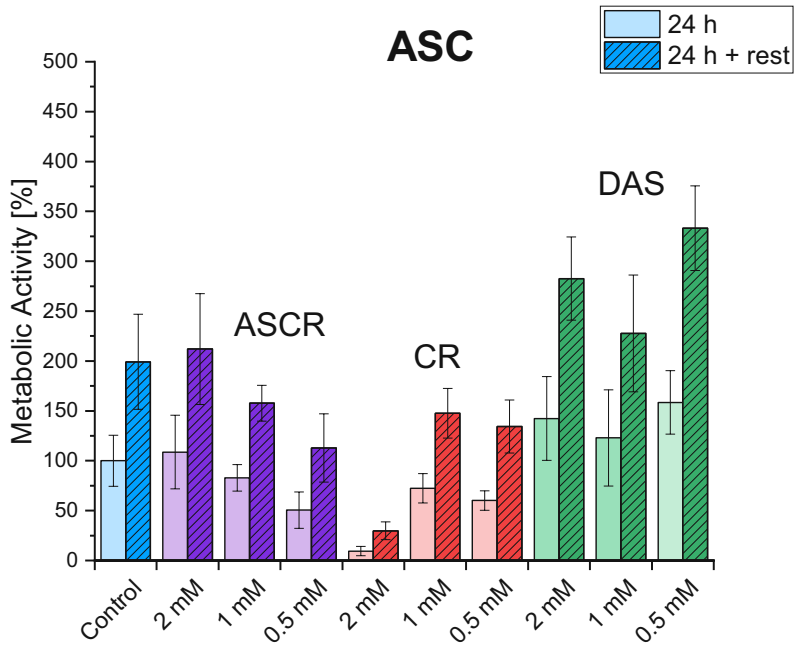

Figure 75: PrestoBlue® assay of adipose-derived stem cells (ASC) exposed to different concentrations of 2PI (2 mM, 1 mM, 0.5 mM, CR, ASCR, DAS). The control group was cultivated in cell medium. The metabolic activity of the cells was repeatingly assessed after an additional resting period (24 h + rest, medium exchange).

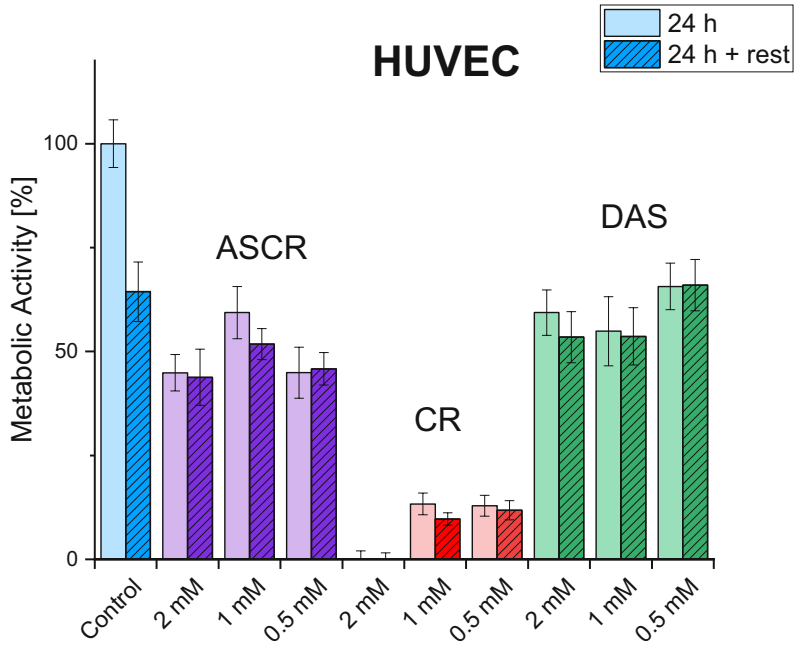

Figure 76: PrestoBlue® assay of human umbilical vein endothelial cells (HUVEC) exposed to different concentrations of 2PI (2 mM, 1 mM, 0.5 mM, CR, ASCR, DAS). The control group was cultivated in cell medium. The metabolic activity of the cells was repeatingly assessed after an additional resting period (24 h + rest, medium exchange).

Here, the metabolic activity was used to assess the biocompatibility of ASCR compared to the starting material (CR) and the reference 2PI (DAS). Promising metabolic activity was observed for cells exposed to ASCR and DAS, while limited metabolic activity was assessed for cells treated with

Die approbierte gedruckte Originalversion dieser Dissertation ist an der TU Wien Bibliothek verfügbar.
The approved original version of this doctoral thesis is available in print at TU Wien Bibliothek.
TU Bibliothek Your knowledge hub WIEN

CR solution, originating from the presence of excessive amount of CR-precipitate. Commonly, extensive heating and ultrasonication would be necessary, to dissolve CR in aqueous media. In general, the non-polar biphenyl backbone and amphoteric character of the azo dye contribute to the cumbersome dissolution of CR. Experimental preparation of CR usually requires long lead times, resulting in colloidal suspensions rather than homogeneous solutions. Contrary to the limited metabolic activity observed for CR, promising cell viability was observed for the novel 2PI (ASCR) as well as for the reference 2PI (DAS). However, the metabolic activity was used as indirect measure of cytotoxicity, being a guideline for future cell encapsulation experiments. The assay is based on a cell-permeable resazurin indicator, which can be reduced inside the mitochondria of living cells.[373] This method is a straightforward approach to quantify the mitochondrial metabolic activity of cells via absorption measurements. While a low metabolic activity of cells indicates low biocompatibility, increased metabolic activity (which is observed for 2 mM ASCR, Figure 75) does not necessarily imply increased cell viability. Cells can tolerate moderately toxic compounds, while experiencing increased metabolic activity as a consequence of stress.[374] The traditional believe that metabolic activity measurements are synonymous to viability assays are misleading.[375] Cells, which maintain a certain membrane integrity or metabolic activity should not automatically be considered as viable. Additionally, it is vital to assess the metabolic activity over the course of a few days, in order to observe a reliable trend regarding biocompatibility. Hence, additional resting periods were included here. Nevertheless, the performed experiments represent a first indication of the promising biocompatibility of ASCR. ASCR (2 – 0.5 mM) was well tolerated for all tested cell-lines (L929, ASC, HUVECs). Since ASCR and DAS are predominantly interesting, the experiment was repeated, testing 2PI-concentrations of down to 0.125 mM. The solutions were homogenized using sonication and left overnight at 37°C (Figure 77).

Die approbierte gedruckte Originalversion dieser Dissertation ist an der TU Wien Bibliothek verfügbar.
The approved original version of this doctoral thesis is available in print at TU Wien Bibliothek.

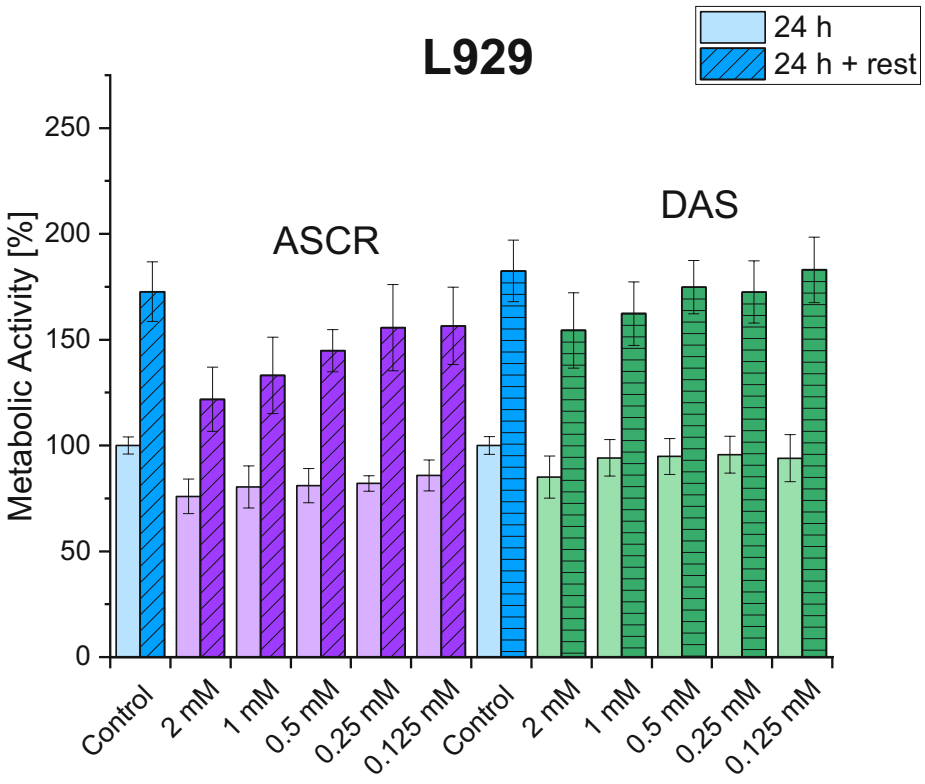

Figure 77: PrestoBlue® assay of mouse fibroblasts (L929) exposed to different concentrations of 2PI (2 mM, 1 mM, 0.5 mM, 0.25 mM, 0.125 mM ASCR, DAS).

Cells, which were exposed to ASCR showed a metabolic activity of 80- 85 % after 24h and remained constant for all tested concentrations (2-0.1 mM). Still, the control group exhibited a higher metabolic activity. After an additional resting period (24 h + medium exchange), the cells recovered and increased in metabolic activity represented in an increased cell number. The metabolic activity of ASCR-exposed cells was lower compared to the control group and significantly lower for higher concentrations (0.5-2.0 mM ASCR). Statistical analyses (Post hoc, Bonferroni) were performed by Marica Markovic and are mentioned in the experimental section (Table 15). Cells, which were exposed to 2 mM DAS showed a metabolic activity of ~85% after 24h and ~95% for lower concentrations (1-0.1 mM). The cells recovered after the additional resting period (24 h + medium exchange) and increased in metabolic activity represented by an increased cell number. Higher metabolic activity was observed for the control group with significant difference for the highest concentration of DAS (2 mM) in comparison to the control. Here, the metabolic activity was used as indirect measure of cytotoxicity and the PrestoBlue® assay showed excellent cell response to a broad range of both 2PI concentrations (2 – 0.1 mM ASCR and DAS). Statistical analyses (Post hoc, Bonferroni) were performed by Marica Markovic and are mentioned in the experimental section (Table 15).

Cytotoxicity in general is a function of concentration, and should always be considered when 2PIs are used for 2PP. For future 2PP cell encapsulation experiments, the appropriate concentration tolerable for cells must first be tested. Subsequently, 2PP structuring parameters for the chosen

Die approbierte gedruckte Originalversion dieser Dissertation ist an der TU Wien Bibliothek verfügbar.
The approved original version of this doctoral thesis is available in print at TU Wien Bibliothek.
TU Bibliothek Your knowledge hub WIEN

concentration must be set accordingly, while in the same time considering possible phototoxic parameters (irradiation intensity, writing speed, layer spacing). Oxidative stress during 2PP additionally influences cell viability. Oxidative stress is a major factor in tissue damage and is occurring when the production of reactive oxygen species (ROS) suppresses the antioxidant capacity of living organisms.[158] Acute and chronic oxidative injury may produce selective cell death and irreparable DNA damage. Due to their proposed sensitizing mechanism, the potential of ASCR and DAS to induce oxidative damage needs to be investigated in the future. Additionally, 2PIs can potentially penetrate through lipophilic cell membranes inducing cell damage within cells. The cell permeability of novel 2PIs (CR, ASCR) should be additionally tested.

Die approbierte gedruckte Originalversion dieser Dissertation ist an der TU Wien Bibliothek verfügbar.
The approved original version of this doctoral thesis is available in print at TU Wien Bibliothek.

2.5.2 Cell Permeability

Since lipophilic primary aromatic amines are suspected to induce carcinogenicity[376] a study was performed to investigate the cell permeability of the commercially available azo dye (CR) in comparison with its modification (ASCR). The cell membrane is a complex barrier, allowing merely certain molecules to pass according to their polarity and hydrophilicity.[377] First, a preliminary experiment was performed, investigating the cell permeability of the starting material (CR) by immersing L929 mouse fibroblasts attached on a well plate in a 2PI solution (1 mM, PBS). The sample was incubated for various time spans (10, 45 min) with CR solution, subsequently removing the 2PI solution and re-immersing the cells in PBS. The cellular uptake of CR was imaged using LSM700 (excitation channel: mRFP 555 nm, Figure 78). The control was imaged without immersion in 2PI solution.

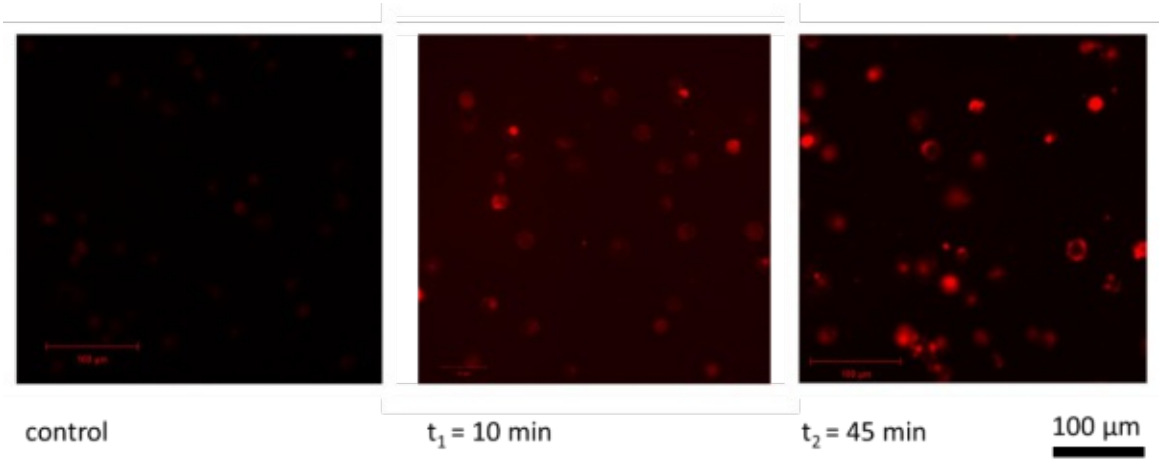

Figure 78: Accumulation of CR was observed within the cytosol of the cells (L929 mouse fibroblasts) upon treatment of the cells with 2PI solution (1 mM) for up to 45 min.

Over the course of 45 min, increased amount of fluorescence was detected within the cytosol of the cells at constant LSM laser settings. The accumulation of CR was visualized as ring-shaped fluorescence at certain areas of the cells. Marginal fluorescence was detected for the control group, corresponding to the auto-fluorescence of cells, which can be observed when relative high laser intensities (4.5%) and detector gain settings (639 V) are required for visualization. For a detailed investigation on cell permeability, additional experiments were performed at the LSM800 (laser channel 488 nm). Here, highly dedifferentiated ASCs were used, which were cultivated on an 8-well plate (ibidi) and immersed in 2PI solutions (2; 1 mM CR) in cell culture medium (DMEM). In contrast to the preliminary experiment (Figure 78), where the PI solution was removed after incubation, here the cells were kept immersed in 2PI solution over the course of 24h. An electronically switchable illumination and detection module (ESID) enabled additional monitoring of the cells via transmitted light illumination.

Die approbierte gedruckte Originalversion dieser Dissertation ist an der TU Wien Bibliothek verfügbar.
The approved original version of this doctoral thesis is available in print at TU Wien Bibliothek.

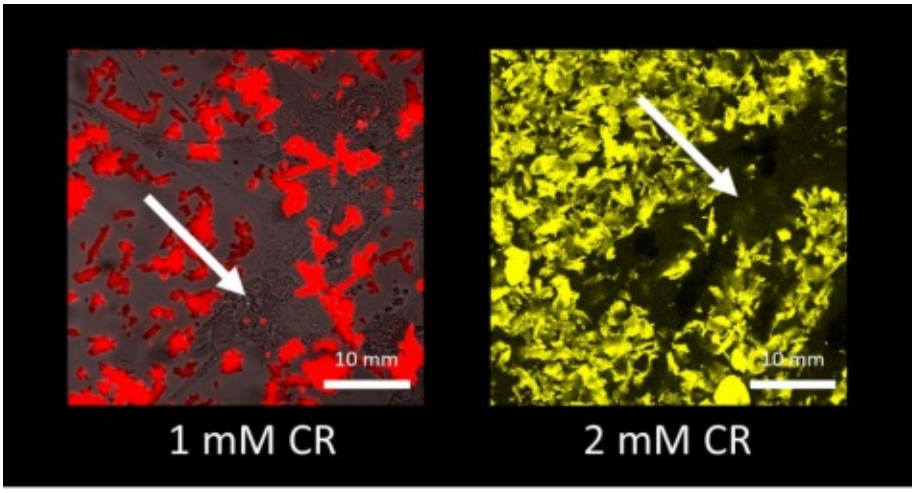

Figure 79: Precipitation of CR (DMEM cell medium) was observed, which severely limited the proliferation of the cells (adipose derived stem cells).

Severe precipitation of CR was observed for both concentrations, although stock solutions were beforehand investigated via the microscope. The cells were successfully imaged using the ESID detection channel in combination with the fluorescence image (depicted as overlay). However, cell-death was observed within 1h of treatment (arrows, Figure 79). Similar behavior was assessed for CR previously (PrestoBlue® assay, Figure 75). E2CK was tested additionally as reference 2PI, since it is known for its severe transmembrane migration into cells, which was investigated in a previous study.[329] Higher dilutions were tested for E2CK and CR (2 mM, 0.2 mM) but severe photodamage was observed for ASCs within the first 4h of incubation, presumably triggered by the high amount of precipitate. 2PIs can potentially induce phototoxicity upon transmembrane migration as a consequence of photoexcitation. Cell death is the most extreme manifestation of phototoxicity. Other effects may be much more subtle, such as in the case of CR the failure to move freely.[378,379]

To evaluate the cellular uptake of CR in comparison to the synthesized modification (ASCR) and the state-of-the-art 2PI (DAS), additional experiments were performed. Concentrations were chosen according to the commonly applied conditions during 2PP. Cells (ASCs) were cultivated and immersed in 1 mM 2PI solutions (CR, ASCR, DAS in cell culture medium (DMEM). Predefined sections of the cells were monitored every 30 min over the course of 24 h using an automated setup (LSM800, laser channel 488 nm, 4.5% laser intensity), enabling cell imaging with parallel incubation at 37°C (5% CO_2, Figure 80). The fluorescence of the control group was additionally imaged to compare the serial images of treated cells (Figure 81). An electronically switchable illumination and detection module (ESID) enabled additional transmitted light illumination of the cells. Time-lapse videos were taken additionally (not depicted) using ZEN imaging software (Zeiss).

Die approbierte gedruckte Originalversion dieser Dissertation ist an der TU Wien Bibliothek verfügbar.
The approved original version of this doctoral thesis is available in print at TU Wien Bibliothek.

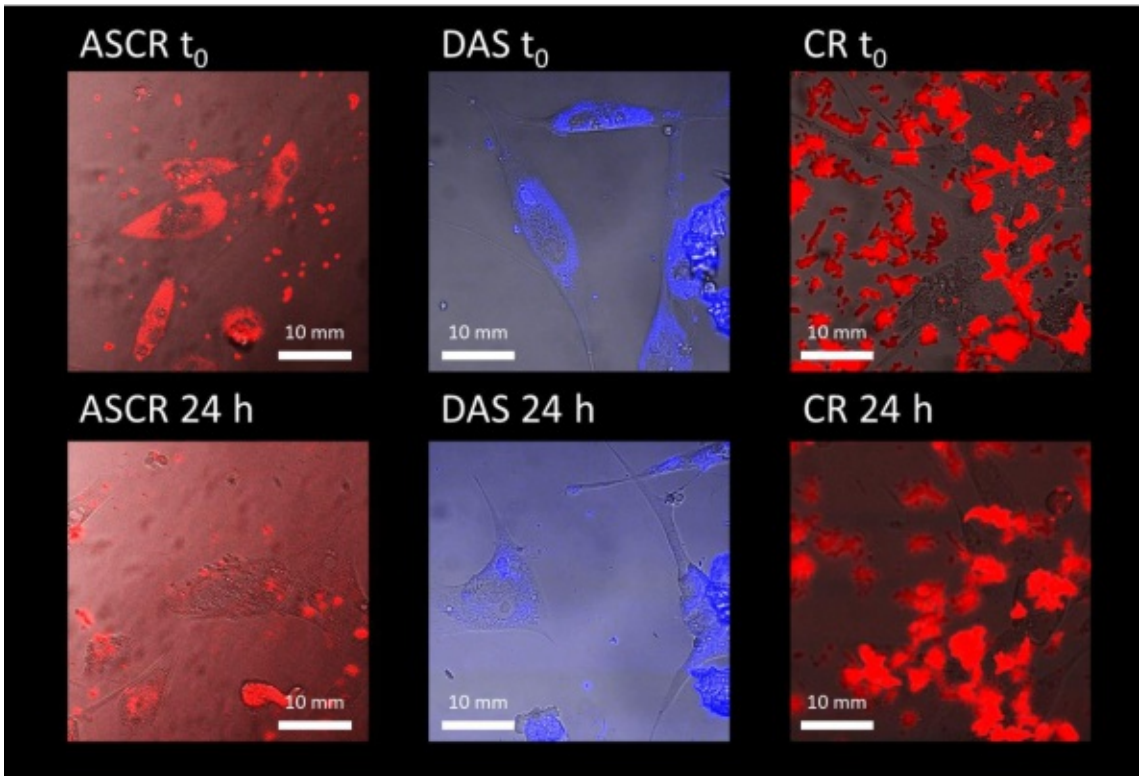

Figure 80: Fluorescence (auto-fluorescence) of adipose-derived stem cells (ASC) after treatment with 1 mM ASCR, DAS and CR solution in cell culture medium (DMEM). Precipitation of CR (agglomeration) was observed upon immersion with cell culture medium. Cell proliferation was observed over the course of 24h for cells immersed in ASCR and DAS solutions. Fluorescence was observed at the beginning (t_0) and after 24h (bottom) of immersing the cell in 2PI media. Reduced fluorescence derived from inaccurate focal plane settings over the course of the experiment observed.

The solubility of ASCR and of DAS surpassed the solubility of CR by far. Cell survival and -proliferation was successfully studied for ASCR and DAS over the period of 24h. Despite multiple trials to avoid the precipitation of CR (sonication at 40°C for 3h, change from cell medium to PBS), extensive amount of agglomeration was observed. Hence, cell-proliferation and -viability was again severely limited by the precipitation of CR. In general, reduced fluorescence was observed for all formulations over the course of 24h, deriving from the extensive mobility of the cells and inaccurate focal plane settings over the course of the experiment. Future experiments should include z-stack images (z > 20 µm) and larger observation windows (> 42x6 mm), to ensure cell imaging across an extended range at high proliferation rates. Since auto-fluorescence of the control group was detected, the observed fluorescence cannot be entirely assigned to the fluorescence of 2PIs. Multiple trials of finding appropriate laser settings failed to exclusively image fluorescence of 2PIs instead of the auto-fluorescence of the cells. High values for laser intensity (4.5%) and detector gain (639 V) were necessary in order to detect fluorescence at all, presumably due to the low 2PI concentrations (1 mM) the 2PIs. To compare the fluorescence with the results from the control group, a cell-section (without 2PIs in cell medium) was imaged additionally (Figure 81).

Die approbierte gedruckte Originalversion dieser Dissertation ist an der TU Wien Bibliothek verfügbar.
The approved original version of this doctoral thesis is available in print at TU Wien Bibliothek.

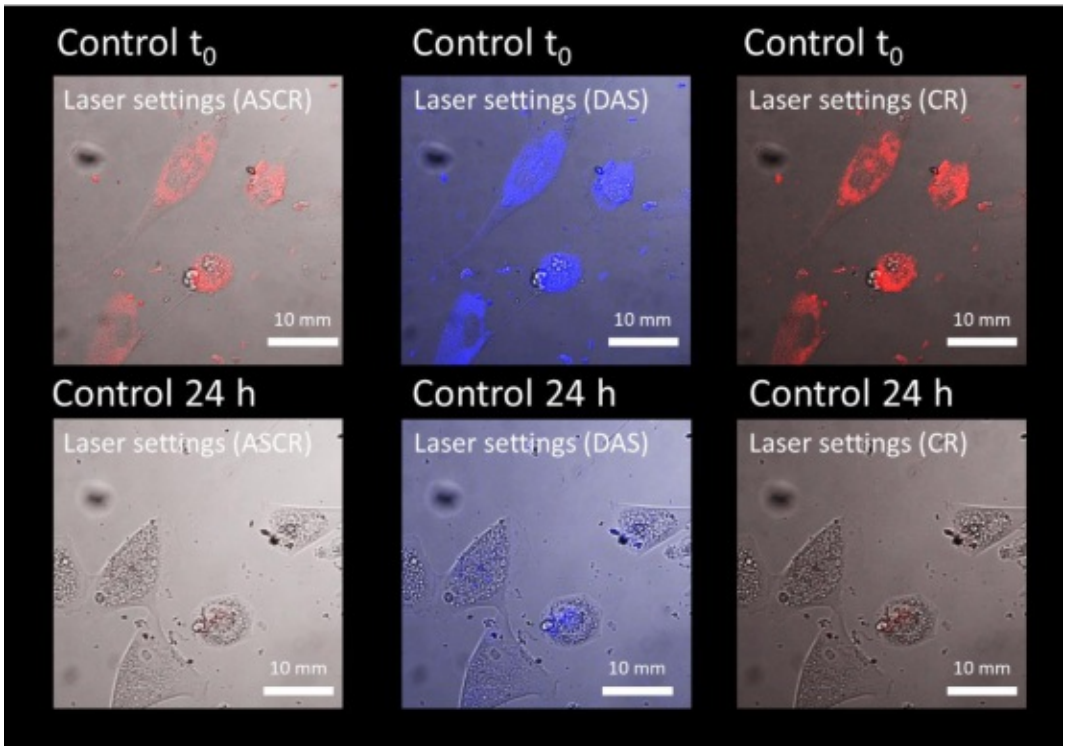

Figure 81: Auto-fluorescence of the control group (adipose-derived stem cells) without treatment of 2PI solutions. The control group (cells in DMEM medium) was imaged using the laser settings applied to image the different 2PIs (ASCR, DAS, CR). Colors were chosen accordingly (red: ASCR, CR; blue: DAS) to visualize the different 2PIs.

Limited fluorescence was detected for the control group as well (after 24h), due to the high proliferation rate of the cells and inaccurate focal plane settings over the course of the experiment. Nevertheless, cell-imaging of the viable cells was enabled via transmitted light illumination using the ESID detection module. The sections in Figure 81 are given by an overlay of ESID- and fluorescence images. The control group was imaged to investigate, whether the applied laser settings are affecting the viability of the cells. Since the development of low-fluorescent 2PIs (such as DAS), LSM imaging at reasonable settings remained a difficult task. High laser powers and detector gain was necessary to image 3D hydrogel constructs in general. Nevertheless, whenever cells are included, increased laser powers might decrease cell viability during LSM imaging.

In conclusion, many factors are determining phototoxicity (excitation wavelength, -intensity, -duration, 2PI concentration and -localization, cell type and -medium).[160] However, being aware that many of the literature-known azo dyes are listed as mutagenic or carcinogenic,[376] ASCR was proven biocompatible within the here tested concentrations (see also PrestoBlue® assay Figure 75) comparable to the state-of-the-art 2PI (DAS). ASCs were highly confluent and stretching outside of the observation window, however leading to a loss of focal plane. Although, 2PI cell permeability was attempted, the desired migration could not be proven here due to insufficient fluorescence of the 2PIs. Additionally, auto-fluorescence of the cells hindered the attempted imaging of 2PI-fluorescence. The results suggest a low fluorescence quantum yield for ASCR and DAS, which is usually desired and beneficial for and effective two-photon induced radical polymerization. Since high cell-proliferation was observed (similar to

Die approbierte gedruckte Originalversion dieser Dissertation ist an der TU Wien Bibliothek verfügbar.
The approved original version of this doctoral thesis is available in print at TU Wien Bibliothek.
TU Bibliothek Your knowledge hub WIEN

the control group), the chance of apoptosis (cell-death) due to the applied laser settings (e.g. irradiation intensity) was neglected. Extensive effort was spent on the visualization of the respective 2PIs to find appropriate settings (laser intensity and detector gain) using different LSM laser channels.[380] However, the auto-fluorescence of cells could not be sufficiently suppressed. Being an amphoteric dye, CR is heavily suffering from solute-aggregation, limiting its solubility in the tested formulations. The reduced solubility of CR is suggested to derive from the applied cell medium, since DMEM is containing increased levels of amino acids and vitamins beneficial for cell proliferation.[381]

Die approbierte gedruckte Originalversion dieser Dissertation ist an der TU Wien Bibliothek verfügbar.
The approved original version of this doctoral thesis is available in print at TU Wien Bibliothek.

2.6 Conclusion

In this thesis, novel water-soluble two-photon initiators (2PIs) were developed aiming to extend the absorption profile of current state of the art 2PIs towards the far-IR region (900 nm). Especially for biological applications, biocompatible alternatives are required, since current state-of-the-art 2PIs (P2CK) can possibly induce photodamage due to the generation of radical oxygen species upon excitation, which is proposed to derive from long triplet state lifetimes. The introduction of photolabile moieties (azo-sulfonates, AS) should tackle the issue by irreversible azo-bond cleavage, while ensuring efficient radical generation rate necessary for two-photon induced radical polymerization. This thesis was focusing on an extension of the AS-portfolio since AS-2PIs already showed enhanced biocompatibility compared to their cycloketone counterparts. In contrast to the previously introduced stilbene-based AS-2PI (DAS), here extended aromatic azo dyes were chosen as starting materials for the development of the novel 2PIs.The distinct UV-Vis absorption bands close to 500 nm, were expected to result in appropriate two-photon absorption (2PA) cross section upon two-photon polymerization (2PP). Congo Red (CR) was selected as starting material, susceptible towards diazotization of the terminal amino groups (Scheme 30). The synthesis of ASCR was performed by subsequent coupling of the transient diazonium salt to sulfite ions in alkaline media.

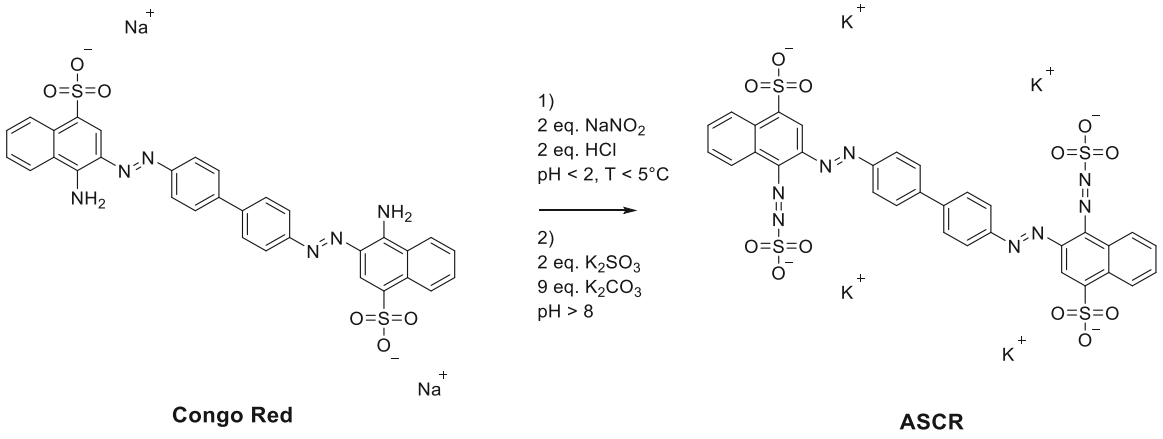

Scheme 30: Synthesis of azo-sulfonate congo red (ASCR).

The issues arising from the amphoteric character of CR (formation of colloidal dye-aggregates) were overcome by recrystallization of the commercially available starting material, applying low analyte concentrations and sonication if necessary. A moderate bathochromic shift of the absorption maximum was observed ($\Delta\lambda_{max}$ = 12 nm) upon modification compared to the starting material CR. For a detailed investigation of the synthesized 2PIs, photoreactor studies were performed, irradiating 2PI solutions with high-energy LED-light (365, 460 nm). In contrast to the novel 2PIs (ASCR, CR) photobleaching was observed for the state-of-the-art 2PI (DAS, Figure 83, right) including its commercially available starting material (DADS, Figure 84, right). Since both compounds are based on a stilbene-backbone and the C=C double bond is contributing with

Die approbierte gedruckte Originalversion dieser Dissertation ist an der TU Wien Bibliothek verfügbar.
The approved original version of this doctoral thesis is available in print at TU Wien Bibliothek.
TU Bibliothek Your knowledge hub WIEN

additional rotational freedom of the molecule, the observed loss of absorption maximum was proposed to be a consequence of photoisomerization instead of azo-bond cleavage.

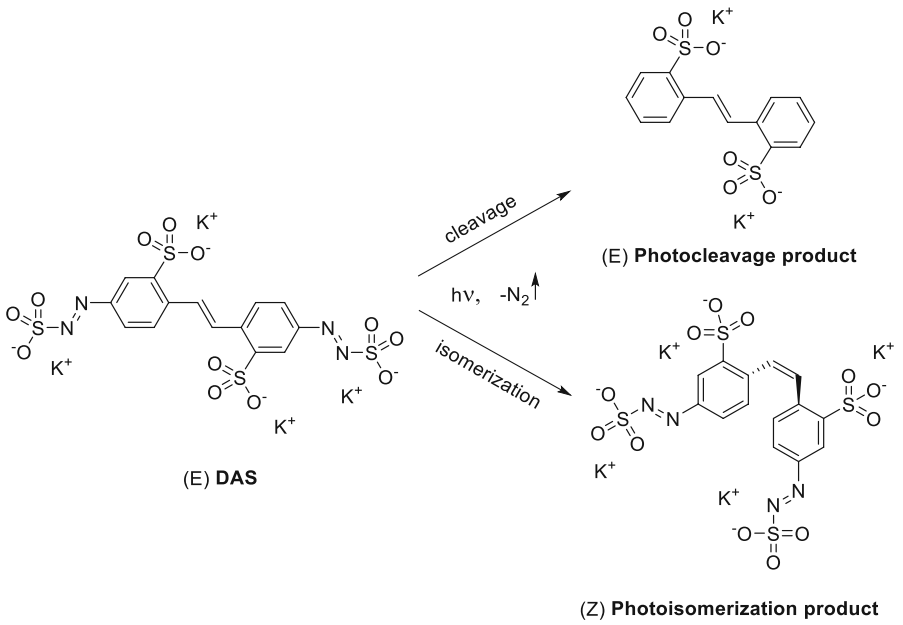

Figure 82: Proposed two-photon (and UV-) induced photoisomerization of stilbene 2PIs and the eventual photocleavage of azo-sulfonate moieties.

The mechanism upon irradiation for both compounds (DAS, DADS) was additionally investigated via NMR- and HPLC studies. The characteristic photoisomerization was confirmed for DADS (Figure 84, left). Neither photoisomerization nor photoproducts were confirmed for DAS (Figure 83, right).

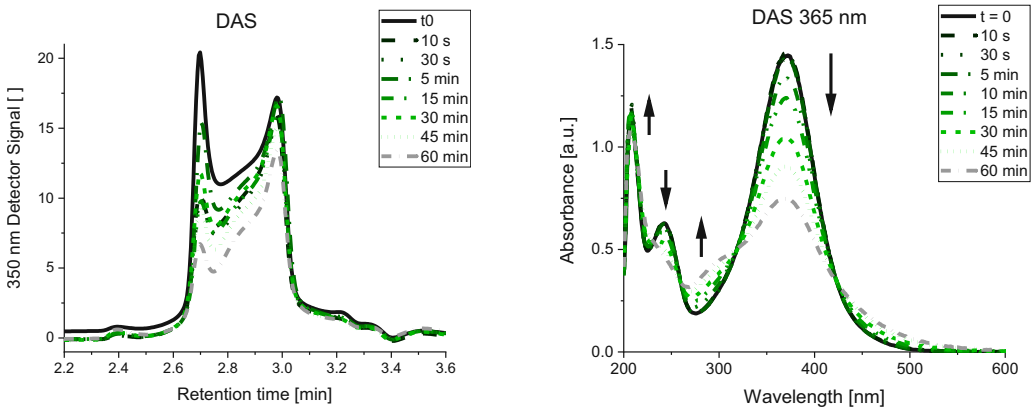

Figure 83: HPLC elution spectra (left)and UV-Vis absorption spectra (right) of DAS at specified timepoints during the photoreactor study.

Die approbierte gedruckte Originalversion dieser Dissertation ist an der TU Wien Bibliothek verfügbar.
The approved original version of this doctoral thesis is available in print at TU Wien Bibliothek.

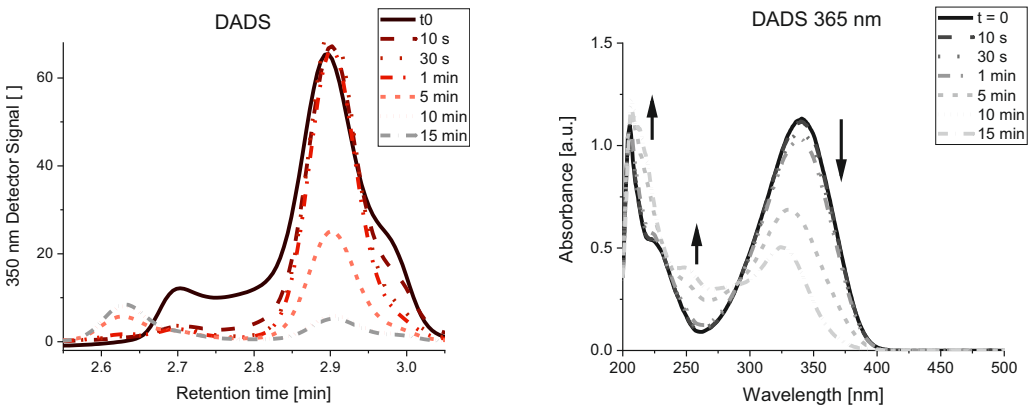

Figure 84: HPLC elution spectra (left)and UV-Vis absorption spectra (right) of DADS at specified timepoints during the photoreactor study.

Still, the proposed mechanism of azo-bond cleavage (DAS) might also be induced after an initial photoisomerization mechanism.[70] The enhanced biocompatibility of DAS, might be explained by the proposed photoisomerization mechanism, since a lower radical generation rate might induce less photodamage as a consequence of less radical oxygen species. Nevertheless, the irradiation intensities applied within the photoreactor studies, are of multiple magnitudes lower compared to the peak intensities at the focal point of the applied pulsed laser beam (200 mW cm^{-2} for 365 nm LED compared to 25 TW cm^{-2} for 800 nm 2PP). To assess the 2PA cross section of the novel 2PIs, z-scan measurements were performed and CR exhibited extraordinarily high values across the measured wavelength region (700-900 nm, σ^{2PA}_{max} = 1490 GM at 700 nm), overruling many state of the art 2PIs (180 GM P2CK, 90 GM DAS). Since a broad processing window was expected for the novel 2PIs, wavelength-dependent threshold tests were performed using 2PP (200-10 mW average laser power; 200-1000 mm s^{-1}writing speed). High-resolution microfabrication of gelatin-modified hydrogels (GelMA) was possible across a broad range of applied wavelength (725, 800, 900 nm).

Die approbierte gedruckte Originalversion dieser Dissertation ist an der TU Wien Bibliothek verfügbar.
The approved original version of this doctoral thesis is available in print at TU Wien Bibliothek.

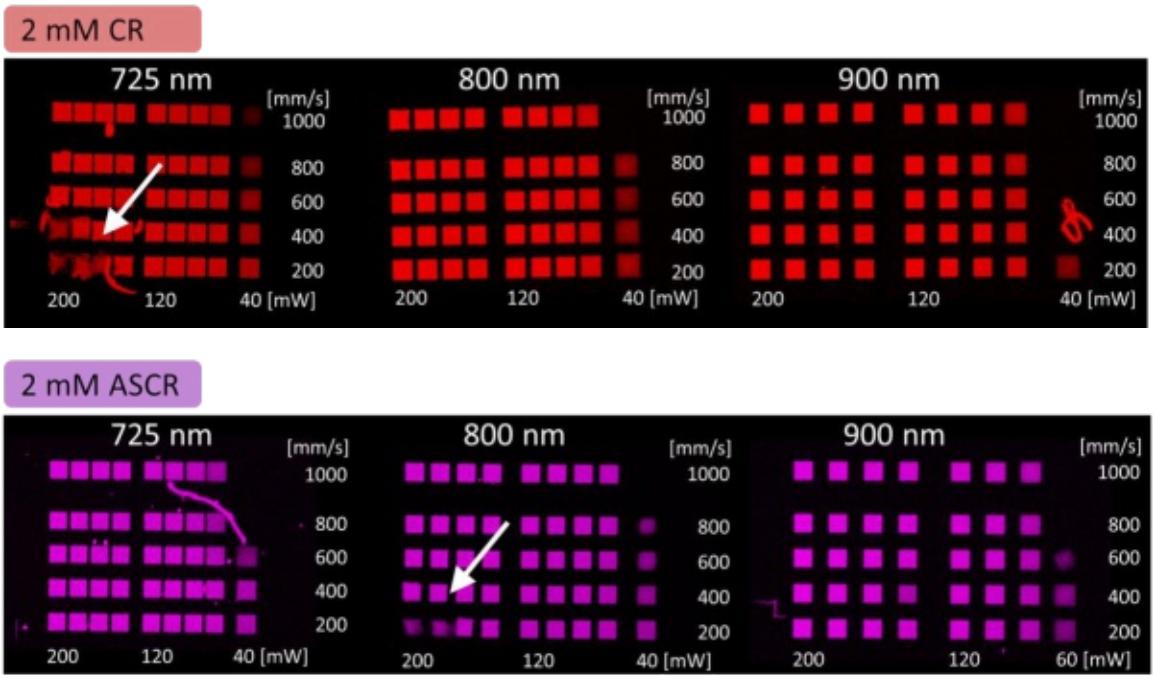

Figure 85: Two-photon polymerization of methacrylate modified gelatin hydrogels in the presence of CR and ASCR.

A wavelength-dependent laser ablation of hydrogel cubes was observed for the novel 2PIs (at 725 nm for CR, at 800 nm for ASCR) assumed to be derived from the high 2PA of the novel chromophores. Still, the hydrogel-cleavage might also be derived from harsh structuring conditions and overlapping focal spots in combination with the enhanced absorbance of the novel 2PIs. The observed bubble formation was proposed as indication for nitrogen gas-formation as a consequence of azo-bond cleavage or as indication for thermally induced hydrogel decomposition (evaporation of water). Still, the novel 2PIs are extremely versatile since highly-resolved hydrogel microstructures and extraordinarily low polymerization thresholds could be obtained. Besides the excellent processability of the novel AS-2PIs, great potential was found during cell-viability studies. ASCR was tested on dedifferentiated adipose-derived stem cells and showed comparable biocompatibility to the state-of-the-art 2PI (DAS). However, low solubility of CR in cell medium hindered the cells from proliferating, exhibiting high dark-toxicity at tested concentrations (2-0.1 mM). For the application of ASCR in future cell-encapsulation experiments it is of crucial importance to investigate whether the applied 2PI is penetrating inside the cell membranes, which is an additional determining factor of phototoxicity. Cell-permeability tests were performed over the course of 24h however, the low sample concentrations (1 mM) resulted in low fluorescence of the tested 2PIs. Cell-penetration of the 2PIs could not be observed, since the auto-fluorescence of the cells overruled the distinct fluorescence signals of the 2PIs. Still, cell-proliferation could be observed via transmitted light illumination for the novel biocompatible 2PI (ASCR) over a period of 24h.

Die approbierte gedruckte Originalversion dieser Dissertation ist an der TU Wien Bibliothek verfügbar.
The approved original version of this doctoral thesis is available in print at TU Wien Bibliothek.

3 Hydrogel Materials for Two-Photon Polymerization

3.1 State-of-the-Art Hydrogel Materials

The constant development of hydrogel materials is of crucial importance to ensure their successful application in biomedicine. The fundamental principles of tissue engineering (TE) need to be fulfilled, while at the same time meeting the ever-changing demands for every specific application (e.g. water-solubility, biocompatibility, biodegradability, bioactivity, structural similarity to the desired type of tissue, mechanical support for cell-regulative behavior). There is already a great variety of hydrogel materials available and an even broader range of their respective crosslinking mechanism.[3,7,9,12,39,91,92,137] In general, hydrogels can either be interconnected by physical or chemical crosslinks (non-covalent or covalent bonds). However, hydrogel assembly is strongly dependent on the chemistry and respective type of macromer precursor (Figure 86).

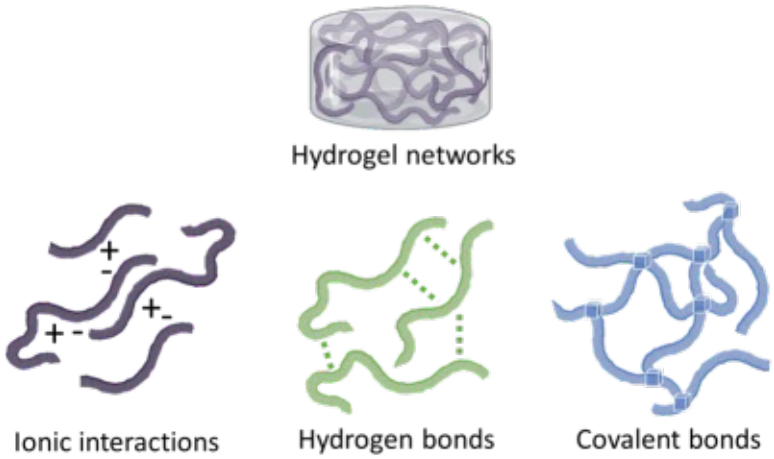

Figure 86: Hydrogel matrices can be assembled either by non-covalent bonds (ionic interactions, hydrogen bonds) or by covalent crosslinks between macromer molecules.

This thesis is focusing on photopolymerizable, covalently crosslinked hydrogel materials for 3D cell encapsulation. Two-photon polymerization (2PP) is an attractive technology to fabricate highly-resolved hydrogel matrices in the presence of cells. An effective approach to introduce covalent crosslinks is realized by 2PP, in particular by scanning a focused NIR laser beam across a photosensitive precursor formulation. By this, precise microfabrication of the cell microenvironment and mechanical fine-tuning of hydrogel matrices are possible. The effective crosslinking of macromers is essential, to ensure a successful additive manufacturing process. Therefore, highly reactive functional groups must be introduced. Naturally occurring proteins (gelatin) as well as polysaccharides (alginate, hyaluronic acid) are especially attractive model compounds, since they possess multiple functional groups available for modification (carboxylic acids, primary alcohol and -amino groups).[50,382] Besides the biocompatibility of the polymer backbone itself, the cytotoxicity of introduced photocrosslinkable moieties is a major factor in

Die approbierte gedruckte Originalversion dieser Dissertation ist an der TU Wien Bibliothek verfügbar.
The approved original version of this doctoral thesis is available in print at TU Wien Bibliothek.
TU Bibliothek Your knowledge hub WIEN

determining the successful application of hydrogels in TE. Vinyl ester (VE) moieties were established as biocompatible alternatives compared to state-of-the-art (meth-)acrylic monomer mixtures, which are known for their acute and chronic toxicity (Figure 87).[383]

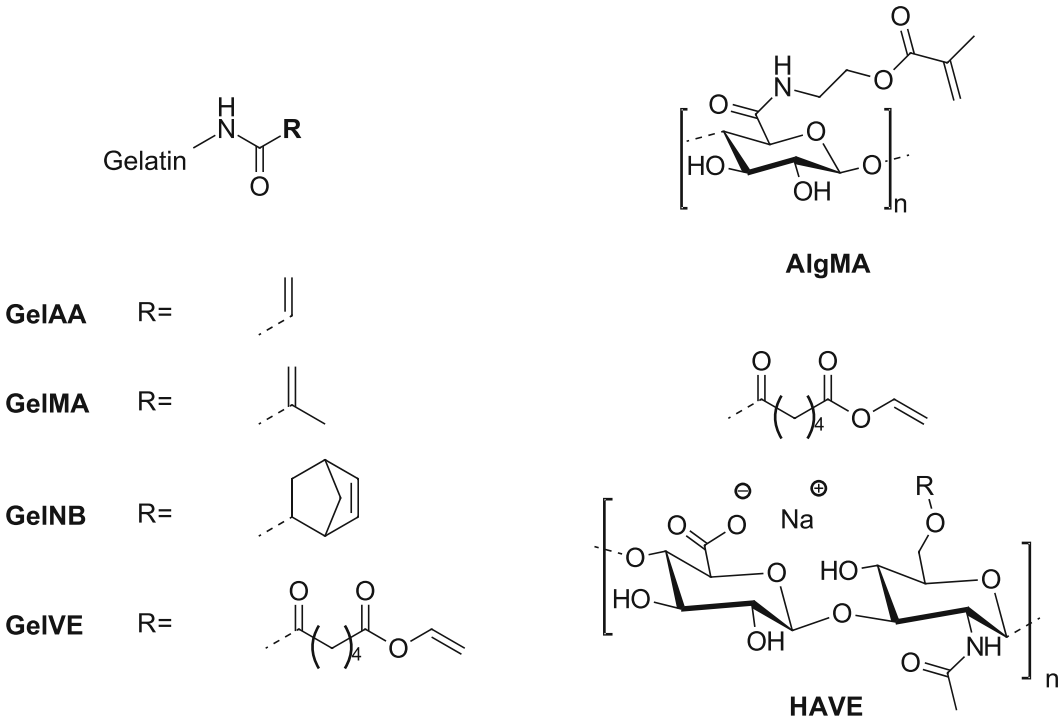

Figure 87: Naturally-derived proteins such as gelatin (Gel),[50-54] polysaccharides such as alginate (Alg)[40] and hyaluronic acid (HA)[43] are highly relevant biomaterial for the design of photopolymerizable hydrogels. Reactive -ene functionalities such as (meth-)acrylate and vinyl ester groups can be introduced by the chemical modification of functional groups of native model compounds (carboxylic acids, primary amines and -alcohols). Most common modifications include acrylates (GelAA), methacrylates (GelMA, GelMA-AEMA, AlgMA),[347] norbornenes (GelNB),[113] and vinyl esters (GelVE, HAVE).[115]

Due to their relatively high reactivity, (meth-)acrylates are widely used for the fabrication of hydrogels, however the risk of harming native tissue when unreacted monomer is still present in the final 3D construct, is still an issue to be solved. VEs became more and more attractive, due to the possibility to boost their initial low reactivity via thiol-ene chemistry.[81] Since unreacted VE groups show reduced cytotoxicity compared to acrylic monomer mixtures they have been widely studied as suitable macromers for bio-based applications.[76] By the fine-tuning of multiple parameters, such as crosslinking density, molecular weight as well as blending with other polymers or nanomaterials, the mechanical stiffness of hydrogels can be adjusted. This led to the development of a broad range of homopolymers as well as hybrid-materials.[384]

Amongst the available natural biopolymers, hyaluronic acid (HA) is an attractive material platform for the fabrication of hydrogels owing to its broad bioavailablility.[43] The clinical use of HA-hydrogels ranges from dermal fillers, corneal and dermal wound repair to pharmacological active scaffolds and viscosupplements in ophthalmology and otology.[61]

Die approbierte gedruckte Originalversion dieser Dissertation ist an der TU Wien Bibliothek verfügbar.
The approved original version of this doctoral thesis is available in print at TU Wien Bibliothek.

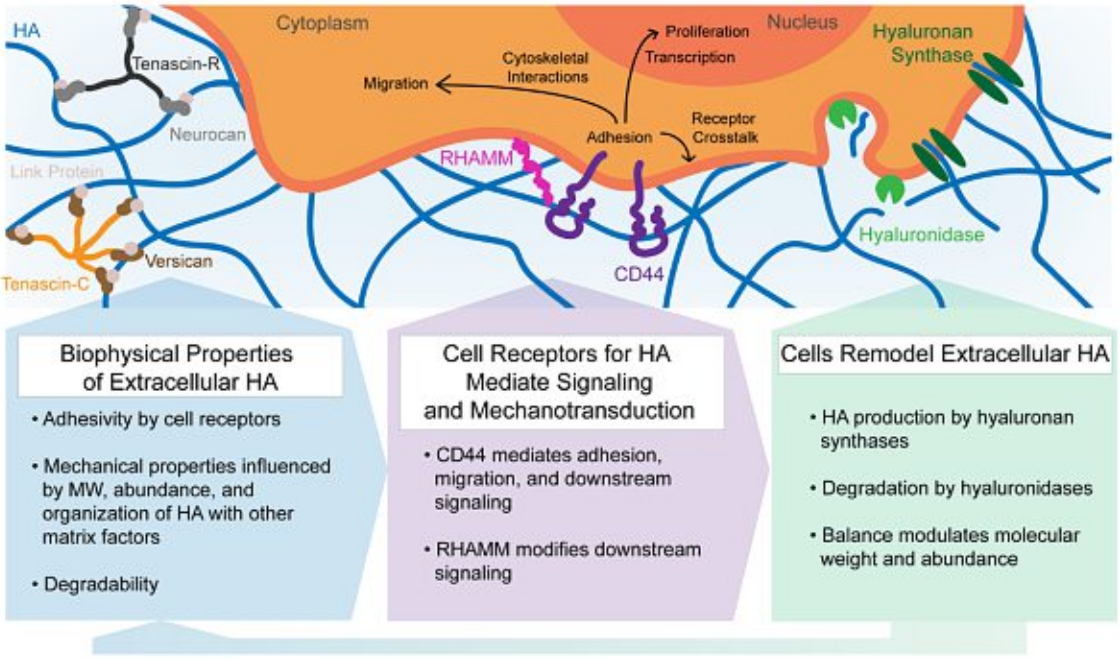

Figure 88: HA-selective enzymes and receptors are naturally present in the human body.[59] Cells are able to selectively sense the biophysical properties of extracellular HA (left) by surface receptors (CD44, RHAMM, middle). The natural remodeling of HA is promoted by hyaluronan-synthases and hyaluronidases (right).

An average human adult possesses approximately 15 g HA throughout the body, with a daily turn-over-rate of about 30%, whereas the abundance and molecular weight of HA is strongly tissue-dependent.[385-387] Cells within the body are equipped with membrane receptors (CD44, RHAMM), capable of selectively binding to HA. These receptors can transduce biochemical signals, which then can influence cell adhesion and motility. Hence, the biophysical properties of extracellular HA are supposed to have an impact on cell adhesion, -migration and -proliferation. However, the role between receptor interactions and cells and their dependence on the microenvironment is a complex issue, which remains unclear. However, during the clinical application of HA it was soon discovered, that injected HA was exhibiting a rapid degradation-rate, reducing its therapeutic benefit.[59] Nevertheless, biodegradability as well as mechanical properties of HA-hydrogels can be guided by the modification of HA's functional groups (carboxylic acids, primary alcohols). Hyaluronic acid vinyl ester (HAVE) for example was vigorously investigated as material for hydrogel fabrication.[388] Additionally, the processability via 2PP was studied enabling high resolution 3D cell encapsulation.[115] However, the coordination of system parameters, such as molecular weight of the precursor and degree of functionalization always remained a practical issue. The solubility of the precursor formulation is strongly influenced by the degree of substitution, hence determining the practicability in the laboratory and the successful application in combination with cells. Therefore, accurate fine-tuning of system parameters are an integral element for the design of hydrogel macromers as well as for their successful application in high-resolution 3D printing.

Die approbierte gedruckte Originalversion dieser Dissertation ist an der TU Wien Bibliothek verfügbar.
The approved original version of this doctoral thesis is available in print at TU Wien Bibliothek.
TU Bibliothek Your knowledge hub WIEN

3.2 Synthesis of Hyaluronic Acid-based Macromers

Several improvements for the synthesis of HAVE macromers were explored, in contrast to the previously reported methods.[388-390] Depending on the desired final molecular weight (m.w.), HA can be degraded via acidic hydrolysis, while monitoring the m.w. via GPC analysis. Degradation of high-m.w. HA (2 MDa) is usually performed in aqueous solution at elevated temperature (60 °C) in the presence of hydrochloric acid. After neutralization and dialysis, HA sodium salt is obtained as a white solid after lyophilization. Instead of an acidic degradation, a defined m.w. of HA can be purchased and modified according to the subsequent method. The counter-ion (Na^+ vs. TBA^+) must be exchanged to increase HA's solubility in DMSO. This was performed by adding highly acidic ion-exchange monomer mixture to an aqueous solution of HA, stirring the suspension for 4 h at room temperature. After filtering off the ion-exchange monomer mixture and neutralization with an aqueous solution of tert-butyl ammonium hydroxide (TBA-OH) the TBA-salt of HA was obtained (HA-TBA) after dialysis and lyophilization. Esterification of the primary alcohol was then performed in DMSO in the presence of excessive amount of divinyl adipate (DVA, 15 eq., Scheme 31). Hydroquinone (HQ, 0.05 eq.) was added to reduce the chance of premature crosslinking. After stopping the reactions at defined timepoints, the macromers were purified via dialysis and observed as white solids.

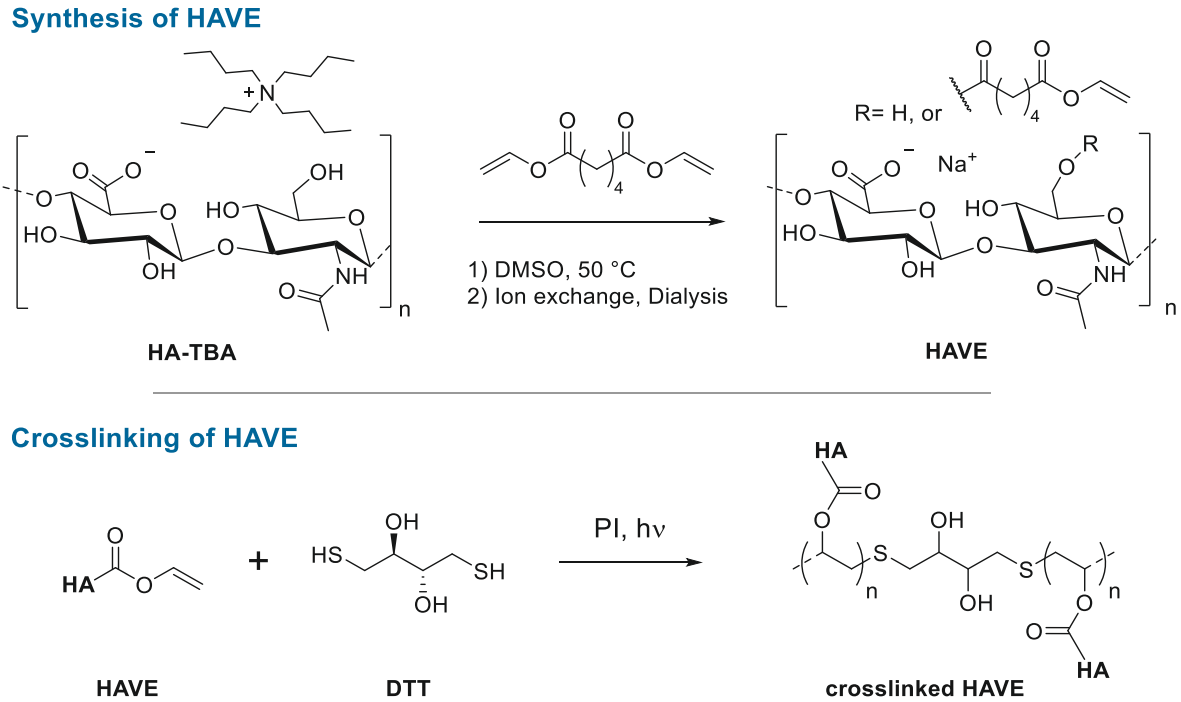

Scheme 31: The synthesis of hyaluronic acid vinyl ester precursors (HAVE) is performed via a transesterification reaction of HA-TBA in DMSO with excessive amount of divinyl adipate (top). The principle of the mixed thiol-ene/homopolymerization crosslinking reaction with dithiothreitol (DTT) in the presence of a photo initiator is depicted above (bottom).

A toolbox of HAVE macromers were available from previous studies (HA22- HA80) and were collectively used with the newly synthesized macromers, to extend the knowledge on HA-based

Die approbierte gedruckte Originalversion dieser Dissertation ist an der TU Wien Bibliothek verfügbar.
The approved original version of this doctoral thesis is available in print at TU Wien Bibliothek.

materials. Compared to synthesis methods described in literature,[388] following adaptations were made. Generally, any type of HA-intermediate can be precipitated in 50-fold amount of isopropyl alcohol, stirred with a mechanical stirrer in a large beaker, instead of diluting the reaction mixture[388] or precipitation in EA.[389] Depending on the m.w., the precipitate can be either centrifuged or decanted and washed with distilled isopropyl alcohol to remove unreacted DVA, HQ and DMSO. HA with high m.w. usually forms spongy and rubbery aggregates upon precipitation. The aggregates can be mechanically unpicked and extensively washed with isopropyl alcohol. HAVE can also be synthesized without the addition of Candida Antarctica Lipase B (CAL-B), since it was found that the transesterification of primary alcohols is promoted by simply stirring HA-TBA in DMSO in the presence of excessive amount of DVA. A broad range of macromers were available from previous studies (HA22- and HA80- macromers) with m.w. ranging from 22 kDa up to 80 kDa and a wide spectrum of DS (5-95%). The portfolio was extended by the synthesis of a novel macromer (HA50VE05) based on a commercially available sodium hyaluronate (50 kDa, Contipro). Generally, the reaction time during transesterification reaction cannot be taken as a measure for the expected DS. The effective esterification of primary alcohols highly depends on the viscosity of the HA solution during the reaction. Like effects described in literature, in general slightly higher DS were obtained for low-m.w. precursors compared to same reaction conditions used for high-m.w. HA. This is potentially explained due to the decreased viscosity for low-m.w. HA, leading to increasing mobility of various species during the reaction.[391] In contrast to synthesis methods previously reported in literature, several improvements were found. Regarding the m.w. of HA, there is an immense variability on the market, starting from relatively low (20 kDa) to high macromer sizes of up to 1 MDa. Nowadays, outstanding research in the field of TE is published using m.w. in the range of 10 kDa,[392] 20 kDa,[393] 50 kDa,[391,394,395] 100 kDa[396] and rarely up to 350 kDa.[391] Due to the immense increase in water-solubility and improved practicability within the laboratory, it is strongly recommended to maintain a precursor-m.w. below or at ~50 kDa. Whenever the m.w. of HA exceeds a certain limit (~100 kDa) the precursor becomes more and more difficult to dissolve, at least for HAVE precursors with a moderate to relative high DS. Still, the effect on cells of hydrogels, consisting of ultra-low m.w. precursors, remains relatively unclear. The discussion on CD44 receptor activation derived from low-m.w. HA, led to the temptation to synthesize high-m.w. hydrogel precursors, but as mentioned above, these precursors became more and more insoluble and impractical to work with. Additionally, upon photopolymerization and covalent crosslinking of precursor molecules, the chance for receptor activation is proposed to be lowered. Nevertheless, there is still the risk of cell-receptor activation derived from degradation of the hydrogel. But key factors such as the water-solubility and handling of the final precursor formulation should always play a major role in the development of novel macromers. After the synthesis of HAVE precursors, several characterization methods are necessary. First, the determination of DS (via ^{1}H-NMR), the final m.w. before and after modification (via GPC) and the material properties of final hydrogel matrices (photorheology, swelling ratio).

Die approbierte gedruckte Originalversion dieser Dissertation ist an der TU Wien Bibliothek verfügbar.
The approved original version of this doctoral thesis is available in print at TU Wien Bibliothek.
TU Bibliothek Your knowledge hub WIEN

3.3 Characterization of HAVE Hydrogels

3.3.1 NMR Analysis

The degree of substitution (DS) was determined via ^{1}H-NMR spectra in D_2O upon addition of 4% v/v NaOD (Figure 89). NaOD is added since the resolution of recorded spectra is increased because of reduced viscosity of the solution. Furthermore, hydrolysis of the vinyl ester moiety is expected, resulting in cleavage of the functional groups followed by the release of acetaldehyde. Nevertheless, the quantification of the DS is still possible, since remaining adipate can be observed. High reproducibility and increased resolution of the spectra were key reasons why the DS was determined upon addition of NaOD. In the following the nomenclature HA(m.w.)VE(DS) was chosen for HAVEs originating from HA with a certain m.w. and DS, e.g. HA50VE05 was derived from HA with a m.w. of 50 kDa having a DS of 5% as determined via NMR. The well separated methyl signal of the acetamido group (2.0 ppm) was used as reference signal to assess the DS for the synthesized macromer. Signals from 4.5-4.8 ppm represent the protons at the anomeric C-atoms (C1, C1') and signals from 3.3-3.9 ppm can be interpreted as the ring-protons of the HA backbone and the CH_2 signal of the primary -OH group. Spectra were measured on a 600 MHz spectrometer (16 scans, Figure 89).

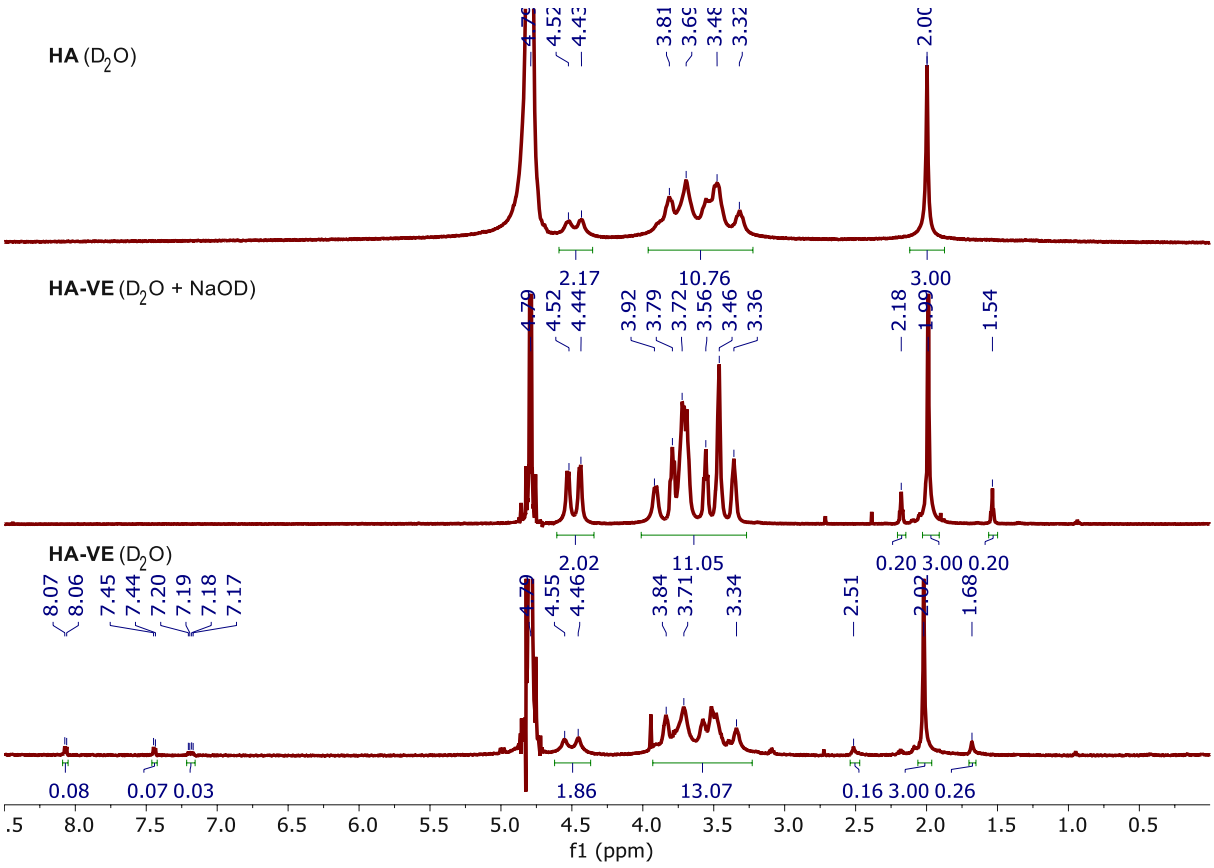

Figure 89: ^{1}H-NMR spectra of HA (top) and HA50VE05 (bottom) in D_2O. For the determination of the degree of substitution, HAVE macromers were recorded in D_2O with addition of 4% NaOD (middle) to increase the resolution of the spectrum as a consequence of reduced viscosity.

Die approbierte gedruckte Originalversion dieser Dissertation ist an der TU Wien Bibliothek verfügbar.
The approved original version of this doctoral thesis is available in print at TU Wien Bibliothek.

3.3.2 GPC Analysis

GPC elugrams of HA22VE95 and HA50VE05 before and after functionalization are depicted hereafter (Figure 90). A minor increase in molecular weight is indicated, which was expected to be a consequence of functionalization but also proved that the excess of DVA is sufficient as no interlinking of HA chains took place.

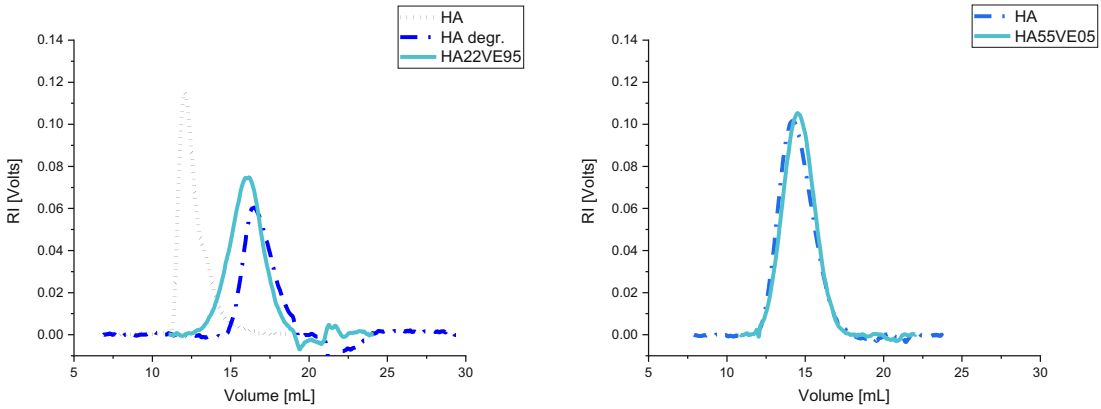

Figure 90: GPC elugrams of HA22VE95 (left) and HA50VE05 (right) before (dot-dashed line) and after functionalization (solid line). HA22VE95 was prepared via acidic degradation starting from HA with M_n of 1.5 MDa (black dotted line).

3.3.3 Photorheology

To investigate the influence of synthesis as well as formulation originated parameters, photorheology was performed. By this versatile tool the photoreactivity and crosslink efficiency of hydrogel formulations can be investigated.[397,398] Measurements were performed in oscillation mode by in situ photopolymerization of hydrogel formulations upon irradiation with filtered light (320 – 500 nm) through the bottom glass plate of the plate-to-plate measuring system. The light intensity at the tip of the light guide was determined via radiometer (3.16 W cm^{-2}), referring to a light intensity of 30 mW cm^{-2} directly above the glass plate. Important system parameters were obtained from storage modulus (G') curves (Figure 91).

Die approbierte gedruckte Originalversion dieser Dissertation ist an der TU Wien Bibliothek verfügbar.
The approved original version of this doctoral thesis is available in print at TU Wien Bibliothek.

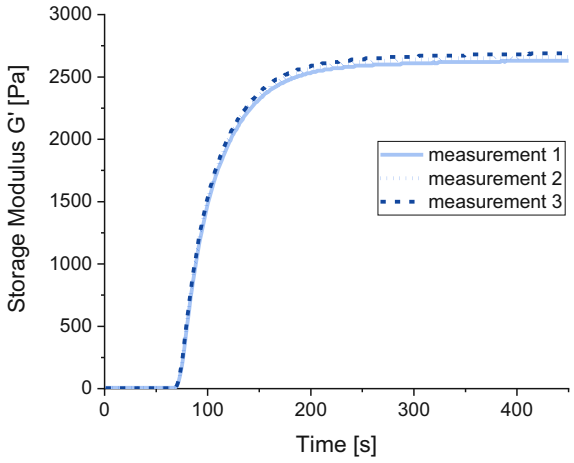

Figure 91: Photorheology curves of HA50VE05 triplicates (15 wt.% macromer content, 0.5 mM LiTPO, 80 mol% (thiol to ene) DTT representing conditions used for UV-encapsulation of ASC-GFPs. Samples were irradiated with filtered light (320 – 500 nm) bottom-up through the glass plate. Storage moduli G' were measured every second and the light was automatically activated after 60 seconds.

G'_{max} was used to calculate the average mesh size (L) of the networks as a measure of the crosslink density of the hydrogels (equation (2)).[399]

Equation $$L = \left(\frac{R \cdot T}{G'_{max} \cdot N_A}\right)^{1/3} \quad (2)$$

Additionally, the slope ($\Delta G' \Delta t^{-1}$), delay time (t_d) and the time to reach 90% of G'_{max} ($t_{G'_{max}}^{90\%}$) were calculated to assess the quality of photopolymerization of the hydrogel systems.[398] The influence of the photoinitiator concentration (lithium phenyl-2,4,6-trimethylbenzoylphosphinate LiTPO) was reported and an optimum concentration of 0.05 wt.% LiTPO was found .[115] A broad range of photorheology experiments were conducted, to investigate important structure parameters (macromer content, macromer chain length and degree of substitution) on the reactivity and mechanical properties of final hydrogels.[115] Additionally, a model system based on HA22VE95 in combination with a difunctional thiol (DL-dithiothreitol DTT) was analyzed in order to optimize the thiol to ene ratio by photorheology. Here, an excessive amount of thiol led to a predominant ratio of mono-reacted groups and therefore retarded network formation and decreased final crosslink densities. The best results were found to be delivered by a ratio of 80 mol% thiols compared to ene. Further experiments were performed, where the influence of macromer content and DS on thiol-ene optimized formulations were investigated.[115]

3.3.4 Hydrogel Swellability

Complementary to the photorheological study the swellability of ready-cured hydrogels was investigated, providing useful information about the crosslink density of the networks. The influence of increased macromer size, addition of thiol (DTT), and DS was already investigated in literature.[115] Here, two selected macromers were studied in detail, especially interesting for UV cell encapsulation (HA50VE05, HA22VE95). To obtain sufficient hydrogel stability and due to

Die approbierte gedruckte Originalversion dieser Dissertation ist an der TU Wien Bibliothek verfügbar.
The approved original version of this doctoral thesis is available in print at TU Wien Bibliothek.
TU Bibliothek Your knowledge hub WIEN

HAVE's relatively low DS, a high macromer content was chosen [15% (w/v)]. Stock solutions of LiTPO (0.1%) and DTT (0.2%) were separately prepared and combined with PBS and pipetted on top of lyophilized HAVE. The formulation was transferred into silicone molds and polymerized in a UV curing system for 4 min.

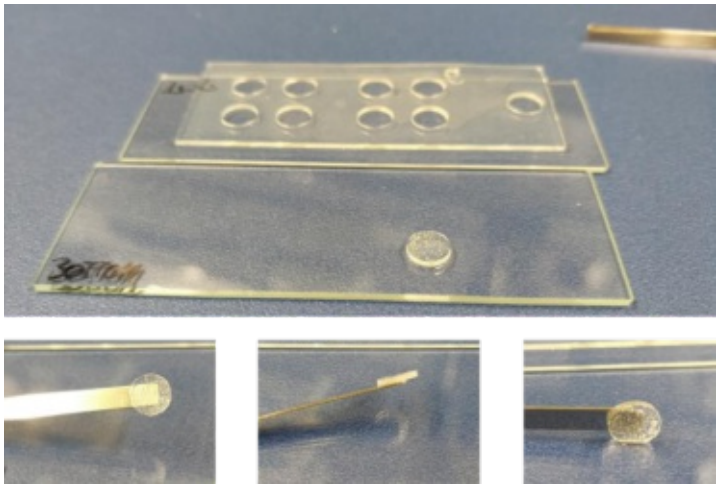

Figure 92: Hydrogel pellets were UV polymerized using silicone molds applied on glass cover slips. (HA50VE05/80 mol% thiol to ene DTT, 15 wt.% macromer content, 0.5 mM LiTPO)

The swelling ratio is defined as the fractional increase in the weight of the hydrogel due to water absorption. The mass swelling ratio Q_m was calculated from the swollen mass and the dry mass of the lyophilized hydrogels according to equation (3). Furthermore, the sol fraction was calculated, representing the fraction of the polymer following a crosslinking reaction that is not part of a crosslinked network. Mass loss was calculated according to equation (4), where w_0 is the initial weight of the macromer needed per hydrogel pellet and wd is the weight of the dried hydrogel pellet. The mass percentage was calculated using equation (5). Mass of the gels was obtained after UV-polymerization (w_{uv}), after lyophilization (w_i), after swelling in PBS for 24h (w_s) and after repeated lyophilization (wd).

Equation $$mass\ swelling\ ratio\ Q_m[\%] = \frac{w_s - w_d}{w_d} \times 100 \quad (3)$$

Equation $$mass\ loss\ [\%] = \frac{w_i - w_d}{w_i} \times 100 \quad (4)$$

Equation $$mass\ percentage\ [\%] = 100 - mass\ loss \quad (5)$$

Increasing swellability of the hydrogels was observed with decreasing DS derived from increased mesh size and increased hydrophilicity. Furthermore, the swellability also increased with increasing macromer size. However, this finding must be reconsidered in sight of the steep curve progression of Q_m with DS and the different values of DS obtained for the two macromer sizes.

Die approbierte gedruckte Originalversion dieser Dissertation ist an der TU Wien Bibliothek verfügbar.
The approved original version of this doctoral thesis is available in print at TU Wien Bibliothek.

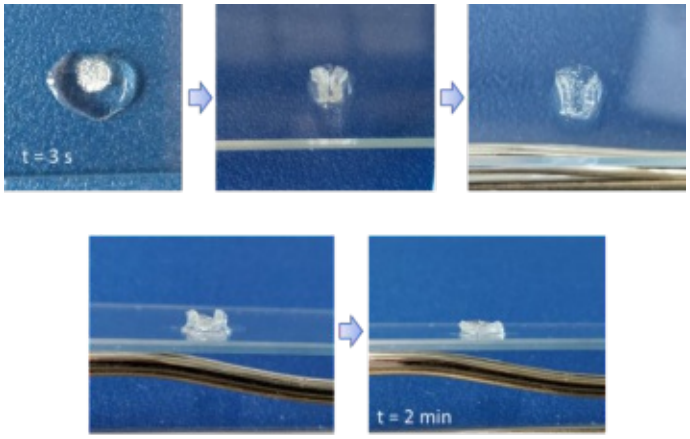

Figure 93: Swelling behavior of HA50VE05 hydrogel after addition of PBS (15 wt.% macromer content, 80 mol% thiol to ene DTT, 0.5 mM LiTPO).

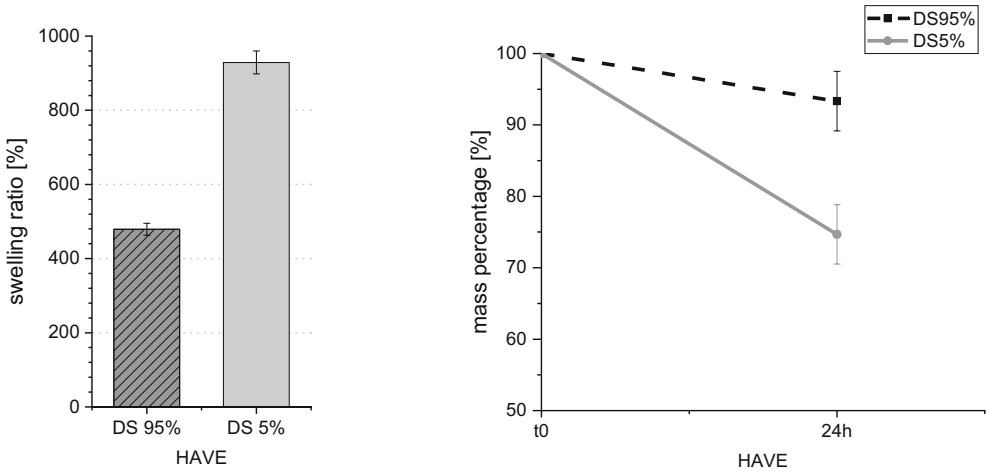

Figure 94: Hydrogel swelling ratio (left) of HA22VE95 (479 ± 16%) and HA50VE05 (928 ± 31%) both containing 80 mol% thiol-to-ene DTT, 15 wt.% macromer content and 0.5 mM LiTPO. Mass loss profiles (mass percentage) are depicted on the right (93 ± 4% for HA22VE95 and 75 ± 4% for HA50VE05 after 24h).

Increased swellability is observed for HA50VE05 most probably due to the increased hydrophilicity of the macromer due to reduced DS, compared to HA22VE95 with an increased number of hydrophobic side chains (Figure 94). This effect is explained by the decreased mesh size observed for macromers with high DS (as found by photorheology measurements). Full characterization of HAVE hydrogels resulted in a broad range of HAVE macromer materials with tunable mechanical properties. Suitable HAVE precursors with enhanced solubility in aqueous media were selected to test their performance towards 3D cell encapsulation.

3.4 Cell Encapsulation

To investigate material biocompatibility, cells (ASC GFP) were encapsulated in HAVE hydrogels. Cells were encapsulated into HAVE hydrogel matrices using two different techniques (UV and 2PP). For these experiments, hydrogel formulations with relatively low viscosity and improved

Die approbierte gedruckte Originalversion dieser Dissertation ist an der TU Wien Bibliothek verfügbar.
The approved original version of this doctoral thesis is available in print at TU Wien Bibliothek.
TU Bibliothek Your knowledge hub WIEN

handling are required. Therefore, suitable macromers were chosen (HA50VE05) for UV encapsulation and HA22VE95 for 2PP encapsulation.

3.4.1 UV-Cell Encapsulation

Cell morphology as well as differentiation, which is central to many biological processes, is highly sensitive to the environmental substrate stiffness.[37,400,401] Due to the enhanced solubility of HA50VE05 as a consequence of the moderate degree of functionalization and m.w. as well as the increased chance to supply cells with a suitable surrounding microenvironment, HA50VE05 was chosen as material for UV cell encapsulation experiments. Increased solubility facilitates straightforward handling procedures of stock solutions and reduces time-consuming matrix homogenization, unfavorable when cells involved. Furthermore, an increased amount of macromer content (15 wt.%) was selected compared to 2PP (5 wt.%) to ensure sufficient crosslink density of hydrogels. UV encapsulation of ASC-GFPs was performed in a laminar flow hood under sterile conditions (Figure 95).

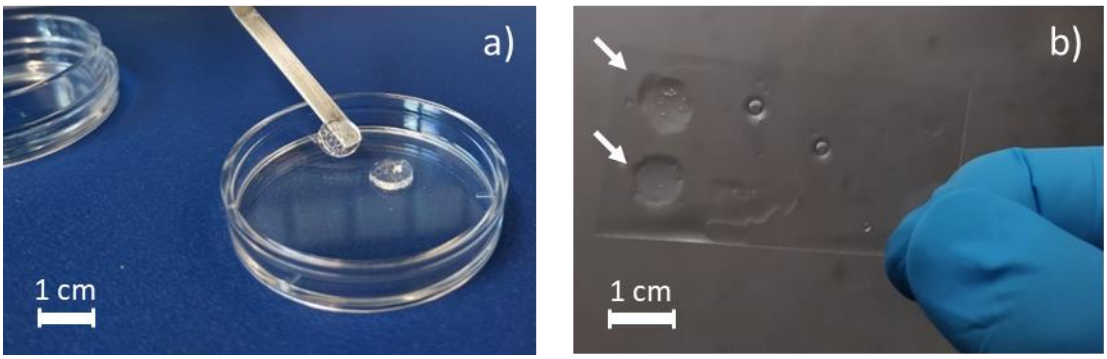

Figure 95: Hydrogel pellets of UV polymerized HA50VE05 cell-free (a) and hydrogel pellets on a glass cover slip containing adipose derived stem cells (b) prepared in a laminar flow hood under sterile conditions with a macromer content of 15 wt.% HA50VE05 and 0.5 mM LiTPO containing 80 mol% (thiol to ene) DTT.

A formulation based on HA50VE05 was prepared and mixed 1:1 (v/v) with cells in medium containing LiTPO and DTT as crosslinking agent in order to reach final concentrations of 15 wt% HAVE macromer content, 0.5 mM LiTPO, and 80 mol% DTT (thiol to ene). UV-polymerized gels were transferred to sterile µ-dishes, immersed in cell medium, and incubated at 37°C up to 14 days. Cell-survival was monitored via LSM imaging (Figure 96).

Die approbierte gedruckte Originalversion dieser Dissertation ist an der TU Wien Bibliothek verfügbar.
The approved original version of this doctoral thesis is available in print at TU Wien Bibliothek.

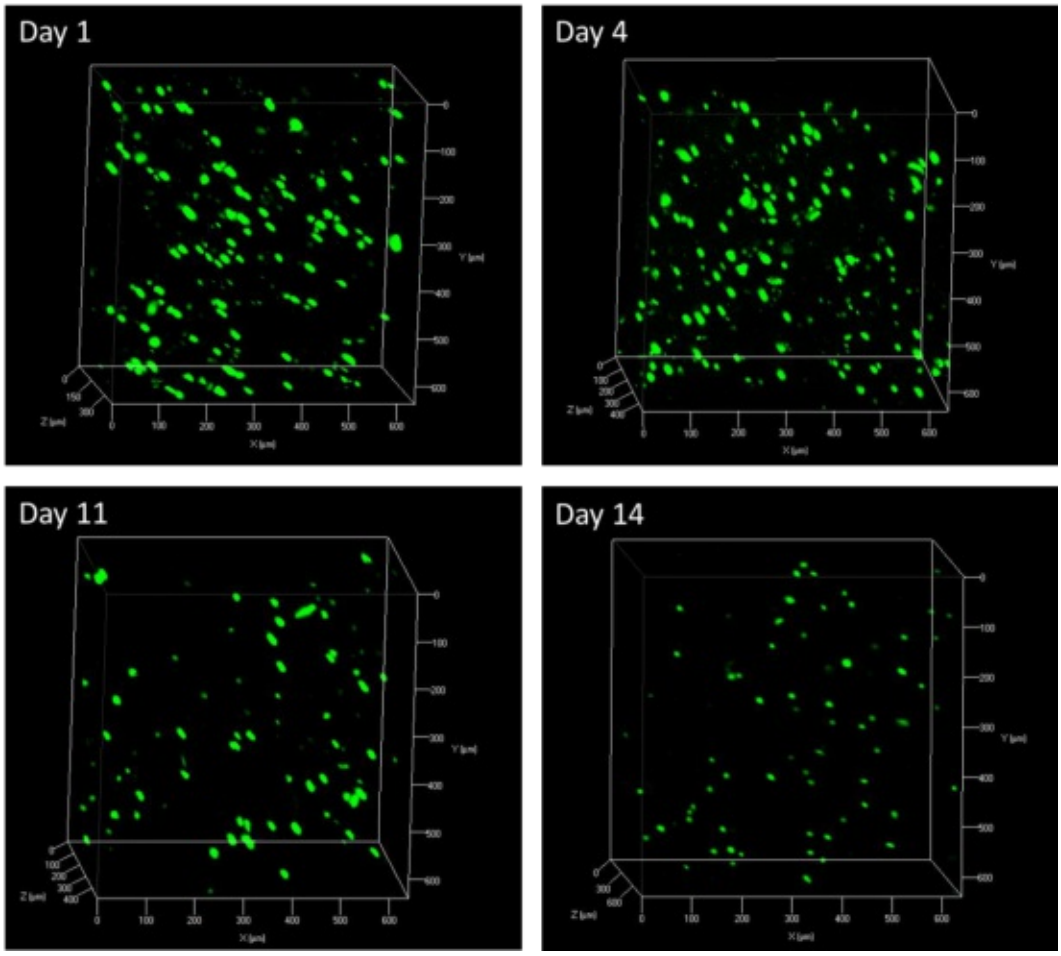

Figure 96: Confocal images of human adipose-derived mesenchymal stem cells labelled with green fluorescent protein (ASC-GFP) after UV encapsulation and 3D cultivation in HAVE hydrogels for up to 14 days (HA50VE05/80 mol% thiol-to-ene DTT, 15 wt.% macromer content, 0.5 mM LiTPO)

Bright fluorescence of ASC-GFPs was observed over the course of 2 weeks. The cell number (proliferation rate) was determined by counting the fluorescent (living) cells using ImageJ within the recorded section (600 × 600 × 400 µm). Cell numbers were counted on day 4, 11 and 14 and the data were normalized to day 1 (100%) (Figure 97).

Die approbierte gedruckte Originalversion dieser Dissertation ist an der TU Wien Bibliothek verfügbar.
The approved original version of this doctoral thesis is available in print at TU Wien Bibliothek.

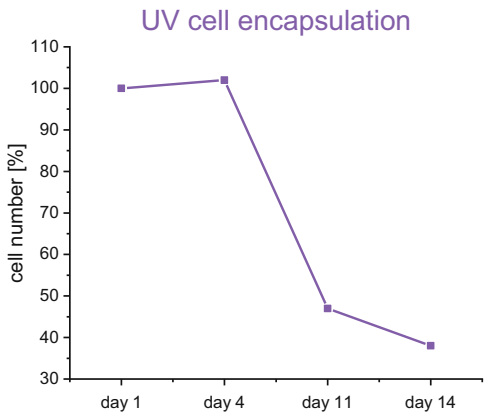

Figure 97: Cell numbers (proliferation rate) of UV encapsulated cells over the course of encapsulation time, referenced to cell numbers on day 1 (100%).

Hydrogels on day 1 and 4 supported the highest viability of differentiated mammalian cells. Within the first 4 days cell numbers remained constant (102%) whereas they decreased up to day 11 (47%) and day 14 (38%). Reasons for a decreased cell proliferation is supposed to be derived from swelling and disintegration of the hydrogels indicated by the low crosslink density originating from the low DS of HA50VE05. These arguments can be underlined by the swelling ratios as well as mass loss profiles depicted in Figure 94. Swelling ratio for HA50VE05 (928 ± 31%) was observed to be twice as high as for HA22VE95 (479 ± 16%). Additionally, mass loss profiles after 24 h were calculated and a higher decrease of mass percentage was observed for HA50VE05 hydrogels (25 ± 4%) compared to HA22VE95 (7 ± 4%). Round morphology of the cells was observed, which is most likely due to the missing cell-interactive properties of HA. Future experiments can be performed to incorporate protein motifs Arg-Gly-Asp (RGD) into HAVE hydrogels using gelatin to enhance cell adhesion.

Furthermore, low cell numbers may also derive from a low nutrient permeability as already suggested by literature, where studies showed that compromised cell viability can also derive from nutrient transport-restrictions within hydrogel networks.[391] Loosely crosslinked hydrogels were shown to be beneficial for cells due to an increase in nutrient and waste transport. Nevertheless, the approach to UV encapsulate cells in hydrogel matrices with relatively low macromer content is a key finding, because rapid hydrogel degradation with a larger hydrogel mesh size may increase the distribution of ECM components. Additionally, the low viscosity of the solution increases processability (first in the distribution of encapsulated cells and second for future clinical applications e.g. low viscosity is needed for arthroscopic techniques).[395]

However, cells were successfully encapsulated using UV-polymerization and showed promising performance during 2 weeks, although many parameters are free for optimization (macromer content, crosslinking density, adjustment of matrix using cell-interactive motifs).

Die approbierte gedruckte Originalversion dieser Dissertation ist an der TU Wien Bibliothek verfügbar.
The approved original version of this doctoral thesis is available in print at TU Wien Bibliothek.

3.4.2 Cell Encapsulation using Two-Photon Polymerization

Cell encapsulation was performed using HA22VE95 as macromer, to study cells within a two-photon polymerized matrix. Highly reactive formulations and a high degree of functionalization are required to ensure sufficient polymerization during 2PP. Furthermore, the improved solubility of HA22VE95 was a key reason, why this macromer was chosen, compared to HA50VE05. Furthermore, the high reactivity of the macromer enables hydrogels fabrication with lower laser power and higher writing speed. Consequently, a formulation based on HA22VE95 and P2CK (0.5 mM) was prepared and mixed 1:1 (v/v) with cells in medium or PBS solution (cell-free control experiment). Cubic hydrogel constructs (100x100x100 µm TU Wien Logos) were manufactured according to a CAD-file. Images of the printed constructs were captured via LSM up to 7 days (Figure 98).

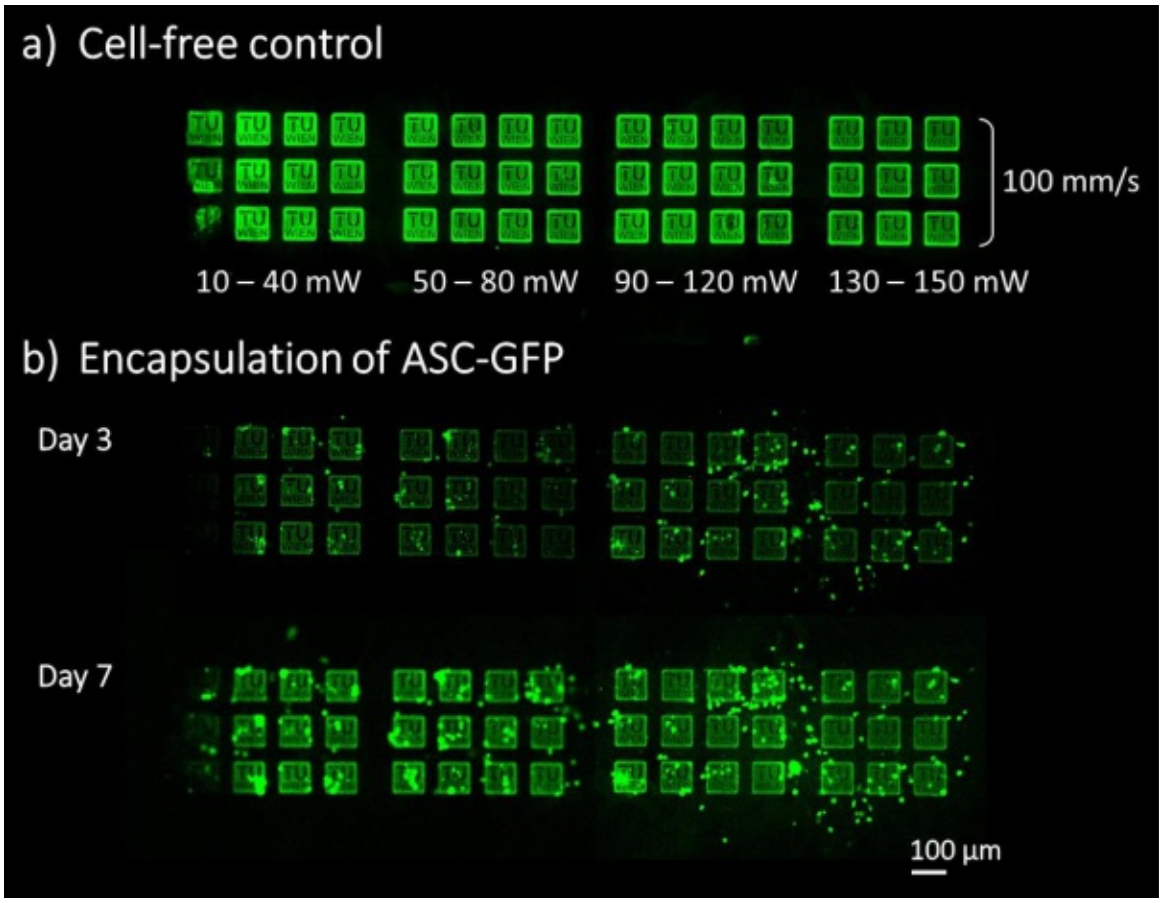

Figure 98: Laser scanning microscopy images of hyaluronic acid- based hydrogel constructs (HA22VE95/80 mol% thiol-to-ene DTT, 5 wt.% macromer content), printed with varied laser powers (Δ = 10 mW) and a constant writing speed of 100 mm s^{-1} (triplicates) according to a CAD-model (TU Wien Logo, 100x100x100 µm) in the presence of 0.5 mM P2CK (cell-free control, a). Fluorescent-labelled ASCs were imaged after 3 and 7 days of encapsulation (b).

A 2D array was successfully fabricated in a reproducible quality by structuring logos with constant writing speed (100 mm s^{-1}, y-axis) and varying laser power (10-150 mW, x-axis). hydrogel constructs printed with laser power < 20 mW seemed to be very fragile, which indicated a low crosslink density due to underexposure at the applied laser power. Presumably, these structures

Die approbierte gedruckte Originalversion dieser Dissertation ist an der TU Wien Bibliothek verfügbar.
The approved original version of this doctoral thesis is available in print at TU Wien Bibliothek.
TU Bibliothek Your knowledge hub WIEN

were destroyed, detached, and washed away during excessive rinsing procedures. Numerous viable ASC GFP cells were imaged for up to 7 days of incubation however, round cell morphology was observed similar to UV cell encapsulation (Figure 96). To quantify the cells, structures were divided into groups and the cell-number normalized to day 3 (Figure 99).

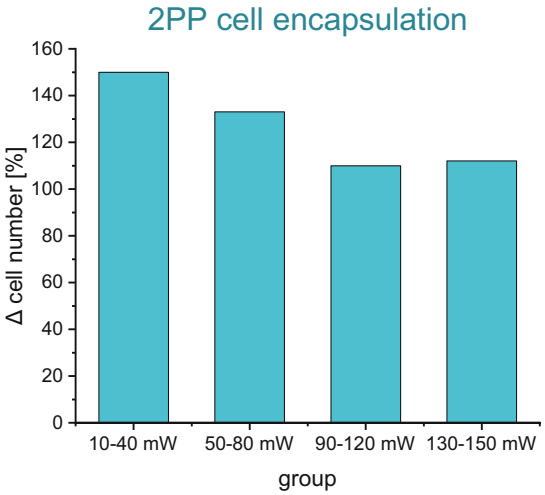

Figure 99: 2PP encapsulated cells (after 7 days) are divided into four groups (according to structuring parameters) and referenced to day 3 (100%).

Higher cell proliferation rates were observed for structures, which were fabricated with lower laser power (10-40 mW) compared to structures, which were fabricated with higher laser power (120-150 mW) expected to be derived from the stiffer hydrogel structures. Similar to the results published in literature, the gel stiffness is majorly important for the promotion of cell viability, since increased stiffness showed reduced cell viability presumably, due to reduced nutrient permeability.[391] Cell morphology as well as -differentiation, is highly sensitive to the environmental substrate stiffness. In this context, modification of material stiffness can modulate the efficiency of the material to recruit cells and change their behavior. Consequently, the reduced cell proliferation correlates with hydrogel substrate rigidity. Macromers can be modified with protein sequences giving a deeper understanding on cell adhesion. The importance of cellular adhesion molecules (integrins), cell surface proteins that contain the Arg-Gly-Asp (RGD) attachment site is of obvious importance.[402,403] Gelatin serves the advantage of already included RGD motifs since it is a naturally bioactive material. Additionally, various photopolymerizable modifications of gelatin are available.[382]

Die approbierte gedruckte Originalversion dieser Dissertation ist an der TU Wien Bibliothek verfügbar.
The approved original version of this doctoral thesis is available in print at TU Wien Bibliothek.

3.5 Conclusion

A wide variation of HAVE macromers were available and the portfolio of hydrogel materials was extended by the synthesis of a novel macromer based on a commercially available HA with defined molecular weight. A straightforward synthesis method was developed obtaining macromers with multiple parameters open for variation. The transesterification reaction was not necessary to be performed in the presence of a lipase (Cal-B) since the synthesis proceeds equally in the absence of the lipase. Various limitations of the naturally occurring polysaccharide (HA) were overcome by precise engineering of the macromer backbone. On the one hand, efficient photopolymerization is only possible, when a relative high degree of modification is available. On the other hand, increased degree of modification resulted in excessive degree of hydrophobic moieties present within the backbone, lowering the overall water-solubility of HAVE. The initial low water-solubility of the highly functionalized macromer was met by reducing the molecular weight to 20 – 50 kDa. Based on the findings from previously performed photorheology experiments, the hydrogels were prepared using an optimum thiol to ene ratio of 80 mol%. Tailor-made hydrogel precursor formulations were prepared leading to successful encapsulation of cells in HAVE-based 3D hydrogel constructs monitoring their cell survival after the encapsulation process. Two different HAVEs were chosen to perform UV- and 2PP cell encapsulation experiments, respectively. HA50VE05 with a m.w. of 50 kDa was found to be an excellent candidate for UV-cell encapsulation. By using higher macromer concentrations (15wt.%) but lower DS (5%) relatively soft hydrogels were prepared, especially suited for cell culture ensuring pleasant cell environment. ASC GFPs were successfully encapsulated in bulk HAVE pellets and their viability was studied for up to 14 days. Numerous viable cells were observed over the whole course although high degree of swelling was observed for HA50VE05. On the other hand, low m.w. HA22VE95 (22 kDa) was found to be an optimum material for 2PP cell encapsulation with good solution properties, when used in low macromer concentrations (5wt.%) while maintaining consistent quality of crosslinking owing to the high DS (95%). Highly-resolved hydrogel microstructures (100x100x100 µm TU Wien Logos) were fabricated with enhanced long-term stability. ASC-GFPs were successfully encapsulated via 2PP and their survival monitored for up to 7 days. Good cell proliferation rates were observed for all different structuring parameters, however, microstructures fabricated with higher laser power resulted in stiffer hydrogel constructs with reduced cell proliferation rates. Structures fabricated with lower laser power led to softer hydrogels prone to disintegration as a result of the low crosslink density yet showing increased cell proliferation rates. This study illustrates how HAVE is expected to be one versatile contributor in the broad field of hydrogel materials. Further studies will increase the knowledge of the system and enhance its properties towards the potential application in the fields of tissue engineering and regenerative medicine.

Die approbierte gedruckte Originalversion dieser Dissertation ist an der TU Wien Bibliothek verfügbar.
The approved original version of this doctoral thesis is available in print at TU Wien Bibliothek.
TU Bibliothek Your knowledge hub WIEN

Experimental Part

1 Two-Photon Initiators based on Oxime Esters

1.2 Synthesis of Oxime Ester-based Two-Photon Initiators

1.2.1 Preliminary Investigation on a Bimolecular System

1.2.1.1 Synthesis of M2CMK

All procedures were performed in an orange light laboratory (filter foils with a cut-off < 520 nm) or in a red-light laboratory (LED light source: 620 nm).

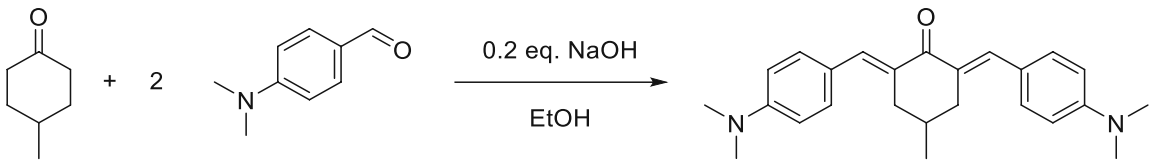

MCK **DMBA** **M2CMK**

Chemicals	M [g/mol]	eq.	n [mmol]	ρ [g/ml]	m [g]	V [mL]
4-Methylcyclohexan-1-one (MCK)	112.17	1	35.7	0.8	4.0	5
4-(Dimethylamino)benzaldehyde (DMBA)	149.19	2	71.3		10.6	
NaOH		0.2	7.1		0.3	
EtOH						120

The synthesis was performed according to literature.[153] 4-Methylcyclohexanone (4.0 g, 35.7 mmol, 1 eq.) was dissolved in 50 mL EtOH and stirred at room temperature in a three-necked round bottom flask. Finely powdered sodium hydroxide (0.3 g, 7.1 mmol, 0.2 eq.) was dissolved in 2 mL EtOH and slowly added dropwise to the MCK-solution. 4-(dimethylamino)benzaldehyde (10.6 g, 71.3 mmol, 2 eq.) was dissolved in 68 mL EtOH and slowly added to the reaction solution. The reaction mixture was heated to reflux and stirred for 4h, while monitoring the reaction progress via TLC. As soon as MCK was consumed, the solvent was reduced to 10 mL and the dark red reaction mixture dissolved in chloroform. Extraction with NH_4Cl solution (twice), drying over Na_2SO_4, evaporation of the solvent and recrystallization from diethyl ether yielded in the pure orange product.

Yield: 7.5 g orange crystals (56% of theory)

TLC: R_f = 0.43 (PE:$CHCl_3$ = 1:3)

M.p.: 208-211 °C (Lit: 212-214 °C)[404]

UV-Vis: λ_{max} = 432 nm (THF), ε_{max} = 51 x 10^3 M^{-1} cm^{-1}

Die approbierte gedruckte Originalversion dieser Dissertation ist an der TU Wien Bibliothek verfügbar.
The approved original version of this doctoral thesis is available in print at TU Wien Bibliothek.

^{1}H-NMR (400 MHz, CD_2Cl_2) δ **7.65** (s, 2H, C<u>H</u>-C_0), **7.44** (d, 4H, Ar-H, J = 8.8 Hz), **6.73** (d, 4H, Ar-H, J = 8.9 Hz,), **3.10 – 3.05** (dd, 2H, C<u>H_2</u>), **3.01** (s, 12H, 2x N-$(CH_3)_2$), **2.51** (m, 2H, CH_2), **1.87** (m, 1H, C<u>H</u>-CH_3), **1.11** (d, 3H, CH-C<u>H_3</u>, J = 6.5 Hz)

^{13}C-NMR (101 MHz, CD_2Cl_2) δ **189.39** (C4, C=O), **150.93** (C4, N-Ar-C), **136.96** (C3, C(=O)-C_0-<u>C</u>H), **132.72** (C3, Ar-C), **132.11** (C(=O)-<u>C_0</u>), **124.41** (C4, Ar-C), **111.98** (C3, Ar-C), **40.33** (C3, N-CH_3), **37.28** (C2, CH-<u>C</u>H_2), **29.96** (C3, <u>C</u>H-CH_3), **22.05** (C1, CH-<u>C</u>H_3)

1.2.1.2 Testing

To investigate the influence of molar ratio between sensitizer M2CMK and the oxime ester (OE) co-initiator benzaldehyde O-benzoyl oxime (BABO) on 2PP processability a thorough study was performed. Different formulations with varying molar ratios were prepared (1:1, 1:2, 1:5, 1:10) and the P_{th} for each formulation was examined. Different CAD-files were chosen to investigate the P_{th}. Either a single between two-pillars (single-line writing) or complex 3D structures (TU Wien Logo, Atomium). For a 1:1 molar ratio, 0.5 mM BABO and 0.5 mM M2CMK were used. A molar ratio of 2:1 was prepared by combining stock solution accordingly leading to final concentrations of 0.5 mM BABO and 0.25 mM M2CMK. Concentrations of M2CMK were lowered up to a molar ratio of down to 0.05 mM M2CMK (1:10 molar ratio M2CMK:BABO) keeping a constant concentration of 0.5 mM BABO.

Table 6: Overview on molar ratios of BABO and M2CMK as well as final concentrations for formulations based on acrylic monomer mixture (ETA:TTA, 1:1).

	Single Line		*Atomium*		TU Wien Logo	
Molar ratio BABO:M2CMK	**BABO [mM]**	**M2CMK [mM]**	**BABO [mM]**	**M2CMK [mM]**	**BABO [mM]**	**M2CMK [mM]**
Control 1	0.50	-	0.50	-	1.00	-
Control 2	-	0.50	-	0.50	-	0.10
1:10	0.05	0.50	0.05	0.50	1.00	0.10
1:5	0.10	0.50	0.10	0.50	n.a.	
1:2	0.25	0.50	0.25	0.50	n.a.	
1:1	0.50	0.50	0.50	0.50	0.10	0.10

Die approbierte gedruckte Originalversion dieser Dissertation ist an der TU Wien Bibliothek verfügbar.
The approved original version of this doctoral thesis is available in print at TU Wien Bibliothek.

Table 7: Polymerization thresholds (P_{th}) determined via single-line writing and fabrication of TU Wien Logos/Atomium structures according to CAD-files. Formulations were based on acrylic monomer mixture (ETA:TTA, 1:1) containing various molar ratio of BABO and M2CMK (10:1, 5:1, 2:1, 1:1). The Ti:sapphire laser system was calibrated either to 760 nm or 800 nm.

	P_{th} [mW] Single-line		P_{th} [mW] Atomium	P_{th} [mW] TU Wien Logo
Molar ratio (BABO:M2CMK)	760 nm	800 nm	760 nm	760 nm
Control 1 (BABO)	No polymerization			
Control 2 (M2CMK)	34	37	70	70
1:1	26	30	50	60
2:1	38	53	80	n.a.
5:1	72	62	100	n.a.
10:1	124	120	>120	80

Synthesis of 5M

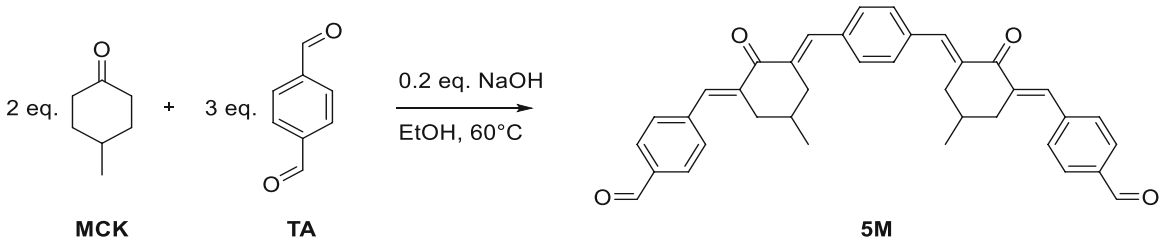

Chemicals	M [g/mol]	eq.	n [mmol]	ρ [g/ml]	m [g]	V [mL]
4-Methylcyclohexan-1-one (MCK)	112.17	2.0	39.8	0.91	4.46	4.88
Terephthalaldehyde (TA)	134.13	3.0	59.6		8.00	
NaOH	39.997	0.2	4.0		0.16	
EtOH						200

TA (8.00 g, 59.6 mmol, 3 eq.) was dissolved in 270 mL distilled ethanol at 40°C in a three-necked round-bottom flask. 4-Methylcyclohexan-1-one (MCK) (4.46 g, 39.8 mmol, 2 eq.) was diluted in 5 mL ethanol and added slowly to the reaction solution. Finely powdered sodium hydroxide (0.16 g, 4.0 mmol, 0.2 eq.) was dissolved in 1 mL ethanol and added slowly to the reaction solution. During addition of sodium hydroxide, the colorless reaction solution turned bright red. After complete addition and stirring for 30 min at 60°C a bright yellow precipitate formed. The reaction was controlled via TLC and stirred under reflux overnight. The yellow precipitate was separated from the bright red mother liquor by hot filtration, washed extensively with hot ethanol to remove residual MCK and dried in high vacuo. Additional 5M fractions were obtained after evaporation of the solvent by half and storage of the mother liquor at 7°C for 24 h.

Yield: 14.2 g bright yellow solid (64% of theory)

TLC: R_f = 0.30 (PE:EE=3:1)

M.p.: 176-179 °C

UV-Vis: λ_{max} = 366 nm (THF), ε_{max} = 62 x 10^3 M^{-1} cm^{-1}

Die approbierte gedruckte Originalversion dieser Dissertation ist an der TU Wien Bibliothek verfügbar.
The approved original version of this doctoral thesis is available in print at TU Wien Bibliothek.
TU Bibliothek Your knowledge hub WIEN

HR-MS: $[ESI]^+$ $[M+H]^+$ m/z
calculated for $C_{38}H_{35}O_4^+$: 555.2529, found: 555.2536

^{1}H-NMR (200 MHz, CD_2Cl_2) δ **10.03** (s, 2H, 2x C<u>H</u>O), **7.92** (d, 4H, Ar-H), **7.77** (d, 4H, Ar-H), **7.62** (d, 4H, Ar-H), **7.56** (s, 4H, C<u>H</u>=C_0) **3.09** (m, 4H, 2x C<u>H</u>$_2$), **2.58** (m, 4H, 2x C<u>H</u>$_2$), **1.93** (m, 2H, 2x CH_3-C<u>H</u>), **1.10** (d, 6H, 2x C<u>H</u>$_3$)

^{13}C-NMR (151 MHz, CD_2Cl_2) δ **191.94** (C3, -H<u>C</u>=O), **189.51** (C4, <u>C</u>$_0$=O), **142.41** (C4, -<u>C</u>$_0$-C_0=O), **142.25** (C4, -<u>C</u>'$_0$-C_0=O), **136.81** (C3, C_0=<u>C</u>H), **136.65** (C4, <u>C</u>$_0$-CHO), **136.47** (C4, <u>C</u>$_0$=Ar-H), **136.20** (C4, <u>C</u>$_0$=Ar-H), **135.46** (C3, C_0=<u>C</u>H), **131.10** (C3, Ar-<u>C</u>), **130.93** (C3, Ar-<u>C</u>), **129.87** (C3, Ar-<u>C</u>), **36.97** (C2, CH-<u>C</u>H$_2$), **36.81** (C2, C_0-<u>C</u>H$_2$'), **29.69** (C3, <u>C</u>H-CH_2), **21.70** (C1, <u>C</u>H$_3$)

Synthesis of 5MOx

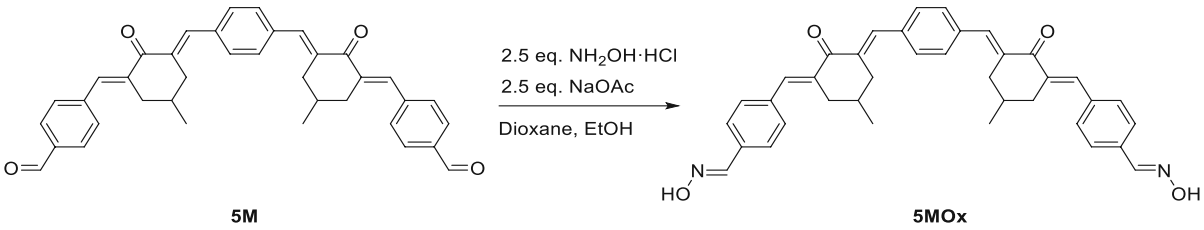

5M **5MOx**

Chemicals	M [g/mol]	eq.	n [mmol]	ρ [g/ml]	m [g]	V [mL]
5M	554.25	1	5.4		3.00	
NH_2OH HCl	69.49	2.5	13.5		0.91	
NaOAc	82.03	2.5	13.5		1.11	
Dioxane						700
EtOH						3

5M (3.0 g, 5.4 mmol, 1 eq.) was dissolved in 700 mL dioxane, while stirring for 2 h under reflux. Sodium acetate (1.1 g, 13.5 mmol, 2.5 eq.) was dissolved in 1.5 mL EtOH and added to the orange reaction solution. Hydroxylamine hydrochloride (0.9 g, 13.5 mmol, 2.5 eq.) was dissolved in 1.5 mL EtOH and added slowly to the reaction solution. After stirring the solution overnight under reflux, the solvent was reduced by half under vacuum. The reaction solution was poured onto a cooled solution of hydrochloric acid in water (10%). The precipitate was centrifuged, the aqueous phase discarded, and the precipitate washed with saturated $NaHCO_3$ and brine. The product is dissolved in THF and dried over Na_2SO_4.

Yield: 1.6 g vibrant orange solid (51% of theory)

TLC: R_f = 0.55 (PE:EE=1:1)

UV-Vis: λ_{max} = 360 nm (Dioxane), ε_{max} = 69 x 10^3 M^{-1} cm^{-1}

M.p.: 131-134 °C

HR-MS: $[ESI]^+$ $[M+H]^+$ m/z
calculated for $C_{38}H_{37}N_2O_4^+$ 585.2746, found: 585.2757

Die approbierte gedruckte Originalversion dieser Dissertation ist an der TU Wien Bibliothek verfügbar.
The approved original version of this doctoral thesis is available in print at TU Wien Bibliothek.
TU Bibliothek Your knowledge hub WIEN

^{1}H-NMR (200 MHz, $(CD_3)_2SO$) δ **11.41** (s, 2H, 2x C=N-OH), **8.18** (s, 2H, 2x HC=N), **7.65** (m, 16H, 12x Ar-H 4x CH=C_0), **2.98** (m, 4H, 2x CH_2), **2.59** (m, 4H, 2x CH_2), **1.85** (m, 2H, 2x CH-CH_3), **1.03** (d, 6H, 2x -CH_3)

^{13}C-NMR APT (151 MHz, $(CD_3)_2SO$) δ **188.58** (C4, C_0=O), **149.54** (C3, CH=N), **147.72** (C4, C_0-C_0=O), **136.15** (C3, C_0=CH), **135.80** (C3, C_0'-CH), **135.55** (C4, C_0-CH=N), **133.40** (C4, C_0-Ar-H); **130.59** (C3, Ar-C) **35.75** (C2, CH-CH_2), **28.63** (C3, CH-CH_3), **21.26** (C1, CH_3)

Synthesis of BAOx

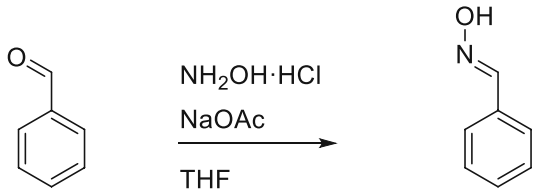

BA **BAOx**

Chemicals	M [g/mol]	eq.	n [mol]	ρ [g/ml]	m [g]	V [mL]
Benzaldehyde (BA)	106.12	1	47.1	1.04	5.00	4.81
NH_2OH HCl	69.49	1.1	51.8		3.60	
NaOAc	82.03	1.1	51.8		4.25	
THF						200.00

Hydroxylamine hydrochloride (3.60 g, 51.8 mmol, 1.1 eq.) and sodium acetate (4.25 g, 51.8 mmol, 1.1 eq.) were dissolved in 150 mL THF. BA (5.00 g, 47.1 mmol, 1 eq.) was dissolved in 50 mL THF and slowly added to the reaction solution. The solution was refluxed for 7 h and the reaction progress controlled via TLC. After cooling the flask to room temperature, the reaction was reduced to 50 mL and extracted with 0.1 M aqueous HCl, saturated $NaHCO_3$ and brine discarding the aqueous layers. The organic layer was dried over Na_2SO_4 and dried in vacuo.

Yield: 4.0 g clear liquid (70% of theory)

TLC: R_f = 0.45 (PE:EE 3:1)

UV-Vis: λ_{max} = 252 nm (THF), ε_{max} = 2 x 10^3 M^{-1} cm^{-1}

^{1}H-NMR (400 MHz, $(CD_3)_2SO$) δ **11.24** (bs, 1H, C=N-OH), **8.15** (s, 1H, HC=N), **7.59** (m, 2H, -C_0-CH,) **7.39** (m, 3H, -C_0-CH-CH)

^{13}C-NMR APT (50 MHz, $(CD_3)_2SO$) δ **148.18** (C3, HC=N-OH), **133.17** (C4, C_0-CH=N-), **129.28** (C3, Ar-C), **128.73** (C3, Ar-C), **126.47** (C3, Ar-C)

Die approbierte gedruckte Originalversion dieser Dissertation ist an der TU Wien Bibliothek verfügbar.
The approved original version of this doctoral thesis is available in print at TU Wien Bibliothek.

Synthesis of TAOx

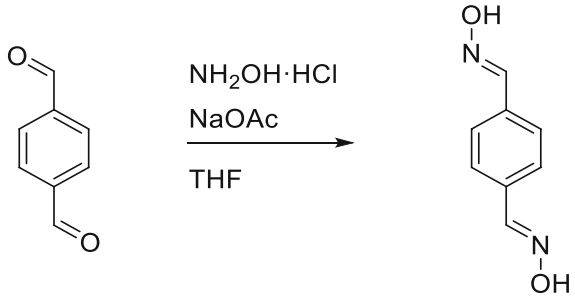

TA **TAOx**

Chemicals	M [g/mol]	eq.	n [mmol]	ρ [g/ml]	m [g]	V [mL]
Terephthalaldehyde (TA)	134.13	1	37.3		5.00	
NH_2OH HCl	69.49	2.2	82.0		5.70	
NaOAc	82.03	2.2	82.0		6.73	
THF						200
EtOH						6

TA (5.0 g, 37.3 mmol, 1 eq.) was dissolved in 40 mL THF at 50 °C. Sodium acetate (6.7 g, 82.0 mmol, 2.2 eq.) and hydroxylamine hydrochloride (5.7 g, 82.0 mmol, 2.2 eq.) were dissolved in 3 mL EtOH each and added to the reaction solution. The reaction was heated to reflux and stirred overnight. The reaction progress was controlled via TLC. The reaction solution was poured onto a cooled solution of hydrochloric acid in water (10%). The precipitate was centrifuged, washed with saturated $NaHCO_3$ and brine while discarding the aqueous layers. The product is dissolved in THF and dried over Na_2SO_4. A pale-yellow solid was obtained after drying in high vacuum.

Yield: 2.9 g pale-yellow solid (48% of theory)

TLC: R_f = 0.24 (PE:EE=3:1)

M.p.: 207-209 °C (Lit: 202-204 °C)[405]

UV-Vis: λ_{max} = 298 nm (THF), ε_{max} = 5 x 10^3 M^{-1} cm^{-1}

^{1}H-NMR (400 MHz, $(CD_3)_2SO$) δ **11.33** (s, 2H, 2x C=N-OH), **8.14** (s, 2H, 2x HC=N), **7.61** (s, 4H, Ar-H)

^{13}C-NMR APT (50 MHz, $(CD_3)_2SO$) δ **147.77** (C3, HC=N-OH), **133.82** (C4, C_0-CH=N-), **126.71** (C3, Ar-C)

Die approbierte gedruckte Originalversion dieser Dissertation ist an der TU Wien Bibliothek verfügbar.
The approved original version of this doctoral thesis is available in print at TU Wien Bibliothek.

Synthesis of BABC

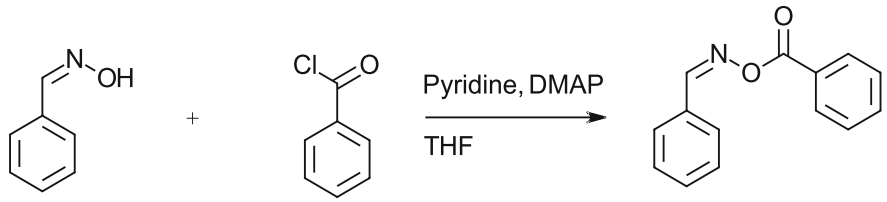

BAOx **BC** **BABC**

Chemicals	M [g/mol]	eq.	n [mmol]	ρ [g/ml]	m [mg]	V [mL]
BAOx	121.14	1	4.13		500	
Pyridine, dry	79.10	1.4	5.78	0.98	457	0.47
Benzoyl chloride (BC)	140.57	1.2	4.95	1.21	696	0.57
4-(Dimethylamino)pyridine (DMAP)	122.17	0.1	0.41		5	
THF, dry						13

BAOx (500 mg, 41 mmol, 1 eq.) was dissolved in 10 mL dry THF under inert atmosphere. Pyridine (457 mg, 58 mmol, 1.4eq.) was diluted with 1 mL THF and slowly added while cooling the reaction solution to 0°C. BC (696 mg, 50 mmol, 1.2 eq.) was diluted with 2 mL dry THF and added. Immediately after addition of BC, a white precipitate was observed. Additionally, DMAP (5 mg, 0.4 mmol, 0.1 eq.) was added in Ar-counter flow. The reaction was stirred for 24 h at 50 °C, while monitoring the reaction progress via TLC. The white precipitate (pyridine-chloride salt) was separated from the reaction solution and the solvent removed by evaporation. The residue was dissolved in DCM and extracted 2 x with 1 N HCl, once with $NaHCO_3$ and with brine. The organic phase was dried over Na_2SO_4 and the solvent evaporated.

Yield: 316.1 mg white solid (34% of theory)

TLC: R_f = 0.74 (PE:EE=2:1)

M.p.: 97-99 °C (Lit: 100-102°C)[406]

^{1}H-NMR (200 MHz, $(CD_3)_2SO$) δ **8.93** (s, 1H, CH=N), **8.08** (d, 2H, Ar-H, J = 6.9 Hz), **7.84 - 7.53** (m, 8H, Ar-H)

^{13}C-NMR (APT, 50 MHz, $(CD_3)_2SO$) δ **163.14** (C4, C_1=O), **158.03** (C3, C_8=N), **133.82** (C3, Ar-C_{12}), **131.88** (C3, Ar-C_5), **130.06** (C4, Ar-C_9), **129.24** (C3, Ar-C_6 + Ar-C_4), **129.11** (C3, Ar-C_{11} + Ar-C_{13}), **128.97** (C3, Ar-C_{10} + Ar-C_{14}), **128.22** (C3, Ar-C_3 + Ar-C_7), **128,12** (C4, Ar-C_2)

Die approbierte gedruckte Originalversion dieser Dissertation ist an der TU Wien Bibliothek verfügbar.
The approved original version of this doctoral thesis is available in print at TU Wien Bibliothek.

Synthesis of BAPAC

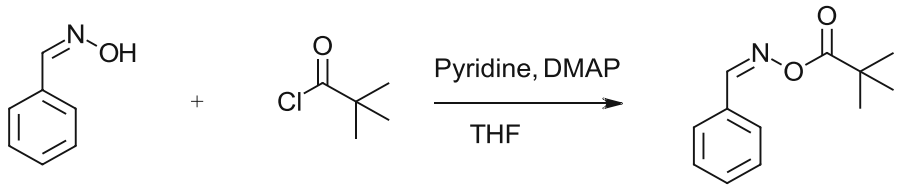

BAOx **PAC** **BAPAC**

Chemicals	M [g/mol]	eq.	n [mmol]	ρ [g/ml]	m [mg]	V [mL]
BAOx	121.14	1	4.13		500	
Pivalic acid chloride (PAC)	120.58	1.2	4.95	0.979	597	0.61
Pyridine, dry	79.10	1.4	5.78	0.982	457	0.47
4-(Dimethylamino)pyridine (DMAP)	122.17	0.1	0.41		50	
THF, dry						10

BAOx (1 eq., 4.1 mmol, 500 mg) was dissolved in 4 mL dry THF under inert atmosphere. The reaction solution was cooled to 0°C and pyridine (1.4 eq., 5.8 mmol, 457 mg) was dissolved in 2 mL dry THF and added via a syringe. PAC (1.2 eq., 5.0 mmol, 597 mg) was dissolved in 4 mL dry THF and slowly added to the reaction solution via a syringe using a septum. DMAP (0.1 eq., 0.4 mmol, 50 mg) was added in Ar-counter flow and the reaction solution was stirred for 24 h at 50°C. A white precipitate formed after 30 min of addition of reactants. After 24h the white precipitate (pyridine-chloride salt) was separated from the reaction solution and the mother liquor was reduced to a minimum. The yellow liquid was dissolved in DCM, extracted 2x with 1M HCl, 1x with $NaHCO_3$ and with brine. The organic phase was dried over Na_2SO_4 and the solvent evaporated, obtaining the product as clear liquid.

Yield: 387.5 mg colorless liquid (46% of theory)

TLC: R_f = 0.31 (PE:EE 5:1)

^{1}H-NMR (400 MHz, CD_2Cl_2) δ **8.40** (s, 1H, C<u>H</u>=N), **7.75** (d, 2H, Ar-H), **7.43** (m, 3H, Ar-H), **1.31** (s, 9H, C<u>H</u>$_3$)

^{13}C-NMR (101 MHz, CD_2Cl_2) δ **184.92** (C4, C(=O)-O), **156.62** (C3, CH=N), **130.85** (C4, Ar-C), **132.55** (C3, Ar-C), **129.35** (C3, Ar-C), **128.58** (C3, Ar-C), **38.84** (C4, <u>C</u>(-CH_3)$_3$), **27.17** (C1, C(-<u>C</u>H_3)$_3$)

Die approbierte gedruckte Originalversion dieser Dissertation ist an der TU Wien Bibliothek verfügbar.
The approved original version of this doctoral thesis is available in print at TU Wien Bibliothek.

Synthesis of TAPAC

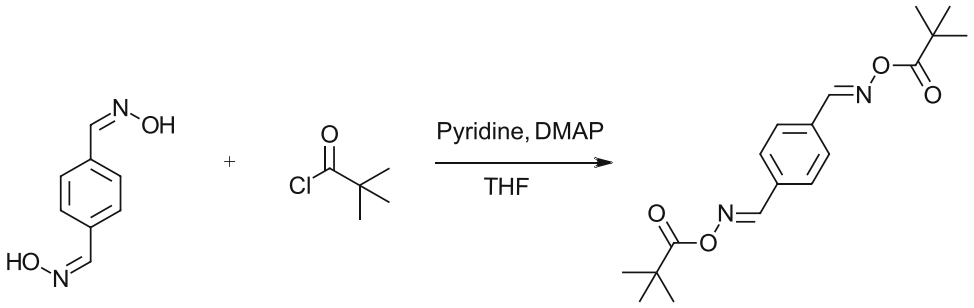

TAOx **PAC** **TAPAC**

Chemicals	M [g/mol]	eq.	n [mmol]	ρ [g/ml]	m [mg]	V [mL]
TAOx	164.16	1	3.1		500	
Pivalic acid chloride (PAC)	120.58	2.2	6.7	0.979	808	0.83
Pyridine, dry	79.10	2.4	7.3	0.982	578	0.59
4-(Dimethylamino)pyridine (DMAP)	122.17	0.1	0.3		37	
THF, dry						110

TAOx (1 eq., 3.1 mmol, 500 mg) was dissolved in 100 mL dry THF under inert atmosphere. Gentle heating was required to dissolve TAOx. The reaction solution was cooled to 0°C and pyridine (2.4 eq., 7.3 mmol, 578 mg) was dissolved in 5 mL dry THF and added via a syringe. PAC (2.2 eq., 6.7 mmol, 808 mg) was dissolved in 5 mL dry THF and slowly added at 0°C via a syringe and septum. Immediately, a white precipitate was observed. DMAP (0.1 eq., 0.3 mmol, 37 mg) was added in Ar-counter flow and the reaction solution was stirred for 24 h at 50°C. The white precipitate was separated by centrifugation (5000 rpm, 2 min) and the mother liquor was reduced to 3 mL by evaporation of the solvent in vacuo. The product was obtained by dropwise addition of the concentrated reaction solution into a stirred solution of 1 M HCl. The collected white solids (centrifugation) were washed multiple times with diethyl ether, ethyl acetate and 0.5 M HCl to remove residual reactants. The product was obtained as white solid upon drying in vacuo.

Yield: 98.9 mg white solid (10% of theory)

TLC: R_f = 0.34 (PE:EE 2:1)

M.p.: 167-170 °C

^{1}H-NMR (400 MHz, CD_2Cl_2) δ **8.42** (s, 1H, CH=N), **7.80** (s, 4H, Ar-H), **1.30** (s, 18H, CH_3)

^{13}C-NMR (101 MHz, CD2Cl2) δ **175.32** (C4, C(=O)-O), **155.61** (C3, CH=N), **129.02** (C3, Ar-C), **117.55** (C4, Ar-C), **38.70** (C4, $\underline{C}(-CH_3)_3$), **27.29** (C1, $C(-\underline{C}H_3)_3$)

Die approbierte gedruckte Originalversion dieser Dissertation ist an der TU Wien Bibliothek verfügbar.
The approved original version of this doctoral thesis is available in print at TU Wien Bibliothek.

Synthesis of TASA

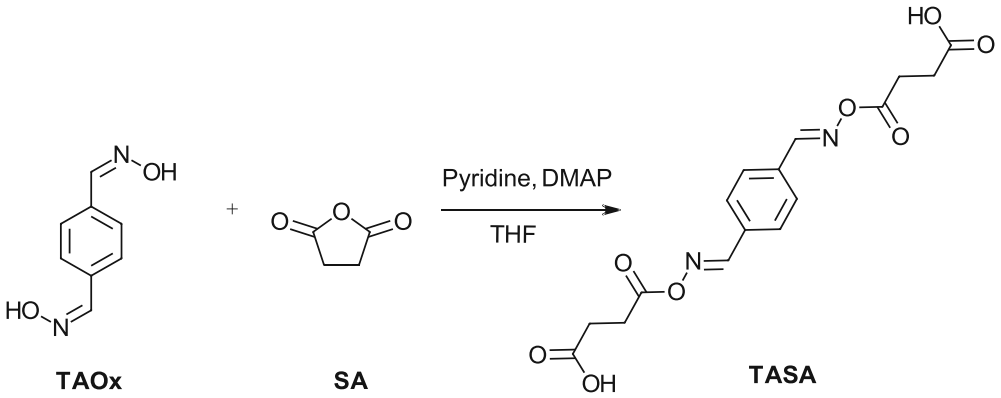

Chemicals	M [g/mol]	eq.	n [mmol]	ρ [g/ml]	m [g]	V [mL]
TAOx	164.16	1	6.1		1.00	
Pyridine, dry	79.10	2.4	14.6	0.73	1.16	0.8
Succinic anhydride (SA)	100.07	2.2	13.4		1.34	
4-(Dimethylamino)pyridine (DMAP)	122.17	0.1	0.6		0.07	
THF, dry						170

TAOx (1.0 g, 6.1 mmol, 1 eq.) was dissolved in 140 mL dry THF under inert atmosphere. Gentle heating is required to dissolve TAOx in THF. The reaction solution was cooled to 10°C and pyridine (1.2 g, 14.6 mmol, 2.4 eq.) dissolved in 10 mL THF was added via a septum and syringe. SA (1.3 g, 13.4 mmol, 2.2 eq.) was dissolved in 20 mL hot THF and slowly added to the reaction solution. The reaction progress was controlled via TLC. A white precipitate formed after stirring the reaction under reflux overnight. After 48 h, the solid was separated by centrifugation (5000 rpm), extracted with THF, and the solvent evaporated. The solid product was dissolved in water and extracted 5x with toluene. The organic phase was discarded, and the aqueous phase was then extracted 5x with EA. A white solid was obtained after evaporation of the organic phases in vacuo.

Yield: 0.72 g white solid (32% of theory)

TLC: R_f = 0.31 (PE:EE 7:1)

M.p.: 182-184 °C

^{1}H-NMR (400 MHz, $(CD_3)_2SO$) δ **8.28** (s, 2H, CH=N), **7.70** (s, 4H, Ar-H), **2.62** (s, 8H, 4x -CH_2)

^{13}C-NMR APT (50 MHz, $(CD_3)_2SO$) δ **178.33** (C4, C_0=O), **157.95** (C4, C_0(=O)-O-N), **151.26** (C3, CH=N), **127.48** (C4, Ar-C_0), **127.46** (C3, Ar-C), **29.96** (C2, CH_2)

Die approbierte gedruckte Originalversion dieser Dissertation ist an der TU Wien Bibliothek verfügbar.
The approved original version of this doctoral thesis is available in print at TU Wien Bibliothek.

Synthesis of TASBA

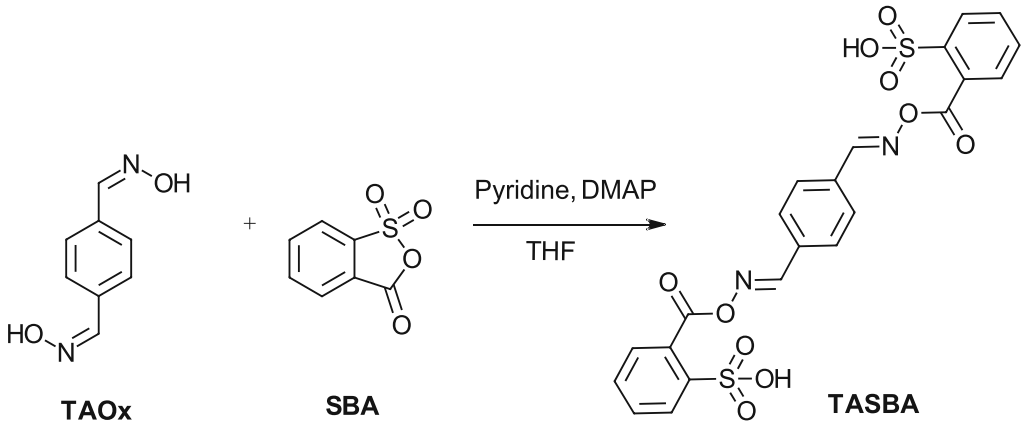

Chemicals	M [g/mol]	eq.	n [mmol]	ρ [g/ml]	m [g]	V [mL]
TAOx	164.16	1	6.1		1.0	
Pyridine, dry	79.10	2.4	14.6	0.73	1.2	1.69
Sulfobenzoic anhydride (SBA)	184.17	2.2	13.4		2.5	
4-(Dimethylamino)pyridine (DMAP)	122.17	0.1	0.06		0.1	
THF, dry						200

TAOx (1.00 g, 6.09 mmol, 1 eq.) was dissolved in 150 mL dry THF at 40 °C under inert atmosphere. The reaction solution was cooled to 10°C and pyridine (1.2 g, 15 mmol, 2.4 eq.) was dissolved in 5 mL THF and added to the stirred reaction solution. SBA (2.5 g, 13 mmol, 2.2 eq.) was dissolved in 20 mL THF and added slowly to the cooled reaction solution. The reaction was stirred for 48 h under reflux and the formed precipitates were separated by centrifugation while washing the precipitate with THF (5000 rpm, 3 min). The mother liquor was precipitated in 0.1 M HCl, the solids collected, redissolved in THF and dried over Na_2SO_4.

Yield: 1.38 g pale yellow solid (43% of theory)

TLC: R_f = 0.20 (PE:EE=7:3)

M.p.: 112-118 °C

^{1}H-NMR (400 MHz, $(CD_3)_2SO$) δ **8.92** (bs, 2H, 2x SO_3H), **8.72** (s, 2H, HC=N), **7.92** (s, 4H, central Ar-H), **7.51** (m, 4H, Ar-H), **7.44** (m, 4H, Ar-H)

^{13}C-NMR APT (151 MHz, $(CD_3)_2SO$) δ **166.00** (C4, C=O), **156.50** (C3, CH=N), **145.77** (C4, C-SO_3H), **133.21** (C4, Ar-C), **129.96** (C3, Ar-C), **129.23** (C4, C-C=O), **128.72** (C3, Ar-C) **127.54** (C3, Ar-C), **127.35** (C3, Ar-C)

Die approbierte gedruckte Originalversion dieser Dissertation ist an der TU Wien Bibliothek verfügbar.
The approved original version of this doctoral thesis is available in print at TU Wien Bibliothek.

Synthesis of 5MBC

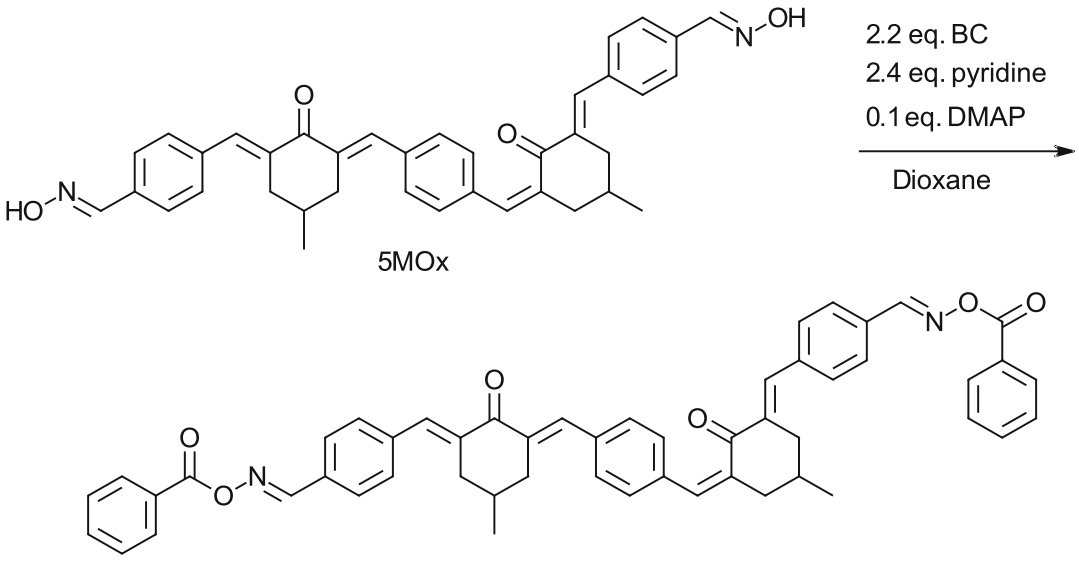

Chemicals	M [g/mol]	eq.	n [mmol]	ρ [g/ml]	m [mg]	V [mL]
5MOx	584.72	1	0.17		100	
Benzoyl chloride (BC)	140.57	2.2	0.38	1.21	53	
Pyridine, dry	79.1	2.4	0.41	0.73	32	
4-(Dimethylamino)pyridine (DMAP)	122.17	0.1	0.02		2	
Dioxane, dry						50

5MOx (1 eq., 100 mg, 0.17 mmol) was dissolved in 40 mL dioxane under inert atmosphere and cooled to 15 °C. Pyridine (2.4 eq., 32 mg, 0,41 mmol) and DMAP (0.1 eq., 2 mg, 0.02 mmol) were dissolved in 3 mL dioxane and slowly added to the reaction mixture. BC (2.2 eq., 53 mg, 0.38 mmol) was dissolved in 7 mL dioxane and slowly added via a syringe. During addition of BC the reaction solution turns bright orange. The reaction solution was allowed to be warmed to room temperature and after 1h a pale-yellow precipitate (pyridine-chloride salt) was observed in the orange reaction solution. The reaction solution was heated to reflux and stirred for 48 h. Upon increasing reaction time, the amount of precipitate increased. The mother liquor was reduced to 5 mL and the product precipitated in aqueous HCl (1 M). The orange precipitate was re-dissolved in DCM, dried over Na_2SO_4 and the solvent removed in vacuum. Recrystallization from EA led to the desired product.

Yield: 44.8 mg orange crystals (33% of theory)

TLC: R_f = 0.32 (CH_2Cl_2:EE=20:1)

M.p.: 242-246 °C

HR-MS: $[ESI]^+$ $[M+H]^+$ m/z

calculated for $C_{52}H_{45}N_2O_6^+$ 793,3270; found 793.3297

Die approbierte gedruckte Originalversion dieser Dissertation ist an der TU Wien Bibliothek verfügbar.
The approved original version of this doctoral thesis is available in print at TU Wien Bibliothek.
TU Bibliothek Your knowledge hub WIEN

^{1}H NMR (400 MHz, CD_2Cl_2) δ **8.14** (s, 2H, HC=N), **7.87 -7.46** (m, 26H, 22x Ar-H, 4x CH=C0), **3.10** (m, 4H, 2x C$\underline{H}_2$), **2.56** (m, 4H, 2x C$\underline{H}_2$), **1.92** (m, 2H, 2x CH_3-C$\underline{H}$), **1.10** (d, 6H, 2x C$\underline{H}_3$)

^{13}C NMR APT (101 MHz, CD_2Cl_2) δ **189.49** (C4, $\underline{C}$=O), **165.61** (C4, C(=O)-O), **164.08** (C3, $\underline{C}$H=N), **136.65 - 127.90** (C4, C=$\underline{C}$-(C=O), C3, Ar-C), **36.69** (C2, C_0-$\underline{C}H_2$), **29.66** (C3, $\underline{C}$H-CH_3), **21.67** (C1, $\underline{C}H_3$).

Synthesis of 5MPAC

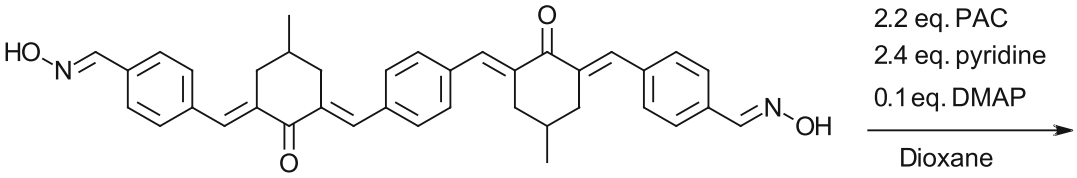

5MOx

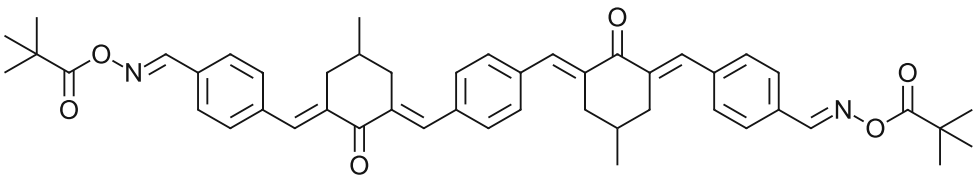

5MPAC

Chemicals	M [g/mol]	eq.	n [mmol]	ρ [g/ml]	m [mg]	V [mL]
5MOx	584.72	1	0.86		500	
Pivalic acid chloride (PAC)	120.58	2.2	1.88	0.98	210	0.2
Pyridine, dry	79.1	2.4	2.05	0.73	140	0.2
4-(Dimethylamino)pyridine (DMAP)	122.17	0.1	0.09		10	
Dioxane, dry						51.0

5MOx (1 eq., 500 mg, 0.86 mmol) was dissolved in 40 mL dry dioxane under inert atmosphere. The solution was cooled to 10°C and pyridine (2.4 eq., 2.05 mmol, 140 mg) dissolved in 5 mL dioxane was slowly added via a syringe. PAC (2.2 eq., 210 mg, 1.88 mmol) was dissolved in 5 mL dioxane and added slowly via a syringe. The reaction solution was warmed to room temperature and DMAP (0.1 eq., 0.09 mmol, 10 mg) was dissolved in 1 mL dioxane and added to the reaction solution. After addition of PAC, a yellow-white precipitate (pyridinium-chloride salt) was observed. The reaction solution was heated to reflux and stirred for 48 h, while controlling the reaction progress via TLC. The precipitate was separated from the reaction solution by centrifugation (5 min, 5000 rpm) and thoroughly washed with dioxane. The red mother liquor was reduced to a minimum and precipitated in 0.5 M aqueous HCl. The orange precipitate was separated from the aqueous phase, dissolved in DCM, dried over Na_2SO_4 and the solvent evaporated in vacuum. The target compound was obtained via recrystallization in EA.

Yield: 433.4 mg orange crystals (64% of theory)

TLC: R_f = 0.29 (CH_2Cl_2:EE=20:1)

M.p.: 221-224°C

Die approbierte gedruckte Originalversion dieser Dissertation ist an der TU Wien Bibliothek verfügbar.
The approved original version of this doctoral thesis is available in print at TU Wien Bibliothek.

HR-MS: $[ESI]^+$ $[M+H]^+$ m/z

calculated for $C_{48}H_{53}N_2O_6^+$ 753.3825; found 753.3913

^{1}H-NMR (400 MHz, CD_2Cl_2) δ **8.41** (s, 2H, C<u>H</u>=N), **7.79** - **7.56** (m, 16H, 12x Ar-H, 4x CH=(C=O), **3.10** (s, 4H, CH_2), **2.56** (m, 4H, CH_2), **1.91** (m, 2H, 2x C<u>H</u>-CH_3), **1.31** (s, 18H, CH_3), **1.09** (d, 6H, 2x -C<u>H</u>$_3$)

^{13}C-NMR (101 MHz, CD_2Cl_2) δ **189.60** (C4, <u>C</u>=O), **175.44** (C4, <u>C</u>(=O)-O-N), **156.01** (C3, <u>C</u>H=N), **139.69** (C4, C(=O)-<u>C</u>=CH), **137.45** (C4, Ar-C), **136.68** (C4, Ar-C), **136.60** (C3, Ar-C), **135.84** (C3, Ar-C), **131.21** (C3, Ar-C), **130.73** (C4, Ar-C), **128.52** (C3, Ar-C), **127.34** (C3, Ar-C), **36.87** (C2, CH-<u>C</u>H$_2$), **29.74** (C3, <u>C</u>H-CH$_2$), **27.33** (C1, (<u>C</u>H$_3$)$_3$), **21.73** (C1, <u>C</u>H$_3$)

Synthesis of 5MSA

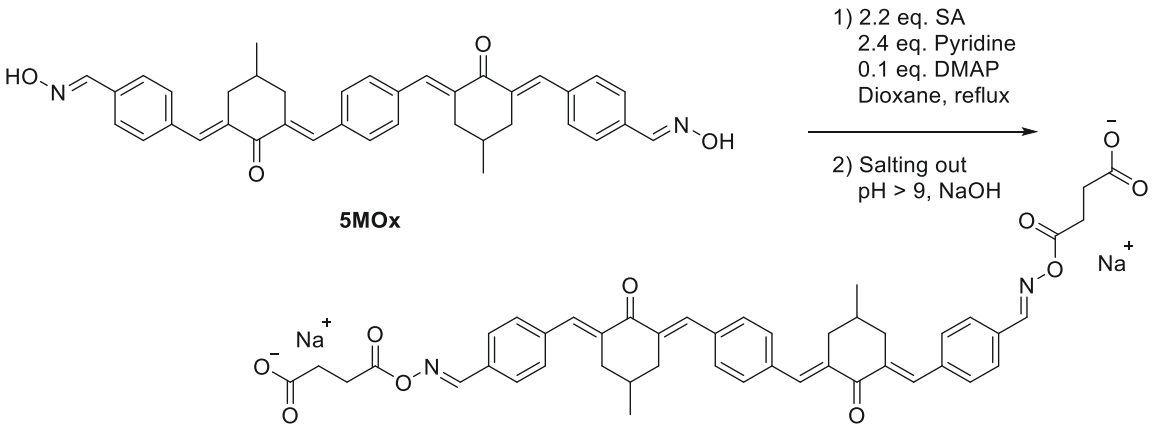

Chemicals	M [g/mol]	eq.	n [mmol]	ρ [g/ml]	m [mg]	V [mL]
5MOx	584.27	1.0	0.9		500	
Succinic anhydride (SA)	100.07	2.2	1.9		188	
Pyridine, dry	79.10	2.4	2.1		162	
4-(Dimethylamino)pyridine (DMAP)	122.17	0.1	0.1		10	
Dioxane, dry						25

5MOx (500 mg, 0.9 mmol, 1.0 eq.) was dissolved in 20 mL dry dioxane at room temperature under inert atmosphere. The solution was cooled to 10 °C and dry pyridine (162 mg, 2.1 mmol, 2.4 eq.) dissolved in 2 mL dry dioxane was slowly added via a syringe. Succinic anhydride (SA, 0.188 mg, 1.9 mmol, 2.2 eq.) was dissolved in 2 mL dry dioxane and added to the reaction solution through a septum via a syringe. The reaction solution was warmed to 50 °C and DMAP (10 mg, 0.1 mmol, 0.1 eq.) was dissolved in 1 mL dry dioxane and added via a syringe. The orange solution was heated and stirred for 4 days at 100°C, while controlling the reaction progress via TLC. The orange suspension was filtered and the fine, pale-yellow precipitate (pyridine-chloride salt) was removed from the red dioxane mother liquor. The dark red mother liquor was reduced to 3 mL and precipitated in aqueous HCl. The resulting precipitate was separated via centrifugation, dissolved in THF, dried over Na_2SO_4 and dried in vacuo. Recrystallization from EA resulted in the corresponding acid. The target compound was salted out via suspension of the orange solid in

Die approbierte gedruckte Originalversion dieser Dissertation ist an der TU Wien Bibliothek verfügbar.
The approved original version of this doctoral thesis is available in print at TU Wien Bibliothek.
TU Bibliothek Your knowledge hub WIEN

distilled water and addition of 0.5 M NaOH (and minimum amount of THF), while monitoring the suspension until a pH of 9 was reached. The remaining solids were separated via centrifugation and the obtained orange aqueous solution freeze-dried at 0.01 mbar.

Yield: 170 mg orange solid (24% of theory)

UV-Vis: λ_{max} = 370 nm (PBS), ε_{max} = 69 x 10^3 M^{-1} cm^{-1}

TLC: R_f = 0.31 (CH_2Cl_2:EE:MeOH=80:5:1)

M.p.: Decomposition at 262 °C

HR-MS: $[ESI]^+$ $[fragment+H]^+$ m/z
calculated for fragment $C_{42}H_{40}N_2O_6^+$ 668.2806 found: 668.2824

^{1}H-NMR (400 MHz, DMSO-d_6) δ **12.18** (s, 2H, COOH), **8.18** (s, 2H, CH=N), **7.91 - 7.52** (m, 16H, 12x Ar-H, 4x CH=C_0), **3.02** (m, 4H, 2x CH_2-COOH), **2.62** (m, 4H, CH_2), **2.40** (d, 4H, 2x CH_2-CH_2-COOH), **1.83** (m, 2H, 2x CH-CH_3), **1.04** (d, 6H, 2x -CH_3)

^{13}C-NMR (101 MHz, DMSO) δ **188.60** (C4, C=O), **173.84** (C4, COOH), **166.25** (C4, C(=O)-O-N), **147.76** (C3, CH=N), **146.07** (C4, C(=O)-C=CH), **140.08** (C4, Ar-C), **139.72** (C4, Ar-C), **138.11** (C4, Ar-C), **135.75** (C3, Ar-C), **134.04** (C4, Ar-C), **133.42** (C4, Ar-C), **132.36** (C3, Ar-C), **130.91** (C3, Ar-C), **130.68** (C3, Ar-C), **126.52** (C3, Ar-C), **35.79** (C2, CH_2-CH_2), **35.50** (C2, CH-CH_2), **29.29** (C2, CH_2-CH_2), **28.50** (C3, CH-CH_3), **21.22** (C1, CH_3)

Die approbierte gedruckte Originalversion dieser Dissertation ist an der TU Wien Bibliothek verfügbar.
The approved original version of this doctoral thesis is available in print at TU Wien Bibliothek.

Synthesis of 5MSBA

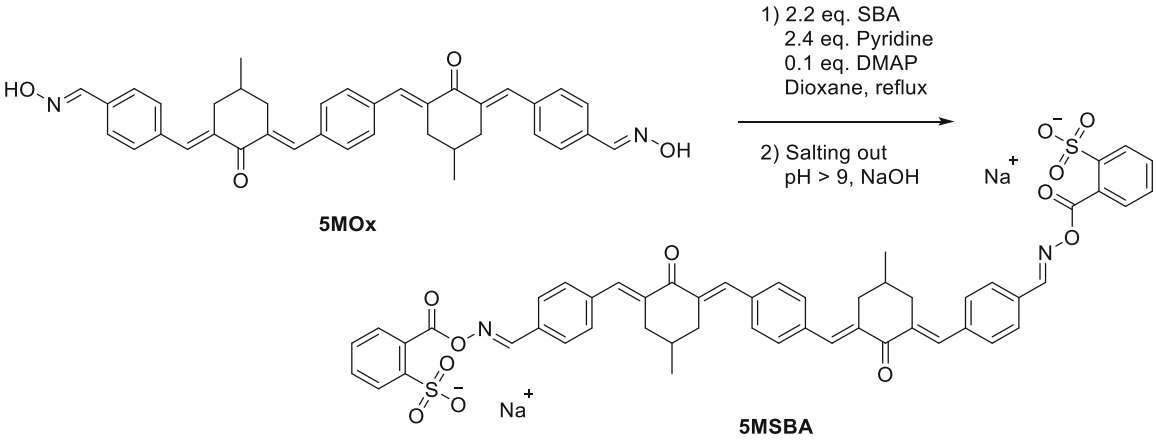

Chemicals	M [g/mol]	eq.	n [mmol]	ρ [g/ml]	m [mg]	V [mL]
5MOx	584.27	1	0.86		500	
Sulfobenzoic anhydride (SBA)	184.17	2.2	1.88		346	
Pyridine dry	79.1	2.4	2.05		162	
4-(Dimethylamino)pyridine (DMAP)	122.17	0.1	0.08		10	
Dioxane, dry						70

5MOx (500 mg, 0.9 mmol, 1 eq.) was dissolved in 50 mL dry dioxane at room temperature under inert atmosphere. The solution was cooled to 10 °C and dry pyridine (162 mg, 2.1 mmol, 2.4 eq.) dissolved in 5mL dioxane was slowly added via a syringe. Sulfobenzoic anhydride (SBA, 346 mg, 1.9 mmol, 2.2 eq.) was dissolved in 6 mL dioxane and slowly added to the reaction solution through a septum via a syringe. DMAP (10 mg, 0.1 mmol, 0.1 eq.) was dissolved in 1 mL dry dioxane and added via a syringe. The orange solution was refluxed for 4 days, while controlling the reaction progress via TLC. The orange suspension was filtered and the fine, pale-yellow precipitate (pyridine-chloride salt) was removed from the red dioxane mother liquor. The red oily residue was separated from the reaction solution by decantation, dissolution in DMF and slow precipitation in 0.5 M HCl. The red precipitate was carefully centrifuged (2200 rpm, 3 min), dissolved in DMF, dried over Na_2SO_4 and the solvent evaporated. The target compound was salted-out via suspension of the red solid in distilled water, while adding 0.5 M NaOH (pH 9). The remaining solids were separated via centrifugation and the red aqueous solution freeze-dried at 0.01 mbar.

Yield: 0.26 g red viscous liquid (25% of theory)

UV-Vis: λ_{max} = 376 nm (PBS), ε_{max} = 67 x 10^3 M^{-1} cm^{-1}

TLC: R_f = 0.22 (CH_2Cl_2:EE:MeOH=80:5:1)

M.p.: Decomposition at 285 °C

HR-MS: $[ESI]^+$ $[fragment+H]^+$ m/z

calculated for fragment $C_{45}H_{39}N_2O_7S^+$ 751.2402; found: 751.2490

Die approbierte gedruckte Originalversion dieser Dissertation ist an der TU Wien Bibliothek verfügbar.
The approved original version of this doctoral thesis is available in print at TU Wien Bibliothek.
TU Bibliothek Your knowledge hub WIEN

^{1}H NMR (400 MHz, CD_2Cl_2) δ **10.02** (s, 2H, SO_3H), **8.86** (s, 2H, HC=N), **8.38 - 7.45** (m, 24H, 20x Ar-H, 4x CH=C_0), **3.08** (m, 4H, 2x CH_2), **2.58** (m, 4H, 2x CH_2), **1.89** (m, 2H, 2x CH_3-CH), **1.08** (d, 6H, 2x CH_3)

^{13}C NMR APT (101 MHz, CD_2Cl_2) δ **189.44** (C4, C=O), **169.26** (C4, C(=O)-O), **146.49** (C3, CH=N), **142.36 - 127.65** (C4, C=C-(C=O), C3, Ar-C), **36.90** (C2, C_0-CH_2), **29.68** (C3, CH-CH_3), **21.65** (C1, CH_3)

Die approbierte gedruckte Originalversion dieser Dissertation ist an der TU Wien Bibliothek verfügbar.
The approved original version of this doctoral thesis is available in print at TU Wien Bibliothek.
TU Bibliothek Your knowledge hub WIEN

1.3 Steady-State Photolysis of Oxime Ester-2PIs

UV-Vis absorption spectra of 2PI solutions (5MSA, 5MSBA, P2CK, 5M) were recorded in quartz cuvettes using a Thermo Scientific NanoDrop One/OneC Microvolume UV-Vis Spectrophotometer, measuring PBS as background spectra and THF/DMSO as background for 5M, respectively. Absorption spectra were recorded before (t_0) and upon irradiation with either 365 or 460 nm for up to 60 min at 25°C. Cuvettes filled with 2PI solutions (0.02 mM) were irradiated using an OmniCure LX500 controller at a distance of 1 cm at irradiation intensities of 30 mW cm^{-2} for 365 nm and 50 mW cm^{-2} for 460 nm. An overview on the measured local absorption maxima and maximum molar extinction coefficients are given below.

Table 8: Overview on local absorption maxima (λ_{max}) and the applied irradiation source (LED) of selected 2PIs.

2PI	λ_{max} [nm]	LED [nm]
5M	366	365
5MSA	370	365
5MSBA	376	365
P2CK	508	460

1.4 Two-Photon Polymerization of Oxime Ester-2PIs

2PI stock solutions (2 mM, 1000 µL) were prepared separately (P2CK, 5MSA, 5MSBA) from GelMA samples (15 mg/vial). 2PI stock solutions (100 µL) were pipetted to the vials containing GelMA, equilibrated for 10 min at 37°C, centrifuged and equilibrated for 5 min at 37°C. The formulation was transferred to a methacrylate-modified µ-dish (ibidi) and processed immediately. Structuring of TU Wien Logos (2D array: 100x100x60 µm) was performed at varying laser power (starting at 400 mW decreasing along x-axis Δ = -20 mW, count 10) and writing speed (starting at 200 mm s^{-1} increasing along y axis Δ = +200 mm s^{-1}, count 3) objective: Olympus 10x/(NA 0.4), hatch: 0.5 µm, dz: 0.5 µm, write type: woodpile, element first, scanner mode: pixelline, line hatch: alternate xy. After 2PP, µ-dishes (ibidi) were immersed in 3 mL PBS and incubated for 15 min at 37°C. Unpolymerized gelatin was dissolved and washed away (post-processing). The dish was re-immersed in PBS and imaged in the brightfield as well as with LSM700 (channel 555 nm).

Table 9: Polymerization thresholds determined via structuring 2D arrays of TU Wien Logos (100x100x60 µm) in the presence of 2 mM 2PI (5MSA, 5MSBA, P2CK) in hydrogel formulations (GelMA95, 15 wt%) varying laser power along the x-axis and writing speed along the y-axis.

Writing speed	**Polymerization Threshold**		
[mm s^{-1}]	[mW]	[mW]	[mW]
	5MSA	5MSBA	P2CK
400	340	320	60
600	360	340	80
800	380	360	100

Die approbierte gedruckte Originalversion dieser Dissertation ist an der TU Wien Bibliothek verfügbar.
The approved original version of this doctoral thesis is available in print at TU Wien Bibliothek.

2 Two-Photon Initiators based on Azosulfonates

2.2 Synthesis of Azosulfonate-based Two-Photon Initiators

Synthesis of DAS

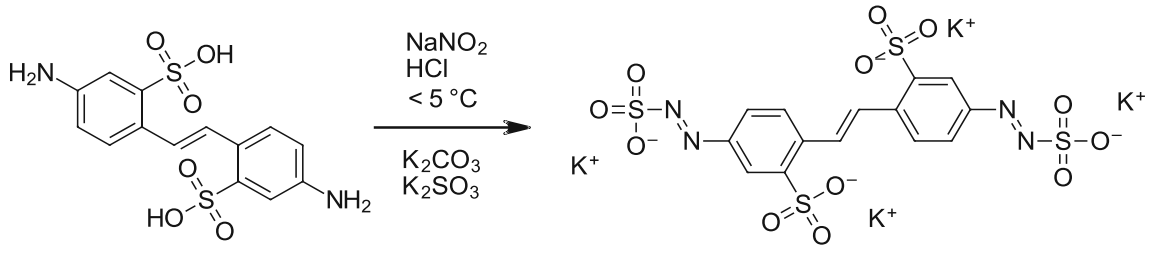

DADS

CAS: 81-11-8

DAS

Chemicals	M [g/mol]	eq.	n [mmol]	ρ [g/ml]	m [g]	V [mL]
DADS	370.39	1	27		10	
$NaNO_2$	68.99	2.3	61		4.2	
HCl 37%						6
H_2O purified						70
K_2CO_3	138.21	1	11		1.6	
K_2SO_3	158.26	2	23		4.0	

Hydrochloric acid (6.0 mL, 37% aq.) was added dropwise to a magnetically stirred suspension of DADS (10 g, 27 mmol, 1 eq.) in purified water (54 mL). The stirred yellow suspension was then cooled to 0°C, while slowly adding a cooled aqueous solution (31,5%) of sodium nitrite ($NaNO_2$, 4.23 g, 61.3 mmol, 2.27 eq.), avoiding the formation of NOx-gas by controlling the temperature (5°C). The yellow suspension was stirred at room temperature for 30 min and for another 2.5 h at 35°C. The suspension was cooled to 4°C, the solids collected by centrifugation (2500 rpm for 2 min) and washed with purified water (2x 40 mL), MeOH (2x 40 mL), Et_2O (2x 40 mL), collecting the yellow solids via centrifugation (1500 rpm, 2 min) and discarding the liquid phases via decantation. The precipitate was dried in vacuo at room temperature. Recrystallization from purified water resulted in the yellow tetrazonium salt (5.5 g, 44% yellow powder TAZ). Powdered K_2CO_3 (1.0 eq.) and K_2SO_3 (90% purity, 2.0 eq.) were mixed and added slowly to a magnetically stirred yellow suspension of TAZ (1 eq.) in purified water. During addition, the suspension turned dark orange. The solution was stirred for 18 h at room temperature and then left to crystallize overnight at 4°C. The resulting precipitate was centrifuged and washed with mother liquor. Recrystallization from purified water and drying in high vacuum led to the isolation of the reference compound (DAS).

Yield: 8.1 g orange solid (34% of theory)

UV-Vis: λ_{max} = 372 nm (PBS), ε_{max} = 36 x 10^3 M^{-1} cm^{-1}

Die approbierte gedruckte Originalversion dieser Dissertation ist an der TU Wien Bibliothek verfügbar.
The approved original version of this doctoral thesis is available in print at TU Wien Bibliothek.
TU Bibliothek Your knowledge hub WIEN

M.p.: Decomposition at 368 °C

^{1}H-NMR (400 MHz, D_2O) δ **8.47** (d, 2H, J = 2.1 Hz, Ar-H), **8.22** (s, 2H, -CH=CH-), **8.21** (d, 2H, 8.1 Hz, Ar-H), **8.14** (dd, 2H, J = 8.6 Hz and 2.2 Hz, Ar-H).

^{13}C-NMR APT (101 MHz, D_2O) δ **148.53** (C4, -C-SO_3), **141.74** (C4, C-N_2-), **139.63** (C4, -C-CH=CH-), **130.01** (C3, -CH=CH-), **129.13** (C3, Ar-C), **126.01** (C3, Ar-C), **122.90** (C3, Ar-C)

Synthesis of ASCR

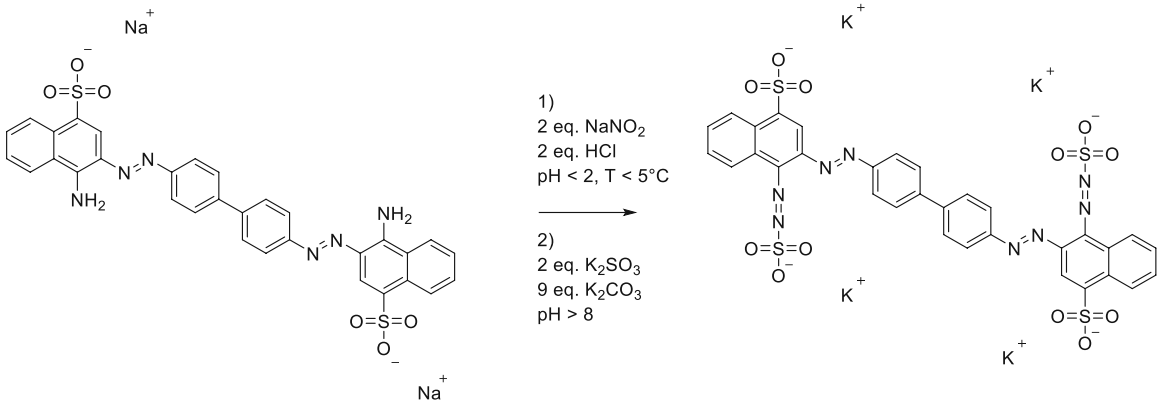

Congo Red

CAS: 14684-01-6

[696.66 g/mol]

ASCR

[991.17 g/mol]

Chemicals	M [g/mol]	eq.	n [mmol]	ρ [g/ml]	m [mg]	V [mL]
Congo Red (CR)	696.7	1	0.7		500	
HCl (37%)	36.5	2	1.4	1.19	52	0.1
$NaNO_2$	69.0	2	1.4		99	
K_2SO_3	174.3	2	1.4		250	
K_2CO_3	138.2	9	6.5		893	
H_2O purified						680

The commercially available CR was first recrystallized from purified water (5% suspension, sonication at 40 °C for 10 min) removing the undissolved agglomerates from the hot aqueous solution before recrystallization at 7°C for 4d. For diazotization CR (500 mg, 0.7 mmol, 1 eq.) was dissolved in 500 mL purified water. The dark red solution (pH = 7) was cooled to 5°C under constant stirring. $NaNO_2$ (99 mg, 1.4 mmol, 2 eq) was dissolved in 30 mL purified water and combined with HCl (37%, 0.1 mL, 2 eq.). The cooled solution of CR was added dropwise to the vigorously stirred acidic $NaNO_2$ solution, until a pH of 1 was reached. The violet reaction suspension was stirred overnight at 5°C.The conversion of CR was monitored via TLC staining (anisaldehyde, CAM). A solution of K_2SO_3 (2 eq., 1.4 mmol, 250 mg) in purified water was prepared and K_2CO_3 (9 eq., 6.5 mmol, 893 mg) was added until the solution was set to pH = 9. The reaction solution was slowly added to the cooled vigorously stirred basic solution. The solution was stirred for 8 h at room temperature. The volume of the reaction solution was reduced via evaporation (25 wt%), removing any remaining solids via centrifugation. The solution was left to crystallize over the course of 7 days at 7°C. The obtained olive-green solid was separated via suction filtration

Die approbierte gedruckte Originalversion dieser Dissertation ist an der TU Wien Bibliothek verfügbar.
The approved original version of this doctoral thesis is available in print at TU Wien Bibliothek.
TU Bibliothek Your knowledge hub WIEN

and washed with minimum amount of purified water. Recrystallization from purified water resulted in the pure product (30% th.). An aliquot of the precipitate was dissolved in water, set to pH = 1 and dried in vacuo to obtain the acidic form of ASCR.

Yield: 211 mg violet solid (30% of theory)

UV-Vis: λ_{max}^{ASCR} = 510 nm (PBS), ε_{max}^{ASCR} = 90 x 10^3 M^{-1} cm^{-1};
λ_{max}^{CR} = 498 nm (PBS), ε_{max}^{CR} = 122 x 10^3 M^{-1} cm^{-1}

M.p.: Decomposition at 320 °C

HR-MS: $[ESI]^+$ m/z calculated for

$C_{32}H_{18}K_4N_8NaO_{12}S_4^+$ 1012.8367; found: $[M+Na]^+$ 1012.8541

^{1}H-NMR potassium salt (400 MHz, D_2O) δ **8.49** (d, 2H, Ar-H), **8.42** (d, 2H, Ar-H), **8.37** (s, 2H, C_0-Ar-H-C_0), **7.89** (m, 8H, Ar-H), **7.69** (t, 2H, Ar-H), **7.54** (t, 2H, Ar-H)

^{1}H-NMR acid form (400 MHz, DMSO) δ **14.70** (bs, 1H, -SO3-H), **8.60** (d, 2H, Ar-H), **8.36** (d, 2H, Ar-H), **7.99** (s, 2H, C_0-Ar-H-C_0), **7.92** (s, 8H, Ar-H), **7.62** (bs, 2H, Ar-H), **7.47** (bs, 2H, Ar-H)

Die approbierte gedruckte Originalversion dieser Dissertation ist an der TU Wien Bibliothek verfügbar.
The approved original version of this doctoral thesis is available in print at TU Wien Bibliothek.

2.3 Characterization of Azosulfonate-2PIs

2.3.1 Photoreactor Studies

2PI solutions (1 mM in 20 mL PBS) were stirred in a photoreactor at 23.1°C and irradiated with LED light from the top (distance 1 cm) through a quartz adapter at irradiation intensities of 100 mW cm^{-2} at the solution level, corresponding to 290 mW cm^{-2} behind quartz for 365 nm and 350 mW cm^{-2} for 460 nm. LED Heads (365 nm, 460 nm) were coupled to an EXFO OmniCure LX400 UV LED spot curing system controller purchased from Excelitas Technologies. LED MAX Head 365 nm x 125 mm (Part Number: 010-00274R) and LED Head 460 nm x 55mm (Part Number: SR8084K) was used as irradiation source. LED head was coupled to a lightguide (EXFO; Part Number 805-00002; S/N LG6031194) via an adapter (8 mm diameter (silver) for 365 nm, 9 mm diameter (black) for 460 nm) and the end of the lightguide was coupled to a quartz adapter. The distance between solution filling level in the photoreactor and the lightguide immersed in a quartz adapter was 1.0 cm. LED Intensities were measured using an Ocean Optics USB 2000+ spectrophotometer device. The photoreactor was covered with aluminum foil to reduce potential loss of scattered radiation. Samples (300 µL each) were collected in brown glass vials at defined intervals (0 min, 5 min, 10 min, 15 min, 30 min, 45 min, 60 min/additionally 10 s, 30 s, 1 min for DAS and DADS) and diluted with PBS accordingly in order to maintain linearity of Lambert-Beer's law at the photometer (0.01 mM for CR, 0.02 mM for P2CK, 0.04 mM for ASCR, DAS and DADS). UV-Vis spectra were recorded in quartz cuvettes using a Thermo Scientific NanoDrop One/OneC Microvolume UV-Vis Spectrophotometer, measuring PBS as background spectra.

Table 10: Absorption maxima (λ_{max}) as well as molar extinction coefficients at λ_{max} (ε_{max}) of tested 2PIs. CR and ASCR show additional absorbance bands at 344 nm and 314 nm. (0.01 mM for CR, 0.04 mM for ASCR, DAS and DADS in PBS).

2PI	λ_{max} [nm]	ε_{max} [M^{-1} cm^{-1}]	M [g mol^{-1}]
CR	498	121,920	696.66
ASCR	510	89,606	991.17
DADS	341	28,300	370.41
DAS	372	36,175	708.87

A full database of chromophores including CR was published in literature (absorption spectra, molar absorption coefficients, fluorescence spectra and fluorescence quantum yields).[358,363,407-410]

Die approbierte gedruckte Originalversion dieser Dissertation ist an der TU Wien Bibliothek verfügbar.
The approved original version of this doctoral thesis is available in print at TU Wien Bibliothek.

2.3.2 NMR Study

The samples taken from the photoreactor were transferred into brown-glass vials and placed into a wide-neck, flat-bottom filter bottle (600 mL, ChristMartin®). The bottles were connected via rubber valves to the freeze-dryer and the samples were freeze-dried (0.01 mbar) for 2 days. The samples were dissolved in deuterated water and analyzed via NMR spectroscopy. ^{1}H-NMR spectra were recorded at 600 MHz on a Bruker Avance spectrometer. Spectra of photosensitive compounds were exclusively measured in brown-glass NMR tubes. Spectra of the starting materials were recorded separately.

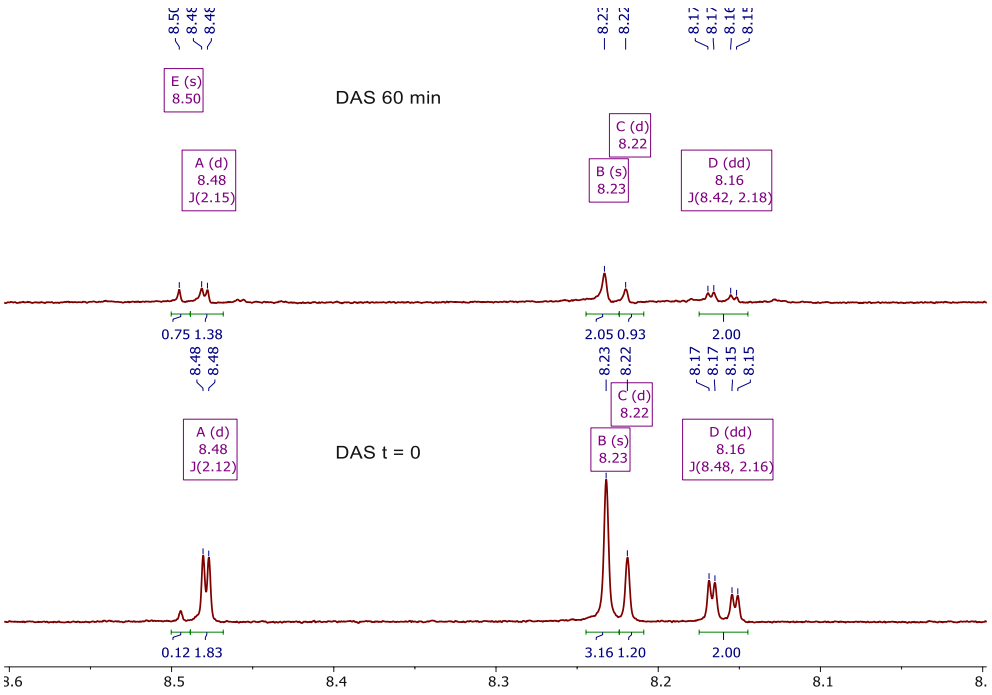

Figure 100: ^{1}H-NMR Spectra of DAS photoreactor samples before (t = 0) and upon irradiation with 365 nm LED light (60 min) with equal y-axis scaling (600 MHz, deuterium oxide). Overall, a decrease in peak-intensity is observed over time and the integral of peak E (8.50 ppm) is increasing and the integral of peak B (8.23 ppm) is decreasing upon irradiation.

Die approbierte gedruckte Originalversion dieser Dissertation ist an der TU Wien Bibliothek verfügbar.
The approved original version of this doctoral thesis is available in print at TU Wien Bibliothek.

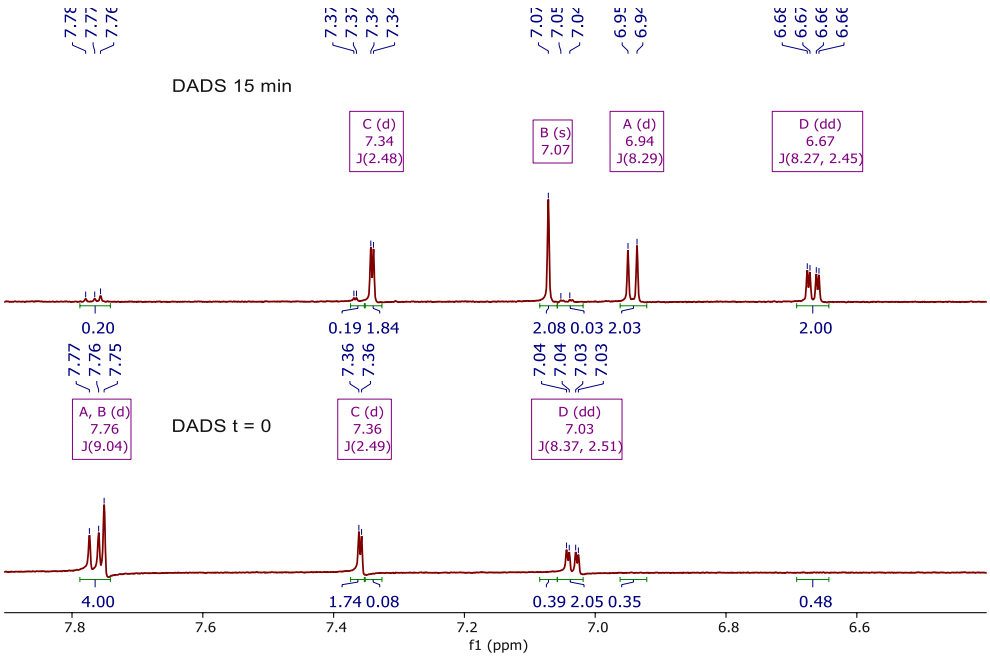

Figure 101: Trans-cis isomerization od DADS was monitored via NMR (600 MHz, deuterium oxide). Peak A is shifting from 7.76 to 6.94 ppm, peak B (s) from 7.75 to 7.05 ppm and peak D (dd) from 7.03 to 6.67 ppm.

Die approbierte gedruckte Originalversion dieser Dissertation ist an der TU Wien Bibliothek verfügbar.
The approved original version of this doctoral thesis is available in print at TU Wien Bibliothek.

2.3.3 HPLC Study

The samples of the NMR study were transferred into brown glass vials and placed into a wide neck, flat bottom filter bottle (600 mL, ChristMartin®). The bottles were connected via rubber valves to the freeze dryer and the samples were freeze dried (0.01 mbar) for 2 days. The samples were dissolved in the mobile phase (MeOH:H_2O, 10:90) and analyzed with a HP-1100 Chemstation HPLC system using a phenyl-modified reversed phase column and an UV detector (350 nm). Samples were exclusively measured in brown glass vials. Elution spectra of the starting materials (inital) were recorded separately.

*Table 11: Retention times (min) and relative integration area (%) of photoreactor samples (t_0 - 60 min). *prepared separately without irradiation.*

DADS			DAS		
	Retention time [min]	Area [%]		Retention time [min]	Area [%]
Initial*	2.89	82	**Initial***	2.50	100
	4.43	18		-	-
t_0	2.70	12	**t_0**	2.69	29
	2.89	85		2.99	71
	4.48	3		-	-
10 s	2.71	6	**10 s**	2.69	31
	2.90	92		2.98	69
	4.48	2		-	-
30 s	2.70	5	**30 s**	2.7	20
	2.90	88		2.69	80
	4.48	7		-	-
1 min	2.70	6	**5 min**	2.7	25
	2.90	88		2.99	75
	4.48	6		-	-
5 min	2.63	20	**15 min**	2.7	19
	2.90	69		2.98	81
	4.48	11		-	-
10 min	2.63	47	**30 min**	2.7	22
	2.91	37		2.98	78
	4.48	16		-	-
15 min	2.63	53	**45 min**	2.7	20
	2.90	38		2.98	80
	4.48	9		-	-
			60 min	2.7	17
				2.98	83

Die approbierte gedruckte Originalversion dieser Dissertation ist an der TU Wien Bibliothek verfügbar.
The approved original version of this doctoral thesis is available in print at TU Wien Bibliothek.

The resolution of the DADS spectrum was improved by the addition of 1vol.% NaOD (sample in D_2O). The singlet of the ethylene moiety (7.72 ppm) was overlapping with the doublet of the aromatic protons at 7.73 ppm.

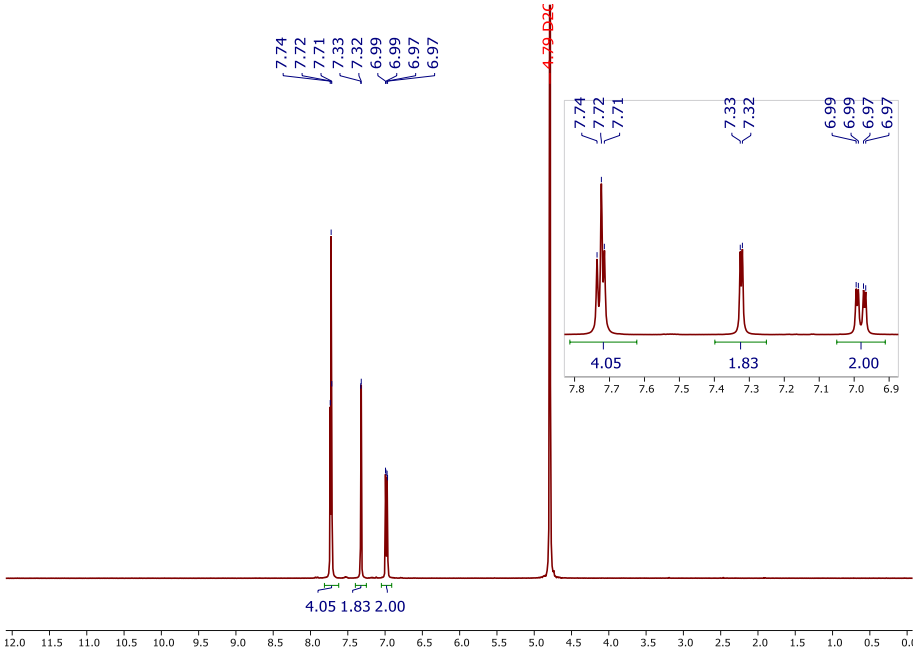

Figure 102: ^{1}H-NMR of DADS (400 MHz, D_2O+1vol% NaOD) δ7.73 (d, 8.4 Hz, 2H), 7.72 (s, 2H), 7.32 (d, J = 2.5 Hz, 2H), 6.98 (dd, J = 8.4, 2.5 Hz, 2H).

Die approbierte gedruckte Originalversion dieser Dissertation ist an der TU Wien Bibliothek verfügbar.
The approved original version of this doctoral thesis is available in print at TU Wien Bibliothek.

2.3.4 Z-Scan Measurements

Z-scan measurements were performed under static conditions. 2PI solutions were filled into quartz-glass cuvettes (120 µl volume, 170-000-1-40, Hellma-Analytics, Müllheim, Germany) and placed onto a motorized stage using a 3D printed socket. The data were acquired using a chopper by triggering the oscilloscope to the rising flank of the signal. The average signal for a given stage position was recorded. For the final z-scan 90 Hz rotation frequency was selected, resulting in an on-time of 78 µs and 11.9 ms off-time, which was proposed to be sufficient for the sample to return to equilibrium after exposure.

Table 12: Mean two-photon absorption (2PA) cross section (σ2) of Congo Red including standard deviation at the measured wavelength.

Wavelength λ [nm]	Mean 2PA Cross Section σ_2 [GM]	±Standard Deviation [GM]
700	1489.87	70.17
710	1223.12	112.59
720	970.819	91.61
740	738.961	126.26
750	644.769	79.92
760	539.564	89.54
770	531.112	51.44
780	487.992	55.68
790	544.521	104.44
800	552.359	148.05
810	414.362	45.75
820	433.103	104.65
830	401.387	33.60
840	393.488	30.10
850	341.452	38.33
860	277.152	39.61
870	257.438	12.37
880	255.993	172.65
890	222.288	36.90
900	198.111	16.70
910	191.486	17.75
920	191.726	35.30
940	151.301	10.27

Die approbierte gedruckte Originalversion dieser Dissertation ist an der TU Wien Bibliothek verfügbar.
The approved original version of this doctoral thesis is available in print at TU Wien Bibliothek.
TU Bibliothek Your knowledge hub WIEN

2.4 Two-Photon Polymerization of Azosulfonate-2PIs

Table 13: Overview on molecular weight (MW), maximum absorbance (λ_{max}) of selected 2PIs.

2PI	λ_{max} [nm]	MW [g/mol]
CR	498	696.66
ASCR	510	991.17
DAS	370	708.87
P2CK	508	506.51

2PI stock solutions (2 mM, 1000 µL PBS) were prepared separately (DAS, P2CK, ASCR, CR) from the GelMA samples (10 mg/vial). 2PI stock solution (100 µL) was pipetted to the vials containing GelMA, equilibrated for 10 min at 37°C, centrifuged and equilibrated for 5 min at 37°C. The formulation was transferred to a methacrylate-modified µ-dish (ibidi) and processed immediately. Structuring of cubes (2D array: 100x100x100 µm) was performed varying laser power (starting at 200 mW decreasing along x-axis Δ = -20 mW, count 10) and writing speed (starting at 200 mm s^{-1} increasing along y axis Δ = +200 mm s^{-1}, count 5) objective: Olympus 10x/(NA 0.4), hatch: 0.5 µm, dz: 0.5 µm, write type: woodpile, element first, scanner mode: pixelline, line hatch: alternate xy. After 2PP, µ-dishes (ibidi) were immersed in 3 mL PBS and incubated for 15 min at 37°C. Unpolymerized gelatin was dissolved and washed away (post-processing). The dish was re-immersed in PBS and imaged in the brightfield as well as with LSM700 (channel 555 nm).

Table 14: Polymerization thresholds determined via structuring 2D arrays of cubes (100x100x100 µm) in the presence of 2 mM 2PI (DAS, P2CK, CR, ASCR) in hydrogel formulations (GelMA95, 10 wt%) varying laser power along the x-axis and writing speed along the y-axis.

Wavelength	**Writing speed**	**Polymerization Threshold**			
[nm]	[mm s^{-1}]	[mW] DAS	[mW] P2CK	[mW] CR	[mW] ASCR
725	200	40	160	40	40
	400	60	180	40	40
	600	80	-	40	40
	800	80	-	40	60
	1000	80	-	60	60
800	200	60	160	40	40
	400	80	180	40	40
	600	100	200	40	60
	800	100	200	40	60
	1000	100	200	60	60
900	200	120	160	40	40
	400	140	180	60	40
	600	160	200	60	60
	800	180	-	60	60
	1000	180	-	60	60

Die approbierte gedruckte Originalversion dieser Dissertation ist an der TU Wien Bibliothek verfügbar.
The approved original version of this doctoral thesis is available in print at TU Wien Bibliothek.
TU Bibliothek Your knowledge hub WIEN

2.5 Biocompatibility Studies

2.5.1 Metabolic Activity

Cells (L929) were seeded on a 96 well plate (5,000 cells/well) and incubated overnight (37°C). 2PI solutions (4 mM) were prepared in DMEM and incubated overnight at 37°C after 30 min sonication at 40°C. The attached cells were immersed with 2PI stock solutions (ASCR, DAS) on the next day, preparing 1:1 dilution with medium (2.0; 1.0; 0.5; 0.25; 0.125 mM final concentrations, 8 repetitions) and incubated for another 24h. The 2PI solutions were removed from the well plate, the cells washed with 37°C DMEM and the viability assessed using PrestoBlue® assay (1h). Fluorescence values were observed at the plate reader (560/590nm, gain 50, bottom read). The cells were incubated for another 24h (resting period) after immersion in new DMEM. The viability was determined again using PrestoBlue® assay.

Table 15: Fluorescence values of the plate reader after 24h and after 48h including a resting period of 24h.

ASCR	**Control**	**2 mM**	**1 mM**	**0.5 mM**	**0.25 mM**	**0.125 mM**
24h, mean	100	75.9	80.4	81.0	82.1	85.9
Standard Deviation	4.1	8.2	10.0	8.1	3.7	7.3
24h + resting period, mean	172.7	121.9	133.2	144.8	155.7	156.5
Standard Deviation	14.1	15.2	18.0	9.9	20.4	18.3
DAS	**Control**	**2 mM**	**1 mM**	**0.5 mM**	**0.25 mM**	**0.125 mM**
24h, mean	100	85.1	94.2	94.8	95.7	94.0
Standard Deviation	4.2	9.9	8.6	8.5	8.7	11.2
24h + resting period, mean	182.5	154.4	162.3	174.8	172.5	183.1
Standard Deviation	14.6	17.9	15.0	12.6	14.7	15.5

Statistical analyses (Post hoc, Bonferroni) were performed by Marica Markovic at the department of material science and technology (E308, TU Wien). Analysis of variance for ASCR (24h) proved the significant difference between the groups, and PostHoc Bonferonni confirmed the significant difference between control and the tested concentrations ($p<0.05$), however no significant difference was observed between the different concentrations of ASCR. After a resting period of 24 h, the cells recovered and increased in metabolic activity reflected by increased cell numbers, which were slightly lower than in the control samples, but significantly lower for 2.0, 1.0 and 0.5 mM in comparison to the control.

Analysis of variance for DAS (24h) using Post hoc analysis proved the difference between the control and 2.00 mM ($p=0.022$). After a resting period of 24 h, the cells recovered and increased the metabolic activity reflected by increased cell numbers, which were slightly lower compared to the control. A significant difference was solely found for 2 mM in comparison to the control (Post hoc; control vs. 2 mM $p=0.009$; 2 mM vs. 0.125 mM $p=0.007$).

Die approbierte gedruckte Originalversion dieser Dissertation ist an der TU Wien Bibliothek verfügbar.
The approved original version of this doctoral thesis is available in print at TU Wien Bibliothek.

2.5.2 Cell Permeability

Cultivation of the cells (ASCs) was prepared on a µ-slide glass bottom dish (8 well, ibidi). 2PI stock solutions (1 mM, 1 mL) were prepared separately in the laminar flow hood using cell culture medium (DMEM). The cells were immersed with the 2PI stock solutions (1 mM) and immediately imaged using the LSM800 (Zeiss). Zeiss LSM800 was used (equipped with an incubator), enabling cell-imaging every 30 min over the course of 24. The reference well was measured additionally with the applied laser settings for each 2PI. An electronically switchable illumination and detection module (ESID) additionally enabled transmitted light illumination. A 20x/0.8 NA objective (ZEISS) was used and an excitation wavelength of the laser of 488 nm.

3 Hydrogel Materials for Two-Photon Polymerization

3.2 Synthesis of Hyaluronic Acid-based Macromers

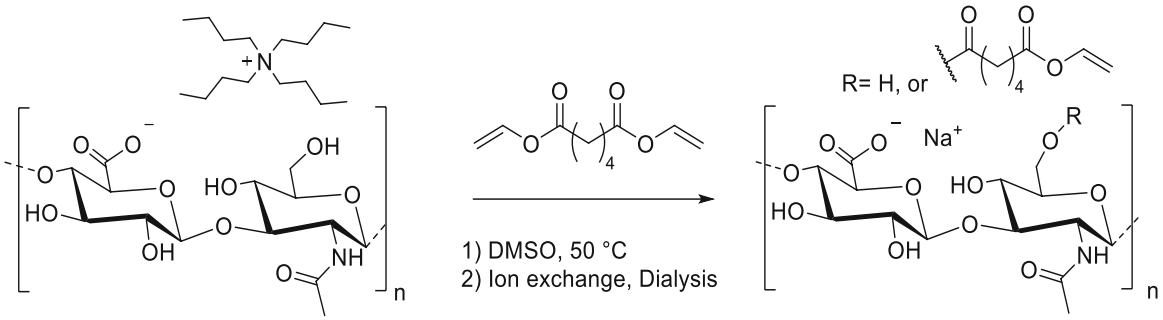

The synthesis of HAVEs with different macromer sizes and degrees of substitution (DS) was performed in a similar procedure as described previously.[115,388] HA with different molecular weight (m.w.) was either purchased or prepared by acidic degradation of HA ($\overline{M_n} \approx$ 1.5 MDa, Fluka) by hydrochloric acid (0.1 M) in a 0.5 wt.% aqueous solution for 12 and 24 h at 60 °C. Subsequently, the solution was neutralized (to a pH of 7.0, monitored by pH meter) with aqueous sodium hydroxide (3 M) and dialyzed (m.w. cut-off 3.5 kDa, Carl Roth) against purified water for at least 60 h (with at least 7 changes of water). Low m.w. HA sodium salt (96% th. after 12 h and 49% th. after 24 h) was obtained as a white solid by means of lyophilization. The sodium salt was dissolved in purified water under gentle agitation to avoid solution degradation processes[411] and the 3 wt.% aqueous solution was stirred with 15 wt.% highly acidic ion-exchange resin (IR120, Amberlite) for 4 h at r.t. After filtration, the solution was neutralized to a pH of 7.0 with tetrabutylammonium hydroxide (40 wt.% aqueous solution) and lyophilized to obtain HA tetrabutylammonium salt (HA-TBA) as a slightly pink solid. Finally, HAVEs were obtained by the conversion of HA-TBA with a 15-fold excess of divinyl adipate (TCI GmbH) in an anhydrous dimethyl sulfoxide (DMSO) solution (4 wt.%) in a transesterification reaction at 50 °C. For the work-up, HAVEs were precipitated in the 50-fold amount of cold isopropyl alcohol, dialyzed against saline solution (48 h with at least

Die approbierte gedruckte Originalversion dieser Dissertation ist an der TU Wien Bibliothek verfügbar.
The approved original version of this doctoral thesis is available in print at TU Wien Bibliothek.
TU Bibliothek Your knowledge hub WIEN

7 changes of solution) and against purified water (72 h, with at least 7 changes of water), and lyophilized to obtain the products as white solids.

3.3 Characterization of HAVE Hydrogels

3.3.1 NMR Analysis

^{1}H-NMR spectra were recorded at 25 °C in D_2O upon addition of 4% NaOD (grade of deuteration ≥ 99.5%, Sigma Aldrich) at 400 MHz using a Bruker DPX-200 Fourier transform spectrometer. The signal of non-deuterated H_2O at 4.79 ppm was used as reference.

^{1}H-NMR (400 MHz, 512 scans, D_2O), δ [ppm]): 8.07 (d, xH, CH=CH_2), 7.45 (d, xH, CH=CH_2), 7.20 (q, xH, CH=CH_2), 4.55 - 4.46 (d, 2H, C^{1}H and C$^{1'}$H), 3.34 – 3.84 (m, 11H, [ring]CH and ring-CH_2), 2.51 (bs, 4xH, CH_2C(O)O), 2.02 (s, 3H, CH_3C(O)N), 1.68 (bs, 4xH, CH_2-CH_2); x represents the degree of substitution (DS).

^{1}H-NMR (400 MHz, 512 scans, D_2O+NaOD), δ [ppm]): 4.52 - 4.44 (d, 2H, C^{1}H and C$^{1'}$H), 3.36 – 3.92 (m, 11H, [ring]CH and ring-CH_2), 2.18 (t, 4xH, CH_2C(O)O), 1.99 (s, 3H, CH_3C(O)N), 1.54 (t, 4xH, CH_2-CH_2); x represents the degree of substitution (DS).

3.3.2 GPC Analysis

Gel permeation chromatography (GPC) analysis was performed using a Viscotek GPC system, including a Viscotek GPCmax VE2001 GPC solvent/sample module (100 µL loop), a solvent degasser, a Viscotek VE3580 refractive index concentration detector, a Waters pre-column, a Waters ultrahydrogel linear 7.8×30mm column, and a Waters ultrahydrogel 250 7.8×30mm column with 10 µm particle size. The eluent was Phosphate buffered saline (NaH_2PO_4 0.05 M, NaCl 0.1 M, NaN_3 0.05%) at a temperature of 30 °C and a flow rate of 0.5 mL min 1. Polyethylene glycol standards (American Polymer Standards Corporation) were used for standard calibration to determine the number average of the molecular weight $\overline{M_n}$ and the polydispersity ($Đ_M$).

3.3.3 Photorheology

Photorheological measurements were performed on an Anton Paar Modular Compact Rheometer MCR 302 WESP with a plate-to-plate measuring system with a 25 mm steel stamp, a glass plate, and a gap size of 50 µm in oscillation mode with 10 Hz and an amplitude of 10% strain at 25 °C.40 Samples were irradiated with filtered light (320 – 500 nm, EXFO Omnicure S2000) bottom-up through the glass plate with a light intensity of 3.2 W cm^2 at the tip of the light guide as measured with an EXFO Omnicure R2000 radiometer. This referred to a light intensity of 40 mW cm^2 directly above the glass plate. Storage modulus G' and loss modulus G'' were measured every second; light was automatically activated after 60 seconds and the measurement was continued until a constant G' was attained.

Die approbierte gedruckte Originalversion dieser Dissertation ist an der TU Wien Bibliothek verfügbar.
The approved original version of this doctoral thesis is available in print at TU Wien Bibliothek.
TU Bibliothek Your knowledge hub WIEN

3.3.4 Hydrogel Swellability

To investigate the swellability of UV-polymerized hydrogels, HAVE formulations were polymerized in a silicone mold from ibidi (5.8 x 0.7 mm). Stock solutions of LiTPO (0.1%) and DTT (0.2%) were combined with PBS and pipetted on top of lyophilized HAVE. The formulation was transferred into molds and polymerized in the UVitron IntelliRay 600 curing system (175 mW cm^{-2}, 320-390nm, 4 min).

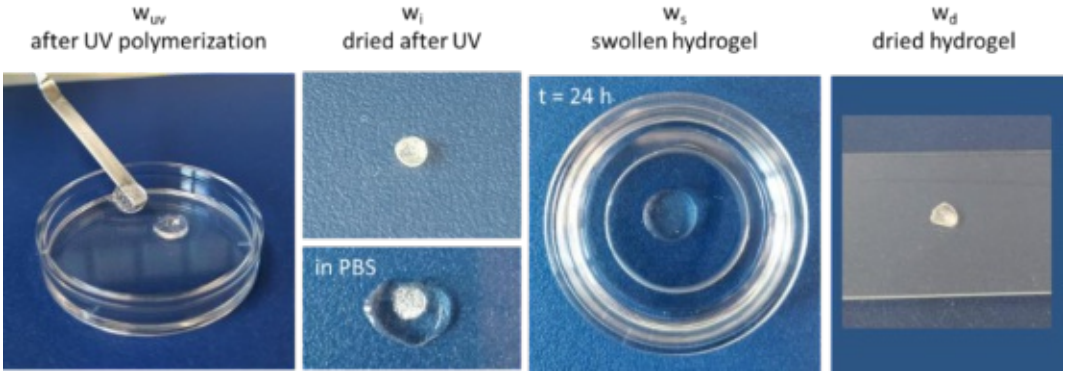

Figure 103: Mass of the hydrogels was obtained after UV-polymerization (wuv), after lyophilization (wi), after swelling in PBS for 24 h (ws) and after repeated lyophilization (wd).

Mean values for the mass of the gels after UV-polymerization (w_{uv}), after lyophilization (w_i), after swelling in PBS for 24h (w_s) and after repeated lyophilization (w_d) were calculated.

Die approbierte gedruckte Originalversion dieser Dissertation ist an der TU Wien Bibliothek verfügbar.
The approved original version of this doctoral thesis is available in print at TU Wien Bibliothek.

Table 16: Hydrogel pellets of two different HAVEs and their weight in dried and swollen states.

HAVE	w_{uv} [mg]	w_i [mg]	w_s [mg]	w_d [mg]	swelling ratio [%]
DS 95%	23.8	4.1	26.0	4.5	4.8
	25.0	4.3	27.4	4.6	5.0
	25.1	4.4	27.6	4.9	4.6
Mean	24.6 ± 0.7	4.3 ± 0.2	27.0 ± 0.9	4.7 ± 0.2	4.8 ± 0.2
DS 5%	20.6	3.3	37.2	3.5	9.6
	20.2	3.7	39.6	3.9	9.2
	21.4	3.7	38.2	3.8	9.1
Mean	20.7 ± 0.6	3.6 ± 0.2	38.3 ± 1.2	3.7 ± 0.2	9.3 ± 0.3

3.4 Cell Encapsulation

3.4.1 UV-Cell Encapsulation

UV-cell encapsulation was performed by mixing HAVE based hydrogel precursor formulation in a 1:1 ratio (v/v) with a cell suspension in medium (ASC GFP) to reach final concentrations of 15 wt.% HA50VE05/80 mol% (thiol-to-ene) dithiothreitol (DTT) and 0.5 mM lithium phenyl-2,4,6-trimethylbenzoylphosphinate (LiTPO). Hydrogels were polymerized using silicone gaskets applied on glass cover slips. Labelled cells (ASC GFP) were used enabling straightforward cell imaging without staining. All formulations were prepared in a laminar flow hood under sterile conditions. Cells were cultured and maintained in EGM 2 supplemented with 10% fetal bovine serum. Cells were incubated in humidified atmosphere at 37°C with 5% CO_2. Cells were detached using 0.5% trypsin EDTA solution. Afterwards, cell culture medium with serum was added to inactivate trypsin. Cells were collected in Falcon tubes and centrifuged at 300 rpm (3 min). Cells were counted, spun down once more, and resuspended in the calculated amount of polymer solution to reach final concentrations of 10^6 cells mL^{-1}. Hydrogels were polymerized using Grace Bio Labs CultureWell™ reusable gaskets (CW 8R 1.0, 8 x 6 mm diameter × 1 mm depth) and Boekel Scientific UV crosslinker (1 J, 368 nm, 4 min). Gels were transferred to a sterile µ-dish (ibidi GmbH, Germany), immersed in cell medium and incubated in a humidified atmosphere with 5% CO_2 at 37 °C. Cell survival was monitored via confocal laser scanning microscopy (LSM) (Zeiss, Germany), changing cell medium every day. The proliferation rate (cell number) was determined by counting the living cells using ImageJ within the recorded section and normalizing values on day 4, 11 and 14 to the data of day 1 (100%).

Die approbierte gedruckte Originalversion dieser Dissertation ist an der TU Wien Bibliothek verfügbar.
The approved original version of this doctoral thesis is available in print at TU Wien Bibliothek.

3.4.2 Cell Encapsulation using Two-Photon Polymerization

Cell encapsulation experiments were performed by mixing equal parts (1:1, v/v) of a cell suspension in medium (ASC-GFP, 10^6 cells mL^{-1}) with HAVE based hydrogel precursor formulation to reach final concentrations of 5 wt.% HA22VE95/80 mol% DTT. The photoinitiator 3,3'-((((1E,1'E)-(2-oxocyclopentane-1,3-diylidene) bis(methanylylidene)) bis(4,1-phenylene)) bis(methylazanediyl))dipropanoate (P2CK)[165] was used in a concentration of 0.5 mM. The formulation was pipetted into a surface-treated ibidi µ-dish (35 mm with glass bottom, ibidi GmbH, Martinsried, Germany). Glass surfaces were treated with 3-(trimethoxysilyl)propyl methacrylate in order to avoid hydrogel detachment during incubation.[348] Another formulation was prepared by mixing equal amount (1:1, v/v) of hydrogel precursor formulation with the same amount of Dulbecco's Phosphate Buffered Saline (PBS) solution without calcium and magnesium in order to perform a cell-free control experiment. Microfabrication was performed by means of a two-photon polymerization (2PP) system. The used 2PP system was based on a Ti:sapphire laser system (wavelength 800 nm, pulse width 70 fs, objective Olympus 10x/(NA 0.4), scanning speed 100 mm s^{-1}, hatch 0.3 µm, layer spacing 0.5 µm) and was also employed in a previous study.[412] A detailed description of the setup and the process can be found in literature.[113] Hydrogel structures (TU Wien Logos, 100x100x100 µm) were printed by scanning the focused laser beam with a writing speed of 100 mm s^{-1} (triplicates) with varied laser power (10 - 150 mW, 10 mW steps) through the hydrogel precursor formulation according to the layer information from the sliced CAD file. The samples were developed in medium or PBS solution, respectively and remaining precursor solution was washed away. GFP-labelled cells (ASCs) were visualized by a confocal LSM 700 (Zeiss, Germany) using ZEN11 software for cell imaging. Viable cells emitted green fluorescence at excitation/emission set to 488/530 nm. After imaging, hydrogels were immersed in cell medium and incubated in a humidified atmosphere with 5% CO_2 at 37 °C. Cell quantification was performed by counting the cells within the 4 divided groups using ImageJ on day 7 and normalizing the data to day 3 (100%) after encapsulation.

Die approbierte gedruckte Originalversion dieser Dissertation ist an der TU Wien Bibliothek verfügbar.
The approved original version of this doctoral thesis is available in print at TU Wien Bibliothek.
TU Bibliothek Your knowledge hub WIEN

Summary

Two-photon polymerization (2PP) is a powerful technology to fabricate complex tissue scaffolds with outstanding resolution in the (sub)micrometer range. In contrast to conventional lithography (one-photon absorption), the polymerization is limited to the focal spot of the pulsed infrared-laser beam. The high photon flux required for 2PP, is realized by scanning an ultrafast femtosecond laser pulse through a photosensitive formulation. Commonly, hydrogels are used as functional material platform to imitate biological matrices as best as possible. Two-photon initiators (2PIs) play a major role in this technology, since amongst other factors their biocompatibility heavily influences the overall biocompatibility of the fabricated tissue. Although, major findings were made in the molecular design of 2PIs, biological systems require sensitive fine-tuning of the chromophores aiming to enhance biocompatibility for tissue engineering applications. A wide variety of available 2PIs are based on aromatic ketone structures, which are known to be potentially cytotoxic. Furthermore, excited species are considered to induce radical oxygen species during two-photon processing, leading to notable oxidative stress amongst living organisms. Therefore, the optimization and engineering of highly efficient, water-soluble 2PIs is of major importance for biomedical applications.

Hence, the key elements of this thesis were the development of novel 2PIs for tissue engineering. Two main approaches were followed to introduce photolabile moieties into different classes of chromophores in order to enhance biocompatibility. Besides the development of 2PIs, further focus was placed on macromers for tissue engineering. For this purpose, a natural biopolymer (hyaluronic acid) was chosen as endogenous substance to extend the portfolio of industrially available hydrogel materials.

The first approach followed the synthesis of 2PIs by introducing photolabile oxime ester (OE) moieties into benzylidene cycloketone core structures. OEs were of special interest, since they tend to decompose upon irradiation, where the excitation energy dissipates by cleavage of the nitrogen-oxygen bond. The initiation mechanism required for polymerization, subsequently involves a decarboxylation reaction, resulting in the generation of initiating radicals.

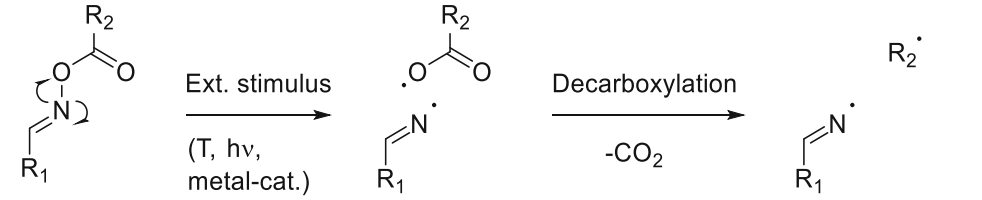

Oxime ester | Iminyl- and acyloxy radical | Iminyl- and reactive radical R•

First, the proposed concept towards improved structuring efficiency was investigated through a comprehensive 2PP study of a bimolecular model system. The determination of the polymerization threshold values via single-line writing was a sensitive tool to assess the reactivity

Die approbierte gedruckte Originalversion dieser Dissertation ist an der TU Wien Bibliothek verfügbar.
The approved original version of this doctoral thesis is available in print at TU Wien Bibliothek.
TU Bibliothek Your knowledge hub WIEN

of the precursor formulations, which were based on an OE-model compound (co-initiator) in the presence of a state-of-the-art benzylidene cycloketone sensitizer. Accordingly, the proposed concept was pursued by designing a monomolecular OE-2PI via a straightforward synthesis approach. OE-functionalities were introduced via oxime-functionalities that followed a classical aldol-condensation of commercially available starting materials.

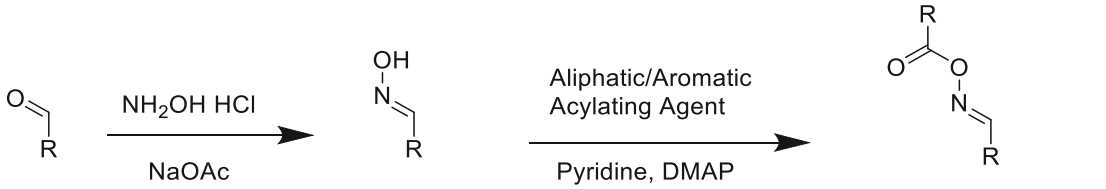

Several coupling agents were chosen enabling the introduction of ionizable functional groups via inorganic acid derivatives, favorable for the preparation of hydrophilic derivatives. Moreover, aliphatic- and aromatic substituents were incorporated to obtain a broad spectrum of target compounds. The organo-soluble derivatives were primarily synthesized as reference compounds in order to establish the experimental conditions for the synthesis of the water-soluble derivatives.

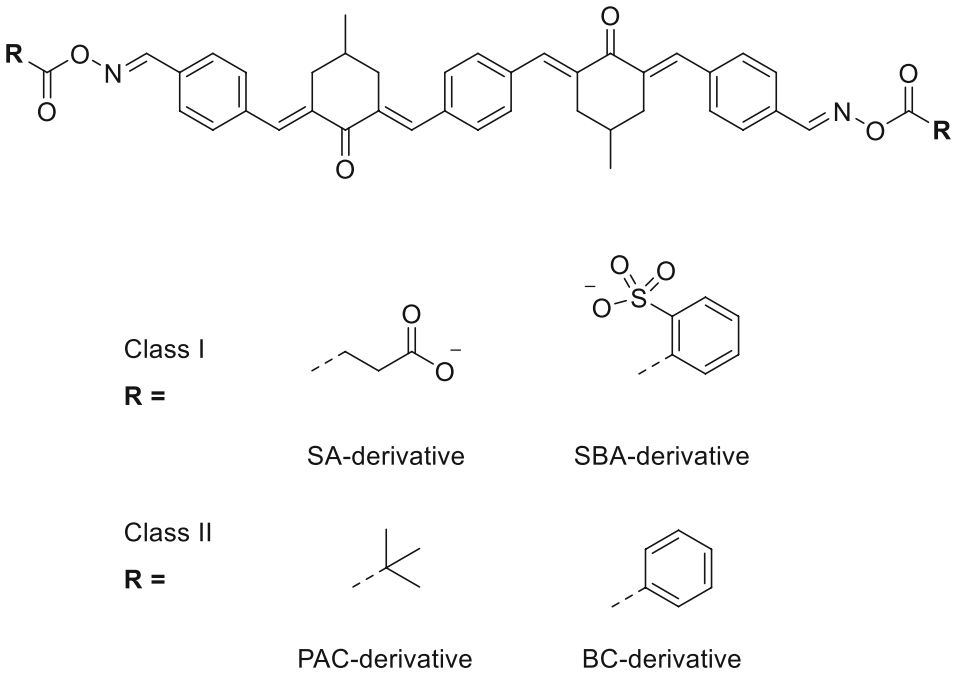

The water-soluble derivatives (5MSA, 5MSBA) were assessed via steady-state photolysis experiments to evaluate their photobleaching behavior upon irradiation with LED-light. UV-Vis measurements revealed a significant loss of the initial absorption maximum of the tested OE-derivatives. The reference compounds, which were not based on OE-functionalities, did not exhibit notable photobleaching behavior. Although, the restoration of the parent system was expected, considerable photofragmentation of the chromophores was observed, likely to be

Die approbierte gedruckte Originalversion dieser Dissertation ist an der TU Wien Bibliothek verfügbar.
The approved original version of this doctoral thesis is available in print at TU Wien Bibliothek.
TU Bibliothek Your knowledge hub WIEN

derived by a loss of conjugation length. However, a thorough study on the photochemical behavior of OE-derivatives might be necessary to understand the mechanistic behavior and to draw profound conclusions on their photolabile behavior.

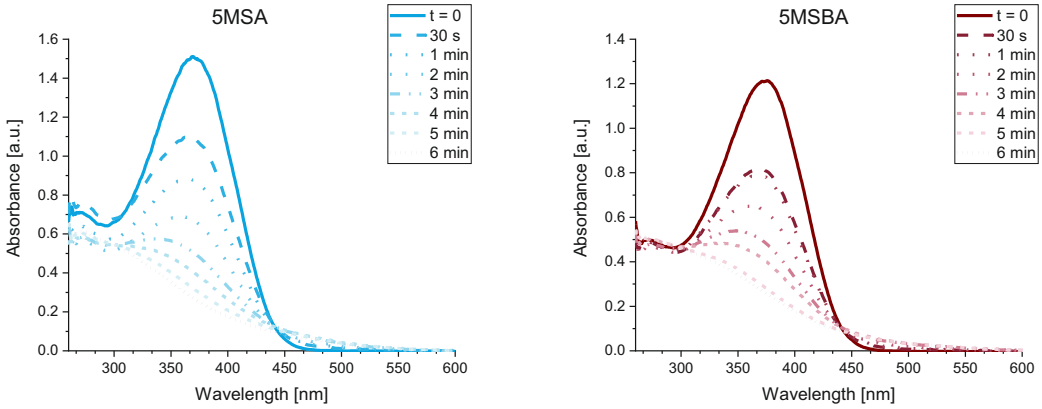

Subsequently, the processing window of the water-soluble 2PIs was determined via a parametric study on laser power and writing speed in hydrogel formulations based on gelatin. However, the polymerization thresholds of the novel 2PIs remained considerably higher compared to the state-of-the-art cycloketone 2PI, corresponding to a higher laser power required to initiate polymerization. Nonetheless, bubble formation during 2PP indicated an eventual 2PI-cleavage during processing, which was expected based on the results from the steady-state photolysis. The assessment of optimum structuring parameters could give further evidence on an eventual thermal decomposition as a consequence of harsh processing conditions. Still, the synthesis of OE-2PIs was successfully performed and the conducted experiments provided initial findings on the subject. Nevertheless, tedious synthesis routes and the harsh structuring conditions, required to initiate polymerization led to the development of a more accessible class of 2PIs.

The second approach of this thesis was the development of novel 2PIs based on commercially available azo dyes. Here, photolabile azosulfonate moieties (AS) were introduced, since they enhance water-solubility in general, which is beneficial for biomedical applications. Moreover, ASs are promising candidates for the development of photolabile 2PIs, due to their photochemically triggered tendency to decompose, driven by the release of gaseous nitrogen. For a straightforward synthesis approach, commercially available azo dyes were used as starting materials. Congo Red was chosen as suitable precursor, since terminal amino groups were available for modification. In the first step, diazotization of the aromatic amines was performed in the presence of $NaNO_2$ in strong acidic aqueous solution. In the second step, sulfites were coupled to the in-situ generated diazonium salts. An effective salting-out approach resulted in the successful isolation of the target compound (ASCR).

Die approbierte gedruckte Originalversion dieser Dissertation ist an der TU Wien Bibliothek verfügbar.
The approved original version of this doctoral thesis is available in print at TU Wien Bibliothek.

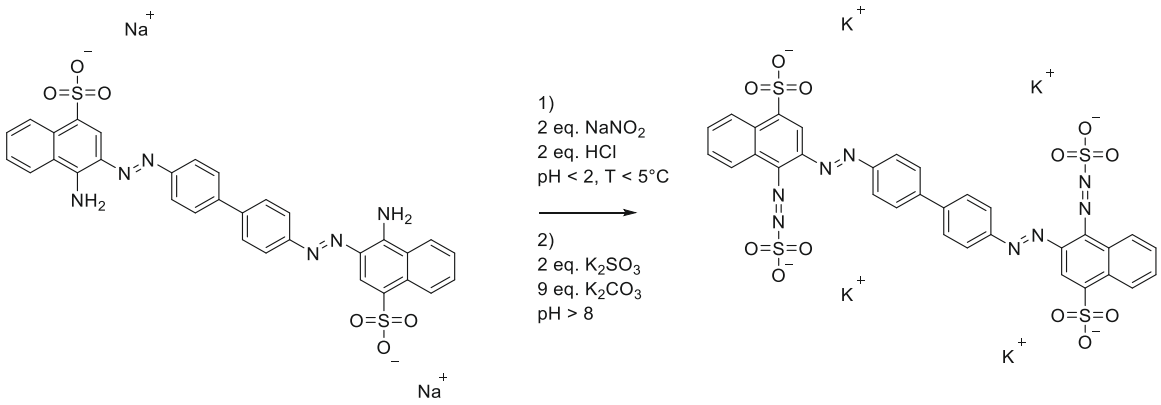

Congo Red **ASCR**

Although azo dyes in general exhibit a high tendency to form water-insoluble dye aggregates, as a consequence of H-bonds, electrostatic- and hydrophobic interactions, these limitations were overcome by accurate monitoring of the analytes' concentration and the pH of the reaction solution. UV-Vis measurements revealed a decent bathochromic shift of the absorption profile upon modification. The photochemical behavior of the novel 2PI (ASCR) and its starting material (CR) was investigated during photoreactor studies. Here, high-energy LED-light was chosen and selected according to the absorption profile of the 2PIs. However, the applied irradiation intensities were insufficient to induce 2PI-decomposition of the chromophores. However, extensive photobleaching was observed for the stilbene-based reference compounds (DAS, DADS), which was proposed to be a consequence of a conformational twist about the ethylene bond.

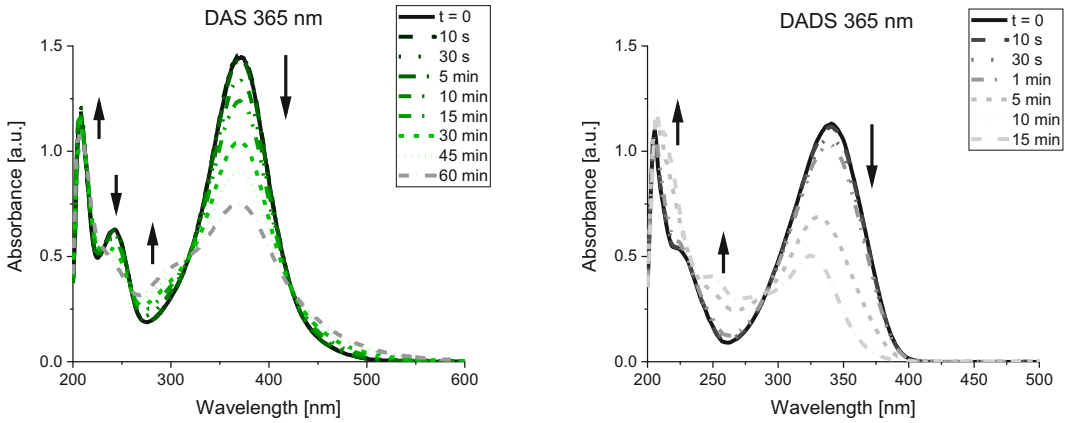

Consequently, photoisomerization was proposed to be in major competition with the desired photodecomposition. The photodegradation products or rather photoisomerization products were meant to be clarified via extensive NMR and HPLC studies, however a full elucidation of the complex mechanism is open for future investigations. Still, photoisomerization was confirmed for the stilbene-precursor molecule, but could not be verified for the state-of-the-art stilbene-based 2PI.

Die approbierte gedruckte Originalversion dieser Dissertation ist an der TU Wien Bibliothek verfügbar.
The approved original version of this doctoral thesis is available in print at TU Wien Bibliothek.
TU Bibliothek Your knowledge hub WIEN

DAS

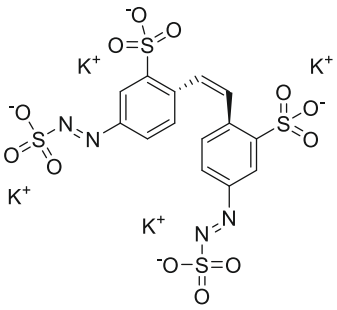

(Z) **Photoisomerization product**

DADS

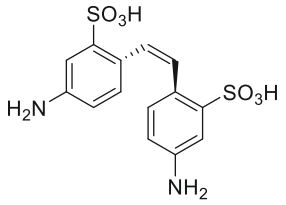

(Z) **Photoisomerization product**

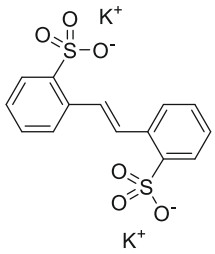

(E) **Photocleavage product**

Z-Scan measurements of the commercially available azo dye (CR) revealed extraordinarily high two-photon absorption (2PA) cross section, especially in the region around 700 nm (1490 GM), overruling many of the available state-of-the-art 2PIs. Likewise, expectations for the synthesized 2PI (ASCR) are high and the Z-Scan is planned for the near future, since the setup required maintenance. Moreover, exceptional 2PP-processability was observed in gelatin-based hydrogels for both azo dye-based 2PIs over a broad range of applied laser wavelengths, laser powers and writing speed. Interestingly, laser-ablation of preliminary structured hydrogel cubes was observed for high laser powers and low writing speed, presumably as a consequence of the extraordinarily high 2PA-cross sections of the azo dyes. Besides that, harsh structuring conditions play a major factor in hydrogel laser-ablation. By careful adjustment of the laser settings (increasing the slicing distance in z-direction), hydrogel-ablation was successfully reduced. Additionally, hydrogel-ablation was deliberately induced by a double-exposure of the photosensitive resin. This opens the pathway towards photodegradable hydrogels. Besides the excellent processability of the novel 2PIs, great potential was found during cell-viability studies. ASCR was tested on various different cell-lines and exhibited comparable biocompatibility to the state-of-the-art 2PIs. Being aware that many of the literature-known azo dyes are listed as mutagenic or carcinogenic, the cell permeability of CR and ASCR is strongly recommended to be tested in the near future.

The last part of this thesis focused on the development of hyaluronic acid (HA)-based macromers. The accurate fine-tuning of the system parameters was an integral element of this study in order to successfully synthesize hydrogel macromers for high-resolution 3D printing. Besides the numerous available synthetic biomaterials, which are heavily dependent on the petroleum-industry, HA was chosen as endogenous substance, which is well-established in

Die approbierte gedruckte Originalversion dieser Dissertation ist an der TU Wien Bibliothek verfügbar.
The approved original version of this doctoral thesis is available in print at TU Wien Bibliothek.
TU Bibliothek Your knowledge hub WIEN

biomedicine. In order to ensure crosslinkability for photopolymerization, vinyl esters (VE) were chosen as modification, in contrast to the potentially cytotoxic (meth)acrylates usually used to synthesize highly reactive macromers. Since, macromer length and crosslinking density are key factors in determining characteristic hydrogel network properties (swelling ratio and mass loss profile), a suitable selection of the system parameters was made, facilitating the synthesis of a wide selection of HAVE macromers.

Synthesis of HAVE

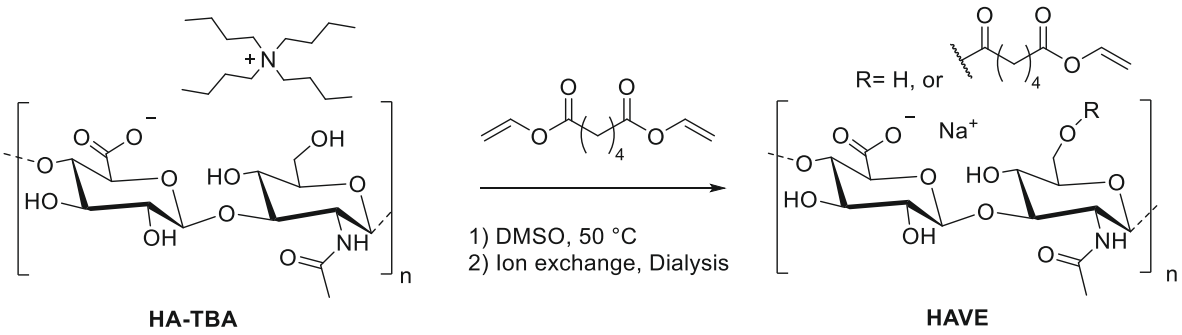

Crosslinking of HAVE

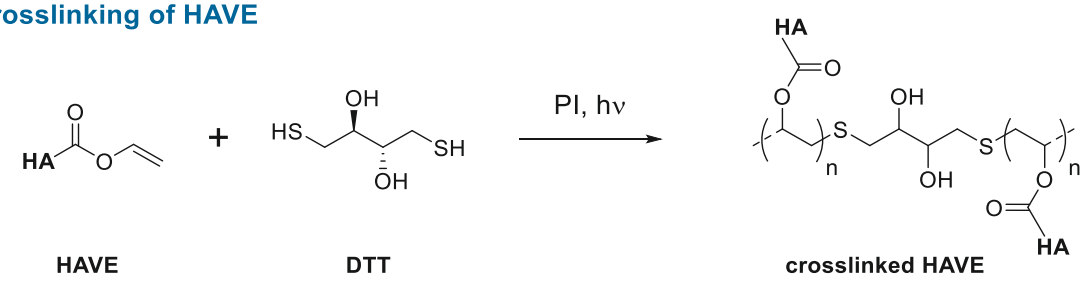

Out of the pool of available macromers, molecular weight and degree of substitution was tuned according to the subsequent application (UV- and 2PP cell encapsulation). Generally speaking, long-term UV-cell encapsulation experiments were observed to require relatively soft and flexible hydrogels for cells to sufficiently proliferate and provide adequate nutrient transport over the course of the experiment. Future encapsulation approaches might also include protein motifs Arg-Gly-Asp (RGD), especially suited for cell culture in order to enhance cell-interactive properties of the macromer and provide a pleasant cell environment. In contrast to UV-polymerized hydrogel pellets, 2PP required macromers with relatively high degree of substitution and low molecular weight in order to obtain high macromer content within the photosensitive formulations and sufficient polymerization rate along the focal volume of the pulsed laser beam. In general, the initial low water-solubility of the functionalized macromers was met by reducing the molecular weight to 20–50 kDa. As a result, highly-resolved hydrogel microstructures in the presence of adipose-derived stem cells were fabricated with enhanced long-term stability. Still, round morphology of the cells was observed being derived by a combination of stiff hydrogel network and eventual missing cell-interactive behavior of HAVE.

Overall, this thesis illustrates how the introduction of photolabile functionalities into two-photon absorbing chromophores is a powerful technique for the fine-tuning of 2PIs. The novel concept of

Die approbierte gedruckte Originalversion dieser Dissertation ist an der TU Wien Bibliothek verfügbar.
The approved original version of this doctoral thesis is available in print at TU Wien Bibliothek.
TU Bibliothek Your knowledge hub WIEN

cleavable 2PIs is proposed to overcome the current limitations of state-of-the-art 2PIs, which require relatively low writing speed with the risk to induce reactive oxygen species upon irradiation. The novel 2PIs are proposed to decrease the generation-rate of reactive oxygen species, as a consequence of fast unimolecular cleavage and reduced lifetimes of excited triplet states. Still, photoproducts and their cell-permeability are considered to play a considerable role in the biocompatibility of hydrogel materials and need to be assessed carefully. The aim of this thesis was to enhance biocompatibility of 2PIs as well as macromers for tissue engineering applications, being realized by the introduction of photolabile moieties into 2PI backbones as well as by the use of natural polysaccharides as hydrogel precursors.

Die approbierte gedruckte Originalversion dieser Dissertation ist an der TU Wien Bibliothek verfügbar.
The approved original version of this doctoral thesis is available in print at TU Wien Bibliothek.

Materials and Methods

Materials

Chemicals were purchased from Sigma Aldrich or TCI and used without further purification. Hyaluronic Acid (sodium hyaluronate- technical, 50-90 kDa) was purchased from Contipro.

Confocal Microscopy

Cell-viability was assessed via confocal laser scanning microscopy (LSM700 and LSM800, Zeiss Germany) in collaboration with Stefan Binder at the department of material science and technology (E308, TU Wien). Confocal 3D image stacks of the microfabricated scaffolds were taken with a Zeiss Axio Observer Z1. Data processing was performed using ZEN11 software from Zeiss.

Cell Culture

Cell culture experiments and statistical analyses (Post hoc, Bonferroni) were performed by Marica Markovic at the department of material science and technology (E308, TU Wien).

Dialysis

The purification and the cation exchange of the synthesized polymers was performed with Pre-wetted RC Tubing dialysis membranes Spectra/Por®6 from Spectrum®Labs.com with a molecular weight cutoff (MWCO) of 50 kDa. The dialysis tubes, which were delivered in a wet state were thoroughly washed with distilled water to remove the sterile storage solution. To seal one side of the dialysis tube, it was clamped with a clip and the polymer solution transferred into the tube via a funnel. The volume of the solution inside the dialysis tube did not exceed 2/3 of the maximum volume of the tube. Air bubbles were removed by pressing the dialysis walls onto each other before sealing the second end of the tube with another clip. Dialysis tubes were immersed into a 5 L beaker, filled with a 0.3 M NaCl solution. After 3h of stirring the solution the diffusion was accelerated by exchanging the used NaCl solution to a new one. The solvent change of NaCl solution was performed at least 7 times and afterwards the dialysis was performed with demineralized water with 7 changes of solvent. After complete dialysis, the clamps were opened, and the purified polymer solution transferred into a flask and lyophilized.

Functionalization of µ-Dishes for Two-Photon Polymerization

Glass bottom µ-dishes were first treated for 10 min in a plasma cleaner (PDC-002, Harrick Plasma, USA). Purified water (50% v/v), ethanol (48% v/v), glacial acetic acid (0.3% v/v) and 3-(trimethoxysilyl)propyl methacrylate (2% v/v, Sigma-Aldrich) was mixed and stirred for 15 min. Aliquots (~1 mL) were pipetted into µ-dishes and the glass surface modified for 30 min. The dishes were rinsed with purified water and dried in a drying oven (50 °C) for 1 h.

Die approbierte gedruckte Originalversion dieser Dissertation ist an der TU Wien Bibliothek verfügbar.
The approved original version of this doctoral thesis is available in print at TU Wien Bibliothek.
TU Bibliothek Your knowledge hub WIEN

GPC Analysis

Gel permeation chromatography (GPC) analysis was performed using a Viscotek GPC system, including a Viscotek GPCmax VE2001 GPC solvent/sample module (100 µL loop), a solvent degasser, a Viscotek VE3580 refractive index concentration detector, a Waters pre-column, a Waters ultrahydrogel linear 7.8×30mm column, and a Waters ultrahydrogel 250 7.8×30mm column with 10 µm particle size. The eluent was Phosphate-buffered saline (NaH_2PO_4 0.05 M, NaCl 0.1 M, NaN_3 0.05%) at a temperature of 30 °C and a flow rate of 0.5 mL min^{-1}. Polyethylene glycol standards (American Polymer Standards Corporation) were used for standard calibration to determine the number average of the molecular weight ($\overline{M_n}$) and the polydispersity ($Đ_M$).

Handling of Photosensitive Compounds

Preparation of photosensitive materials was performed in a laboratory equipped with UV-filter films (cut-off: 520 nm). Sensitive formulations including 2PIs were processed in a dark-room laboratory using 620 nm LEDs as light source.

HPLC Analysis

Samples were analyzed on a reversed-phase HP-1100 Chemstation HPLC system with a diode array detector and a Waters Xterra MS C18 column, particle size 5 µm, 150 x 145 mm using a flow rate of 0.8 mL/min at column temperature of 25 °C. Measurements were performed using a solvent ratio of 58/42% ACN/H_2O for 20 min. UV-Vis detector signals (200 – 600 nm) were recorded continuously during the measurement.

HR-MS Analysis

HR-MS spectra (m/z 50-1900) were obtained on a maXis ESI-Qq-TOF mass spectrometer (Bruker Daltonics, Bremen, Germany) in the positive-ion mode by direct infusion. The sum formulas of the detected ions were determined using Bruker Compass DataAnalysis 4.0 based on the mass accuracy (Δm/z ≤ 5 ppm) and isotopic pattern matching (SmartFormula algorithm). Samples were dissolved in analytical grade solvents (THF) in a concentration of 10 µM and measured using an HTC PAL system autosampler (CTC Analytics AG, Zwingen, Switzerland), an Agilent 1100/1200 HPLC with binary pumps, degasser and column thermostat (Agilent Technologies, Waldbronn, Germany) and Agilent 6230 AJS ESI–TOF mass spectrometer (Agilent Technologies, Palo Alto, United States). A silica-based C-18 column (4.6 x 50 mm) from Agilent was used as stationary phase with a Phenomenex C-18 Security Guard Cartridge. Data evaluation was performed using Agilent MassHunter Qualitative Analysis B.07.00. Identification was based on peaks obtained from extracted ion chromatograms (extraction width ± 20 ppm).

Die approbierte gedruckte Originalversion dieser Dissertation ist an der TU Wien Bibliothek verfügbar.
The approved original version of this doctoral thesis is available in print at TU Wien Bibliothek.
TU Bibliothek Your knowledge hub WIEN

Lyophilization

Aqueous solutions were freeze-dried by immersing the flask containing the sample in liquid nitrogen for minimum 15 minutes. The solvent was removed by sublimation on a Christ freeze-drying system Gamma 2-20 at a pressure of 0.01 mbar and a temperature of the cooling coils of -85°C.

Melting Points

Melting points were obtained using a Stanford Research Systems Optimelt MPA100 automated melting point system.

Nuclear Magnetic Resonance

NMR spectra were recorded on a Bruker Avance spectrometer at 400 MHz/600 MHz for ^{1}H and 100 MHz for ^{13}C. Spectra of photosensitive compounds were exclusively measured in brown-glass NMR tubes. Data for ^{1}H-NMR are reported as follows: chemical shift (δ) in units of parts per million (ppm) from tetramethylsilane (TMS) using the residual non-deuterated solvent signal of CD_2Cl_2 (δ = 5.32 ppm), $CDCl_3$ (δ = 7.26 ppm), D_2O (δ = 4.79 ppm) or DMSO-d_6 (δ = 2.50 ppm) as internal reference.[413] Multiplicities are reported by using the following abbreviations; bs: broad singlet; s: singlet; d: doublet; t: triplet; m: multiplet. Abbreviations for multiplicities are: C1 primary, C2 secondary, C3 tertiary, C4 quaternary carbon. ^{13}C-NMR data are reported in ppm from TMS using the central peak of the solvent as reference (CD_2Cl_2: δ = 53.84 ppm, $CDCl_3$: δ = 77.16 ppm, DMSO-d6: δ = 39.52 ppm).

pH- Meter

pH measurements were performed with a WTW pH meter 330i. Measurements for small-volumes were performed with a Mettler Toledo InLab Micro pH electrode with an S7 screw head equipped with a F2 FiveGoTM pH Meter.

Photorheology

Photorheological measurements were performed on an Anton Paar Modular Compact Rheometer MCR 302 WESP with a plate-to-plate measuring system with a 25 mm steel stamp, a glass plate, and a gap size of 50 µm in oscillation mode with 10 Hz and an amplitude of 10% strain at 25 °C.[398] Samples were irradiated with filtered light (320 – 500 nm, EXFO Omnicure S2000) bottom-up through the glass plate with a light intensity of 3.2 W cm^{-2} at the tip of the light guide as measured with an EXFO Omnicure R2000 radiometer. This referred to a light intensity of 40 mW cm^{-2} directly above the glass plate. Storage modulus *G'* and loss modulus *G''* were measured every second; light was automatically activated after 60 seconds and the measurement was continued until a constant *G'* was attained.

Die approbierte gedruckte Originalversion dieser Dissertation ist an der TU Wien Bibliothek verfügbar.
The approved original version of this doctoral thesis is available in print at TU Wien Bibliothek.
TU Bibliothek Your knowledge hub WIEN

Symbols

Symbols for figures were created using »biorender.com«

Thin Layer Chromatography Analysis

Thin layer chromatography (TLC) was performed on silica gel 60 F_{254} aluminum sheets from Merck.

Two-Photon Polymerization

A tunable femtosecond oscillator with a repetition rate of 80 MHz (MaiTai eHP DeepSee, Spectra-Physics) was operated at 720-900 nm, with a pulse duration of ~ 70 fs at 800 nm after the microscope objective (Olympus 10x/0.4). A motorized microscope stage and two-axis galvanometric scanners were used to ensure high-resolution 3D printing. Formulations were pipetted on sterile glass bottom methacrylate-modified substrates (diameter: 35 mm) purchased from ibidi. The processing window was established by producing arrays of 100 x 100 x 100 µm cubes based on STL files. Linespacing was set to 0.5 µm and layer height was 1 µm for all geometries, while varying scanning speed (50 – 1000 mm s^{-1}) and average power (50 - 200 mW). Structuring was performed using voxel slice mode and infill alternating x-y. The laser was each time calibrated according to the used 2PI (720 nm for DAS, 800 nm for CR, ASCR, and P2CK).

UV-VIS Absorption Spectra

UV-Vis absorption spectra were recorded in quartz cuvettes using a Thermo Scientific NanoDrop One/OneC Microvolume UV-Vis Spectrophotometer (MolChemBio/Mikula Lab, IAS, TU Wien).

Z-Scan

2PA-cross sections of CR at various wavelength were determined by Franziska Gantner at the department of material science and technology (E308, TU Wien).

Die approbierte gedruckte Originalversion dieser Dissertation ist an der TU Wien Bibliothek verfügbar.
The approved original version of this doctoral thesis is available in print at TU Wien Bibliothek.

Abbreviations

AMT	Additive manufacturing technology
AS	Azosulfonates
ASC-GFP	Adipose-derived stem cells marked with green-fluorescent protein
CAD	Computer-aided design
CIDNP	Chemically Induced Dynamic Nuclear Polarization
$Đ_M$	Polydispersity
DMBA	4-(Dimethylamino)benzaldehyde
DMEM	Dulbecco's Modified Eagle's Medium
DTT	DL-Dithiothreitol
DVA	Divinyl adipate
ECM	Extracellular matrix
ESR	Electron spin resonance
ETA	Ethoxylated trimethylolpropane triacrylate
fs	Femtosecond
G'	Storage modulus [Pa]
GelMA	Methacrylate-modified gelatin (also referred as: GelMOD)
GM	Göppert-Mayer [10^{-50}·cm^4·s·$photon^{-1}$·$molecule^{-1}$]
HA	Hyaluronic acid
HAVE	Hyaluronic acid modified with vinyl ester functionalities
HUVEC	Human umbilical vein endothelial cells
LFP	Laser Flash Photolysis
LSM	Laser scanning microscopy
L929	Mouse fibroblasts
MCK	4-Methylcyclohexanone
M_n	Number average of the molecular weight
NA	Numerical aperture
NIR	Near-infrared
OE	Oxime ester
OE-2PIs	Two-photon initiators based on oxime ester moieties
PBS	Phosphate buffered saline
PEGDA	Poly(ethylene glycol) diacrylate
PDT	Photodynamic therapy
P_{th}	Polymerization threshold
PI	Photoinitiator
Q	Swelling ratio
ROS	Reactive oxygen species
STL	Stereolithography
TA	Terephthalaldehyde
TICT	Twisted Internal Charge-Transfer
2PA	Two-photon absorption
TTA	Trimethylolpropane triacrylate
Voxel	Volumetric pixel
VE	Vinyl ester
δ	Chemical shift [ppm]
ε	Molar extinction coefficient at λ_{max} [L·mol^{-1}·cm^{-1}]

Die approbierte gedruckte Originalversion dieser Dissertation ist an der TU Wien Bibliothek verfügbar.
The approved original version of this doctoral thesis is available in print at TU Wien Bibliothek.
TU Bibliothek Your knowledge hub WIEN

$h\upsilon$	Planck constant · frequency (photon energy)
λ_{max}	Absorption maximum
σ_{2PA}	Two-photon absorption cross-section
1PA	One-photon absorption
2D	Two-dimensional
2PA	Two-photon absorption
2PI	Two-photon initiator
2PP	Two-photon polymerization
3D	Three-dimensional

Initiators

ASCR	Azosulfonate-modified Congo Red
BABO	Benzaldehyde O-benzoyl oxime
BB	4,4'-(m-Phenylenebisazo)bis-m-phenylenediamine dihydrochloride (CAS: 10114-58-0)
CR	Congo Red (CAS: 573-58-0)
DADS	4,4’-Diamino-2,2’-stilbenedisulfonic acid (CAS: 81-11-8)
DAS	Diaminostilbene- azosulfonate (also referred as: AS7)
M2CMK	2,6-Bis[p-(dimethylamino)phenyl]methylene-4-methylcyclohexanone
P2CK	3-(((2-Carboxyethyl)-N-methylaminophenylmethylene)-2-oxocyclopentylidenemethylphenyl-N-methylamino)propionic acid
Li-TPO	Lithium phenyl (2,4,6-trimethylbenzoyl)phosphinate
5M	4,4'(1,4-Phenylenebis(methaneylylidene))bis(5-methyl-2-oxocyclohexane-3,1-diylidene))bis (methaneylylidene))dibenzaldehyde
5MBC	Benzoylchloride modified oxime ester 2PI based on 5M
5MPAC	Pivalicacid chloride modified oxime ester 2PI
5MSA	succinic anhydride modified oxime ester 2PI
5MSBA	2-sulfobenzoic anhydride modified oxime ester 2PI

Die approbierte gedruckte Originalversion dieser Dissertation ist an der TU Wien Bibliothek verfügbar.
The approved original version of this doctoral thesis is available in print at TU Wien Bibliothek.
TU Bibliothek Your knowledge hub WIEN

References

(1) Langer, R. and Vacanti, J. P., *Tissue engineering.* Science (New York, NY), 1993. **260**(5110): p. 920-926.

(2) Place, E. S., Evans, N. D. and Stevens, M. M., *Complexity in biomaterials for tissue engineering.* Nature Materials, 2009. **8**(6): p. 457-470.

(3) Rosales, A. M. and Anseth, K. S., *The design of reversible hydrogels to capture extracellular matrix dynamics.* Nature Reviews Materials, 2016. **1**: p. 15012.

(4) Nelson, C. M. and Bissell, M. J., *Of extracellular matrix, scaffolds, and signaling: tissue architecture regulates development, homeostasis, and cancer.* Annu. Rev. Cell Dev. Biol., 2006. **22**: p. 287-309.

(5) Ratner, B. D., Hoffman, A. S., Schoen, F. J. and Lemons, J. E., *Biomaterials science: an introduction to materials in medicine*. 2004: Elsevier.

(6) Buwalda, S. J., Boere, K. W., Dijkstra, P. J., Feijen, J., Vermonden, T. and Hennink, W. E., *Hydrogels in a historical perspective: From simple networks to smart materials.* Journal of controlled release, 2014. **190**: p. 254-273.

(7) Caliari, S. R. and Burdick, J. A., *A practical guide to hydrogels for cell culture.* Nature methods, 2016. **13**(5): p. 405.

(8) Hench, L. L. and Wilson, J., *Surface-active biomaterials.* Science, 1984. **226**(4675): p. 630-636.

(9) Burdick, J. A. and Murphy, W. L., *Moving from static to dynamic complexity in hydrogel design.* Nature communications, 2012. **3**(1): p. 1-8.

(10) Bhat, S. and Kumar, A., *Biomaterials and bioengineering tomorrow's healthcare.* Biomatter, 2013. **3**(3): p. e24717.

(11) Huang, G., Li, F., Zhao, X., Ma, Y., Li, Y., Lin, M., Jin, G., Lu, T. J., Genin, G. M. and Xu, F., *Functional and biomimetic materials for engineering of the three-dimensional cell microenvironment.* Chemical reviews, 2017. **117**(20): p. 12764-12850.

(12) Zhu, J. and Marchant, R. E., *Design properties of hydrogel tissue-engineering scaffolds.* Expert review of medical devices, 2011. **8**(5): p. 607-626.

(13) Ratner, B. D., *Biomaterials science: an interdisciplinary endeavor*, in *Biomaterials science*. 1996, Elsevier. p. 1-8.

(14) He, W. and Benson, R., *Polymeric biomaterials*, in *Applied Plastics Engineering Handbook*. 2017, Elsevier. p. 145-164.

(15) Deible, C. R., Petrosko, P., Johnson, P. C., Beckman, E. J., Russell, A. J. and Wagner, W. R., *Molecular barriers to biomaterial thrombosis by modification of surface proteins with polyethylene glycol.* Biomaterials, 1998. **19**(20): p. 1885-1893.

(16) Yang, F., Williams, C. G., Wang, D.-a., Lee, H., Manson, P. N. and Elisseeff, J., *The effect of incorporating RGD adhesive peptide in polyethylene glycol diacrylate*

Die approbierte gedruckte Originalversion dieser Dissertation ist an der TU Wien Bibliothek verfügbar.
The approved original version of this doctoral thesis is available in print at TU Wien Bibliothek.
TU Bibliothek Your knowledge hub WIEN

hydrogel on osteogenesis of bone marrow stromal cells. Biomaterials, 2005. **26**(30): p. 5991-5998.

(17) Frazer, R. Q., Byron, R. T., Osborne, P. B. and West, K. P., *PMMA: an essential material in medicine and dentistry.* Journal of long-term effects of medical implants, 2005. **15**(6).

(18) Ossipov, D. A., Brännvall, K., Forsberg-Nilsson, K. and Hilborn, J., *Formation of the first injectable poly (vinyl alcohol) hydrogel by mixing of functional PVA precursors.* Journal of applied polymer science, 2007. **106**(1): p. 60-70.

(19) Wichterle, O. and LÍM, D., *Hydrophilic Gels for Biological Use.* Nature, 1960. **185**(4706): p. 117-118.

(20) Zhang, Z., Liu, R., Zepeda, H., Zeng, L., Qiu, J. and Wang, S., *3D Printing Super Strong Hydrogel for Artificial Meniscus.* ACS Applied Polymer Materials, 2019. **1**(8): p. 2023-2032.

(21) Tekin, H., Sanchez, J. G., Tsinman, T., Langer, R. and Khademhosseini, A., *Thermoresponsive Platforms for Tissue Engineering and Regenerative Medicine.* AIChE journal. American Institute of Chemical Engineers, 2011. **57**(12): p. 3249-3258.

(22) De La Rosa, V., Van Den Bulcke, A. and Hoogenboom, R., *Poly (2-oxazoline) s: the Versatile Polymer Platform for Biomedicine.* Material Matters, Aldrich, 2016. **11**(3): p. 75-78.

(23) Podevyn, A., Arys, K., de la Rosa, V. R., Glassner, M. and Hoogenboom, R., *End-group functionalization of poly(2-oxazoline)s using methyl bromoacetate as initiator followed by direct amidation.* European Polymer Journal, 2019. **120**: p. 109273.

(24) Hoogenboom, R., *Chapter 2 - Temperature-Responsive Polymers: Properties, Synthesis, and Applications*, in *Smart Polymers and their Applications (Second Edition)*, Aguilar, M.R. and San Román, J., Editors. 2019, Woodhead Publishing. p. 13-44.

(25) Bucher, P. J., Büchi, E. R. and Daicker, B. C., *Dystrophic calcification of an implanted hydroxyethylmethacrylate intraocular lens.* Archives of Ophthalmology, 1995. **113**(11): p. 1431-1435.

(26) Lopes, M. S., Jardini, A. and Maciel Filho, R., *Poly (lactic acid) production for tissue engineering applications.* Procedia Engineering, 2012. **42**: p. 1402-1413.

(27) Van Hoorick, J., Delaey, J., Vercammen, H., Van Erps, J., Thienpont, H., Dubruel, P., Zakaria, N., Koppen, C., Van Vlierberghe, S. and Van den Bogerd, B., *Designer Descemet Membranes Containing PDLLA and Functionalized Gelatins as Corneal Endothelial Scaffold.* Advanced Healthcare Materials, 2020. **9**(16): p. 2000760.

(28) Day, R. M., Boccaccini, A. R., Shurey, S., Roether, J. A., Forbes, A., Hench, L. L. and Gabe, S. M., *Assessment of polyglycolic acid mesh and bioactive glass for soft-tissue engineering scaffolds.* Biomaterials, 2004. **25**(27): p. 5857-5866.

Die approbierte gedruckte Originalversion dieser Dissertation ist an der TU Wien Bibliothek verfügbar.
The approved original version of this doctoral thesis is available in print at TU Wien Bibliothek.
TU Bibliothek Your knowledge hub WIEN

(29) Benatti, A. C. B., Pattaro, A. F., Rodrigues, A. A., Xavier, M. V., Kaasi, A., Barbosa, M. I. R., Jardini, A. L., Maciel Filho, R. and Kharmandayan, P., *Bioreabsorbable polymers for tissue engineering: PLA, PGA, and their copolymers*, in *Materials for Biomedical Engineering*. 2019, Elsevier. p. 83-116.

(30) Siddiqui, N., Asawa, S., Birru, B., Baadhe, R. and Rao, S., *PCL-based composite scaffold matrices for tissue engineering applications.* Molecular biotechnology, 2018. **60**(7): p. 506-532.

(31) Arslan, A., Steiger, W., Roose, P., Van den Bergen, H., Gruber, P., Zerobin, E., Gantner, F., Guillaume, O., Ovsianikov, A., Van Vlierberghe, S. and Dubruel, P., *Polymer architecture as key to unprecedented high-resolution 3D-printing performance: The case of biodegradable hexa-functional telechelic urethane-based poly-ε-caprolactone.* Materials Today, 2020.

(32) Jeong, S. I., Kim, B.-S., Kang, S. W., Kwon, J. H., Lee, Y. M., Kim, S. H. and Kim, Y. H., *In vivo biocompatibilty and degradation behavior of elastic poly (l-lactide-co-ε-caprolactone) scaffolds.* Biomaterials, 2004. **25**(28): p. 5939-5946.

(33) Pitt, C. G., Hendren, R. W., Schindler, A. and Woodward, S. C., *The enzymatic surface erosion of aliphatic polyesters.* Journal of Controlled Release, 1984. **1**(1): p. 3-14.

(34) Guhathakurta, S. and Galla, S., *Progress in cardiovascular biomaterials.* Asian Cardiovascular and Thoracic Annals, 2019. **27**(9): p. 744-750.

(35) Ehrmann, K., Potzmann, P., Dworak, C., Bergmeister, H., Eilenberg, M., Grasl, C., Koch, T., Schima, H., Liska, R. and Baudis, S., *Hard Block Degradable Polycarbonate Urethanes: Promising Biomaterials for Electrospun Vascular Prostheses.* Biomacromolecules, 2019.

(36) DeForest, C. A. and Anseth, K. S., *Advances in bioactive hydrogels to probe and direct cell fate.* Annual review of chemical and biomolecular engineering, 2012. **3**: p. 421-444.

(37) Rice, J. J., Martino, M. M., De Laporte, L., Tortelli, F., Briquez, P. S. and Hubbell, J. A., *Engineering the regenerative microenvironment with biomaterials.* Advanced healthcare materials, 2013. **2**(1): p. 57-71.

(38) Hench, L. L. and Polak, J. M., *Third-generation biomedical materials.* Science, 2002. **295**(5557): p. 1014-1017.

(39) Van Vlierberghe, S., Dubruel, P. and Schacht, E., *Biopolymer-based hydrogels as scaffolds for tissue engineering applications: a review.* Biomacromolecules, 2011. **12**(5): p. 1387-1408.

(40) Hashimoto, T., Suzuki, Y., Kitada, M., Kataoka, K., Wu, S., Suzuki, K., Endo, K., Nishimura, Y. and Ide, C., *Peripheral nerve regeneration through alginate gel: Analysis of early outgrowth and late increase in diameter of regenerating axons.* Experimental Brain Research, 2002. **146**(3): p. 356-368.

(41) Balgude, A. P., Yu, X., Szymanski, A. and Bellamkonda, R. V., *Agarose gel stiffness determines rate of DRG neurite extension in 3D cultures.* Biomaterials, 2001. **22**(10): p. 1077-1084.

Die approbierte gedruckte Originalversion dieser Dissertation ist an der TU Wien Bibliothek verfügbar.
The approved original version of this doctoral thesis is available in print at TU Wien Bibliothek.
TU Bibliothek Your knowledge hub WIEN

(42) Haipeng, G., Yinghui, Z., Jianchun, L., Yandao, G., Nanming, Z. and Xiufang, Z., *Studies on nerve cell affinity of chitosan-derived materials.* Journal of Biomedical Materials Research, 2000. **52**(2): p. 285-295.

(43) Highley, C. B., Prestwich, G. D. and Burdick, J. A., *Recent advances in hyaluronic acid hydrogels for biomedical applications.* Current Opinion in Biotechnology, 2016. **40**: p. 35-40.

(44) Herbert, C. B., Nagaswami, C., Bittner, G. D., Hubbell, J. A. and Weisel, J. W., *Effects of fibrin micromorphology on neurite growth from dorsal root ganglia cultured in three-dimensional fibrin gels.* Journal of Biomedical Materials Research, 1998. **40**(4): p. 551-559.

(45) Knezevic, L., Schaupper, M., Mühleder, S., Schimek, K., Hasenberg, T., Marx, U., Priglinger, E., Redl, H. and Holnthoner, W., *Engineering blood and lymphatic microvascular networks in fibrin matrices.* Frontiers in bioengineering and biotechnology, 2017. **5**: p. 25.

(46) Satou, T., Nishida, S., Hiruma, S., Tanji, K., Takahashi, M., Fujita, S., Mizuhara, Y., Akai, F. and Hashimoto, S., *A MORPHOLOGICAL STUDY ON THE EFFECTS OF COLLAGEN GEL MATRIX ON REGENERATION OF SEVERED RAT SCIATIC NERVE IN SILICONE TUBES.* Pathology International, 1986. **36**(2): p. 199-208.

(47) Wells, M. R., Kraus, K., Batter, D. K., Blunt, D. G., Weremowitz, J., Lynch, S. E., Antoniades, H. N. and Hansson, H. A., *Gel Matrix Vehicles for Growth Factor Application in Nerve Gap Injuries Repaired with Tubes: A Comparison of Biomatrix, Collagen, and Methylcellulose.* Experimental Neurology, 1997. **146**(2): p. 395-402.

(48) Tytgat, L., Dobos, A., Markovic, M., Van Damme, L., Van Hoorick, J., Bray, F., Thienpont, H., Ottevaere, H., Dubruel, P., Ovsianikov, A. and Van Vlierberghe, S., *High-resolution 3D bioprinting of photo-crosslinkable recombinant collagen to serve tissue engineering applications.* Biomacromolecules, 2020.

(49) Sierpinski, P., Garrett, J., Ma, J., Apel, P., Klorig, D., Smith, T., Koman, L. A., Atala, A. and Van Dyke, M., *The use of keratin biomaterials derived from human hair for the promotion of rapid regeneration of peripheral nerves.* Biomaterials, 2008. **29**(1): p. 118-128.

(50) Tamura, M., Yanagawa, F., Sugiura, S., Takagi, T., Sumaru, K. and Kanamori, T., *Click-crosslinkable and photodegradable gelatin hydrogels for cytocompatible optical cell manipulation in natural environment.* Scientific reports, 2015. **5**: p. 15060.

(51) Van Vlierberghe, S., Samal, S. K. and Dubruel, P., *Development of Mechanically Tailored Gelatin-Chondroitin Sulphate Hydrogel Films.* Macromolecular Symposia, 2011. **309-310**(1): p. 173-181.

(52) De Moor, L., Fernandez, S., Vercruysse, C., Tytgat, L., Asadian, M., De Geyter, N., Van Vlierberghe, S., Dubruel, P. and Declercq, H., *Hybrid Bioprinting of Chondrogenically Induced Human Mesenchymal Stem Cell Spheroids.* Frontiers in Bioengineering and Biotechnology, 2020. **8**(484).

Die approbierte gedruckte Originalversion dieser Dissertation ist an der TU Wien Bibliothek verfügbar.
The approved original version of this doctoral thesis is available in print at TU Wien Bibliothek.
TU Bibliothek Your knowledge hub WIEN

(53) Van Hoorick, J., Delaey, J., Vercammen, H., Van Erps, J., Thienpont, H., Dubruel, P., Zakaria, N., Koppen, C., Van Vlierberghe, S. and Van den Bogerd, B., *Designer Descemet Membranes Containing PDLLA and Functionalized Gelatins as Corneal Endothelial Scaffold.* Advanced Healthcare Materials, 2020. **n/a**(n/a): p. 2000760.

(54) Adib, A. A., Sheikhi, A., Shahhosseini, M., Simeunović, A., Wu, S., Castro, C. E., Zhao, R., Khademhosseini, A. and Hoelzle, D. J., *Direct-write 3D printing and characterization of a GelMA-based biomaterial for intracorporeal tissue engineering.* Biofabrication, 2020. **12**(4): p. 045006.

(55) Allison, D. D. and Grande-Allen, K. J., *Hyaluronan: a powerful tissue engineering tool.* Tissue engineering, 2006. **12**(8): p. 2131-2140.

(56) https://klinik-am-ring.de/en/orthopedics/injuries-conditions/knee-joint/anatomy-knee-joint/. Dowloaded 30.04.2020.

(57) MacNeil, S., *Progress and opportunities for tissue-engineered skin.* Nature, 2007. **445**(7130): p. 874-880.

(58) https://www.iris-pharma.com/eye-structures. Downloaded 30.04.2020.

(59) Wolf, K. J. and Kumar, S., *Hyaluronic Acid: Incorporating the Bio into the Material.* ACS Biomaterials Science & Engineering, 2019. **5**(8): p. 3753-3765.

(60) Shazeeb, M. S., Corazzini, R., Konowicz, P. A., Fogle, R., Bangari, D. S., Johnson, J., Ying, X. and Dhal, P. K., *Assessment of in vivo degradation profiles of hyaluronic acid hydrogels using temporal evolution of chemical exchange saturation transfer (CEST) MRI.* Biomaterials, 2018. **178**: p. 326-338.

(61) Bukhari, S. N. A., Roswandi, N. L., Waqas, M., Habib, H., Hussain, F., Khan, S., Sohail, M., Ramli, N. A., Thu, H. E. and Hussain, Z., *Hyaluronic acid, a promising skin rejuvenating biomedicine: A review of recent updates and pre-clinical and clinical investigations on cosmetic and nutricosmetic effects.* International Journal of Biological Macromolecules, 2018. **120**: p. 1682-1695.

(62) Green, J. J. and Elisseeff, J. H., *Mimicking biological functionality with polymers for biomedical applications.* Nature, 2016. **540**(7633): p. 386-394.

(63) Terzaki, K. and Farsari, M., *Polymer Processing Through Multiphoton Absorption*, in *Polymer and Photonic Materials Towards Biomedical Breakthroughs*, Van Hoorick, J., Ottevaere, H., Thienpont, H., Dubruel, P. and Van Vlierberghe, S., Editors. 2018, Springer International Publishing: Cham. p. 49-69.

(64) Žigon-Branc, S., Markovic, M., Van Hoorick, J., Van Vlierberghe, S., Dubruel, P., Zerobin, E., Baudis, S. and Ovsianikov, A., *Impact of hydrogel stiffness on differentiation of human adipose-derived stem cell microspheroids.* Tissue Engineering Part A, 2019. **25**(19-20): p. 1369-1380.

(65) Stuart, M. A. C., Huck, W. T., Genzer, J., Müller, M., Ober, C., Stamm, M., Sukhorukov, G. B., Szleifer, I., Tsukruk, V. V. and Urban, M., *Emerging applications of stimuli-responsive polymer materials.* Nature materials, 2010. **9**(2): p. 101-113.

(66) Aguilar, M. R. and San Román, J., *Smart polymers and their applications*. 2019: Woodhead Publishing.

Die approbierte gedruckte Originalversion dieser Dissertation ist an der TU Wien Bibliothek verfügbar.
The approved original version of this doctoral thesis is available in print at TU Wien Bibliothek.
TU Bibliothek Your knowledge hub WIEN

(67) Tambiev, A. K. and Skalny, A., *Electromagnetic radiation and life: bioelementological point of view.* Biophysics, 2012: p. 193-220.

(68) Moad, G. and Solomon, D. H., *The chemistry of radical polymerization*. 2006: Elsevier.

(69) Crivello, J. V., Dietliker, K. and Bradley, G., *Photoinitiators for Free Radical Cationic & Anionic Photopolymerisation*. 1999: Wiley.

(70) Klán, P. and Wirz, J., *Photochemistry of organic compounds: from concepts to practice*. 2009: John Wiley & Sons.

(71) Ullrich, G., Burtscher, P., Salz, U., Moszner, N. and Liska, R., *Phenylglycine derivatives as coinitiators for the radical photopolymerization of acidic aqueous formulations.* Journal of Polymer Science Part A: Polymer Chemistry, 2006. **44**(1): p. 115-125.

(72) Fouassier, J.-P., Morlet-Savary, F., Lalevée, J., Allonas, X. and Ley, C., *Dyes as photoinitiators or photosensitizers of polymerization reactions.* Materials, 2010. **3**(12): p. 5130-5142.

(73) Zahoranova, A., Vojtova, L., Dusicka, E., Michlovska, L., Krivankova, N. and Baudis, S., *Hybrid Hydrogel Networks by Photocrosslinking of Thermoresponsive α,ω-Itaconyl-PLGA-PEG-PLGA Micelles in Water: Influence of the Lithium Phenyl-2,4,6-Trimethylbenzoylphosphinate Photoinitinator.* Macromolecular Chemistry and Physics, 2020. **221**(17): p. 2000165.

(74) Fouassier, J.-P., *Photoinitiation, photopolymerization, and photocuring: fundamentals and applications*. 1995: Hanser.

(75) Husar, B. and Liska, R., *Vinyl carbonates, vinyl carbamates, and related monomers: Synthesis, polymerization, and application.* Chemical Society Reviews, 2012. **41**(6): p. 2395-2405.

(76) Orman, S., Hofstetter, C., Aksu, A., Reinauer, F., Liska, R. and Baudis, S., *Toughness enhancers for bone scaffold materials based on biocompatible photopolymers.* Journal of Polymer Science Part A: Polymer Chemistry, 2019. **57**(2): p. 110-119.

(77) Bowman, C. N. and Peppas, N. A., *Coupling of kinetics and volume relaxation during polymerizations of multiacrylates and multimethacrylates.* Macromolecules, 1991. **24**(8): p. 1914-1920.

(78) Gou, L., Opheim, B., Coretsopoulos, C. N. and Scranton, A. B., *Consumption of the molecular oxygen in polymerization systems using photosensitized oxidation of dimethylanthracene.* Chemical Engineering Communications, 2006. **193**(5): p. 620-627.

(79) Hoyle, C. E. and Bowman, C. N., *Thiol–ene click chemistry.* Angewandte Chemie International Edition, 2010. **49**(9): p. 1540-1573.

(80) Kolb, H., Finn, M. and Sharpless, K., *Click chemistry in glycoscience: new developments and strategies.* Angew Chem Int Ed, 2001. **40**(11): p. 2004-2021.

(81) Mautner, A., Qin, X., Wutzel, H., Ligon, S. C., Kapeller, B., Moser, D., Russmueller, G., Stampfl, J. and Liska, R., *Thiol-ene photopolymerization for efficient curing of*

Die approbierte gedruckte Originalversion dieser Dissertation ist an der TU Wien Bibliothek verfügbar.
The approved original version of this doctoral thesis is available in print at TU Wien Bibliothek.
TU Bibliothek Your knowledge hub WIEN

vinyl esters. Journal of Polymer Science Part A: Polymer Chemistry, 2013. **51**(1): p. 203-212.

(82) Fouassier, J.-P. and Rabek, J. F., *Radiation curing in polymer science and technology: Fundamentals and methods*. Vol. 1. 1993: Springer Science & Business Media.

(83) Lu, H., Carioscia, J. A., Stansbury, J. W. and Bowman, C. N., *Investigations of step-growth thiol-ene polymerizations for novel dental restoratives.* Dental Materials, 2005. **21**(12): p. 1129-1136.

(84) Cramer, N. B. and Bowman, C. N., *Kinetics of thiol–ene and thiol–acrylate photopolymerizations with real-time fourier transform infrared.* Journal of Polymer Science Part A: Polymer Chemistry, 2001. **39**(19): p. 3311-3319.

(85) Heller, C., Schwentenwein, M., Russmueller, G., Varga, F., Stampfl, J. and Liska, R., *Vinyl esters: low cytotoxicity monomers for the fabrication of biocompatible 3D scaffolds by lithography based additive manufacturing.* Journal of Polymer Science Part A: Polymer Chemistry, 2009. **47**(24): p. 6941-6954.

(86) Truby, R. L. and Lewis, J. A., *Printing soft matter in three dimensions.* Nature, 2016. **540**: p. 371.

(87) Ngo, T. D., Kashani, A., Imbalzano, G., Nguyen, K. T. and Hui, D., *Additive manufacturing (3D printing): A review of materials, methods, applications and challenges.* Composites Part B: Engineering, 2018. **143**: p. 172-196.

(88) Lee, J., Cuddihy, M. J. and Kotov, N. A., *Three-dimensional cell culture matrices: state of the art.* Tissue Engineering Part B: Reviews, 2008. **14**(1): p. 61-86.

(89) Melchels, F. P. W., Grijpma, D. W. and Kellomäki, M., *A review of rapid prototyping techniques for tissue engineering purposes AU - Peltola, Sanna M.* Annals of Medicine, 2008. **40**(4): p. 268-280.

(90) Ovsianikov, A., Mironov, V., Stampfl, J. and Liska, R., *Engineering 3D cell-culture matrices: multiphoton processing technologies for biological and tissue engineering applications.* Expert Review of Medical Devices, 2012. **9**(6): p. 613-633.

(91) Billiet, T., Vandenhaute, M., Schelfhout, J., Van Vlierberghe, S. and Dubruel, P., *A review of trends and limitations in hydrogel-rapid prototyping for tissue engineering.* Biomaterials, 2012. **33**(26): p. 6020-6041.

(92) Malda, J., Visser, J., Melchels, F. P., Jüngst, T., Hennink, W. E., Dhert, W. J., Groll, J. and Hutmacher, D. W., *25th anniversary article: engineering hydrogels for biofabrication.* Advanced materials, 2013. **25**(36): p. 5011-5028.

(93) Ovsianikov, A., Khademhosseini, A. and Mironov, V., *The Synergy of Scaffold-Based and Scaffold-Free Tissue Engineering Strategies.* Trends in Biotechnology, 2018. **36**(4): p. 348-357.

(94) Chen, S., Duan, B., Takeuchi, S., Hollister, S., Heilshorn, S., Melchels, F. P., Cho, D.-W., Jeon, N. L., Swieszkowski, W. and Pati, F., *Biofabrication and 3D Tissue Modeling*. 2019: Royal Society of Chemistry.

Die approbierte gedruckte Originalversion dieser Dissertation ist an der TU Wien Bibliothek verfügbar.
The approved original version of this doctoral thesis is available in print at TU Wien Bibliothek.
TU Bibliothek Your knowledge hub WIEN

(95) Fetah, K., Tebon, P., Goudie, M. J., Eichenbaum, J., Ren, L., Barros, N., Nasiri, R., Ahadian, S., Ashammakhi, N., Dokmeci, M. R. and Khademhosseini, A., *The emergence of 3D bioprinting in organ-on-chip systems.* Progress in Biomedical Engineering, 2019. **1**(1): p. 012001.

(96) Swieszkowski, W., Dokmeci, M. R. and Khademhosseini, A., *Microfluidics in biofabrication.* Biofabrication, 2020. **12**(3): p. 030201.

(97) Dobos, A., Gantner, F., Markovic, M., Van Hoorick, J., Tytgat, L., Van Vlierberghe, S. and Ovsianikov, A., *On-chip high-definition bioprinting of microvascular structures.* Biofabrication, 2020. **13**(1): p. 015016.

(98) Kim, S. H., Yeon, Y. K., Lee, J. M., Chao, J. R., Lee, Y. J., Seo, Y. B., Sultan, M. T., Lee, O. J., Lee, J. S. and Yoon, S.-i., *Precisely printable and biocompatible silk fibroin bioink for digital light processing 3D printing.* Nature communications, 2018. **9**(1): p. 1-14.

(99) Emons, M., Obata, K., Binhammer, T., Ovsianikov, A., Chichkov, B. N. and Morgner, U., *Two-photon polymerization technique with sub-50 nm resolution by sub-10 fs laser pulses.* Optical Materials Express, 2012. **2**(7): p. 942-947.

(100) N., L. C., T., F. J., Tommaso, B. and A., F. R., *Multiphoton Fabrication.* Angewandte Chemie International Edition, 2007. **46**(33): p. 6238-6258.

(101) Steyrer, B., Neubauer, P., Liska, R. and Stampfl, J., *Visible light photoinitiator for 3D-printing of tough methacrylate resins.* Materials, 2017. **10**(12): p. 1445.

(102) Vyatskikh, A., Delalande, S., Kudo, A., Zhang, X., Portela, C. M. and Greer, J. R., *Additive manufacturing of 3D nano-architected metals.* Nature Communications, 2018. **9**(1): p. 593.

(103) Stampfl, J., Liska, R. and Ovsianikov, A., *Multiphoton Lithography: Techniques, Materials, and Applications*. 2016: Wiley.

(104) DeVoe, R. J., Kalweit, H. W., Leatherdale, C. A. and Williams, T. R. *Voxel shapes in two-photon microfabrication*. in *Multiphoton Absorption and Nonlinear Transmission Processes: Materials, Theory, and Applications*. 2003: International Society for Optics and Photonics.

(105) Hong, G., Antaris, A. L. and Dai, H., *Near-infrared fluorophores for biomedical imaging.* Nature Biomedical Engineering, 2017. **1**(1): p. 1-22.

(106) Cumpston, B. H., Ananthavel, S. P., Barlow, S., Dyer, D. L., Ehrlich, J. E., Erskine, L. L., Heikal, A. A., Kuebler, S. M., Lee, I.-Y. S. and McCord-Maughon, D., *Two-photon polymerization initiators for three-dimensional optical data storage and microfabrication.* Nature, 1999. **398**(6722): p. 51-54.

(107) Sun, H.-B., Matsuo, S. and Misawa, H., *Three-dimensional photonic crystal structures achieved with two-photon-absorption photopolymerization of resin.* Applied physics letters, 1999. **74**(6): p. 786-788.

(108) Lee, C.-W., Pagliara, S., Keyser, U. and Baumberg, J. J., *Perpendicular coupling to in-plane photonics using arc waveguides fabricated via two-photon polymerization.* Applied Physics Letters, 2012. **100**(17): p. 171102.

Die approbierte gedruckte Originalversion dieser Dissertation ist an der TU Wien Bibliothek verfügbar.
The approved original version of this doctoral thesis is available in print at TU Wien Bibliothek.
TU Bibliothek Your knowledge hub WIEN

(109) Doraiswamy, A., Jin, C., Narayan, R., Mageswaran, P., Mente, P., Modi, R., Auyeung, R., Chrisey, D., Ovsianikov, A. and Chichkov, B., *Two photon induced polymerization of organic–inorganic hybrid biomaterials for microstructured medical devices.* Acta Biomaterialia, 2006. **2**(3): p. 267-275.

(110) Sugioka, K., Xu, J., Wu, D., Hanada, Y., Wang, Z., Cheng, Y. and Midorikawa, K., *Femtosecond laser 3D micromachining: a powerful tool for the fabrication of microfluidic, optofluidic, and electrofluidic devices based on glass.* Lab on a Chip, 2014. **14**(18): p. 3447-3458.

(111) Weisgrab, G., Ovsianikov, A. and Costa, P. F., *Functional 3D Printing for Microfluidic Chips.* Advanced Materials Technologies, 2019. **4**(10): p. 1900275.

(112) Mandt, D., Gruber, P., Markovic, M., Tromayer, M., Rothbauer, M., Krayz, S. R. A., Ali, F., van Hoorick, J., Holnthoner, W. and Mühleder, S., *Fabrication of placental barrier structures within a microfluidic device utilizing two-photon polymerization.* International Journal of Bioprinting, 2018. **4**(2).

(113) Dobos, A., Van Hoorick, J., Steiger, W., Gruber, P., Markovic, M., Andriotis, O. G., Rohatschek, A., Dubruel, P., Thurner, P. J., Van Vlierberghe, S., Baudis, S. and Ovsianikov, A., *Thiol–Gelatin–Norbornene Bioink for Laser-Based High-Definition Bioprinting.* Advanced Healthcare Materials, 2019. **n/a**(n/a): p. 1900752.

(114) Ren, T., Steiger, W., Chen, P., Ovsianikov, A. and Demirci, U., *Enhancing cell packing in buckyballs by acoustofluidic activation.* Biofabrication, 2020. **12**(2): p. 025033.

(115) Zerobin, E., Markovic, M., Tomášiková, Z., Qin, X. H., Ret, D., Steinbauer, P., Kitzmüller, J., Steiger, W., Gruber, P. and Ovsianikov, A., *Hyaluronic acid vinyl esters: A toolbox toward controlling mechanical properties of hydrogels for 3D microfabrication.* Journal of Polymer Science, 2020. **1-11**.

(116) Hsieh, T. M., Ng, C. W. B., Narayanan, K., Wan, A. C. and Ying, J. Y., *Three-dimensional microstructured tissue scaffolds fabricated by two-photon laser scanning photolithography.* Biomaterials, 2010. **31**(30): p. 7648-7652.

(117) Zimmermann, R., Hentschel, C., Schrön, F., Moedder, D., Büttner, T., Atallah, P., Wegener, T., Gehring, T., Howitz, S., Freudenberg, U. and Werner, C., *High resolution bioprinting of multi-component hydrogels.* Biofabrication, 2019. **11**(4): p. 045008.

(118) Song, J., Michas, C., Chen, C. S., White, A. E. and Grinstaff, M. W., *From Simple to Architecturally Complex Hydrogel Scaffolds for Cell and Tissue Engineering Applications: Opportunities Presented by Two-Photon Polymerization.* Advanced Healthcare Materials, 2020. **9**(1): p. 1901217.

(119) Geng, Q., Wang, D., Chen, P. and Chen, S.-C., *Ultrafast multi-focus 3-D nano-fabrication based on two-photon polymerization.* Nature Communications, 2019. **10**(1): p. 2179.

(120) Göppert-Mayer, M., *Über Elementarakte mit zwei Quantensprüngen.* Annalen der Physik, 1931. **401**(3): p. 273-294.

Die approbierte gedruckte Originalversion dieser Dissertation ist an der TU Wien Bibliothek verfügbar.
The approved original version of this doctoral thesis is available in print at TU Wien Bibliothek.
TU Bibliothek Your knowledge hub WIEN

(121) Sibbett, W., Lagatsky, A. and Brown, C., *The development and application of femtosecond laser systems.* Optics Express, 2012. **20**(7): p. 6989-7001.

(122) Albota, M., Beljonne, D., Brédas, J.-L., Ehrlich, J. E., Fu, J.-Y., Heikal, A. A., Hess, S. E., Kogej, T., Levin, M. D. and Marder, S. R., *Design of organic molecules with large two-photon absorption cross sections.* Science, 1998. **281**(5383): p. 1653-1656.

(123) Corrigan, N., Yeow, J., Judzewitsch, P., Xu, J. and Boyer, C., *Seeing the light: Advancing materials chemistry through photopolymerization.* Angewandte Chemie International Edition, 2019. **58**(16): p. 5170-5189.

(124) Barner-Kowollik, C., Bastemeyer, M., Blasco, E., Patrick, M., Delaittre, G., Richter, B. and Wegener, M., *3D Laser Micro- and Nano-Printing: Challenges for Chemistry.* Angewandte Chemie International Edition, 2017.

(125) Pawlicki, M., Collins, H. A., Denning, R. G. and Anderson, H. L., *Two-Photon Absorption and the Design of Two-Photon Dyes.* Angewandte Chemie International Edition, 2009. **48**(18): p. 3244-3266.

(126) Gruber, P., *Development of a novel wavelength-tunable high-speed 2-photon lithography setup.* PhD Thesis, Institute of Materials Science and Technology, TU Wien, 2018.

(127) Steiger, W., *Investigation of multi-photon processing parameters and materials.* PhD Thesis, Institute of Materials Science and Technology, TU Wien, 2018.

(128) Matsumoto, S., Kubodera, K. i., Kurihara, T. and Kaino, T., *Nonlinear optical properties of an azo dye attached polymer.* Applied physics letters, 1987. **51**(1): p. 1-2.

(129) Sadovski, O., Beharry, A. A., Zhang, F. and Woolley, G. A., *Spectral tuning of azobenzene photoswitches for biological applications.* Angewandte Chemie International Edition, 2009. **48**(8): p. 1484-1486.

(130) Prasad, P. N., *Introduction to biophotonics*. 2004: John Wiley & Sons.

(131) Lakowicz, J. R., *Principles of fluorescence spectroscopy*. 2013: Springer Science & Business Media.

(132) Whitby, R., Ben-Tal, Y., MacMillan, R., Janssens, S., Raymond, S., Clarke, D., Jin, J., Kay, A. and Simpson, M. C., *Photoinitiators for two-photon polymerisation: effect of branching and viscosity on polymerisation thresholds.* RSC Advances, 2017. **7**(22): p. 13232-13239.

(133) Katan, C., Terenziani, F., Le Droumaguet, C., Mongin, O., Werts, M. H. V., Tretiak, S. and Blanchard-Desce, M. *Branching of dipolar chromophores: effects on linear and nonlinear optical properties*. in *Linear and Nonlinear Optics of Organic Materials V*. 2005. San Diego, United States: SPIE, Bellingham, WA 2005.

(134) Saeva, F., *AdV. Electron Transfer Chem. 1994, 4, 1.(b) DeVoe, RJ; Olofson, PM; Sahyun, MRV.* AdV. Photochem, 1992. **17**: p. 313.

(135) Rumi, M., Barlow, S., Wang, J., Perry, J. W. and Marder, S. R., *Two-Photon Absorbing Materials and Two-Photon-Induced Chemistry*, in *Photoresponsive*

Die approbierte gedruckte Originalversion dieser Dissertation ist an der TU Wien Bibliothek verfügbar.
The approved original version of this doctoral thesis is available in print at TU Wien Bibliothek.
TU Bibliothek Your knowledge hub WIEN

Polymers I, Marder, S.R. and Lee, K.-S., Editors. 2008, Springer Berlin Heidelberg: Berlin, Heidelberg. p. 1-95.

(136) Zhou, R., Malval, J.-P., Jin, M., Spangenberg, A., Pan, H., Wan, D., Morlet-Savary, F. and Knopf, S., *A two-photon active chevron-shaped type I photoinitiator designed for 3D stereolithography.* Chemical Communications, 2019. **55**(44): p. 6233-6236.

(137) Ruskowitz, E. R. and DeForest, C. A., *Photoresponsive biomaterials for targeted drug delivery and 4D cell culture.* Nature Reviews Materials, 2018. **3**: p. 17087.

(138) Holmes, C. P., *Model studies for new o-nitrobenzyl photolabile linkers: Substituent effects on the rates of photochemical cleavage.* The Journal of organic chemistry, 1997. **62**(8): p. 2370-2380.

(139) DeForest, C. A. and Anseth, K. S., *Cytocompatible click-based hydrogels with dynamically tunable properties through orthogonal photoconjugation and photocleavage reactions.* Nature chemistry, 2011. **3**(12): p. 925.

(140) Yoshida, M., Sakuragi, H., Nishimura, T., Ishikawa, S.-i. and Tokumaru, K., *Nature of the excited triplet states in the photolysis of O-acyloximes.* Chemistry Letters, 1975. **4**(11): p. 1125-1130.

(141) McCarroll, A. J. and Walton, J. C., *Exploitation of aldoxime esters as radical precursors in preparative and EPR spectroscopic roles.* Journal of the Chemical Society, Perkin Transactions 2, 2000(12): p. 2399-2409.

(142) Schafer, K. J., Hales, J. M., Balu, M., Belfield, K. D., Van Stryland, E. W. and Hagan, D. J., *Two-photon absorption cross-sections of common photoinitiators.* Journal of Photochemistry and Photobiology A: Chemistry, 2004. **162**(2): p. 497-502.

(143) Ovsianikov, A., Mühleder, S., Torgersen, J., Li, Z., Qin, X.-H., Van Vlierberghe, S., Dubruel, P., Holnthoner, W., Redl, H., Liska, R. and Stampfl, J., *Laser Photofabrication of Cell-Containing Hydrogel Constructs.* Langmuir, 2014. **30**(13): p. 3787-3794.

(144) Li, Z., Siklos, M., Pucher, N., Cicha, K., Ajami, A., Husinsky, W., Rosspeintner, A., Vauthey, E., Gescheidt, G., Stampfl, J. and Liska, R., *Synthesis and structure-activity relationship of several aromatic ketone-based two-photon initiators.* Journal of Polymer Science Part A: Polymer Chemistry, 2011. **49**(17): p. 3688-3699.

(145) Geißler, D., Antonenko, Y. N., Schmidt, R., Keller, S., Krylova, O. O., Wiesner, B., Bendig, J., Pohl, P. and Hagen, V., *(Coumarin-4-yl) methyl esters as highly efficient, ultrafast phototriggers for protons and their application to acidifying membrane surfaces.* Angewandte Chemie International Edition, 2005. **44**(8): p. 1195-1198.

(146) Nazir, R., Balčiūnas, E., Buczyńska, D., Bourquard, F., Kowalska, D., Gray, D., Maćkowski, S., Farsari, M. and Gryko, D. T., *Donor–acceptor type Thioxanthones: synthesis, optical properties, and two-photon induced polymerization.* Macromolecules, 2015. **48**(8): p. 2466-2472.

(147) Nazir, R., Thorsted, B., Balčiūnas, E., Mazur, L., Deperasińska, I., Samoć, M., Brewer, J., Farsari, M. and Gryko, D. T., *π-Expanded 1, 3-diketones–synthesis, optical properties and application in two-photon polymerization.* Journal of Materials Chemistry C, 2016. **4**(1): p. 167-177.

Die approbierte gedruckte Originalversion dieser Dissertation ist an der TU Wien Bibliothek verfügbar.
The approved original version of this doctoral thesis is available in print at TU Wien Bibliothek.
TU Bibliothek Your knowledge hub WIEN

(148) Tromayer, M., Gruber, P., Rosspeintner, A., Ajami, A., Husinsky, W., Plasser, F., González, L., Vauthey, E., Ovsianikov, A. and Liska, R., *Wavelength-optimized two-photon polymerization using initiators based on multipolar aminostyryl-1, 3, 5-triazines.* Scientific reports, 2018. **8**(1): p. 17273.

(149) Nazir, R., Danilevicius, P., Gray, D., Farsari, M. and Gryko, D. T., *Push–Pull Acylo-Phosphine Oxides for Two-Photon-Induced Polymerization.* Macromolecules, 2013. **46**(18): p. 7239-7244.

(150) Xing, J.-F., Zheng, M.-L. and Duan, X.-M., *Two-photon polymerization microfabrication of hydrogels: an advanced 3D printing technology for tissue engineering and drug delivery.* Chemical Society Reviews, 2015. **44**(15): p. 5031-5039.

(151) Xing, J.-F., Chen, W.-Q., Dong, X.-Z., Tanaka, T., Fang, X.-Y., Duan, X.-M. and Kawata, S., *Synthesis, optical and initiating properties of new two-photon polymerization initiators: 2, 7-Bis (styryl) anthraquinone derivatives.* Journal of Photochemistry and Photobiology A: Chemistry, 2007. **189**(2-3): p. 398-404.

(152) Xing, J.-F., Zheng, M.-L., Chen, W.-Q., Dong, X.-Z., Takeyasu, N., Tanaka, T., Zhao, Z.-S., Duan, X.-M. and Kawata, S., *C 2v symmetrical two-photon polymerization initiators with anthracene core: synthesis, optical and initiating properties.* Physical Chemistry Chemical Physics, 2012. **14**(45): p. 15785-15792.

(153) Li, Z., Pucher, N., Cicha, K., Torgersen, J., Ligon, S. C., Ajami, A., Husinsky, W., Rosspeintner, A., Vauthey, E. and Naumov, S., *A straightforward synthesis and structure–activity relationship of highly efficient initiators for two-photon polymerization.* Macromolecules, 2013. **46**(2): p. 352-361.

(154) Basu, S., Rodionov, V., Terasaki, M. and Campagnola, P. J., *Multiphoton-excited microfabrication in live cells via Rose Bengal cross-linking of cytoplasmic proteins.* Optics letters, 2005. **30**(2): p. 159-161.

(155) Dobos, A., Steiger, W., Theiner, D., Gruber, P., Lunzer, M., Van Hoorick, J., Van Vlierberghe, S. and Ovsianikov, A., *Screening of two-photon activated photodynamic therapy sensitizers using a 3D osteosarcoma model.* Analyst, 2019. **144**(9): p. 3056-3063.

(156) Gomer, C. J., *Preclinical examination of first and second generation photosensitizers used in photodynamic therapy.* Photochemistry and photobiology, 1991. **54**(6): p. 1093-1107.

(157) Bulina, M. E., Chudakov, D. M., Britanova, O. V., Yanushevich, Y. G., Staroverov, D. B., Chepurnykh, T. V., Merzlyak, E. M., Shkrob, M. A., Lukyanov, S. and Lukyanov, K. A., *A genetically encoded photosensitizer.* Nature Biotechnology, 2006. **24**(1): p. 95-99.

(158) Klaunig, J. E., Xu, Y., Isenberg, J. S., Bachowski, S., Kolaja, K. L., Jiang, J., Stevenson, D. E. and Walborg Jr, E. F., *The role of oxidative stress in chemical carcinogenesis.* Environmental health perspectives, 1998. **106**(suppl 1): p. 289-295.

(159) Ouédraogo, G. D. and Redmond, R. W., *Secondary Reactive Oxygen Species Extend the Range of Photosensitization Effects in Cells: DNA Damage Produced Via Initial*

Die approbierte gedruckte Originalversion dieser Dissertation ist an der TU Wien Bibliothek verfügbar.
The approved original version of this doctoral thesis is available in print at TU Wien Bibliothek.
TU Bibliothek Your knowledge hub WIEN

Membrane Photosensitization¶. Photochemistry and photobiology, 2003. **77**(2): p. 192-203.

(160) Hoebe, R., Van Oven, C., Gadella, T. W., Dhonukshe, P., Van Noorden, C. and Manders, E., *Controlled light-exposure microscopy reduces photobleaching and phototoxicity in fluorescence live-cell imaging.* Nature biotechnology, 2007. **25**(2): p. 249-253.

(161) Koester, H. J., Baur, D., Uhl, R. and Hell, S. W., *Ca2+ fluorescence imaging with pico- and femtosecond two-photon excitation: signal and photodamage.* Biophysical journal, 1999. **77**(4): p. 2226-2236.

(162) Tirlapur, U. K., König, K., Peuckert, C., Krieg, R. and Halbhuber, K.-J., *Femtosecond near-infrared laser pulses elicit generation of reactive oxygen species in mammalian cells leading to apoptosis-like death.* Experimental cell research, 2001. **263**(1): p. 88-97.

(163) Benedikt, S., Wang, J., Markovic, M., Moszner, N., Dietliker, K., Ovsianikov, A., Grützmacher, H. and Liska, R., *Highly efficient water-soluble visible light photoinitiators.* Journal of Polymer Science Part A: Polymer Chemistry, 2016. **54**(4): p. 473-479.

(164) Tromayer, M., Dobos, A., Gruber, P., Ajami, A., Dedic, R., Ovsianikov, A. and Liska, R., *A biocompatible diazosulfonate initiator for direct encapsulation of human stem cells via two-photon polymerization.* Polymer Chemistry, 2018. **9**(22): p. 3108-3117.

(165) Li, Z., Torgersen, J., Ajami, A., Muhleder, S., Qin, X., Husinsky, W., Holnthoner, W., Ovsianikov, A., Stampfl, J. and Liska, R., *Initiation efficiency and cytotoxicity of novel water-soluble two-photon photoinitiators for direct 3D microfabrication of hydrogels.* RSC Advances, 2013. **3**(36): p. 15939-15946.

(166) Farsari, M., Filippidis, G., Sambani, K., Drakakis, T. S. and Fotakis, C., *Two-photon polymerization of an Eosin Y-sensitized acrylate composite.* Journal of Photochemistry and Photobiology A: Chemistry, 2006. **181**(1): p. 132-135.

(167) Xu, C. and Webb, W. W., *Measurement of two-photon excitation cross sections of molecular fluorophores with data from 690 to 1050 nm.* JOSA B, 1996. **13**(3): p. 481-491.

(168) Griesser, M., Rosspeintner, A., Dworak, C., Höfer, M., Grabner, G., Liska, R. and Gescheidt, G., *Initiators Based on Benzaldoximes: Bimolecular and Covalently Bound Systems.* Macromolecules, 2012. **45**(21): p. 8648-8657.

(169) Vessally, E., Saeidian, H., Hosseinian, A., Edjlali, L. and Bekhradnia, A., *A review on synthetic applications of oxime esters.* Current Organic Chemistry, 2017. **21**(3): p. 249-271.

(170) Gao, Y., Song, J., Shang, S., Wang, D. and Li, J., *Synthesis and antibacterial activity of oxime esters from dihydrocumic acid.* BioResources, 2012. **7**(3): p. 4150-4160.

(171) Sun, I. C., Wang, H.-K., Kashiwada, Y., Shen, J.-K., Cosentino, L. M., Chen, C.-H., Yang, L.-M. and Lee, K.-H., *Anti-AIDS Agents. 34. Synthesis and Structure–Activity*

Die approbierte gedruckte Originalversion dieser Dissertation ist an der TU Wien Bibliothek verfügbar.
The approved original version of this doctoral thesis is available in print at TU Wien Bibliothek.
TU Bibliothek Your knowledge hub WIEN

Relationships of Betulin Derivatives as Anti-HIV Agents. Journal of Medicinal Chemistry, 1998. **41**(23): p. 4648-4657.

(172) Kumar, S. C. S., Kumar, N. V., Srinivas, P. and Bettadaiah, B. K., *Synthesis and Importance of Oxime esters.*

(173) Harini, S. T., Kumar, H. V., Rangaswamy, J. and Naik, N., *Synthesis, antioxidant and antimicrobial activity of novel vanillin derived piperidin-4-one oxime esters: Preponderant role of the phenyl ester substituents on the piperidin-4-one oxime core.* Bioorganic & medicinal chemistry letters, 2012. **22**(24): p. 7588-7592.

(174) Wylie, B. B., Isaacson, E. I. and Delgado, J. N., *Synthesis of oxime esters and ethers as potential psychotropic agents.* Journal of pharmaceutical sciences, 1965. **54**(9): p. 1373-1376.

(175) Karakurt, A., Alagöz, M. A., Sayoğlu, B., Çalış, Ü. and Dalkara, S., *Synthesis of some novel 1-(2-naphthyl)-2-(imidazol-1-yl) ethanone oxime ester derivatives and evaluation of their anticonvulsant activity.* European journal of medicinal chemistry, 2012. **57**: p. 275-282.

(176) Hayashi, I. and Shimizu, K., *Reactivity of aromatic o-hydroxy oximes. II. The use of esters of aromatic o-hydroxy oximes in peptide synthesis.* Bulletin of the Chemical Society of Japan, 1983. **56**(10): p. 3197-3198.

(177) Gotor, V. and Morís, F., *Regioselective acylation of 2'-deoxynucleosides through an enzymatic reaction with oxime esters.* Synthesis (Stuttgart), 1992(7): p. 626-628.

(178) Khlebnicova, T. S., Piven, Y. A., Baranovsky, A. V., Lakhvich, F. A., Shishkina, S. V., Zicāne, D., Tetere, Z., Rāviņa, I., Kumpiņš, V., Rijkure, I., Mieriņa, I., Peipiņš, U. and Turks, M., *Synthesis of novel lupane triterpenoid-indazolone hybrids with oxime ester linkage.* Steroids, 2017. **117**: p. 77-89.

(179) Hwu, J. R., Tsay, S.-C., Hong, S. C., Hsu, M.-H., Liu, C.-F. and Chou, S.-S. P., *Relationship between structure of conjugated oxime esters and their ability to cleave DNA.* Bioconjugate chemistry, 2013. **24**(11): p. 1778-1783.

(180) Bindu, P., Mahadevan, K., Satyanarayan, N. and Naik, T. R., *Synthesis and DNA cleavage studies of novel quinoline oxime esters.* Bioorganic & medicinal chemistry letters, 2012. **22**(2): p. 898-900.

(181) Kloxin, A. M., Kasko, A. M., Salinas, C. N. and Anseth, K. S., *Photodegradable Hydrogels for Dynamic Tuning of Physical and Chemical Properties.* Science, 2009. **324**(5923): p. 59-63.

(182) Dietlin, C., Allonas, X., Morlet-Savary, F., Fouassier, J. P., Visconti, M., Norcini, G. and Romagnano, S., *Investigation of Barton esters as radical photoinitiators.* Journal of Applied Polymer Science, 2008. **109**(2): p. 825-833.

(183) Ingold, K. U., Lusztyk, J., Maillard, B. and Walton, J. C., *EPR detection of free radicals from N-hydroxypyridine-2-thione esters.* Tetrahedron letters, 1988. **29**(8): p. 917-920.

(184) Bohne, C., Boch, R. and Scaiano, J., *Exploratory studies of the photochemistry of N-hydroxypyridine-2-thione esters. Generation of excited radicals by laser flash*

Die approbierte gedruckte Originalversion dieser Dissertation ist an der TU Wien Bibliothek verfügbar.
The approved original version of this doctoral thesis is available in print at TU Wien Bibliothek.
TU Bibliothek Your knowledge hub WIEN

photolysis and in a conventional fluorescence spectrometer. The Journal of Organic Chemistry, 1990. **55**(19): p. 5414-5418.

(185) Aveline, B. M., Kochevar, I. E. and Redmond, R. W., *Photochemistry of N-hydroxypyridine-2-thione derivatives: involvement of the 2-pyridylthiyl radical in the radical chain reaction mechanism.* Journal of the American Chemical Society, 1995. **117**(38): p. 9699-9708.

(186) Aveline, B. M., Kochevar, I. E. and Redmond, R. W., *Photochemistry of the nonspecific hydroxyl radical generator, N-hydroxypyridine-2 (1 H)-thione.* Journal of the American Chemical Society, 1996. **118**(42): p. 10113-10123.

(187) Xuan, J., Zhang, Z. G. and Xiao, W. J., *Visible-Light-Induced Decarboxylative Functionalization of Carboxylic Acids and Their Derivatives.* Angewandte Chemie International Edition, 2015. **54**(52): p. 15632-15641.

(188) Yu, X. Y., Chen, J. R., Wang, P. Z., Yang, M. N., Liang, D. and Xiao, W. J., *A Visible-Light-Driven Iminyl Radical-Mediated C− C Single Bond Cleavage/Radical Addition Cascade of Oxime Esters.* Angewandte Chemie International Edition, 2018. **57**(3): p. 738-743.

(189) Dauncey, E. M., Morcillo, S. P., Douglas, J. J., Sheikh, N. S. and Leonori, D., *Photoinduced remote functionalisations by iminyl radical promoted C− C and C− H bond cleavage cascades.* Angewandte Chemie International Edition, 2018. **57**(3): p. 744-748.

(190) Groenenboom, C. J., Hageman, H. J., Oosterhoff, P., Overeem, T. and Verbeek, J., *Photoinitiators and photoinitiation Part 11. The photodecomposition of some O-acyl 2-oximinoketones.* Journal of Photochemistry and Photobiology A: Chemistry, 1997. **107**(1-3): p. 261-269.

(191) Suyama, K. and Shirai, M., *Photobase generators: recent progress and application trend in polymer systems.* Progress in Polymer Science, 2009. **34**(2): p. 194-209.

(192) Qiu, W., Li, M., Yang, Y., Li, Z. and Dietliker, K., *Cleavable coumarin-based oxime esters with terminal heterocyclic moieties: photobleachable initiators for deep photocuring under visible LED light irradiation.* Polymer Chemistry, 2020.

(193) McCarroll, A. J. and Walton, J. C., *Enhanced radical delivery from aldoxime esters for EPR and ring closure applications.* Chemical Communications, 2000(5): p. 351-352.

(194) Dworak, C. and Liska, R., *Alternative Initiators for Bimolecular Photoinitiating Systems.* Wiley Online Library, 2010.

(195) Fast, D. E., Lauer, A., Menzel, J. P., Kelterer, A.-M., Gescheidt, G. and Barner-Kowollik, C., *Wavelength-Dependent Photochemistry of Oxime Ester Photoinitiators.* Macromolecules, 2017. **50**(5): p. 1815-1823.

(196) Worth, G. A. and Cederbaum, L. S., *Beyond Born-Oppenheimer: molecular dynamics through a conical intersection.* Annu. Rev. Phys. Chem., 2004. **55**: p. 127-158.

Die approbierte gedruckte Originalversion dieser Dissertation ist an der TU Wien Bibliothek verfügbar.
The approved original version of this doctoral thesis is available in print at TU Wien Bibliothek.
TU Bibliothek Your knowledge hub WIEN

(197) Qiu, W., Hu, P., Zhu, J., Liu, R., Li, Z., Hu, Z., Chen, Q., Dietliker, K. and Liska, R., *Cleavable Unimolecular Photoinitiators Based on Oxime-Ester Chemistry for Two-Photon Three-Dimensional Printing.* ChemPhotoChem, 2019. **3**(11): p. 1090-1094.

(198) Ma, X., Gu, R., Yu, L., Han, W., Li, J., Li, X. and Wang, T., *Conjugated phenothiazine oxime esters as free radical photoinitiators.* Polymer Chemistry, 2017. **8**(39): p. 6134-6142.

(199) Lalevee, J., Allonas, X., Fouassier, J., Tachi, H., Izumitani, A., Shirai, M. and Tsunooka, M., *Investigation of the photochemical properties of an important class of photobase generators: the O-acyloximes.* Journal of Photochemistry and Photobiology A: Chemistry, 2002. **151**(1-3): p. 27-37.

(200) Kunimoto, K., Tanabe, J., Kura, H., Oka, H. and Ohwa, M., *Oxime ester photoinitiators having a combined structure*. 2002, Google Patents.

(201) Kunimoto, K., Oka, H., Ohwa, M., Tanabe, J., Kura, H. and Birbaum, J. L., *Oxime ester photoinitiators*. 2005, Google Patents.

(202) Matsumoto, A., Tanabe, J., Kura, H. and Ohwa, M., *Oxime ester photoinitiators, WO2008138732A1*. 2008.

(203) Tanabe, J., Kunimoto, K., Kura, H., Oka, H. and Ohwa, M., *Oxime ester photoinitiators*. 2010, Google Patents.

(204) Matsumoto, A. and Kura, H., *Oxime ester photoinitiators*. 2013, Google Patents.

(205) Nishimae, Y., Kura, H., Kunimoto, K., Yamagami, R. and Tanaka, K., *Oxime ester photoinitiators*. 2017, Google Patents.

(206) Qian, X., *Nitro-containing bisoxime ester photoinitiator and preparation method and use thereof*. 2017, Google Patents.

(207) Turro, N. J., Li, Y., Jockusch, S., Hagiwara, Y., Okazaki, M., Mesch, R. A., Schuster, D. I. and Willson, C. G., *Study of a Two-Stage Photobase Generator for Photolithography in Microelectronics.* The Journal of Organic Chemistry, 2013. **78**(5): p. 1735-1741.

(208) Xu, J., Ma, G., Wang, K., Gu, J., Jiang, S. and Nie, J., *Synthesis and photopolymerization kinetics of oxime ester photoinitiators.* Journal of Applied Polymer Science, 2012. **123**(2): p. 725-731.

(209) Fan, X., Lei, T., Liu, Z., Yang, X.-L., Cheng, Y.-Y., Liang, G., Chen, B., Tung, C.-H. and Wu, L.-Z., *Benzyl C–O and C–N Bond Construction via C–C Bond Dissociation of Oxime Ester under Visible Light Irradiation.* European Journal of Organic Chemistry, 2020. **2020**(10): p. 1551-1558.

(210) Lemercier, G., Martineau, C., Mulatier, J.-C., Wang, I., Stéphan, O., Baldeck, P. and Andraud, C., *Analogs of Michler's ketone for two-photon absorption initiation of polymerization in the near infrared: synthesis and photophysical properties.* New Journal of Chemistry, 2006. **30**(11): p. 1606-1613.

(211) Tian, Y., Zhang, M., Yu, X., Xu, G., Ren, Y., Yang, J., Wu, J., Zhang, X., Tao, X. and Zhang, S., *Two novel two-photon polymerization initiators with extensive application prospects.* Chemical physics letters, 2004. **388**(4-6): p. 325-329.

Die approbierte gedruckte Originalversion dieser Dissertation ist an der TU Wien Bibliothek verfügbar.
The approved original version of this doctoral thesis is available in print at TU Wien Bibliothek.
TU Bibliothek Your knowledge hub WIEN

(212) Lin, T.-C., Hsu, C.-S., Hu, C.-L., Chen, Y.-F. and Huang, W.-J., *Synthesis and two-photon properties of a multipolar chromophore containing indenofluorenyl units.* Tetrahedron Letters, 2009. **50**(2): p. 182-185.

(213) Chinchilla, R. and Nájera, C., *The Sonogashira reaction: a booming methodology in synthetic organic chemistry.* Chemical reviews, 2007. **107**(3): p. 874-922.

(214) Dworak, C.,

(215) Delrot, P., Loterie, D., Psaltis, D. and Moser, C., *Single-photon three-dimensional microfabrication through a multimode optical fiber.* Optics express, 2018. **26**(2): p. 1766-1778.

(216) Haske, W., Chen, V. W., Hales, J. M., Dong, W., Barlow, S., Marder, S. R. and Perry, J. W., *65 nm feature sizes using visible wavelength 3-D multiphoton lithography.* Optics Express, 2007. **15**(6): p. 3426-3436.

(217) Stampfl, J., Baudis, S., Heller, C., Liska, R., Neumeister, A., Kling, R., Ostendorf, A. and Spitzbart, M., *Photopolymers with tunable mechanical properties processed by laser-based high-resolution stereolithography.* Journal of Micromechanics and Microengineering, 2008. **18**(12): p. 125014.

(218) Sticker, D., Rothbauer, M., Ehgartner, J., Steininger, C., Liske, O., Liska, R., Neuhaus, W., Mayr, T., Haraldsson, T. and Kutter, J. r. P., *Oxygen management at the microscale: a functional biochip material with long-lasting and tunable oxygen scavenging properties for cell culture applications.* ACS applied materials & interfaces, 2019. **11**(10): p. 9730-9739.

(219) Ajami, A., Husinsky, W., Tromayer, M., Gruber, P., Liska, R. and Ovsianikov, A., *Measurement of degenerate two-photon absorption spectra of a series of developed two-photon initiators using a dispersive white light continuum Z-scan.* Applied Physics Letters, 2017. **111**(7): p. 071901.

(220) Gibian, M. J. and Corley, R. C., *Organic radical-radical reactions. Disproportionation vs. combination.* Chemical Reviews, 1973. **73**(5): p. 441-464.

(221) Jipa, F., Zamfirescu, M., Velea, A., Popescu, M. and Dabu, R., *Femtosecond Laser Lithography in Organic and Non-Organic Materials.* Updates in Advanced Lithography, 2013. **3**.

(222) Oakdale, J. S., Ye, J., Smith, W. L. and Biener, J., *Post-print UV curing method for improving the mechanical properties of prototypes derived from two-photon lithography.* Optics express, 2016. **24**(24): p. 27077-27086.

(223) Ladner, I. S., Cullinan, M. A. and Saha, S. K., *Tensile properties of polymer nanowires fabricated via two-photon lithography.* RSC Advances, 2019. **9**(49): p. 28808-28813.

(224) Jeong, T.-S., Kim, M. J., Yu, H., Kim, K. S., Choi, J.-K., Kim, S.-S. and Lee, W. S., *(E)-Phenyl-and-heteroaryl-substituted O-benzoyl-(or acyl) oximes as lipoprotein-associated phospholipase A2 inhibitors.* Bioorganic & medicinal chemistry letters, 2005. **15**(5): p. 1525-1527.

Die approbierte gedruckte Originalversion dieser Dissertation ist an der TU Wien Bibliothek verfügbar.
The approved original version of this doctoral thesis is available in print at TU Wien Bibliothek.
TU Bibliothek Your knowledge hub WIEN

(225) Jeong, H. J., Park, Y.-D., Park, H.-Y., Jeong, I. Y., Jeong, T.-S. and Lee, W. S., *Potent inhibitors of lipoprotein-associated phospholipase A2: Benzaldehyde O-heterocycle-4-carbonyloxime.* Bioorganic & medicinal chemistry letters, 2006. **16**(21): p. 5576-5579.

(226) Cheng, Y.-Y., Lei, T., Su, L., Fan, X., Chen, B., Tung, C.-H. and Wu, L.-Z., *Visible Light Irradiation of Acyl Oxime Esters and Styrenes Efficiently Constructs β-Carbonyl Imides by a Scission and Four-Component Reassembly Process.* Organic Letters, 2019. **21**(21): p. 8789-8794.

(227) Woo, H. Y., Liu, B., Kohler, B., Korystov, D., Mikhailovsky, A. and Bazan, G. C., *Solvent effects on the two-photon absorption of distyrylbenzene chromophores.* Journal of the American Chemical Society, 2005. **127**(42): p. 14721-14729.

(228) Xue, J., Zhao, Y., Wu, J. and Wu, F., *Novel benzylidene cyclopentanone dyes for two-photon photopolymerization.* Journal of Photochemistry and Photobiology A: Chemistry, 2008. **195**(2-3): p. 261-266.

(229) Nazir, R., Danilevicius, P., Ciuciu, A. I., Chatzinikolaidou, M., Gray, D., Flamigni, L., Farsari, M. and Gryko, D. T., *π-Expanded ketocoumarins as efficient, biocompatible initiators for two-photon-induced polymerization.* Chemistry of Materials, 2014. **26**(10): p. 3175-3184.

(230) March, J., *Advanced Organic Chemistry 4th Edition, Hoboken*. 1992, New Jersey: Wiley Interscience.

(231) Kalia, J. and Raines, R. T., *Hydrolytic Stability of Hydrazones and Oximes.* Angewandte Chemie (International ed. in English), 2008. **47**(39): p. 7523-7526.

(232) Bittner, S. and Grinberg, S., *Alkylation, acylation, and Beckmann rearrangement of oximes in the presence of an oxidation–reduction system.* Journal of the Chemical Society, Perkin Transactions 1, 1976(16): p. 1708-1711.

(233) Abele, E. and Lukevics, E., *Recent Advances in the Chemistry of Oximes.* Organic Preparations and Procedures International, 2000. **32**(3): p. 235-264.

(234) Heck, L., Müller, P., Müller-Dolezal, H., Regitz, M. and Söll, H., *Houben-Weyl Methods of Organic Chemistry Vol. X/4, 4th Edition: Oximes; Diazo Compounds; N-Oxides*. 2014: Thieme.

(235) Sandler, S. R. and Karo, W., *Organic functional group preparations*. Vol. 2. 2013: Elsevier.

(236) Wipf, P., Fletcher, J. M. and Scarone, L., *Microwave promoted oxazole synthesis: cyclocondensation cascade of oximes and acyl chlorides.* Tetrahedron Letters, 2005. **46**(33): p. 5463-5466.

(237) Ouellette, R. J. and Rawn, J. D., *21 - Carboxylic Acid Derivatives*, in *Organic Chemistry Study Guide*, Ouellette, R.J. and Rawn, J.D., Editors. 2015, Elsevier: Boston. p. 385-418.

(238) Smith, M. B., *Chapter 4 - Acids, Bases, and Functional Group Exchange Reactions: Acyl Addition and Acyl Substitution*, in *Organic Synthesis (Fourth Edition)*, Smith, M.B., Editor. 2017, Academic Press: Boston. p. 161-183.

Die approbierte gedruckte Originalversion dieser Dissertation ist an der TU Wien Bibliothek verfügbar.
The approved original version of this doctoral thesis is available in print at TU Wien Bibliothek.
TU Bibliothek Your knowledge hub WIEN

(239) Ouellette, R. J. and Rawn, J. D., *22 - Carboxylic Acid Derivatives*, in *Organic Chemistry (Second Edition)*, Ouellette, R.J. and Rawn, J.D., Editors. 2018, Academic Press. p. 665-710.

(240) Clayden, J., Greeves, N., Warren, S. and Wothers, P., *Organic Chemistry. New York 2001.* Oxford University Press Inc.

(241) Spivey, A. C. and Arseniyadis, S., *Nucleophilic Catalysis by 4-(Dialkylamino)pyridines Revisited—The Search for Optimal Reactivity and Selectivity.* Angewandte Chemie International Edition, 2004. **43**(41): p. 5436-5441.

(242) Xu, S., Held, I., Kempf, B., Mayr, H., Steglich, W. and Zipse, H., *The DMAP-Catalyzed Acetylation of Alcohols—A Mechanistic Study (DMAP= 4-(Dimethylamino) pyridine).* Chemistry–A European Journal, 2005. **11**(16): p. 4751-4757.

(243) Wheeler, S. E. and Bloom, J. W., *Toward a more complete understanding of noncovalent interactions involving aromatic rings.* The journal of physical chemistry A, 2014. **118**(32): p. 6133-6147.

(244) Bolotin, D. S., Burianova, V. K., Novikov, A. S., Demakova, M. Y., Pretorius, C., Mokolokolo, P. P., Roodt, A., Bokach, N. A., Suslonov, V. V., Zhdanov, A. P., Zhizhin, K. Y., Kuznetsov, N. T. and Kukushkin, V. Y., *Nucleophilicity of Oximes Based upon Addition to a Nitrilium closo-Decaborate Cluster.* Organometallics, 2016. **35**(20): p. 3612-3623.

(245) DeRosa, T. F., *Oximes*, in *Advances in Synthetic Organic Chemistry and Methods Reported in US Patents*, DeRosa, T.F., Editor. 2006, Elsevier: Oxford. p. 478-483.

(246) Pombeiro, A. J. L. and Kukushkin, V. Y., *Reactivity of Coordinated Oximes*, in *Comprehensive Coordination Chemistry II*, McCleverty, J.A. and Meyer, T.J., Editors. 2003, Pergamon: Oxford. p. 631-637.

(247) Allen, C. C. R., Ellinger, J., Ewing, T. and de Gonzalo Calvo, G., *Science of Synthesis: Biocatalysis in Organic Synthesis*. Vol. 3. 2015: Georg Thieme Verlag.

(248) Ritson, D. J., Cox, R. J. and Berge, J., *Indium mediated allylation of glyoxylate oxime ethers, esters and cyanoformates.* Organic & Biomolecular Chemistry, 2004. **2**(13): p. 1921-1933.

(249) Moszner, N., Fischer, U. K., Ganster, B., Liska, R. and Rheinberger, V., *Benzoyl germanium derivatives as novel visible light photoinitiators for dental materials.* Dental Materials, 2008. **24**(7): p. 901-907.

(250) Ganster, B., Fischer, U. K., Moszner, N. and Liska, R., *New photocleavable structures. Diacylgermane-based photoinitiators for visible light curing.* Macromolecules, 2008. **41**(7): p. 2394-2400.

(251) Mitterbauer, M., Knaack, P., Naumov, S., Markovic, M., Ovsianikov, A., Moszner, N. and Liska, R., *Acylstannanes: Cleavable and Highly Reactive Photoinitiators for Radical Photopolymerization at Wavelengths above 500 nm with Excellent Photobleaching Behavior.* Angewandte Chemie International Edition, 2018. **57**(37): p. 12146-12150.

(252) Layer, R. W., *The Chemistry of Imines.* Chemical Reviews, 1963. **63**(5): p. 489-510.

Die approbierte gedruckte Originalversion dieser Dissertation ist an der TU Wien Bibliothek verfügbar.
The approved original version of this doctoral thesis is available in print at TU Wien Bibliothek.
TU Bibliothek Your knowledge hub WIEN

(253) Dinon, F., Richards, E., Murphy, P. J., Hibbs, D. E., Hursthouse, M. B. and Malik, K. A., *Tandem Michael/intramolecular aldol reactions mediated by secondary amines, thiols and phosphines.* Tetrahedron letters, 1999. **40**(16): p. 3279-3282.

(254) Suwa, T., Shibata, I., Nishino, K. and Baba, A., *Synthesis of nitrogen heterocycles by intramolecular Michael Type of amination via reduction of imines with Di-n-butyliodotin Hydride (n-Bu2SnIH).* Organic Letters, 1999. **1**(10): p. 1579-1581.

(255) Movassagh, B., Tahershamsi, L. and Mobaraki, A., *A magnetic solid sulfonic acid modified with hydrophobic regulators: an efficient recyclable heterogeneous catalyst for one-pot aza-Michael-type and Mannich-type reactions of aldehydes, ketones, and amines.* Tetrahedron Letters, 2015. **56**(14): p. 1851-1854.

(256) Roy, T. K., Parhi, B. and Ghorai, P., *Cinchonamine Squaramide Catalyzed Asymmetric aza-Michael Reaction: Dihydroisoquinolines and Tetrahydropyridines.* Angewandte Chemie International Edition, 2018. **57**(30): p. 9397-9401.

(257) Kobayashi, S., Yamaguchi, M., Agostinho, M. and Schneider, U., *Catalytic Use of Strontium Hexamethyldisilazide in the Asymmetric Michael Addition of Malonate to Chalcone Derivatives.* Chemistry letters, 2009. **38**(3): p. 296-297.

(258) Pesyan, N. N., Noori, S., Poorhassan, S. and Şahin, E., *New spiro (thio) barbiturates based on cyclohexanone and bicyclo [3.1. 1] heptan-6-one by nonconcerted [1+ 5] cycloaddition reaction and their conformational structures.* Bulletin of the Chemical Society of Ethiopia, 2014. **28**(3): p. 423-440.

(259) Almaşi, D., Alonso, D. A. and Najera, C., *Organocatalytic asymmetric conjugate additions.* Tetrahedron: Asymmetry, 2007. **18**(3): p. 299-365.

(260) Christoffers, J. and Baro, A., *Construction of quaternary stereocenters: New perspectives through enantioselective Michael reactions.* Angewandte Chemie International Edition, 2003. **42**(15): p. 1688-1690.

(261) Krause, N. and Hoffmann-Röder, A., *Recent advances in catalytic enantioselective Michael additions.* Synthesis, 2001. **2001**(02): p. 0171-0196.

(262) Ito, A., Konishi, K. and Aida, T., *Free bases of chiral N-substituted porphyrins as catalysts for asymmetric reaction.* Tetrahedron letters, 1996. **37**(15): p. 2585-2588.

(263) Sera, A., Takagi, K., Katayama, H., Yamada, H. and Matsumoto, K., *High-pressure asymmetric Michael additions of thiols, nitromethane, and methyl oxoindancarboxylate to enones.* The Journal of Organic Chemistry, 1988. **53**(6): p. 1157-1161.

(264) Kawara, A. and Taguchi, T., *An enantioselective Michael addition of soft nucleophiles to prochiral enone catalyzed by (2-pyrrolidyl) alkyl ammonium hydroxide.* Tetrahedron letters, 1994. **35**(47): p. 8805-8808.

(265) Desmet, G. B., Sabbe, M. K., D'Hooge, D. R., Espeel, P., Celasun, S., Marin, G. B., Du Prez, F. E. and Reyniers, M.-F., *Thiol-Michael addition in polar aprotic solvents: nucleophilic initiation or base catalysis?* Polymer Chemistry, 2017. **8**(8): p. 1341-1352.

Die approbierte gedruckte Originalversion dieser Dissertation ist an der TU Wien Bibliothek verfügbar.
The approved original version of this doctoral thesis is available in print at TU Wien Bibliothek.
TU Bibliothek Your knowledge hub WIEN

(266) Verboom, W., Van Eijk, P., Conti, P. and Reinhoudt, D., *2-(1-Alkenyl)-and 2-aryl-substituted four-membered cyclic nitrones as precursors for 2, 3, 4-substituted pyridines and quinolines.* Tetrahedron, 1989. **45**(10): p. 3131-3138.

(267) Mallavia, R., Sastre, R. and Amat-Guerri, F., *Photofragmentation and photoisomerization of O-acyl-α-oxooximes: Quantum yields and mechanism.* Journal of Photochemistry and Photobiology A: Chemistry, 2001. **138**(3): p. 193-201.

(268) Kassaee, M. and Vessally, E., *Different relative rates for photo-rearrangements of (E)-and (Z)-β-nitrostyrene derivatives to oximinoketones.* Journal of Photochemistry and Photobiology A: Chemistry, 2005. **172**(3): p. 331-336.

(269) Kitamura, M., Mori, Y. and Narasaka, K., *Photochemical radical cyclization of γ, δ-unsaturated ketone oximes to 3, 4-dihydro-2H-pyrroles.* Tetrahedron letters, 2005. **46**(14): p. 2373-2376.

(270) Austin, M., Egan, O. J., Tully, R. and Pratt, A. C., *Quinoline synthesis: scope and regiochemistry of photocyclisation of substituted benzylidenecyclopentanone O-alkyl and O-acetyloximes.* Organic & biomolecular chemistry, 2007. **5**(23): p. 3778-3786.

(271) Huang, H., Cai, J. and Deng, G.-J., *O-Acyl oximes: versatile building blocks for N-heterocycle formation in recent transition metal catalysis.* Organic & biomolecular chemistry, 2016. **14**(5): p. 1519-1530.

(272) Ma, X., Cao, D., Fu, H., You, J., Gu, R., Fan, B., Nie, J. and Wang, T., *Multicomponent photoinitiating systems containing arylamino oxime ester for visible light photopolymerization.* Progress in Organic Coatings, 2019. **135**: p. 517-524.

(273) Padwa, A., *Photochemistry of the carbon-nitrogen double bond.* Chemical Reviews, 1977. **77**(1): p. 37-68.

(274) Fan, X., Lei, T., Liu, Z., Yang, X. L., Cheng, Y. Y., Liang, G., Chen, B., Tung, C. H. and Wu, L. Z., *Benzyl C–O and C–N Bond Construction via C–C Bond Dissociation of Oxime Ester under Visible Light Irradiation.* European Journal of Organic Chemistry, 2020.

(275) McBurney, R. T. and Walton, J. C., *Dissociation or Cyclization: Options for a Triad of Radicals Released from Oxime Carbamates.* Journal of the American Chemical Society, 2013. **135**(19): p. 7349-7354.

(276) Nguyen, A. K. and Narayan, R. J., *Two-photon polymerization for biological applications.* Materials Today, 2017. **20**(6): p. 314-322.

(277) Valeur, B. and Berberan-Santos, M. N., *Molecular fluorescence: principles and applications*. 2012: John Wiley & Sons.

(278) Mahimwalla, Z., Yager, K. G., Mamiya, J.-i., Shishido, A., Priimagi, A. and Barrett, C. J., *Azobenzene photomechanics: prospects and potential applications.* Polymer bulletin, 2012. **69**(8): p. 967-1006.

(279) Kumar, G. S. and Neckers, D., *Photochemistry of azobenzene-containing polymers.* Chemical Reviews, 1989. **89**(8): p. 1915-1925.

Die approbierte gedruckte Originalversion dieser Dissertation ist an der TU Wien Bibliothek verfügbar.
The approved original version of this doctoral thesis is available in print at TU Wien Bibliothek.
TU Bibliothek Your knowledge hub WIEN

(280) Santos, F. d. S., Descalzo, R. R., Gonçalves, P. F. B., Benvenutti, E. V. and Rodembusch, F. S., *Evidence for excited state intramolecular charge transfer in benzazole-based pseudo-stilbenes.* Physical Chemistry Chemical Physics, 2012. **14**(31): p. 10994-11001.

(281) Ried, W. and Junker, P., *Reaktionen mit Diazocarbonylverbindungen, XXV. Umsetzung von o-Chinondiaziden mit Ketenen in alkoholischer Lösung.* Justus Liebigs Annalen der Chemie, 1967. **709**(1): p. 85-96.

(282) Lester, H. A., Krouse, M. E., Nass, M. M., WASSERMANN, N. H. and ERLANGER, B. F., *Light-activated drug confirms a mechanism of ion channel blockade.* Nature, 1979. **280**(5722): p. 509-510.

(283) Beharry, A. A. and Woolley, G. A., *Azobenzene photoswitches for biomolecules.* Chemical Society Reviews, 2011. **40**(8): p. 4422-4437.

(284) Tamesue, S., Takashima, Y., Yamaguchi, H., Shinkai, S. and Harada, A., *Photoswitchable supramolecular hydrogels formed by cyclodextrins and azobenzene polymers.* Angewandte Chemie International Edition, 2010. **49**(41): p. 7461-7464.

(285) Renner, C. and Moroder, L., *Azobenzene as conformational switch in model peptides.* ChemBioChem, 2006. **7**(6): p. 868-878.

(286) Mart, R. J. and Allemann, R. K., *Azobenzene photocontrol of peptides and proteins.* Chemical Communications, 2016. **52**(83): p. 12262-12277.

(287) Fortin, D. L., Banghart, M. R., Dunn, T. W., Borges, K., Wagenaar, D. A., Gaudry, Q., Karakossian, M. H., Otis, T. S., Kristan, W. B. and Trauner, D., *Photochemical control of endogenous ion channels and cellular excitability.* Nature methods, 2008. **5**(4): p. 331.

(288) Sharma, G., Suresh, P., Sharma, S. K. and Roy, M., *Photovoltaic properties of liquid-state photoelectrochemical cells based on PPAT and a composite film of PPAT and nanocrystalline titanium dioxide.* Synthetic metals, 2008. **158**(12): p. 509-515.

(289) Ho, M., Natansohn, A. and Rochon, P., *Azo polymers for reversible optical storage. 7. The effect of the size of the photochromic groups.* Macromolecules, 1995. **28**(18): p. 6124-6127.

(290) Mutlu, H., Geiselhart, C. M. and Barner-Kowollik, C., *Untapped potential for debonding on demand: the wonderful world of azo-compounds.* Materials Horizons, 2018. **5**(2): p. 162-183.

(291) Calvert, J., *u. JN Pitts, jr., Photochemistry*. 1966, John Wiley, New York.

(292) Strausz, O., Lown, J. and Gunning, H., *Unimolecular Homogeneous Decompositions and Isomerizations of Nitrogen Compounds*, in *Comprehensive Chemical Kinetics*. 1972, Elsevier. p. 566-696.

(293) Koenig, T. and Fischer, H., *In Free Radicals; Kochi, J. K., Ed*. 1973, Wiley: New York.

(294) Duismann, W. and Rüchardt, C., *Steric accellerations in thermolysis and solvolysis reactions.* Tetrahedron Letters, 1974. **15**(51-52): p. 4517-4520.

Die approbierte gedruckte Originalversion dieser Dissertation ist an der TU Wien Bibliothek verfügbar.
The approved original version of this doctoral thesis is available in print at TU Wien Bibliothek.
TU Bibliothek Your knowledge hub WIEN

(295) Mark, J. E., *Physical properties of polymers handbook*. Vol. 1076. 2007: Springer.

(296) Engel, P. S., *Mechanism of the thermal and photochemical decomposition of azoalkanes.* Chemical Reviews, 1980. **80**(2): p. 99-150.

(297) Denisov, E. T., Denisova, T. G. and Pokidova, T. S., *Handbook of free radical initiators*. 2005: John Wiley & Sons.

(298) Staško, A., Erentová, K., Rapta, P., Nuyken, O. and Voit, B., *Investigation of the decomposition of compounds containing azo groups by EPR spectroscopy.* Magnetic Resonance in Chemistry, 1998. **36**(1): p. 13-34.

(299) Nuyken, O. and Voit, B., *Water-soluble and photosensitive copolymers from methyl methacrylate and sodium 3-vinylphenylazosulfonate.* Die Makromolekulare Chemie, 1989. **190**(6): p. 1325-1332.

(300) Nuyken, O., Knepper, T. and Voit, B., *Sulfur-containing azoinitiators and their properties.* Die Makromolekulare Chemie: Macromolecular Chemistry and Physics, 1989. **190**(5): p. 1015-1024.

(301) Reinhardt, B. A., Brott, L. L., Clarson, S. J., Dillard, A. G., Bhatt, J. C., Kannan, R., Yuan, L., He, G. S. and Prasad, P. N., *Highly Active Two-Photon Dyes: Design, Synthesis, and Characterization toward Application.* Chemistry of Materials, 1998. **10**(7): p. 1863-1874.

(302) Drobizhev, M., Karotki, A., Rebane, A. and Spangler, C. W., *Dendrimer molecules with record large two-photon absorption cross section.* Optics letters, 2001. **26**(14): p. 1081-1083.

(303) Campagnola, P. J., Delguidice, D. M., Epling, G. A., Hoffacker, K. D., Howell, A. R., Pitts, J. D. and Goodman, S. L., *3-dimensional submicron polymerization of acrylamide by multiphoton excitation of xanthene dyes.* Macromolecules, 2000. **33**(5): p. 1511-1513.

(304) Ifkovits, J. L. and Burdick, J. A., *Photopolymerizable and degradable biomaterials for tissue engineering applications.* Tissue engineering, 2007. **13**(10): p. 2369-2385.

(305) Seybold, G., *Farbenchemie: Color Chemistry. Synthesis, Properties and Applications of Organic Dyes and Pigments. Von H. Zollinger, VCH Verlagsgesellschaft, Weinheim 1987. 367 S., geb. 198,- DM. ISBN 3-527-26200-8.* Nachrichten aus Chemie, Technik und Laboratorium, 1987. **35**(12): p. 1264-1265.

(306) Erkurt, E. A., Erkurt, H. A. and Unyayar, A., *Decolorization of azo dyes by white rot fungi*, in *Biodegradation of Azo Dyes*. 2010, Springer. p. 157-167.

(307) Franzke, D., Scherer, C., Nuyken, O. and Wokaun, A., *Synthesis and photochemical properties of aromatic diazo-phosphonium salts.* Journal of Photochemistry and Photobiology A: Chemistry, 1997. **111**(1-3): p. 47-50.

(308) Staško, A., Nuyken, O., Volt, B. and Biskupič, S., *Azo compounds as spin traps in their photochemical decomposition.* Tetrahedron Letters, 1990. **31**(40): p. 5737-5740.

Die approbierte gedruckte Originalversion dieser Dissertation ist an der TU Wien Bibliothek verfügbar.
The approved original version of this doctoral thesis is available in print at TU Wien Bibliothek.
TU Bibliothek Your knowledge hub WIEN

(309) Backes, J., Krüger, G., Behnisch, P. and Hemmer, R., *Houben-Weyl Methods of Organic Chemistry Vol. E 16d, Supplement: Organic N Compounds IV: Amines, Nitro, Azo, Azoxy Compounds*. 2014: Georg Thieme Verlag.

(310) Merino, E., *Synthesis of azobenzenes: the coloured pieces of molecular materials.* Chemical Society Reviews, 2011. **40**(7): p. 3835-3853.

(311) Mustroph, H., *Dyes, General Survey*, in *Ullmann's Encyclopedia of Industrial Chemistry*. 2014. p. 1-38.

(312) Raue, R., Kunde, K. and Engel, A., *Azo Dyes, 4. Cationic Dyes*, in *Ullmann's Encyclopedia of Industrial Chemistry*. 2011.

(313) Hunger, K. and Herbst, W., *Pigments, Organic*, in *Ullmann's Encyclopedia of Industrial Chemistry*. 2012.

(314) Bering, L. and Antonchick, A. P., *Reactive nitrogen species: Nitrosonium ions in organic synthesis.* Tetrahedron, 2019. **75**(9): p. 1131-1143.

(315) Jean, R., *Diazonium salts and process for their preparation*. 1968, Google Patents.

(316) Merino, E. and Ribagorda, M., *Control over molecular motion using the cis–trans photoisomerization of the azo group.* Beilstein journal of organic chemistry, 2012. **8**(1): p. 1071-1090.

(317) García-Iriepa, C., Marazzi, M., Frutos, L. M. and Sampedro, D., *E/Z Photochemical switches: syntheses, properties and applications.* RSC advances, 2013. **3**(18): p. 6241-6266.

(318) Ahmed, I. and Fruk, L., *The power of light: photosensitive tools for chemical biology.* Molecular BioSystems, 2013. **9**(4): p. 565-570.

(319) Georgi, U., Dissertation, Technischen Universität Dresden, 2014

(320) Cho, J., Cho, J. K., Lee, J., Lee, D., Park, C. and Kim, S., *Optimization of salting-out crystallization for an efficient in situ separation of synthetic anthraquinone- and azo-type reactive dyes.* Separation and Purification Technology, 2009. **68**(2): p. 138-144.

(321) Hyde, A. M., Zultanski, S. L., Waldman, J. H., Zhong, Y.-L., Shevlin, M. and Peng, F., *General principles and strategies for salting-out informed by the Hofmeister series.* Organic Process Research & Development, 2017. **21**(9): p. 1355-1370.

(322) Baughman, G. L., Banerjee, S. and Perenich, T. A., *Dye solubility*, in *Physico-Chemical Principles of Color Chemistry*, Peters, A.T. and Freeman, H.S., Editors. 1996, Springer Netherlands: Dordrecht. p. 145-195.

(323) Ahmed, F., Dewani, R., Pervez, M., Mahboob, S. and Soomro, S., *Non-destructive FT-IR analysis of mono azo dyes.* Bulg. Chem. Commun, 2016. **48**: p. 71-77.

(324) Jia, X.-J., Wang, J., Wu, J., Du, Y., Zhao, B. and Engelsen, D. d., *Bouquet-like calcium sulfate dihydrate: a highly efficient adsorbent for Congo red dye.* RSC Advances, 2015. **5**(88): p. 72321-72330.

Die approbierte gedruckte Originalversion dieser Dissertation ist an der TU Wien Bibliothek verfügbar.
The approved original version of this doctoral thesis is available in print at TU Wien Bibliothek.
TU Bibliothek Your knowledge hub WIEN

(325) Lafi, R., Montasser, I. and Amor, H., *Adsorption of congo red dye from aqueous solutions by prepared activated carbon with oxygen-containing functional groups and its regeneration*. Vol. 37. 2018. 026361741881922.

(326) Furniss, B. S., *Vogel's textbook of practical organic chemistry*. 1989: Pearson Education India.

(327) Marmion, D. M., *Applications of nuclear magnetic resonance spectroscopy to certifiable food colors.* Journal of the Association of Official Analytical Chemists, 1974. **57**(3): p. 495-507.

(328) Fedorov, L. A., *NMR spectroscopy of azo dyes.* Russian Chemical Reviews, 1988. **57**(10): p. 941.

(329) Tromayer, M., *Novel biocompatible initiators for direct cell encapsulation via two-photon induced photopolymerization.* Dissertation (PhD), Institut für angewandte Synthesechemie, TU Wien, 2018.

(330) Budyka, M. F. and Li, V. M., *Visible-light-driven two-way photoisomerization of 1-(1-pyrenyl)-2-(2-quinolyl) ethylene in neutral and protonated forms.* Photochemical & Photobiological Sciences, 2018. **17**(2): p. 213-220.

(331) Szaciłowski, K., *Digital Information Processing in Molecular Systems.* Chemical Reviews, 2008. **108**(9): p. 3481-3548.

(332) Zimmerman, G., Chow, L.-Y. and Paik, U.-J., *The photochemical isomerization of azobenzene1.* Journal of the American Chemical Society, 1958. **80**(14): p. 3528-3531.

(333) Lewis, F. D., Bedell, A. M., Dykstra, R. E., Elbert, J. E., Gould, I. R. and Farid, S., *Photochemical generation, isomerization, and oxygenation of stilbene cation radicals.* Journal of the American Chemical Society, 1990. **112**(22): p. 8055-8064.

(334) Chen, S., Jin, M., Malval, J.-P., Fu, J., Morlet-Savary, F., Pan, H. and Wan, D., *Substituted stilbene-based oxime esters used as highly reactive wavelength-dependent photoinitiators for LED photopolymerization.* Polymer Chemistry, 2019. **10**(48): p. 6609-6621.

(335) Ishitobi, H., Sekkat, Z. and Kawata, S., *Ordering of azobenzenes by two-photon isomerization.* The Journal of chemical physics, 2006. **125**(16): p. 164718.

(336) Pennacchio, F. A., Fedele, C., De Martino, S., Cavalli, S., Vecchione, R. and Netti, P. A., *Three-Dimensional Microstructured Azobenzene-Containing Gelatin as a Photoactuable Cell Confining System.* ACS applied materials & interfaces, 2017. **10**(1): p. 91-97.

(337) Banwell, C. N. and McCash, E. M., *Fundamentals of molecular spectroscopy*. Vol. 851. 1994: McGraw-Hill New York.

(338) Waldeck, D. H., *Photoisomerization dynamics of stilbenes.* Chemical Reviews, 1991. **91**(3): p. 415-436.

(339) Grabowski, Z. R., Rotkiewicz, K. and Rettig, W., *Structural changes accompanying intramolecular electron transfer: focus on twisted intramolecular charge-transfer states and structures.* Chemical reviews, 2003. **103**(10): p. 3899-4032.

Die approbierte gedruckte Originalversion dieser Dissertation ist an der TU Wien Bibliothek verfügbar.
The approved original version of this doctoral thesis is available in print at TU Wien Bibliothek.
TU Bibliothek Your knowledge hub WIEN

(340) Zhu, Y., Morisato, K., Hasegawa, G., Moitra, N., Kiyomura, T., Kurata, H., Kanamori, K. and Nakanishi, K., *High-performance liquid chromatography separation of unsaturated organic compounds by a monolithic silica column embedded with silver nanoparticles.* Journal of separation science, 2015. **38**(16): p. 2841-2847.

(341) Lamuela-Raventos, R. M., Romero-Perez, A. I., Waterhouse, A. L. and De La Torre-Boronat, M. C., *Direct HPLC analysis of cis-and trans-resveratrol and piceid isomers in Spanish red Vitis vinifera wines.* Journal of Agricultural and Food Chemistry, 1995. **43**(2): p. 281-283.

(342) Király-Véghely, Z., Kátay, G., Tyihák, E. and Merillon, J.-M., *Separation of stilbene isomers from red wine by overpressured-layer chromatography.* JPC–Journal of Planar Chromatography–Modern TLC, 2004. **17**: p. 4-8.

(343) Saltiel, J., *Perdeuteriostilbene. The triplet and singlet paths for stilbene photoisomerization.* Journal of the American Chemical Society, 1968. **90**(23): p. 6394-6400.

(344) Letzel, T., Pöschl, U., Wissiack, R., Rosenberg, E., Grasserbauer, M. and Niessner, R., *Phenyl-Modified Reversed-Phase Liquid Chromatography Coupled to Atmospheric Pressure Chemical Ionization Mass Spectrometry: A Universal Method for the Analysis of Partially Oxidized Aromatic Hydrocarbons.* Analytical Chemistry, 2001. **73**(7): p. 1634-1645.

(345) Kathan, M. and Hecht, S., *Photoswitchable molecules as key ingredients to drive systems away from the global thermodynamic minimum.* Chemical Society Reviews, 2017. **46**(18): p. 5536-5550.

(346) Steiger, W., Gruber, P., Theiner, D., Dobos, A., Lunzer, M., Van Hoorick, J., Van Vlierberghe, S., Liska, R. and Ovsianikov, A., *Fully automated z-scan setup based on a tunable fs-oscillator.* Optical Materials Express, 2019. **9**(9): p. 3567-3581.

(347) Steiger, W., Gruber, P., Tromayer, M., Dobos, A., Lunzer, M., Liska, R. and Ovsianikov, A. *Fully automated z-scan setup based on a tunable fs-oscillator (Conference Presentation)*. in *SPIE BiOS*. 2018: SPIE.

(348) Dyanov, H. M. and Dzitoeva, S. G., *Method for attachment of microscopic preparations on glass for in situ hybridization, PRINS and in situ PCR studies.* BioTechniques, 1995. **18**(5): p. 822-4, 826.

(349) Xiong, W., Zhou, Y. S., He, X. N., Gao, Y., Mahjouri-Samani, M., Jiang, L., Baldacchini, T. and Lu, Y. F., *Simultaneous additive and subtractive three-dimensional nanofabrication using integrated two-photon polymerization and multiphoton ablation.* Light: Science & Applications, 2012. **1**(4): p. e6-e6.

(350) Phipps, C., *Laser ablation and its applications*. Vol. 129. 2007: Springer.

(351) Pasparakis, G., Manouras, T., Argitis, P. and Vamvakaki, M., *Photodegradable polymers for biotechnological applications.* Macromolecular rapid communications, 2012. **33**(3): p. 183-198.

(352) Brandenberg, N. and Lutolf, M. P., *In Situ Patterning of Microfluidic Networks in 3D Cell-Laden Hydrogels.* Advanced Materials, 2016. **28**(34): p. 7450-7456.

Die approbierte gedruckte Originalversion dieser Dissertation ist an der TU Wien Bibliothek verfügbar.
The approved original version of this doctoral thesis is available in print at TU Wien Bibliothek.
TU Bibliothek Your knowledge hub WIEN

(353) Srinivasan, R., *Ablation of polymers and biological tissue by ultraviolet lasers.* Science, 1986. **234**(4776): p. 559-565.

(354) Van Hoorick, J., Biopolymers Immobilized on Polyester Membranes: A new Vision Towards Ocular Regeneration, Ghent University, 2019

(355) Tomkiewicz, M. and Klein, M. P., *Photochemically induced dynamic nuclear polarization in hydrosol suspensions of Congo Red.* Journal of the American Chemical Society, 1973. **95**(10): p. 3132-3136.

(356) Bellin, J. S. and Gergel, C. A., *PHYCOCYANIN-SENSITIZED PHOTOREDUCTION OF AZO DYES*.* Photochemistry and Photobiology, 1969. **10**(6): p. 427-439.

(357) Pedersen, M. Ø., Mikkelsen, K., Behrens, M. A., Pedersen, J. S., Enghild, J. J., Skrydstrup, T., Malmendal, A. and Nielsen, N. C., *NMR reveals two-step association of Congo Red to amyloid β in low-molecular-weight aggregates.* The Journal of Physical Chemistry B, 2010. **114**(48): p. 16003-16010.

(358) Iwunze, M. O., *Aqueous Photophysical Parameters of Congo Red.* Spectroscopy Letters, 2010. **43**(1): p. 16-21.

(359) LaPlante, S. R., Carson, R., Gillard, J., Aubry, N., Coulombe, R., Bordeleau, S., Bonneau, P., Little, M., O'Meara, J. and Beaulieu, P. L., *Compound Aggregation in Drug Discovery: Implementing a Practical NMR Assay for Medicinal Chemists.* Journal of Medicinal Chemistry, 2013. **56**(12): p. 5142-5150.

(360) Klunk, W. E., Debnath, M. L. and Pettegrew, J. W., *Development of small molecule probes for the beta-amyloid protein of Alzheimer's disease.* Neurobiology of aging, 1994. **15**(6): p. 691-698.

(361) Wang, L. and Wang, A., *Adsorption properties of congo red from aqueous solution onto N, O-carboxymethyl-chitosan.* Bioresource Technology, 2008. **99**(5): p. 1403-1408.

(362) Panczyk, T., Wolski, P., Jagusiak, A. and Drach, M., *Molecular dynamics study of Congo red interaction with carbon nanotubes.* RSC Advances, 2014. **4**(88): p. 47304-47312.

(363) Childers, W. S., Mehta, A. K., Lu, K. and Lynn, D. G., *Templating Molecular Arrays in Amyloid's Cross-β Grooves.* Journal of the American Chemical Society, 2009. **131**(29): p. 10165-10172.

(364) Qi, S., Zhang, C., Yang, X., Chen, K. and Zhang, L. *Nonlinear optical properties of Congo red in aqueous solution and PVA film*. in *European Symposium on Optics and Photonics for Defence and Security*. 2004: SPIE.

(365) Rudyk, H., Knaggs, M. H., Vasiljevic, S., Hope, J., Birkett, C. and Gilbert, I. H., *Synthesis and evaluation of analogues of congo red as potential compounds against transmissible spongiform encephalopathies.* European Journal of Medicinal Chemistry, 2003. **38**(6): p. 567-579.

(366) Demaimay, R., Harper, J., Gordon, H., Weaver, D., Chesebro, B. and Caughey, B., *Structural Aspects of Congo Red as an Inhibitor of Protease-Resistant Prion Protein Formation.* Journal of Neurochemistry, 1998. **71**(6): p. 2534-2541.

Die approbierte gedruckte Originalversion dieser Dissertation ist an der TU Wien Bibliothek verfügbar.
The approved original version of this doctoral thesis is available in print at TU Wien Bibliothek.
TU Bibliothek Your knowledge hub WIEN

(367) Szadowski, J., *Disazo direct dyes containing cyclic amido, keto and amino groups.* Dyes and Pigments, 1990. **14**(3): p. 217-224.

(368) Conway-Jacobs, A. and Lewin, L. M., *Isoelectric focusing in acrylamide gels: Use of amphoteric dyes as internal markers for determination of isoelectric points.* Analytical Biochemistry, 1971. **43**(2): p. 394-400.

(369) Freeman, H. S., *Aromatic amines: use in azo dye chemistry.* Front Biosci (Landmark Ed), 2013. **18**: p. 145-164.

(370) Hunger, K., Mischke, P., Rieper, W., Raue, R., Kunde, K. and Engel, A., *Azo dyes.* Ullmann's encyclopedia of industrial chemistry, 2005.

(371) Waring, D. R. and Hallas, G., *The chemistry and application of dyes*. 2013: Springer Science & Business Media.

(372) Ventura-Camargo, B. and Marin-Morales, M., *Azo Dyes: Characterization and Toxicity– A Review*. Vol. 2. 2013.

(373) Präbst, K., Engelhardt, H., Ringgeler, S. and Hübner, H., *Basic colorimetric proliferation assays: MTT, WST, and resazurin*, in *Cell viability assays*. 2017, Springer. p. 1-17.

(374) Eisner, V., Picard, M. and Hajnóczky, G., *Mitochondrial dynamics in adaptive and maladaptive cellular stress responses.* Nature cell biology, 2018. **20**(7): p. 755-765.

(375) Kell, D. B., Kaprelyants, A. S., Weichart, D. H., Harwood, C. R. and Barer, M. R., *Viability and activity in readily culturable bacteria: a review and discussion of the practical issues.* Antonie van Leeuwenhoek, 1998. **73**(2): p. 169-187.

(376) Puntener, A. and Page, C., *European ban on certain azo dyes–a report.* Quality and Environment, TFL Leather Technology Limited, Version, 2007. **2**: p. 1-6.

(377) Lombard, J., *Once upon a time the cell membranes: 175 years of cell boundary research.* Biology Direct, 2014. **9**(1): p. 32.

(378) Pawley, J., *Handbook of biological confocal microscopy*. Vol. 236. 2006: Springer Science & Business Media.

(379) Lackie, J. M., *Cell movement and cell behaviour*. 2012: Springer Science & Business Media.

(380) Jerome, W. G. and Price, R. L., *Basic Confocal Microscopy*. 2018: Springer International Publishing.

(381) https://www.sigmaaldrich.com/content/dam/sigma-aldrich/docs/Sigma/Product_Information_Sheet/1/m6514pis.pdf. *Downloaded 26.11.2020*.

(382) Van Hoorick, J., Tytgat, L., Dobos, A., Ottevaere, H., Van Erps, J., Thienpont, H., Ovsianikov, A., Dubruel, P. and Van Vlierberghe, S., *(Photo-)crosslinkable Gelatin Derivatives for Biofabrication Applications.* Acta Biomaterialia, 2019.

(383) Autian, J., *Structure-toxicity relationships of acrylic monomers.* Environmental health perspectives, 1975. **11**: p. 141-152.

Die approbierte gedruckte Originalversion dieser Dissertation ist an der TU Wien Bibliothek verfügbar.
The approved original version of this doctoral thesis is available in print at TU Wien Bibliothek.
TU Bibliothek Your knowledge hub WIEN

(384) Cobo, I., Li, M., Sumerlin, B. S. and Perrier, S., *Smart hybrid materials by conjugation of responsive polymers to biomacromolecules.* Nature materials, 2015. **14**(2): p. 143-159.

(385) Fraser, J. R. E., Laurent, T. C. and Laurent, U., *Hyaluronan: its nature, distribution, functions and turnover.* Journal of internal medicine, 1997. **242**(1): p. 27-33.

(386) Stern, R., *Hyaluronan catabolism: a new metabolic pathway.* European journal of cell biology, 2004. **83**(7): p. 317-325.

(387) Cowman, M. K., Lee, H.-G., Schwertfeger, K. L., McCarthy, J. B. and Turley, E. A., *The content and size of hyaluronan in biological fluids and tissues.* Frontiers in immunology, 2015. **6**: p. 261.

(388) Qin, X.-H., Gruber, P., Markovic, M., Plochberger, B., Klotzsch, E., Stampfl, J., Ovsianikov, A. and Liska, R., *Enzymatic synthesis of hyaluronic acid vinyl esters for two-photon microfabrication of biocompatible and biodegradable hydrogel constructs.* Polymer Chemistry, 2014. **5**(22): p. 6523-6533.

(389) Tomášiková, Z., *Hydrogels for Tissue Engineering*. 2015: Master Thesis, Institut für Angewandte Synthesechemie, Technische Universität Wien.

(390) Zerobin, E., *Two-Photon Structured Hydrogels based on Hyaluronic Acid for Applications in Tissue Engineering*. 2017: Master Thesis, Institut für Angewandte Synthesechemie, Technische Universität Wien.

(391) Burdick, J. A., Chung, C., Jia, X., Randolph, M. A. and Langer, R., *Controlled degradation and mechanical behavior of photopolymerized hyaluronic acid networks.* Biomacromolecules, 2005. **6**(1): p. 386-391.

(392) Oh, E. J., Kang, S. W., Kim, B. S., Jiang, G., Cho, I. H. and Hahn, S. K., *Control of the molecular degradation of hyaluronic acid hydrogels for tissue augmentation.* Journal of Biomedical Materials Research Part A, 2008. **86**(3): p. 685-693.

(393) Chan, A. T., Karakas, M. F., Vakrou, S., Afzal, J., Rittenbach, A., Lin, X., Wahl, R. L., Pomper, M. G., Steenbergen, C. J. and Tsui, B. M., *Hyaluronic acid-serum hydrogels rapidly restore metabolism of encapsulated stem cells and promote engraftment.* Biomaterials, 2015. **73**: p. 1-11.

(394) Gerecht, S., Burdick, J. A., Ferreira, L. S., Townsend, S. A., Langer, R. and Vunjak-Novakovic, G., *Hyaluronic acid hydrogel for controlled self-renewal and differentiation of human embryonic stem cells.* Proceedings of the National Academy of Sciences, 2007. **104**(27): p. 11298-11303.

(395) Chung, C., Mesa, J., Randolph, M. A., Yaremchuk, M. and Burdick, J. A., *Influence of gel properties on neocartilage formation by auricular chondrocytes photoencapsulated in hyaluronic acid networks.* Journal of Biomedical Materials Research Part A: An Official Journal of The Society for Biomaterials, The Japanese Society for Biomaterials, and The Australian Society for Biomaterials and the Korean Society for Biomaterials, 2006. **77**(3): p. 518-525.

(396) Patterson, J., Siew, R., Herring, S. W., Lin, A. S., Guldberg, R. and Stayton, P. S., *Hyaluronic acid hydrogels with controlled degradation properties for oriented bone regeneration.* Biomaterials, 2010. **31**(26): p. 6772-6781.

Die approbierte gedruckte Originalversion dieser Dissertation ist an der TU Wien Bibliothek verfügbar.
The approved original version of this doctoral thesis is available in print at TU Wien Bibliothek.
TU Bibliothek Your knowledge hub WIEN

(397) Fairbanks, B. D., Schwartz, M. P., Bowman, C. N. and Anseth, K. S., *Photoinitiated polymerization of PEG-diacrylate with lithium phenyl-2,4,6-trimethylbenzoylphosphinate: polymerization rate and cytocompatibility.* Biomaterials, 2009. **30**(35): p. 6702-6707.

(398) Gorsche, C., Harikrishna, R., Baudis, S., Knaack, P., Husar, B., Laeuger, J., Hoffmann, H. and Liska, R., *Real Time-NIR/MIR-Photorheology: A Versatile Tool for the in Situ Characterization of Photopolymerization Reactions.* Analytical Chemistry, 2017. **89**(9): p. 4958-4968.

(399) Wang, J. and Ugaz, V. M., *Using in situ rheology to characterize the microstructure in photopolymerized polyacrylamide gels for DNA electrophoresis.* Electrophoresis, 2006. **27**(17): p. 3349-3358.

(400) Sunyer, R., Jin, A. J., Nossal, R. and Sackett, D. L., *Fabrication of hydrogels with steep stiffness gradients for studying cell mechanical response.* PloS one, 2012. **7**(10): p. e46107.

(401) Charrier, E. E., Pogoda, K., Wells, R. G. and Janmey, P. A., *Control of cell morphology and differentiation by substrates with independently tunable elasticity and viscous dissipation.* Nature communications, 2018. **9**(1): p. 1-13.

(402) Ruoslahti, E., *RGD AND OTHER RECOGNITION SEQUENCES FOR INTEGRINS.* Annual Review of Cell and Developmental Biology, 1996. **12**(1): p. 697-715.

(403) LeBaron, R. G. and Athanasiou, K. A., *Extracellular Matrix Cell Adhesion Peptides: Functional Applications in Orthopedic Materials.* Tissue Engineering, 2000. **6**(2): p. 85-103.

(404) Stähler, A., *Chemisches Zentralblatt.*

(405) Aakeröy, C. B., Sinha, A. S., Epa, K. N., Spartz, C. L. and Desper, J., *A versatile and green mechanochemical route for aldehyde–oxime conversions.* Chemical Communications, 2012. **48**(92): p. 11289-11291.

(406) Freeman, J. P., *The Reactions of Certain Oxidized Nitrogen Compounds with Perchloryl Fluoride1.* Journal of the American Chemical Society, 1960. **82**(15): p. 3869-3873.

(407) Taniguchi, M. and Lindsey, J. S., *Database of Absorption and Fluorescence Spectra of >300 Common Compounds for use in PhotochemCAD.* Photochemistry and Photobiology, 2018. **94**(2): p. 290-327.

(408) Zellelow, A. Z., Abiye, M., Fink, D. A., Ford, C. E., Kim, K.-H., Sours, R. E., Yannette, C. M. and Swift, J. A., *Doping Uric Acid Crystals. 1. Uric Acid Dihydrate.* Crystal Growth & Design, 2010. **10**(8): p. 3340-3347.

(409) Bhoi, Y. P., Pradhan, S. R., Behera, C. and Mishra, B., *Visible light driven efficient photocatalytic degradation of Congo red dye catalyzed by hierarchical CuS–Bi 2 Cu x W 1− x O 6− 2x nanocomposite system.* RSC Advances, 2016. **6**(42): p. 35589-35601.

Die approbierte gedruckte Originalversion dieser Dissertation ist an der TU Wien Bibliothek verfügbar.
The approved original version of this doctoral thesis is available in print at TU Wien Bibliothek.
TU Bibliothek Your knowledge hub WIEN

(410) Pérez, A., Poznyak, T. and Chairez, I., *Effect of additives on ozone-based decomposition of Reactive Black 5 and Direct Red 28 dyes.* Water Environment Research, 2013. **85**(4): p. 291-300.

(411) Collins, M. N. and Birkinshaw, C., *Hyaluronic acid solutions—A processing method for efficient chemical modification.* Journal of Applied Polymer Science, 2013. **130**(1): p. 145-152.

(412) Baudis, S., Bomze, D., Markovic, M., Gruber, P., Ovsianikov, A. and Liska, R., *Modular material system for the microfabrication of biocompatible hydrogels based on thiol–ene-modified poly(vinyl alcohol).* Journal of Polymer Science Part A: Polymer Chemistry, 2016. **doi: 10.1002/pola.28073**.

(413) Gottlieb, H. E., Kotlyar, V. and Nudelman, A., *NMR Chemical Shifts of Common Laboratory Solvents as Trace Impurities.* The Journal of Organic Chemistry, 1997. **62**(21): p. 7512-7515.

Die approbierte gedruckte Originalversion dieser Dissertation ist an der TU Wien Bibliothek verfügbar.
The approved original version of this doctoral thesis is available in print at TU Wien Bibliothek.

Curriculum Vitae

Elise Zerobin

Education

- PhD Candidate, Institute of Applied Synthetic Chemistry, TU Wien 2017-2020
- Master of Science in Technical Chemistry, TU Wien 2017
- Study abroad, University of Helsinki, Finland 2014
- Bachelor of Science in Technical Chemistry, TU Wien 2014

Work experience

- PhD Candidate, Institute of Applied Synthetic Chemistry, TU Wien 2017-2020
- Laboratory Assistant, TU Wien, Vienna, Austria 2013-2015
- Internship, DPx Fine Chemicals, Linz, Austria 2014
- Internship, DSM, Linz, Austria 2013
- Internship, Hospital Barmherzige Schwestern, Linz, Austria 2011
- Internship, Voestalpine, Linz, Austria 2011
- Internship, Borealis, Schwechat, Austria 2009

Publications (ORCID-iD: 0000-0003-3937-6083)

- Elise Zerobin, Marica Markovic, Zuzana Tomasikova, Xiao-Hua Qin, Davide Ret, Patrick Steinbauer, Jakob Kitzmüller, Wolfgang Steiger, Peter Gruber, Aleksandr Ovsianikov, Robert Liska, Stefan Baudis (2020). “A toolbox toward controlling mechanical properties of hydrogels for 3D microfabrication." Journal of Polymer Science 1-11.
- Elise Zerobin, Marica Markovic, Franziska Gantner, Stefan Binder, Aleksandr Ovsianikov, Stefan Baudis, Robert Liska (submitted February 2021). “Expanding the Portfolio of Biocompatible Azosulfonate-based Two Photon Initiators” Journal of Polymer Science
- Aysu Arslan, Wolfgang Steiger, Patrice Roose, Hugues Van den Bergen, Peter Gruber, Elise Zerobin, Franziska Gantner, Olivier Guillaume, Aleksandr Ovsianikov, Sandra Van Vlierberghe, Peter Dubruel (2020). “Polymer architecture as key to unprecedented high-resolution 3Dprinting performance: The case of biodegradable hexa-functional telechelic urethane-based poly-e-caprolactone” Materials Today.

Die approbierte gedruckte Originalversion dieser Dissertation ist an der TU Wien Bibliothek verfügbar.
The approved original version of this doctoral thesis is available in print at TU Wien Bibliothek.
TU Bibliothek Your knowledge hub WIEN

- Sara Zigon-Branc, Marica Markovic, Jasper Van Hoorick, Sandra Van Vlierberghe, Peter Dubruel, Elise Zerobin, Stefan Baudis, and Aleksandr Ovsianikov (2019). "Impact of hydrogel stiffness on differentiation of human adipose-derived stem cell microspheroids." Tissue Engineering Part A 25 (19-20): 1369-1380.

International Conferences

- BSTE (Poster Presentation & Speed-talk) Ghent, Belgium, 2018
  Molecular Design towards Two-Photon Initiators with Reduced Phototoxicity (Poster Presentation Award)
- ESPS (Poster Presentation) Mulhouse, France, 2018
  Molecular Design towards Two-Photon Initiators with Reduced Phototoxicity
- VSS (Oral Presentation) Vienna, Austria, 2018
  Molecular Design towards novel Photo Initiators with increased Two-photon absorption cross section
- ViP (Poster Presentation) Vienna, Austria, 2018
  Hydrogel Networks and Two-Photon Initiators based on Hyaluronic Acid
- ViCEM (Poster Presentation) Vienna, Austria, 2017
  Hyaluronic Acid as a Basis for the Development of Hydrogel Networks and Two-Photon Initiators
- ÖGBMT Jahrestagung (Oral Presentation) Vienna, Austria, 2017
  Two-Photon Structured Hydrogels based on Hyaluronic Acid for Applications in Tissue Engineering (Förderpreis für den wissenschaftlichen Nachwuchs)
- DVSPM (Oral Presentation) Vienna, Austria, 2017
  Two-Photon Initiator Development and Hydrogel Networks based on Hyaluronic Acid (Best Lecturer Award)
- AMBA (Oral Presentation) Ghent, Belgium, 2017
  Newly Developed Hydrogel Precursors and Two-Photon Initiators based on Hyaluronic Acid
- CEITEC (Poster Presentation) Brno, Czech Republic, 2017
  Biocompatible Hydrogel Constructs Based on Hyaluronic Acid
- ESPS (Poster Presentation) Leipzig, Germany, 2016
  High Resolved Biocompatible Hydrogel Constructs Based on Hyaluronic Acid
- BYPoS (Oral Presentation) Zdiar, Slovakia, 2016
  Micro Fabrication of Hydrogels based on Hyaluronic Acid

Die approbierte gedruckte Originalversion dieser Dissertation ist an der TU Wien Bibliothek verfügbar.
The approved original version of this doctoral thesis is available in print at TU Wien Bibliothek.
TU Bibliothek Your knowledge hub WIEN